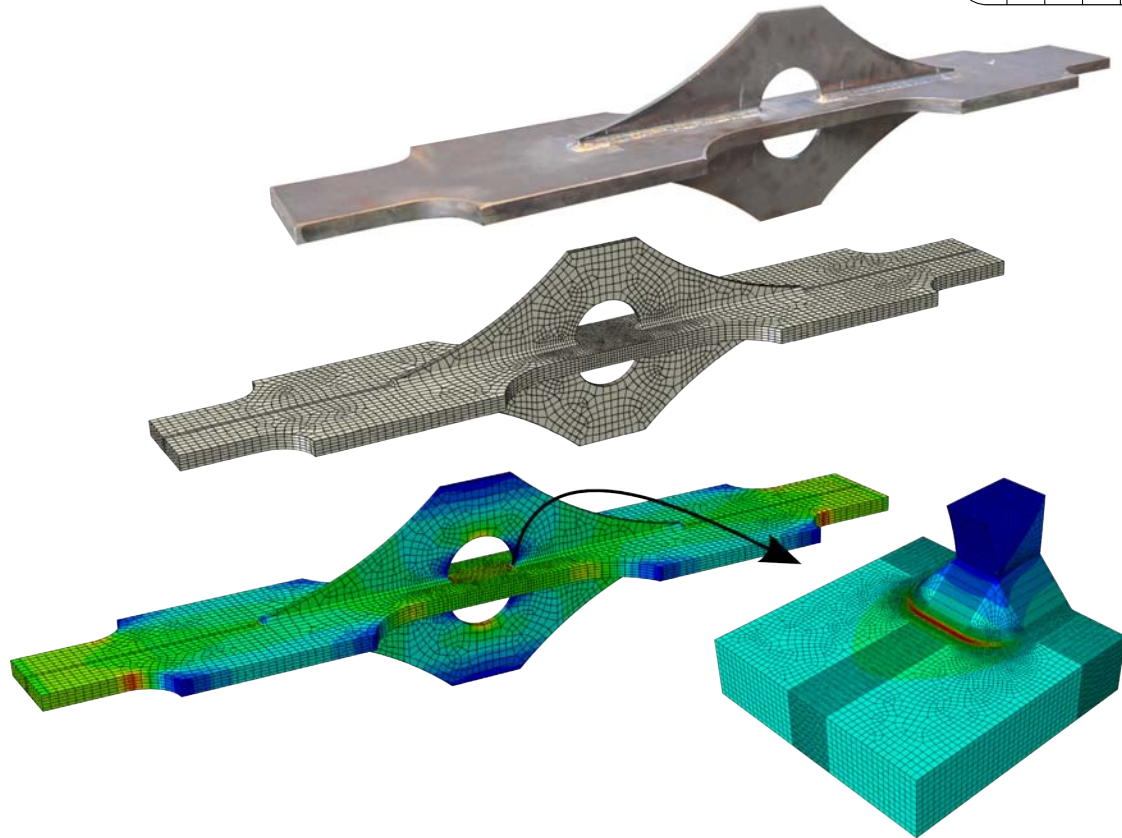


# CHALMERS



## Fatigue Life Assessment of Bridge Details Using Finite Element Method

*Master's thesis in the Master's Programme Structural Engineering and Building Performance Design*

MOHSEN HESHMATI

Department of Civil and Environmental Engineering  
*Division of Structural Engineering*  
*Steel and Timber Structures*  
CHALMERS UNIVERSITY OF TECHNOLOGY  
Gothenburg, Sweden 2012  
Master's thesis 2012:03



MASTERS THESIS 2012:3

# Fatigue Life Assessment of Bridge Details Using Finite Element Method

*Master's Thesis in the Master's Programme Structural Engineering and Building  
Performance Design*

MOHSEN HESHMATI

Department of Civil and Environmental Engineering  
Division of Structural Engineering  
*Steel and Timber Structures*  
CHALMERS UNIVERSITY OF TECHNOLOGY

Göteborg, Sweden, 2012

Fatigue life assessment of bridge details using finite element method  
*Master's Thesis in the Master's Programme Structural Engineering and Building  
Performance Design*  
MOHSEN HESHMATI

©MOHSEN HESHMATI, 2012

Examensarbete 2012:3  
Department of Civil and Environmental Engineering  
Division of Structural Engineering  
*Steel and Timber Structures*  
Chalmers University of Technology  
SE-412 96 Göteborg  
Sweden  
Telephone +46 (0)31-772 1000

Cover:

Photograph of the fatigue tested cope-hole specimen and the corresponding finite element models for the structural hot spot and the effective notch stress calculation

Chalmers Reproservice  
Göteborg, Sweden 2008



Fatigue life assessment of bridge details using finite element method

*Master's Thesis in the Master's Programme Structural Engineering and Building Performance Design*

MOHSEN HESHMATI

Department of Civil and Environmental Engineering

Division of Structural Engineering

Steel and Timber Structures

Chalmers University OF Technology

## Abstract

Eurocode 3 has recently become the governing design code for steel structures in Sweden. In this design code, the nominal stress method is the predominant approach for fatigue design. However, the limitations of this method along with new advanced computational possibilities, have paved the way for more accurate stress based fatigue design approaches. The Structural Hot Spot Stress (SHSS) and the Effective Notch Stress (ENS) methods are among those which have widely drawn engineers' attention since their advent. These approaches take advantage of new computational modeling possibilities and designate the basic stress by taking into account the geometrical variations of the detail at the expected fatigue crack initiation area (hot spot). As a result, a higher variation of constructional details can be assessed more accurately by these methods. Although the SHSS approach has been extensively exploited in other industries, both methods are considered inexperienced in the field of bridge engineering.

In the current study, several frequently used bridge details are investigated using the nominal stress, SHSS and ENS methods. The aim of this investigation is to establish an equivalency between these approaches with reference to the fatigue strengths of the studied details. The finite element modeling is carried out using different modeling techniques mainly based on the well-known IIW modeling instructions. Furthermore, effects of thickness, weld shape and overall member geometry on the computed stress concentration factor are studied and discussed. A large database including available fatigue test results (from 1950s till present) is built up and used to produce SHSS and ENS S-N curves for the studied details. The findings of this study are presented in terms of modeling recommendations along with characteristic fatigue design values based on different assessment methods for the studied details.

Moreover, special consideration is given to details with cope-holes which are often governing the fatigue design of steel and composite bridges due to their relatively low fatigue resistance. In this study, an examination of load effects on two existing bridge sections with cope-hole details is performed. The findings confirm the considerable effect of shear stresses on fatigue strength of these details. Additionally, the effects of altering the geometric shape of the cope-holes are investigated using finite element analysis. Furthermore, the fatigue strength enhancement of cope-hole details by means of post-weld treatment is experimentally evaluated by conducting constant amplitude fatigue tests. Based on the test results, a new fatigue strength category for improved cope-hole details is proposed. The results revealed an approximately 6.8 times fatigue life extension for the Burr Ground cope-hole details.

**Key words:** Fatigue assessment, Steel bridges, Welded joints, Finite element method, Hot spot stress, Effective notch stress, Experimental approach, Fatigue life improvement techniques, Burr grinding, Ultrasonic impact treatment



# Contents

|   |            |
|---|------------|
| <b>Abstract</b>   | <b>I</b>   |
| <b>Contents</b>   | <b>III</b> |
| <b>Preface</b>  | <b>VII</b> |
| <b>Nomenklature</b>   | <b>X</b>   |
| <b>1 Introduction</b>   | <b>1</b>   |
| 1.1 Aim and scope . . . . .                                     | 2          |
| 1.2 Methodology . . . . .                                       | 2          |
| 1.3 Limitations . . . . .                                       | 3          |
| 1.4 Structure of thesis . . . . .                               | 3          |
| <b>2 Introduction to fatigue</b>                                | <b>5</b>   |
| 2.1 What is fatigue? . . . . .                                  | 5          |
| 2.2 Fatigue and failure of structures . . . . .                 | 7          |
| 2.3 Fatigue from a metallurgical point of view . . . . .        | 9          |
| 2.4 Fatigue from a fracture mechanics point of view . . . . .   | 14         |
| 2.5 Fatigue terms . . . . .                                     | 17         |
| 2.5.1 Fatigue loading . . . . .                                 | 17         |
| 2.5.2 S-N curves . . . . .                                      | 19         |
| 2.6 Fatigue of welded structures . . . . .                      | 21         |
| 2.6.1 Weld shape effects . . . . .                              | 21         |
| 2.6.2 Weld defects . . . . .                                    | 22         |
| 2.6.3 Residual stresses . . . . .                               | 25         |
| <b>3 Fatigue assessment methods</b>                             | <b>27</b>  |
| 3.1 Nominal stress approach . . . . .                           | 30         |
| 3.1.1 Basic concepts . . . . .                                  | 30         |
| 3.1.2 Design according to the Nominal Stress Approach . . . . . | 30         |
| 3.1.3 Thickness effect . . . . .                                | 34         |
| 3.1.4 Misalignment effect . . . . .                             | 36         |
| 3.1.5 Limitations . . . . .                                     | 37         |
| 3.2 Structural stress approach . . . . .                        | 38         |
| 3.2.1 Basic concepts . . . . .                                  | 38         |
| 3.2.2 Applications . . . . .                                    | 41         |
| 3.2.3 Experimental evaluation of the SHSS . . . . .             | 44         |

|          |  |           |
|----------|--|-----------|
| 3.2.4    | The SHSS evaluation using finite element method . . . . .                    | 47        |
| 3.2.5    | The SHSS according to surface stress extrapolation . . . . .                 | 52        |
| 3.2.6    | The SHSS according to through thickness stress linearisation                 | 56        |
| 3.2.7    | The SHSS according to Dong . . . . .   | 57        |
| 3.2.8    | The SHSS according to Xiao and Yamada . . . . .                              | 59        |
| 3.2.9    | The SHSS according to Poutiainen and Marquis . . . . .                       | 60        |
| 3.2.10   | Comparison of different SHSS determination procedures . . .                  | 62        |
| 3.2.11   | Limitations . . . . .  | 64        |
| 3.2.12   | Fatigue design based on the SHSS . . . . .                                   | 65        |
| 3.3      | Effective notch stress method . . . . .                                      | 67        |
| <b>4</b> | <b>Fatigue Life Assessment of Longitudinal Non-Load-Carrying Attachments</b> | <b>69</b> |
| 4.1      | Introduction . . . . .   | 69        |
| 4.2      | Test database . . . . .  | 70        |
| 4.3      | Literature review . . . . .  | 71        |
| 4.4      | Finite element modeling and analysis . . . . .                               | 72        |
| 4.4.1    | Geometry . . . . .   | 72        |
| 4.4.2    | Material properties . . . . .  | 74        |
| 4.4.3    | Loading and boundary conditions . . . . .                                    | 74        |
| 4.4.4    | Partitioning, meshing and element types . . . . .                            | 75        |
| 4.4.5    | Post-processing of the results . . . . .                                     | 77        |
| 4.5      | Influencing factors . . . . .  | 78        |
| 4.5.1    | Weld size effect . . . . .   | 78        |
| 4.5.2    | Attachment thickness effect . . . . .  | 78        |
| 4.5.3    | Chamfer angle effect . . . . .   | 80        |
| 4.5.4    | Weld end effect . . . . .  | 83        |
| 4.5.5    | Width effect . . . . .   | 87        |
| 4.5.6    | Thickness effect . . . . .   | 88        |
| 4.5.7    | Detail symmetry effect . . . . .   | 91        |
| 4.5.8    | Length effect . . . . .  | 92        |
| 4.6      | Evaluation according to the nominal stress method . . . . .                  | 95        |
| 4.7      | Evaluation according to the hot spot stress approach . . . . .               | 96        |
| <b>5</b> | <b>Fatigue Life Assessment of Over-Lapped Joints</b>                         | <b>99</b> |
| 5.1      | Introduction . . . . .   | 99        |
| 5.2      | Finite element modeling and analysis . . . . .                               | 101       |
| 5.2.1    | Geometry . . . . .   | 101       |

|          |   |            |
|----------|---|------------|
| 5.2.2    | Partitioning and post-processing of the results . . . . .           | 102        |
| 5.3      | Evaluation according to the nominal stress method . . . . .         | 104        |
| 5.4      | Evaluation according to the hot spot stress approach . . . . .      | 107        |
| 5.5      | Evaluation according to the Dong stress method . . . . .            | 109        |
| <b>6</b> | <b>Fatigue Life Assessment of Cover-Plates</b>                      | <b>111</b> |
| 6.1      | Introduction . . . . .  | 111        |
| 6.2      | Test database . . . . .   | 112        |
| 6.3      | Literature review . . . . .   | 113        |
| 6.4      | Finite element modeling techniques . . . . .                        | 114        |
| 6.4.1    | Global model . . . . .  | 114        |
| 6.4.2    | Sub model . . . . .   | 115        |
| 6.4.3    | The nominal stress calculation . . . . .                            | 118        |
| 6.5      | Cover plate end shape effect . . . . .                              | 119        |
| 6.6      | Evaluation according to the nominal stress method . . . . .         | 121        |
| 6.7      | Evaluation according to the hot spot stress approach . . . . .      | 122        |
| 6.8      | Evaluation according to the effective notch stress method . . . . . | 123        |
| <b>7</b> | <b>Fatigue Life Assessment of Cruciform Joints</b>                  | <b>125</b> |
| 7.1      | Introduction . . . . .  | 125        |
| 7.2      | Test database . . . . .   | 126        |
| 7.3      | Finite element modeling and analysis . . . . .                      | 128        |
| 7.3.1    | Geometry and partitioning . . . . .                                 | 128        |
| 7.3.2    | Meshing, Element type and analysis procedure . . . . .              | 129        |
| 7.4      | Influencing factors . . . . .                                       | 130        |
| 7.4.1    | Stress ratio (R) effect . . . . .                                   | 130        |
| 7.4.2    | Welding method effect . . . . .                                     | 132        |
| 7.4.3    | Weld shape effect . . . . .   | 133        |
| 7.4.4    | Stress calculation effect . . . . .                                 | 136        |
| 7.4.5    | Residual stresses effect . . . . .                                  | 136        |
| 7.4.6    | Detail configuration effect . . . . .                               | 137        |
| 7.5      | Evaluation according to the nominal stress method . . . . .         | 139        |
| 7.6      | Evaluation according to the effective notch stress method . . . . . | 139        |
| 7.7      | An investigation of crack propagation path . . . . .                | 141        |
| <b>8</b> | <b>Fatigue Life Assessment of Cope-Hole Details</b>                 | <b>145</b> |
| 8.1      | Introduction . . . . .  | 145        |
| 8.2      | Existing fatigue tests . . . . .                                    | 148        |

|          |   |            |
|----------|---|------------|
| 8.3      | Influencing factors . . . . .                                       | 150        |
| 8.3.1    | load effect . . . . .   | 150        |
| 8.3.2    | shape effect . . . . .  | 154        |
| 8.4      | Evaluation according to the hot spot stress approach . . . . .      | 157        |
| 8.5      | Evaluation according to the effective notch stress method . . . . . | 157        |
| 8.6      | Experimental study . . . . .  | 159        |
| 8.6.1    | Test specimen . . . . .   | 159        |
| 8.6.2    | Post-weld treatment . . . . .                                       | 160        |
| 8.6.3    | Test procedure . . . . .  | 167        |
| 8.6.4    | Test results . . . . .  | 168        |
| <b>9</b> | <b>Conclusions</b>  | <b>171</b> |
| 9.1      | Concluding remarks . . . . .  | 171        |
| 9.2      | Future work . . . . .   | 174        |
|          | <b>References</b>   | <b>175</b> |
|          | <b>Appendices</b>   | <b>182</b> |
|          | <b>Paper A–C</b>  | <b>205</b> |

# Preface

This Master's thesis deals with the fatigue assessment of welded bridge details using finite element method. The research has been carried out at the Division of Structural Engineering of the Department of Civil and Environmental Engineering at Chalmers University of Technology. The work presented in this research is a part of the research project BriFag - Bridge Fatigue Guidance with a financial grant from the Research Fund for Coal and Steel (contract No. RFSRCT-2008-00033) as well as the Swedish Transport Administration.

This research project would not have been possible without the support of many people. I would like to express my deepest gratitude to my supervisor, Prof. Mohammad Al-Emarani who was abundantly helpful and offered invaluable assistance, support and guidance. I am greatly indebted to him for his insightful comments, stimulating discussions and illuminating guidelines.

My sincere thanks go to Mustafa Aygül, PHD student at the Division of Structural Engineering, without whose knowledge and assistance this study would not have been successful.

Many thanks go in particular to Dr. Reza Haghani Dogaheh who always kindly grants me his time. I gratefully acknowledge him for his valuable advice, fruitful consultation and guidance. Special thanks go to Prof. Bo Edlund who spent his precious time reading this thesis and gave his critical comments about it. I would also like to acknowledge Dr. Zuheir Barsoum for his valuable contribution and guidance.

My most sincere thanks is extended to my family, specially my parents whose continuous support and belief in higher education provided me valuable motivation.

Last, but not least, I send my love and gratitude to my girlfriend, Parisa, for her endless support and encouragement throughout the whole study; more importantly, for understanding and helping in ways others could not.

Gothenburg, February 2012  
Mohsen Heshmati

# Nomenclature

|                    |  |
|--------------------|--|
| $\Delta K$         | Stress intensity factor range                                |
| $\delta$           | Distance from the weld toe in the Dong method                |
| $\gamma_t$         | Fatigue strength thickness reduction factor                  |
| $\nu$              | Poisson's ratio for steel                                    |
| $\sigma_{0.4t}$    | stress in the reference point located 0.4t from the hot spot |
| $\sigma_{0.5t}$    | stress in the reference point located 0.5t from the hot spot |
| $\sigma_{0.9t}$    | stress in the reference point located 0.9t from the hot spot |
| $\sigma_{1.0t}$    | stress in the reference point located 1.0t from the hot spot |
| $\sigma_{1.4t}$    | stress in the reference point located 1.4t from the hot spot |
| $\sigma_{1.5t}$    | stress in the reference point located 1.5t from the hot spot |
| $\sigma_{12mm}$    | stress in the reference point located 12mm from the hot spot |
| $\sigma_{15mm}$    | stress in the reference point located 15mm from the hot spot |
| $\sigma_{4mm}$     | stress in the reference point located 4mm from the hot spot  |
| $\sigma_{5mm}$     | stress in the reference point located 15mm from the hot spot |
| $\sigma_{8mm}$     | stress in the reference point located 8mm from the hot spot  |
| $\sigma_{\perp a}$ | Normal stress amplitude                                      |
| $\sigma_{add}$     | Additional stress due to shear deformation                   |
| $\sigma_a$         | Stress amplitude   |
| $\sigma_{ben}$     | Bending stress component                                     |
| $\sigma_{ben}$     | Non-linear stress peak component                             |
| $\sigma_e$         | Stress range   |
| $\sigma_{Hotspot}$ | Structural hot spot stress                                   |
| $\sigma_{max}$     | Maximum stress   |
| $\sigma_{mean}$    | Mean stress  |
| $\sigma_{mem}$     | Membrane stress component                                    |
| $\sigma_{min}$     | Minimum stress   |
| $\sigma_m$         | Normal stress in flange                                      |



|                      |   |
|----------------------|---|
| $\sigma_{Nominal}$   | Nominal stress  |
| $\sigma_r$           | Stress range  |
| $\sigma_t$           | Total stress at the weld toe  |
| $\tau_{\parallel a}$ | Shear stress amplitude  |
| $\tau_a$             | Shear stress in web at weld ends                                      |
| $\varepsilon_{0.4t}$ | Measured strain in the reference point located 0.4t from the weld toe |
| $\varepsilon_{0.9t}$ | Measured strain in the reference point located 0.9t from the weld toe |
| $\varepsilon_{1.0t}$ | Measured strain in the reference point located 1.0t from the weld toe |
| $\varepsilon_{1.4t}$ | Measured strain in the reference point located 1.4t from the weld toe |
| $\varepsilon_{12mm}$ | Measured strain in the reference point at 12mm from the weld toe      |
| $\varepsilon_{4mm}$  | Measured strain in the reference point at 4mm from the weld toe       |
| $\varepsilon_{8mm}$  | Measured strain in the reference point at 8mm from the weld toe       |
| $\varepsilon_{hs}$   | Structural strain at the weld toe (hot spot)                          |
| $\varepsilon_x$      | Strain in the direction perpendicular to the weld toe)                |
| $\varepsilon_y$      | Strain in the direction parallel to the weld toe                      |
| $a$                  | Crack length  |
| $A_s$                | Shear effective area  |
| $D_\sigma$           | Damage caused by normal stress  |
| $D_\tau$             | Damage caused by shear stress   |
| $D_{tot}$            | Total damage calculated from Palmgren-Miner's rule                    |
| $da/dN$              | Fatigue crack growth rate   |
| $E$                  | Modulus of elasticity for steel                                       |
| $f$                  | Geometry and loading function   |
| $I_f$                | Flange second moment of inertia                                       |
| $K_I$                | Stress intensity factor   |
| $K_t$                | Stress concentration factor   |
| $K_{hs}$             | Structural hot spot stress concentration factor                       |
| $K_{sa}$             | Modified structural stress concentration factor                       |
| $K_{weld}$           | Stress intensity factor for the weldment                              |

|           |  |
|-----------|--|
| $M_K$     | Weld geometry correction factor            |
| $M_{add}$ | Additional moment due to shear deformation |
| $N_i$     | Fatigue crack initiation life of a detail  |
| $N_p$     | Fatigue crack propagation life of a detail |
| $N_t$     | Total fatigue life of a detail             |
| $R$       | Stress ratio                               |
| $R_{cp}$  | Cope-hole radius                           |
| $R_{cp}$  | Cope-hole radius                           |
| $R_{ref}$ | Reference cope-hole radius                 |
| $S$       | Applied remote stress                      |
| $t_f$     | Flange thickness                           |
| $Y$       | Geometry correction factor                 |

# 1 Introduction

Fatigue is a complex phenomenon which becomes even more complicated in case of welded details. Welding process induces residual stresses and distortions, changes the crystalline structure at the weld zone, and produces potential failure points by including weld defects [1–4]. These peculiarities of welded components, as well as other destructive effects of welding, drastically reduce the fatigue strength of welded structures. However, welding offers great flexibility to design details and components. This unique feature of welding has made it one of the most common production techniques of large structures, such as bridges, offshore platforms and crane girders. Considering the wide use of welding process on the one hand, and on the other, its destructive effects with reference to fatigue, an enormous amount of research has been focused on the fatigue design and assessment of welded structures.

The nominal stress method has been the most widely used fatigue assessment method in the field of structural engineering for decades. This method disregards any local stress redistribution due to the weld and makes use of the ‘global stress field’ away from the weld. However, fatigue of welded structures is a very localized phenomenon that is affected by local geometrical complexities and material imperfections and discontinuities. Since these are only roughly accounted for when using the nominal stress method, the fatigue life estimation would not be very accurate. In addition to that, in case of large steel structures with complex details, such as bridges, the nominal stress method has a very limited application. A more accurate fatigue assessment may be achieved by implementing methods that take the stress raising effects caused by the geometrical and/or loading variations into account. These methods are generally known as ‘local approaches’ and are expected to yield relatively better fatigue life estimations for complex structures.

Steel and composite bridges are composed of complex structural components and are generally subjected to multiple loading conditions. Thus, calculating the local stress state in such structures without using a computer-based analysis tool is cumbersome, if not impossible. A precise calculation of local stresses for the fatigue assessment of complex welded bridge details may be obtained by using advanced computational methods such as the Finite Element Method (FEM). The application of FEM for the fatigue assessment of bridge details has paved the way for the development of local methods such as the structural hot spot stress approach and the effective notch stress method. Furthermore, recent developments in the numerical methods and computational possibilities have extended the application range of the mentioned methods.

The structural hot spot stress method is well established and has been widely used for the fatigue assessment of tubular structures [3, 5]. However, since the method has not been comprehensively applied to the plate-type structures, it is still considered as an inexperienced fatigue assessment approach for such structures. The effective notch stress concept is an even newer and consequently less applied method. Moreover, the results of several 3D finite element analysis have shown that certain

instructions regarding the element types and meshing techniques should be followed in order to obtain comparable results [6–8]. Therefore, a number of codes and guidelines have proposed finite element modeling recommendations in that regard [9–11]. However, these recommendations are not generally comprehensive and do not cover complex details. Eurocode3 [9], in particular, has provided very insufficient recommendations regarding the application of these methods.

## 1.1 Aim and scope

The nominal stress method has been based on experimental investigations that were conducted mostly before 1970s. As the welding techniques have undergone significant changes since then, the credibility of this method, considering the newly performed tests, is questionable. In addition to that, the structural hot spot stress approach and the effective notch stress method suggest considerably fewer fatigue design classes compared to the nominal stress method. Thus, the main aim of this study is to investigate the reliability and credibility of the mentioned fatigue assessment methods.

Furthermore, the effect of different modeling techniques on the predicted fatigue lives are investigated. The aim of this investigation is to provide recommendations regarding the finite element modeling of the welded details.

Another aim of this study is to explicitly investigate the fatigue behavior of cope-hole details. The verification of current design classes, identification of different fatigue life influencing factors as well as improving the fatigue life of this detail are pursued.

## 1.2 Methodology

In order to achieve the above defined objectives, firstly, an extensive literature study on the different fatigue assessment methods are done. Secondly, several frequently used bridge details are selected and a comprehensive database including available fatigue test results is built up and pre-evaluated. In the preliminary evaluation phase of the collected fatigue test data, the improper tests, inconsistent with the objectives of this research, were excluded.

Afterwards, to establish an equivalency between the nominal stress, structural hot spot stress and effective notch stress methods with reference to the fatigue strengths of the studied details, the correspondent finite element models were created and analyzed. The analysis results were used to compare the predicted fatigue lives with the experimental results, identify fatigue life influencing factors and investigate the validity of the suggested design recommendations based on the Eurocode 3 [9] and IIW [10]. Since the finite element models were created for different mesh qualities and geometries, modeling recommendations are also given based on the results. In order to achieve the objectives of the special study for the cope-hole details,

a new test series is designed and tested at Chalmers University of Technology, Structural Engineering Laboratory. The tests were conducted to verify the current recommendations and also investigate the fatigue life improvement of post-weld treated cope-hole details.

### 1.3 Limitations

In this study, only the as-welded joints tested under constant-amplitude fatigue loading are selected. Post-weld treated joints and joints tested in temperatures other than the ambient room temperature are not included. Only the specimens made of mild steel and tested in the air are studied. In order to diminish the beneficial effects of compression stress, only the fatigue tested specimens with a positive stress ratio ( $R \geq 0$ ) or included. In addition to that, for axially tested specimens, the test series including bending load cases are not collected.

In case of cope-hole details, the analytical and experimental investigations were carried out only for notches with  $R_{cp} = 50mm$ . Moreover, the dimensions of the designed test specimen were limited by the executable length and grip of the available testing machine.

For finite element modeling, the IIW recommendations [10, 11] for modeling and stress determination are followed. The obtained results are compared to the recommended fatigue classes provided by the Eurocode 3 [9] and IIW [10].

### 1.4 Structure of thesis

A short introduction to fatigue with special consideration given to the fatigue of welded details is presented in Chapter 2. Chapter 3 provides a comprehensive introduction to the different fatigue assessment methods. As the structural hot spot stress and effective notch stress approaches have not been used widely, this chapter is prepared in a descriptive format to provide a sufficient theoretical background for these methods.

Chapters 4–8, provide the results of the investigations for each studied detail, separately. In each chapter, firstly, the investigated detail is introduced and its current pertaining design classes are presented. Secondly, the collected tests for the detail are summarized. Afterwards, the finite element modeling and analysis procedures are presented. Next, the fatigue life influencing factors are investigated and the finite element analysis and experimental results are compared. Eventually, the detail is assessed based on different fatigue life assessment methods and the results are discussed.

Eventually, Chapter 9 includes the concluding remarks and recommendations. Suggestions for the future work are also given.



## 2 Introduction to fatigue

### 2.1 What is fatigue?

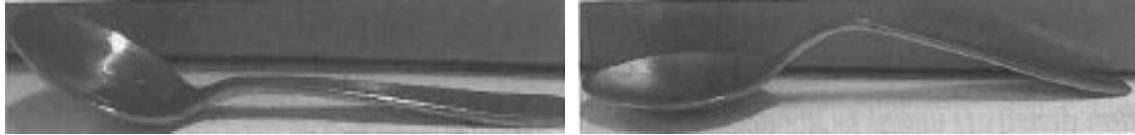
It is a well known fact that if the maximum load acting on a structure becomes higher than its material yield strength limit, a failure is assumed in the structure. However, in a structure that undergoes fluctuating loads, even if they are well below the material elastic limit, a failure can be expected after many loading cycles. The latter situation, which is a result of accumulated damages in the material, is known as fatigue failure. In other words, static loading of a ductile material which increases from zero to a maximum, will cause large deformations. In that case, failure of the structure occurs after a single load application with large plastic deformation, whereas, if the same material is repeatedly loaded to stresses well below the elastic limit, fatigue failure may happen after as little as a few hundred cycles or after, say, several million cycles of load application without any large plastic deformation.

However, it should be noted that fatigue can happen not only in metallic alloys but also in a large number of engineering materials such as polymers and composites, e.g. concrete and fiber reinforced plastics. Although the phenomenological details of the fatigue process might be divergent in different materials, ASTM [12] defines fatigue for all materials as:

Fatigue: The process of *progressive localized permanent structural change* occurring in a material subjected to conditions that produce fluctuating stresses and strains at some point or points and that may culminate in cracks or complete fracture after a sufficient number of fluctuations.

In the above definition, the remarkable features of fatigue are shown in italics. Fatigue is a progressive process that takes time to initiate and develop. Therefore, the process of fatigue is time-consuming and can only happen as an outcome of a repeated loading. In most cases the crack initiates in a confined small area that is either subjected to high local stresses or suffering from local defects in the material. On the contrary, in adjacent parts, where the stress state is insignificantly lower, no crack would initiate. Hence, fatigue is clearly a very localized process in which the crack originates in a location where several micro-cracks are available and grow together into one dominant crack. The mentioned process of crack formation after a coalescence of several micro-cracks is called the initiation phase of fatigue crack growth and is a result of plastic deformations in a small area in front of the crack tip. The presence of plastic deformations also implies that fatigue is an irreversible process which leaves permanent structural damages. This fact will be more elaborated in Section 2.3.

In order to understand the fatigue phenomenon in a more practical sense, a simple experiment performed by Dahlberg and Ekberg [13] is discussed here. This experiment aims to comparatively investigate the failure of a group of repeatedly bent tea spoons with those severely bent only once.



(a) *A teaspoon*

(b) *A statically bent teaspoon*

**Figure 2.1:** *The teaspoon test, after [13]*

It is observed that, by bending the teaspoon statically, a large deformation would occur but a rupture is very unlikely to happen. Conversely, by repeatedly bending the other teaspoon, after a while, it becomes fragile and would easily break a part with a snap. This phenomenon, which is accompanied by some energy dissipation near the fracture region (it can be really hot), is called fatigue. Furthermore, the final fracture of the teaspoon in the second test is surprisingly brittle compared to the ductile behavior of the first test series.

Just before the final fracture of the second test series, by investigating more in details, some small cracks are observed at the failure region. These cracks are formed due to the plastic deformation caused by each bending cycle. The permanent deformation of the teaspoon after each cycle can be regarded as the proof of plastic nature of it. By continuing the test, these small cracks will grow together and form a single dominating crack leading to the final fracture. The characteristics of the final fracture surface will be discussed in more details in Section 2.3.

Eventually, the following conclusions regarding the fatigue nature can be drawn from this simple experiment:

- Small cracks will initiate as an outcome of plastic deformation.
- The cracks will coalesce, resulting in a dominant crack.
- The brittle failure will occur in the end.



(a) *Crack initiation at the sur-*  
*face*

(b) *Formation of larger cracks*

(c) *Single dominating crack just*  
*before failure*

**Figure 2.2:** *Fatigue crack initiation and propagation process in the teaspoon experiment, after [13]*



## 2.2 Fatigue and failure of structures

As it was concluded in the previous section, fatigue failure has a brittle nature. This characteristic of fatigue makes it a potentially dangerous failure mode of structures. These failures happen at extremely high speed without prior large deformations. Moreover, Gurney [2] estimates that 90% of the engineering component failures occur due to fatigue.

On the other hand, very few structures can be regarded as being statically loaded, whereas repeated or fluctuated loading, which can cause fatigue, can be easily found in most of the structures. Bridges, crane girders, chimneys and offshore structures such as oil and production platforms, are among the most common civil engineering structures that frequently experience fatigue loading.

The failure of several welded truss bridges in Europe prior to world war II, shortly after being put into service, drawn the attention of bridge industry and designers. The bridges were lightly loaded and the fractures were sudden. Most of the cracks had initiated in welds and the investigations indicated that the main failure reason was due to inappropriate design, weld defects and poor steel quality. Poor detail design of the Kings Bridge in Melbourne, Australia led to crack initiation in the flange, prior to any service loading, and consequently the brittle fracture of the bridge.

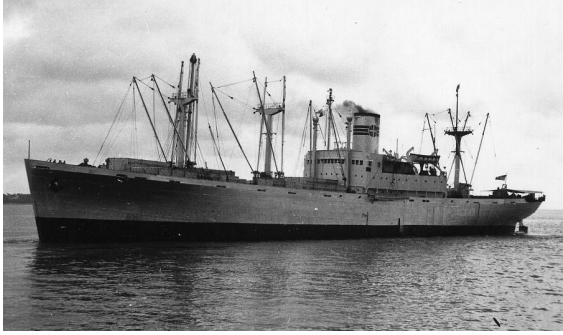
Despite the fact that most of the failures of this kind happened in several bridges throughout the world with noticeably high casualties, the wide-spread attention of bridge engineers hadn't been drawn to the importance of fatigue of bridge details until the Point Pleasant Bridge disaster in West Virginia 1967. The sudden collapse of the bridge took 46 lives and was one of the most catastrophic events at that time. The investigations revealed that the main reason of the collapse was the poor design of a joint which was the crack initiation and propagation region due to fluctuating and repeated loading of the bridge.

Ships, aircrafts and trains are the other major engineering structures that have



(a) *Point Pleasant bridge*      (b) *Point Pleasant bridge after the collapse*      (c) *Point Pleasant bridge after the collapse*

**Figure 2.3:** *Photographs of Point Pleasant bridge before and after collapse in 1967*



(a) *Photograph of one of the liberty ships*



(b) *A liberty ship failure*

**Figure 2.4:** *The failure of liberty ships during 1942-1952*

suffered severe fatigue damages. Although, there were a lot of brittle failures in the aforementioned industries, this problem was not completely comprehended by engineers until the large number of failures of liberty ships during world war II. By 1946, cracks of critical size were seen in more than 1000 out of 5000 ships built in 1942. Between 1942 and 1952, at least 7 liberty ships broke entirely in two halves as a result of fatigue cracking and brittle failure.

The mentioned disasters due to fatigue are not the total number of failures of this kind. Fatigue failures have happened and are happening. They may not be as common as the other structural failures, but when they occur, it might be more devastating in terms of casualties and damages. Therefore, understanding this phenomenon is the prerequisite of a good and efficient design.

## 2.3 Fatigue from a metallurgical point of view

Fatigue life of a detail,  $N_t$ , is often divided into two stages:

- Fatigue crack initiation,  $N_i$
- Fatigue crack propagation,  $N_p$

The separation of these two stages is mainly practical because fatigue crack initiation can be affected by several parameters which the propagation phase is more or less independent. Recent microscopic investigations have shown that, fatigue crack nuclei form almost immediately after the fatigue loading has been applied, providing that the stress is above the fatigue limit<sup>1</sup>, according to Schijve [14]. The crack nuclei commence in slip bands as small invisible microcracks and remain hidden for a significant time. On the other hand, the emergence of cracks indicates that there is not much left of the total fatigue life of the specimen. While the microcracks are being nucleated, the crack growth is in the initiation phase and has an erratic and slow progress. The propagation phase begins when the growth exhibits a steadier behavior.

After having gained basic knowledge of the two phases of fatigue crack growth, their mechanisms and characteristics will be explained further below.

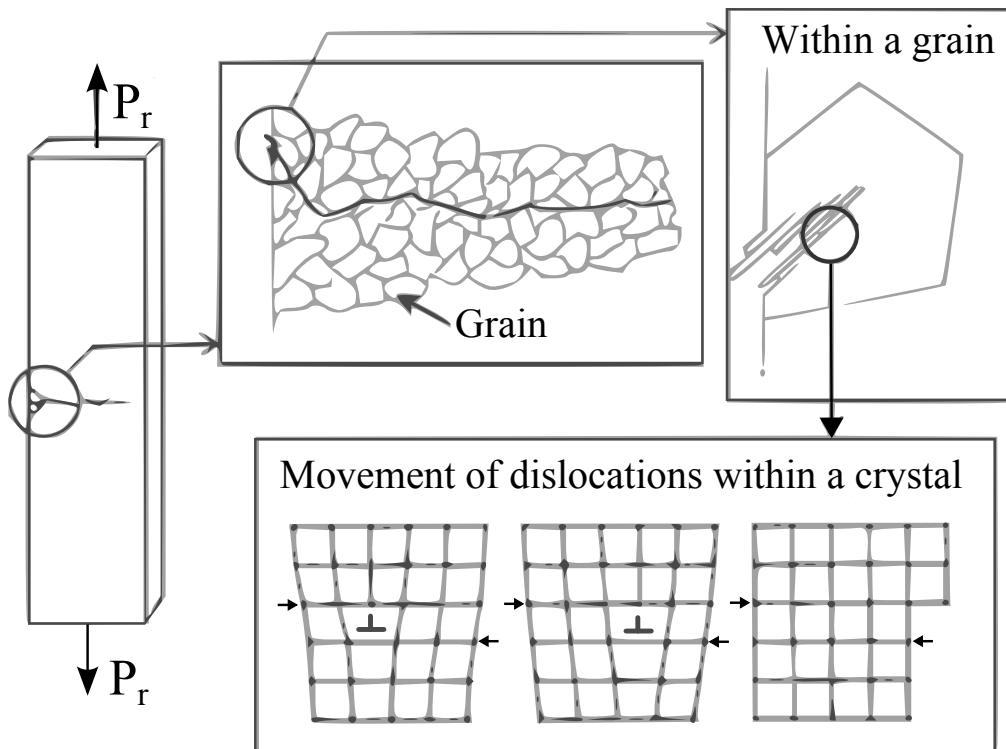
Firstly, metallic alloys are made of grains which are formed by crystals. Within a crystal there might be small line defects that can shift by shear driven forces. These defects which act as very small scale inhomogeneity in the material are called dislocations. Under cyclic loading, dislocations can move and stack up forming a slip band, see Figure 2.5.

Secondly, the stresses that trigger fatigue are often well below the material yield stress limit. Hence, large scale plastic deformations would not occur at such low stress levels and plastic deformations are confined to small areas in the material. Since the material is only available at one side of the free surfaces, grains are less restrained to slip and plastic deformations occur there. Furthermore, the presence of material defects such as pores, inclusions or other sources of inhomogeneity at the surface may also exacerbate the surface condition.

As it was mentioned before, formation of slip bands require shear forces. However, the shear stresses are not distributed evenly between grains, on a microscopic scale. On the one hand, based on each grain size, shape and atomic properties, shear stresses differ at the crystallographic planes. Furthermore, slip bands tend to form along planes that dislocations can move more easily. Eventually, a slip will happen in a grain, see Figure 2.6a. Since the slip is shear driven, it will occur in planes that are oriented  $45^\circ$  to the tensile stress direction.

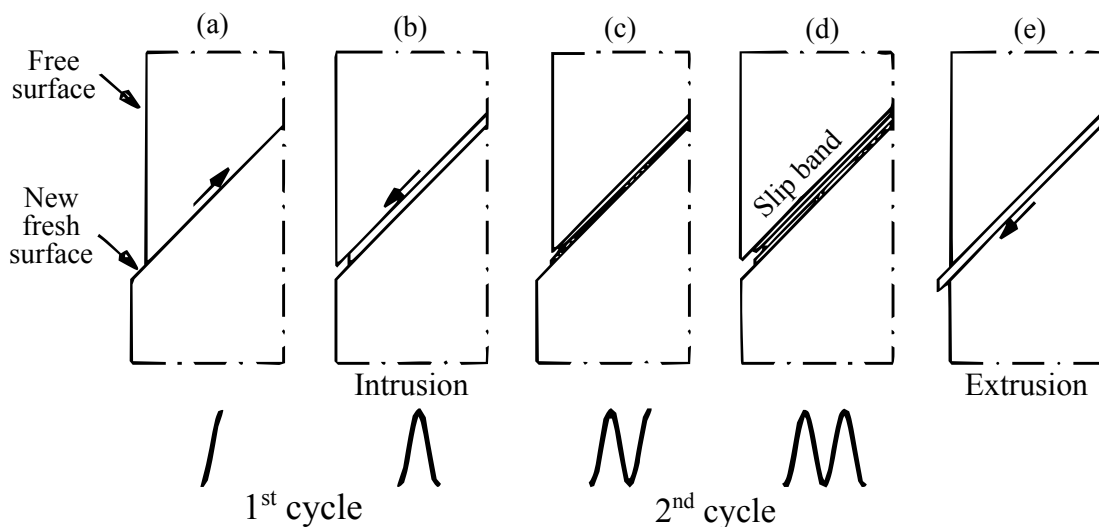
---

<sup>1</sup>Fatigue limit is the stress level in which fatigue cracking doesn't occur if applied stress is below that. More information regarding fatigue limit can be found in section 2.5



**Figure 2.5:** *The process of fatigue and movement of dislocations*

Once a slip happened, a new fresh material will be exposed to the surrounding environment, which is in most cases, air. This new fresh layer will instantly react with the surrounding air and an oxide layer will cover it. The new oxide layer will be bound to the material surface strongly and would not be removed easily. Additionally, upon formation of the slip band, while the load is increasing, strain hardening occurs in the slip band. This indicates that the process of slip band formation is irreversible. The next slip happens during the unloading, while shear



**Figure 2.6:** *Crack initiation as a result of cyclic slip, after [14]*

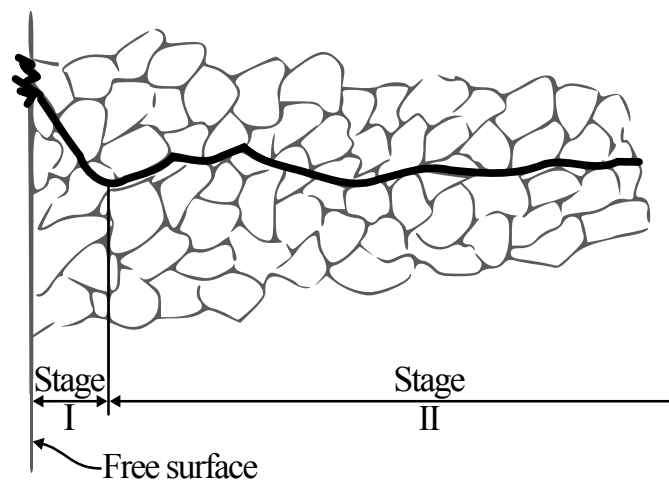
forces are in the reversed direction. The slip, as a consequence, is prone to occur at the same band, but since the presence of irreversible deformations and oxide layer makes it impossible, it will happen at adjacent parallel planes. This process forms an intrusion as it is shown in Figure 2.6b. The same sequence may happen for the other load cycles, see Figure 2.6c and d. It should be noted that the process leading to the intrusion would conversely lead to an extrusion if the slip happen on the lower side of the slip band, Figure 2.6d.

The formed microcrack, grows over a few grains and deviates the uniform stress distribution on a micro level with the stress concentration being at its tip. On the other hand, as the cyclic loading continues, more microcracks will be formed. At some point, these microcracks will coalesce and form one or more dominant cracks. Afterwards, the crack growth direction deviates and becomes perpendicular to the maximum principal stress direction. This is the beginning of the propagation phase of the crack growth. However, crack growth is still dependent on the material crystallographic planes and grows in a zigzag path, see Figure 2.7.

Nevertheless, it should be noted that, as crack initiation and propagation phases are different in nature, the percentage of fatigue life for each phase is variant for different materials and specimens. For instance, experiments have shown that a notched specimen can be considered as a cracked specimen. Therefore, the initiation phase does not take a great portion of the final fatigue life, i.e. about 10% of  $N_t$ , whereas for a plain machined specimen, the initiation phase takes up to 90% of the total fatigue life.

From what has been explained above, the following can be concluded:

- In the initiation phase, the fatigue process depends on the material surface characteristics.
- In the crack growth phase, fatigue is no longer a surface phenomenon.

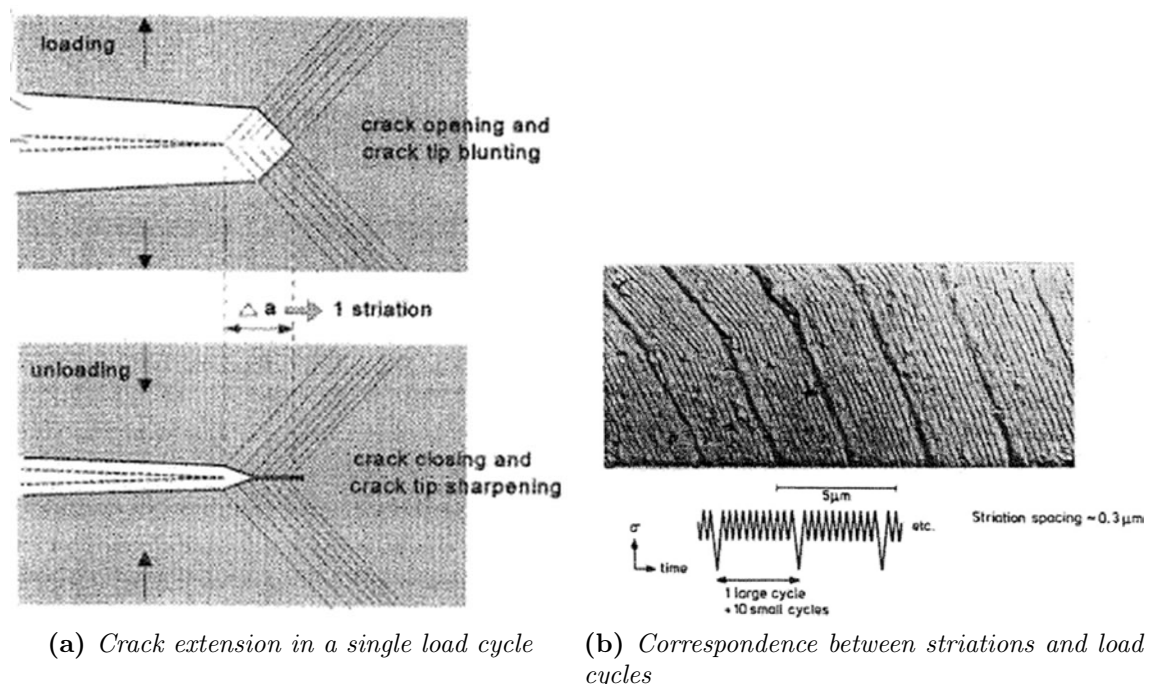


**Figure 2.7:** *Fatigue crack pattern*

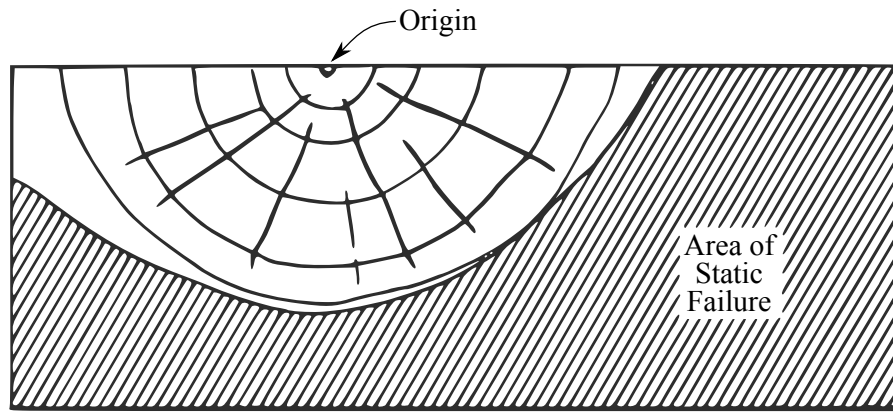
Analogous to the fatigue crack initiation and growth phases that are particular in some aspects, fatigue fracture surfaces have also several characteristic features. These special features make fatigue failures distinguishable from the other failure types such as static failures. These characteristics can be found both in microscopic and macroscopic scale.

A fatigue fracture surface, generally has a very smooth region in the vicinity of crack origin. As the crack slowly propagates, fracture surfaces very close to the crack nuclei rub together for a high number of cycles and create an incredibly smooth and silky surface. The texture becomes rougher as getting further away from the crack origin. The aforementioned microscopic characteristics of fatigue exist in this region.

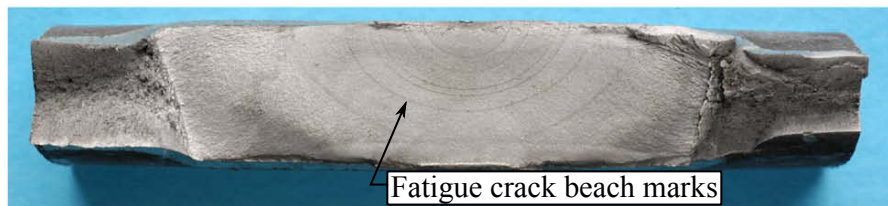
Striations are one of the unique microscopic characteristics of fatigue failures. They are a product of cyclic loading of the material and plastic deformations at the small zone close to the crack tip, Figure 2.8. It was observed before, that after a crack is initiated, a stress concentration will be formed at the tip of the crack. Because of the mechanisms of crack growth at this stage, the stress at this concentration point is the maximum shear stress. The shear stress causes the crack to slip during each cycle accompanied by strain hardening. During the loading sequence, crack will open and extend through the grain, leaving a ridge as a result of microplastic deformation at the upper end, Figure 2.8a. On the other hand, unloading compels the crack to close and leaves a ridge at the lower end in a similar way. These ridges are known as *Striations* and are often visible with electron microscopes.



**Figure 2.8:** Formation of striations during microcrack growth, after [14]



(a) Representation of a typical fatigue fracture surface



(b) Formation of beach marks

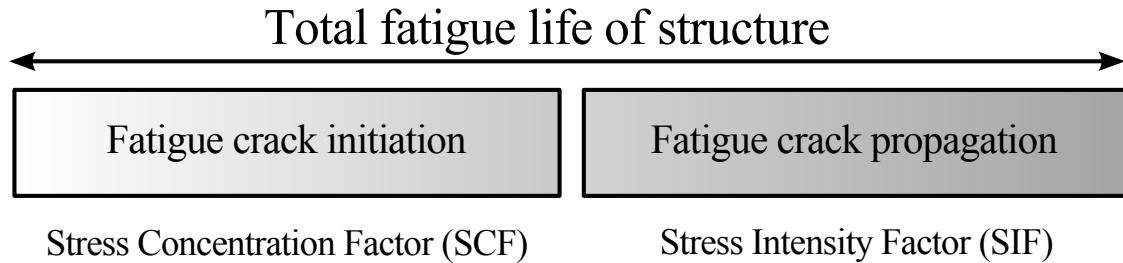
**Figure 2.9:** Macroscopic characteristics of fatigue fracture surfaces, after [15]

As a side note, fatigue cracks prefer to grow through the grain rather than the grain boundaries. This phenomenon is known as *Transgranular crack growth*. Since the slip restraint is minimum inside the grains, transgranular crack growth is consistent with the cyclic slip as the crack growth motivating factor. The zigzag pattern of crack growth is a good supporting evidence for this trend.

Formation of growth bands is also another characteristic of fatigue failures. Growth bands are concentric rings around the crack origin, and are recognizable with different colors. Higher applied stresses, cause darker bands on the fracture surface. These bands which are also called beach marks are visible with naked eye, Figure 2.9b. The presence of beach marks on a fracture surface can be helpful to determine the crack origin and propagation rate.

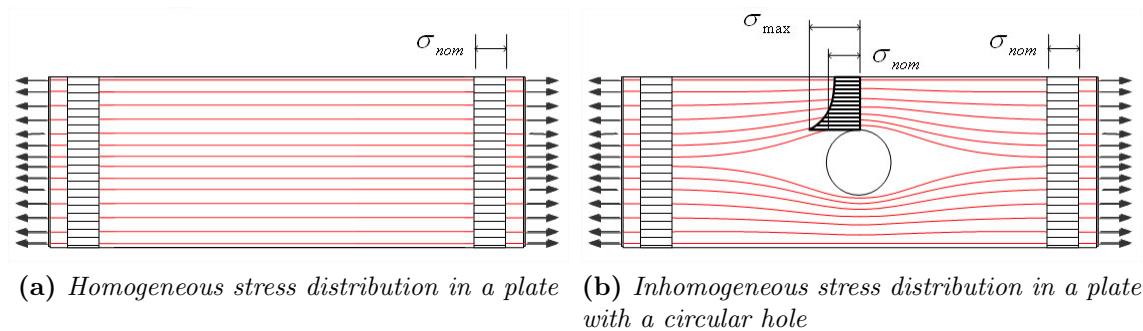
## 2.4 Fatigue from a fracture mechanics point of view

It was discussed in the previous section that fatigue life of a structure is consisted of two stages; Crack initiation and crack propagation. However, these two stages are different in nature and therefore, a quantitative representation of them should also obey different parameters, Figure 2.10.



**Figure 2.10:** *different stages of fatigue life and their relevant factors*

Assume a plate which is subjected to uniaxial tension. The stresses are uniformly distributed throughout the cross section of the plate as long as there is no local changes in the plate dimensions. This uniform stress is called the *nominal stress* ( $\sigma_{nom}$ ). Conversely, any small changes in the cross section such as notches, holes or fillets cause the stress to change rapidly in the vicinity of the inhomogeneity. This abrupt change in the nominal stress is called *stress concentration*. For example, consider a circular hole in the middle of the discussed plate. The hole will deviate the uniformly distributed stress in the area close to it, so that the material around the hole would undergo different stresses as shown in Figure 2.11. It can



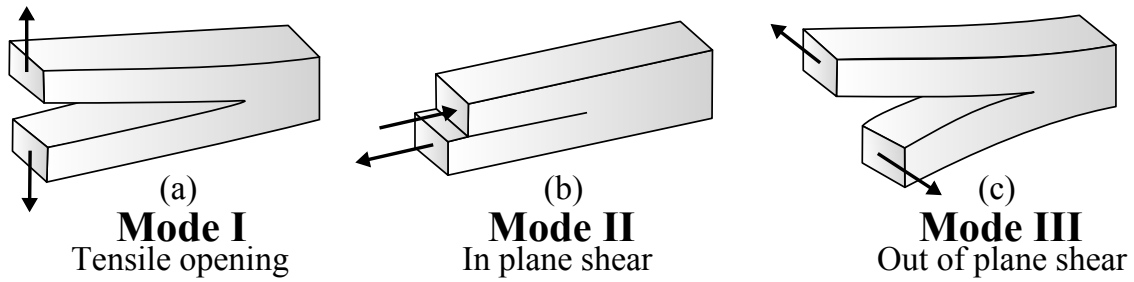
**Figure 2.11:** *Stress distribution in a large plate subjected to uniaxial tension*

be shown that for a linearly elastic material the maximum stress ( $\sigma_{max}$ ) for the specimen shown in Figure 2.11b can be as high as three times more than nominal stress. However, generally the relation between maximum stress and nominal stress can be written as:

$$\sigma_{max} = K_t \cdot \sigma_{nom} \quad (2.1)$$

Where  $K_t$  is called *stress concentration factor (SCF)*. According to Schijve [14], the geometry of the structure is the only parameter that affects the stress concentration factor. SCF indicates the severity of the stress concentration and hence it can be





**Figure 2.12:** *Different modes of loading a crack*

used to predict the fatigue crack initiation. Having said that a good fatigue resistant structure is one with less critical stress concentration points, this parameter becomes a crucial design factor for the structures that are prone to fatigue loading.

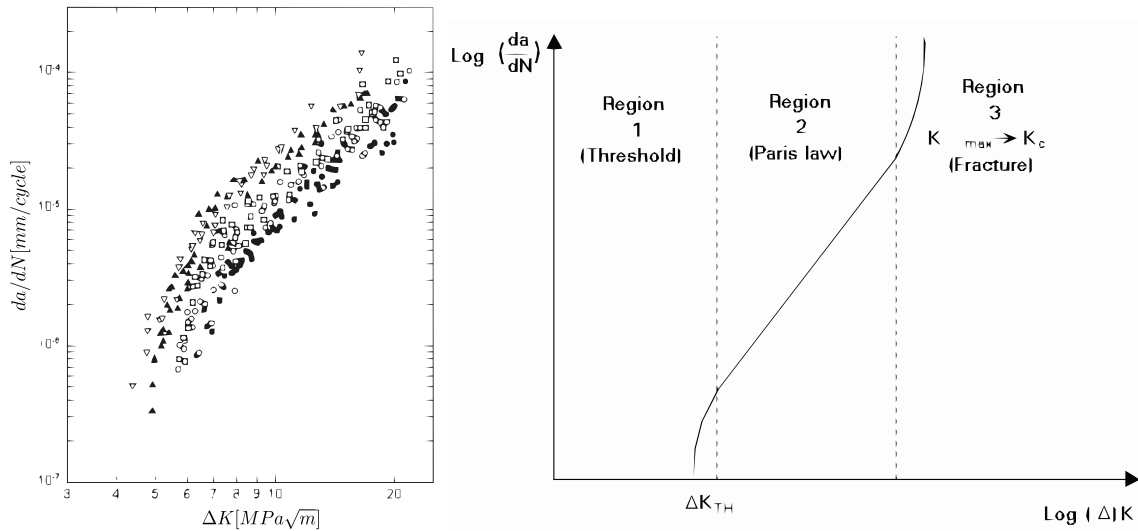
It should be noted that, once a crack initiated,  $K_t$  will approach infinity at its tip and becomes an inappropriate parameter. Thus, a new factor should be used to describe the stress severity at a sharp crack tip. This parameter that gives rise to the magnitude of the applied stresses at the crack tip, is called the *Stress Intensity Factor (SIF)*. The SIF magnitude depends on the geometrical variations of the loading type as well. These effects are categorized based on the different modes that can grow a crack. As discussed in Section 2.3, fatigue cracks grow perpendicular to the principal stress direction which is in most cases the tensile stress direction. This load case that opens the crack is known as *Mode I*, see Figure 2.12a. As shown in Figure 2.12b and c, other failure modes are also possible. Load cases that propagate a crack by rubbing its surfaces against each other are known as *Mode II* and *Mode III*. However, since the crack is entirely opened in the Mode I, it is the most dangerous mode of failure that gives the highest rise to the stress intensity factor. Furthermore, Mode I is the most common load type in engineering components.

The stress intensity factor,  $K_I$ , in its simplest way can be expressed as:

$$K_I = \sigma_{nom} \sqrt{\pi a} \cdot f \quad (2.2)$$

where  $a$  is the crack length and  $f$  is a function of geometry and loading of the detail. Function  $f$  can either be calculated by finite element analysis or taken from handbooks and literature for different load cases and geometries. It should be noted that the stress intensity factor for a crack and stress concentration factor for a notch are not similar concepts. SIF is a function of loading type and geometry of the detail and has the unit  $MPa\sqrt{m}$ , while SCF is a dimensionless parameter that only accounts for geometry of the detail.

The importance of SIF is that, under some circumstances, it is vital for engineers to predict the remaining fatigue life of a cracked structure so that appropriate actions can be taken before it is too late. However, an acceptable and reliable quantitative estimation is only possible with an accurate numerical model. In 1963, Paris and Erdogan [16] proposed that the rate of the crack propagation per cycle may be expressed as a function of the stress intensity factor. It was shown that, plotting the crack growth rate versus the stress intensity factor yields straight lines on a



(a) Test data for a ductile iron sample in the air (b) Different distinguishable regions for a typical fatigue crack propagation behavior

**Figure 2.13:** Typical relation between crack growth rate and the range of stress intensity factor

log-log scale. This general law which is known as the Paris law is expressed in Equation 2.3:

$$\log\left(\frac{da}{dN}\right) = m \log(\Delta K) + \log(C) \quad (2.3)$$

taking out the logs yields:

$$\frac{da}{dN} = C(\Delta K)^m \quad (2.4)$$

where  $(da/dN)$  is the fatigue crack growth rate,  $\Delta K = K_{max} - K_{min}$  is the stress intensity factor range, and  $C$  and  $m$  are material constants. Plotting the experimental work on a logarithmic graph of  $(da/dN)$  against  $\Delta K$ , reveals three regions; threshold region, Paris law region and fracture region, see Figure 2.13.

The region at the bottom left is called the threshold region since the stresses are lower than the minimum required to open the crack. Inversely, at the top right of the graph, the crack growth approaches infinity and is designated as the fracture region. In between these two regions, the Paris law is consistent with the test results and a straight line with the slope  $m$  and position  $C$  can be drawn. Eventually, the Paris law can be integrated in order to calculate the residual lifetime of a structure.

## 2.5 Fatigue terms

In this section, some basic terms regarding fatigue are described. These terms are frequently used in the literature related to fatigue and therefore, understanding them in a good manner is the prerequisite for any further discussion.

### 2.5.1 Fatigue loading

As mentioned before, structures that are subjected to fatigue loading, experience fluctuated loads during their lifetime. Generally, the stress history of such structures varies constantly. However, the simplest stress history that can be assumed for a structure is a *constant amplitude* cyclic stress, as illustrated in Figure 2.14. This type of loading is usually experienced by the specimens tested in the laboratories as it doesn't require advanced testing equipments. A constant amplitude loaded structure, is subjected to a maximum stress ( $\sigma_{max}$ ) and a minimum stress ( $\sigma_{min}$ ). Thus, the stress range and the mean stress can be expressed as:

$$\Delta\sigma = \sigma_{max} - \sigma_{min} \quad (2.5)$$

$$\sigma_{mean} = \frac{\sigma_{max} + \sigma_{min}}{2} \quad (2.6)$$

Stress amplitude ( $\sigma_a$ ) is defined as half of the stress range, and hence it can be calculated as follows:

$$\sigma_a = \frac{\sigma_{max} - \sigma_{min}}{2} \quad (2.7)$$

Stress ratio, which implicitly represents the loading type, is defined as the ratio of the minimum to maximum stress:

$$R = \frac{\sigma_{min}}{\sigma_{max}} \quad (2.8)$$

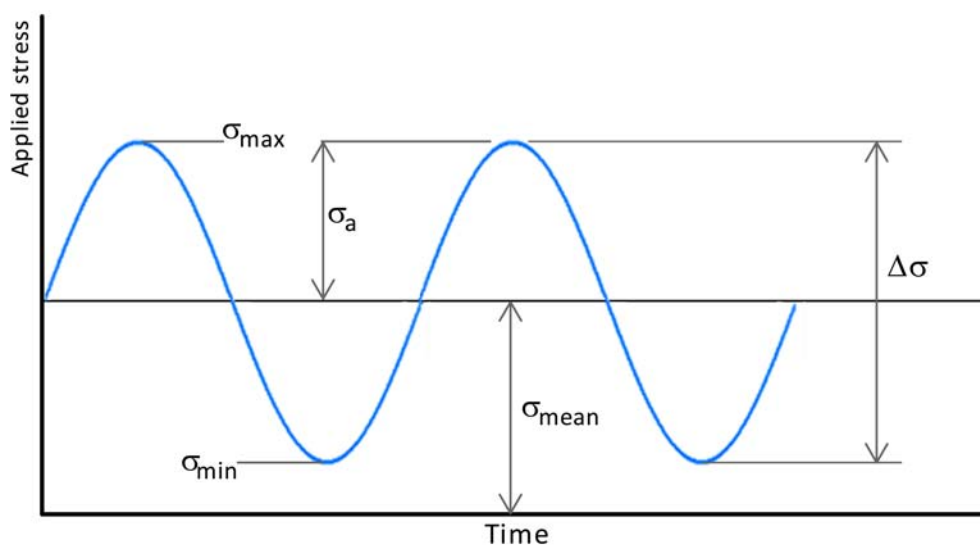
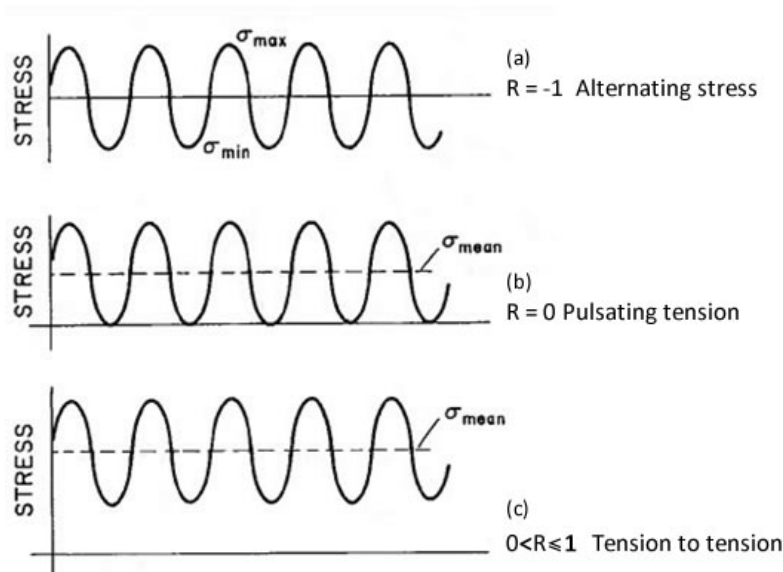


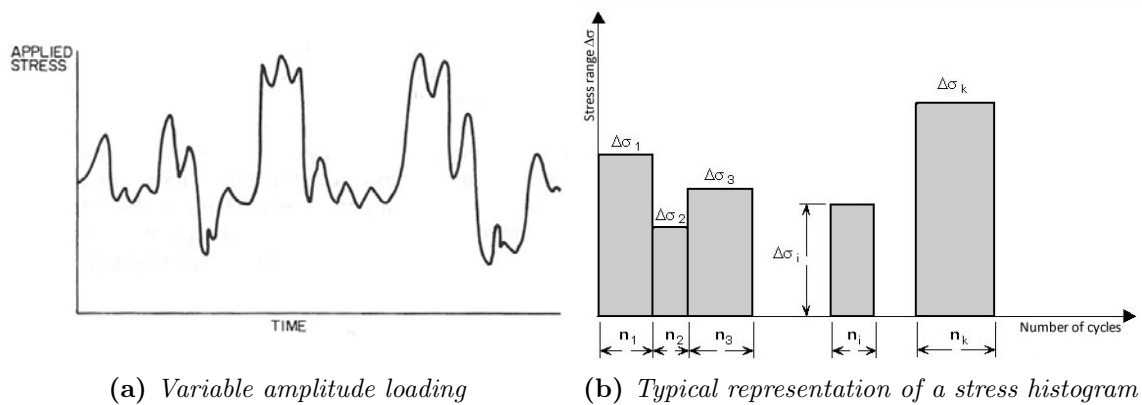
Figure 2.14: Constant amplitude loading



**Figure 2.15:** *Different stress ratios for various loadings*

Therefore, as it is shown in Figure 2.15,  $R = -1$  is followed by reversing the stress state from a compressive stress to an equal tensile stress, while  $0 \leq R \leq 1$  corresponds to any fluctuation of stress from a minimum tensile to a maximum tensile load.

In general, the fatigue life of a specimen depends mainly on the stress range ( $\Delta\sigma$ ) so that a higher stress range would result in a lower fatigue life. Nevertheless, the constant amplitude loading is not a realistic loading pattern for real structures such as bridges, buildings or offshore platforms. The mentioned structures experience random sequence load histories through their life time. This loading pattern is called *variable amplitude loading* and cannot be represented by an analytical model. Figure 2.16a shows an example of a variable amplitude loading which may



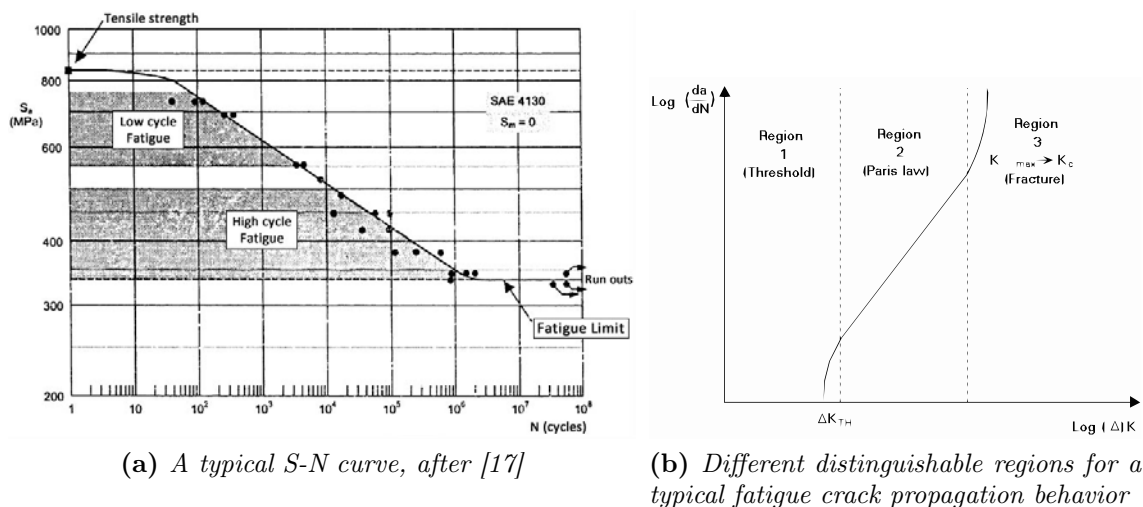
**Figure 2.16:** *An example of variable amplitude loading and stress histogram as a simplification method of variable amplitude loaded structures*

be experienced by a structure. For such loadings, a *stress histogram* is usually used to simplify the problem. A stress histogram is a chart of separate blocks that defines the number of cycles that a constant stress range is repeated during the life time of the structure, see Figure 2.16b.

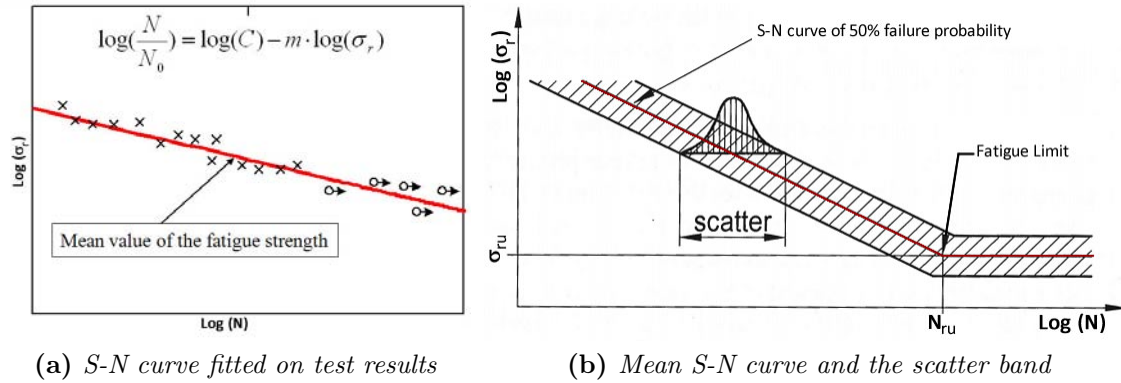
## 2.5.2 S-N curves

As mentioned before, the stress range has the most influence on the fatigue life of a specimen. Accordingly, the most important outcome of fatigue tests is the fatigue life of the specimen in terms of number of cycles ( $n_i$ ) at different stress ranges. A common way to represent these results is the so called S-N curve, also known as Wöhler diagram. Usually, plotting the test results of a specified specimen on a log-log graph with the stress ranges on the vertical axis and the number of cycles to failure on the horizontal axis, would result a large scatter. However, in most cases, it is possible to get a regression line of the test data by running a statistical analysis of the results. The obtained line on the mentioned graph is called a S-N curve for a specified specimen, see Figure 2.17a. Moreover, as it is depicted in Figure 2.17, by rotating the S-N curve 90° clockwise, it becomes analogous to the fatigue crack propagation curves. Therefore, the top left corner of S-N curve is the region in which the applied stress range is so high that plastic deformations occur momentarily. This region is known as *low cycle fatigue* where the fatigue failure usually happens very fast. On the other hand, the bottom right corner represents the region in which the stress is so low that the specimen can be loaded for an infinite number of cycles without any fatigue damage. This stress range is called *fatigue limit*.

Similar to the Paris law region in a crack propagation graph which follows a straight line on a log-log scale, the region between low cycle fatigue and fatigue limit can



**Figure 2.17:** Analogy of S-N curves and fatigue crack propagation regions



**Figure 2.18:** Fatigue S-N curves

be expressed by a linear equation as follows:

$$\log\left(\frac{N}{N_0}\right) = \log(C) - m \log(\sigma_r) \quad (2.9)$$

taking out the logs results:

$$N = N_0 \cdot \left(\frac{C}{\sigma_r}\right)^m \quad (2.10)$$

where  $N$  represents the fatigue life,  $\sigma_r$  is the stress range and  $C$  and  $N_0$  are fatigue strength constants.  $m$  is a material constant and for typical steel welded joints is around 3.

Figure 2.18a demonstrates a typical S-N curve fitted to the test results. As it is mentioned in the figure, this line is the mean value of the fatigue test data. However, for the design purposes, an acceptable safety margin should be provided. This requirement can be satisfied as follows:

- A sufficient number of tests should be carried out at each stress range to ensure the validity of statistical evaluation of the results.
- The design S-N curve should be driven by considering the standard deviation of the test results.

## 2.6 Fatigue of welded structures

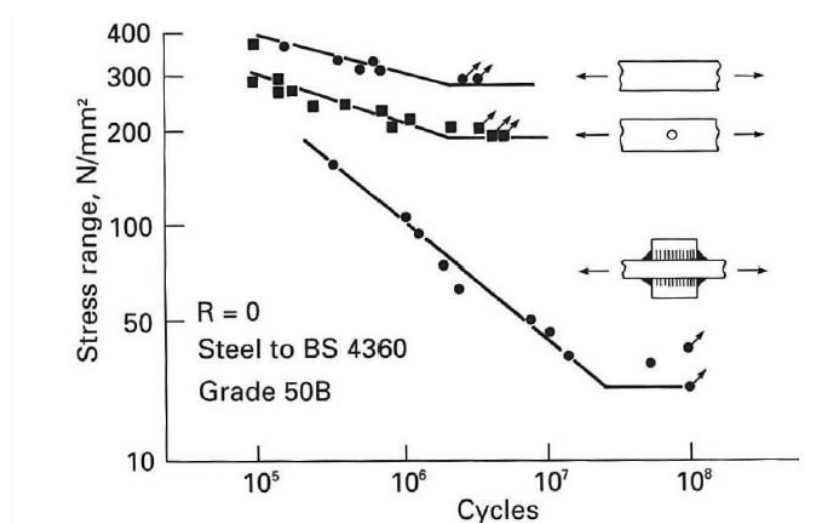
Welding is of great interest of engineers, since it offers great flexibility to design details and components that couldn't be made by any other means. This special feature of welding has made it one of the most common ways of production of large structures such as bridges, offshore platforms and crane girders. However, various issues are related to welding as a production technique. Welding induces stress concentration points as a result of inhomogeneities. Several defects are also attributed to the welding. These known problems as well as other effects of welding, has made it an important subject that an extensive number of literature, codes and standards have been created for.

Tests that have been conducted on both welded and not welded details have shown that there is a significant drop in terms of fatigue life for welded details. As can be seen in Figure 2.19, although the fatigue strength of a hole notched plate is lower than a plain plate, yet a plate with welded longitudinal gusset attachment exhibits an almost 8 times lower fatigue strength. In this section, the reasons for such poor fatigue behavior of welded details are discussed in more details.

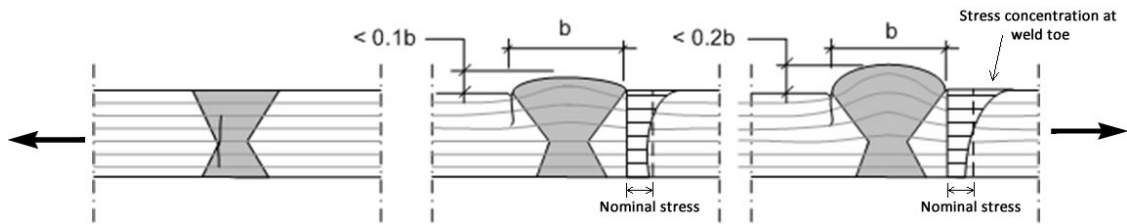
### 2.6.1 Weld shape effects

By welding a plate, inhomogeneities are also being introduced. These inhomogeneities might cause an abrupt change in the stress distribution. As a result, a weld profile can be a potential site of high stress concentrations.

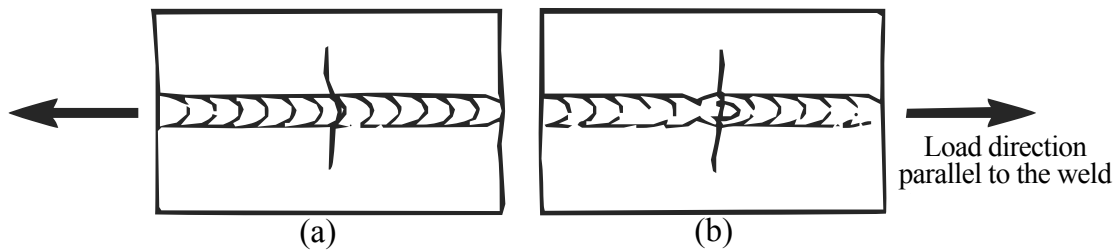
Generally, the stress concentration caused by a stress raiser depends on the orientation of the stress raiser in relation to the direction of the applied load. The maximum stress concentration is expected when the plane of the stress raiser becomes perpendicular to the direction of the tensile stresses. Conversely, as the



**Figure 2.19:** Comparison between fatigue strengths of plain steel plate, hole notched plate and plate with fillet welded attachments, after [4]



**Figure 2.20:** *Stress concentration at the weld toe*



**Figure 2.21:** *Fatigue cracking of continuous welds loaded parallel to weld from: (a) Weld ripples; (b) Stop-start positions.*

stress raiser plane becomes parallel to the applied tensile load direction, the stress concentration factor approaches zero. Hence, if a plate is loaded transverse to the weld, the stress concentration happens at the intersection of plate surface and weld metal, i.e, weld toe. The stress concentration would be lower if the transition between plate and weld is more smooth, Figure 2.20.

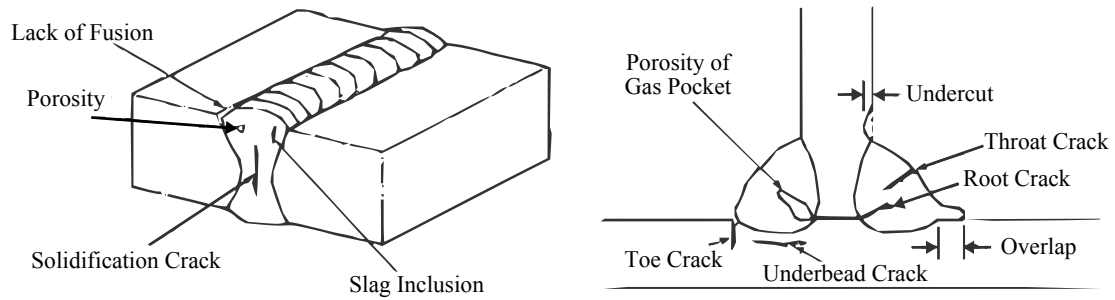
On the other hand, stress raisers also exist for a continuous weld that is loaded parallel to the weld direction. In this case, surface irregularities such as, ripples or weld stop-start positions are the most likely places for stress concentration and consequently cracks to occur, Figure 2.21. Nevertheless, these points are less severe than those of transversely loaded details and a higher fatigue strength is expectable in this case.

## 2.6.2 Weld defects

According to Maddox [4], the stress analysis has shown that the stress concentration factor for a transversely loaded fillet weld is about the same as the edge of a hole. This fact is not consistent with the test results shown in Figure 2.19, where the welded attachment has a significantly lower fatigue strength compared to the detail with the hole. This contrast arises from the fact that weld defects can be present at a weld profile. Figure 2.22 depicts the most common defects and cracks in welded details.

Despite the numerous attempts that have been made to reduce the amount of weld defects, it is inevitable to prevent them. Improper design, inaccessibility of welding location and lack of skilled welders are some of the reasons that can lead to weld defects. Automated welding process has been developed to specifically eliminate





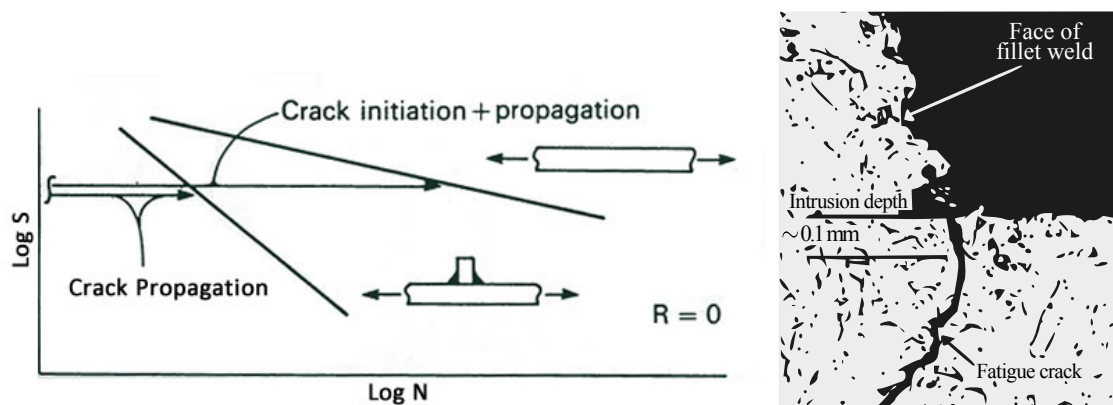
**Figure 2.22:** *The most common defects and cracks in welded details, after [18]*

the human errors.

Overlaps and lack of penetration and fusion, are among the defects that correspond to pre-existing cracks. This implies that, the crack initiation stage for welded details occupies only a very small portion of the total fatigue life. Therefore, the number of cycles to initiate a crack in a welded joint is remarkably reduced. This fact is shown schematically in Figure 2.23 for an as-rolled plate and a plate with fillet welded attachment.

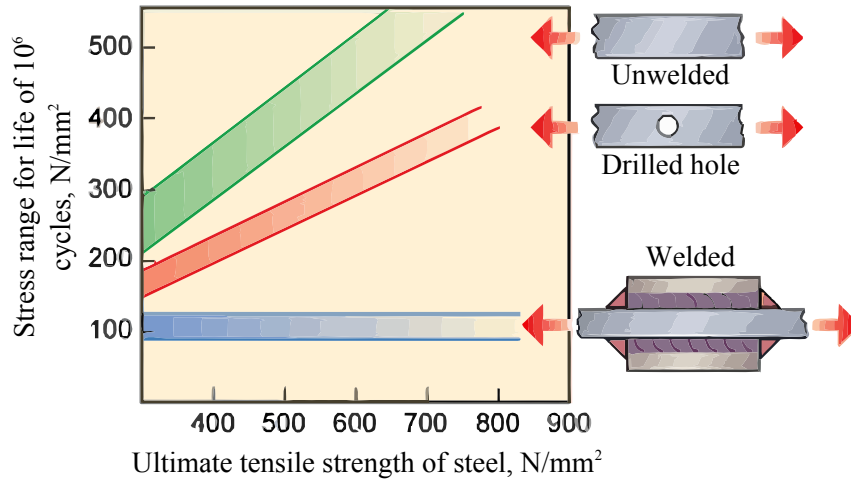
Lack of penetration can cause severe stress concentration in weld roots under repeated loading. As a result, cracks may start to propagate from the root of the weld rather than the weld toe. Due to the fact that the root cracks can be invisible for a long time and consequently develop over a considerable area, they are often regarded as the most serious fatigue cracks. Porosities and Slag inclusions can also be serious defects for the fatigue crack initiation.

Furthermore, undercuts may also be a severe stress concentration point since they introduce a sharp change in the stress distribution at the weld toe. Nevertheless, as discussed in Section 2.6.1, the excessive weld material can also introduce stress



(a) *Fatigue strength representation for a plain plate and welded joint, after [4]* (b) *Weld toe intrusions as a pre-existing fatigue crack*

**Figure 2.23**



**Figure 2.24:** *The benefits of increasing the ultimate tensile strength of steel on different details*

concentration at the weld toe even if an undercut is not present. Additionally, the welding process is capable of leaving small scale crack-like discontinuities at the weld toe. This destructive feature of welding makes the weld toe condition even more severe. Microscopic pictures have shown the existence of these discontinuities, also known as *intrusions*, at the weld toe, see Figure 2.23b. The existence of intrusions exempts the material from taking more number of load cycles for the crack initiation. These findings clearly confirm that the fatigue life of a welded detail is only consisted of the crack propagation phase.

As it was discussed in Section 2.3, crack initiation in a material is a surface phenomenon, whereas, crack propagation depends only on the bulk properties of the material. In other words, by increasing the strength of a material, more number of cycles is required for a crack to initiate, whereas, the crack propagation rate in the material is not influenced. Hence, the fact that fatigue life of welded details is only consisted of propagation phase also implies that, very little or no benefit in fatigue strength of welded details would be accomplished by increasing the strength of the material. Figure 2.24 demonstrates that by increasing the ultimate limit strength of steel in a plain plate, the fatigue strength improves correspondingly while, it has very little effect on the welded detail.

### 2.6.3 Residual stresses

Welding of a material is often associated with stresses that are locked into the welded detail. These stresses form during the cooling period of the deposited molten weld metal. When the weld is cooling down to the room temperature, it shrinks. The shrinking procedure does not occur freely since the weld is restrained by the adjacent colder parent material. The implication of the contraction between the weld metal and the parent plates is that residual stresses would be introduced in both the longitudinal and transverse direction as shown in Figure 2.25. These stresses are both tensile and compressive which are balanced in order to maintain equilibrium at the section.

The actual residual stresses can be measured using a variety of methods, both destructive and nondestructive. Besides, parametric studies and tests have also shown that the magnitude of residual stresses depends on several factors such as tensile strength, joint type and size, and also run size and sequence. However, in the absence of test results, the magnitude of residual stresses is often taken as the maximum tensile yield strength.

The presence of such high tensile residual stresses implies that, on the one hand, fatigue failures can happen under nominally compressive loading conditions, and on the other hand, the fatigue strength of the detail depends only on the stress range irrespective of the applied stress ratio, as illustrated in Figure 2.26.

Therefore, it can be seen that tensile residual stresses can be very harmful so that a fatigue crack could initiate under a compressive applied load. However, these cracks will grow only in the tensile residual stresses region. As the cracks propagate, they cause the stresses to redistribute and some of the tensile residual stresses may relieve as a consequence. As soon as reaching the compressive residual stress zone, the cracks stop propagating further.

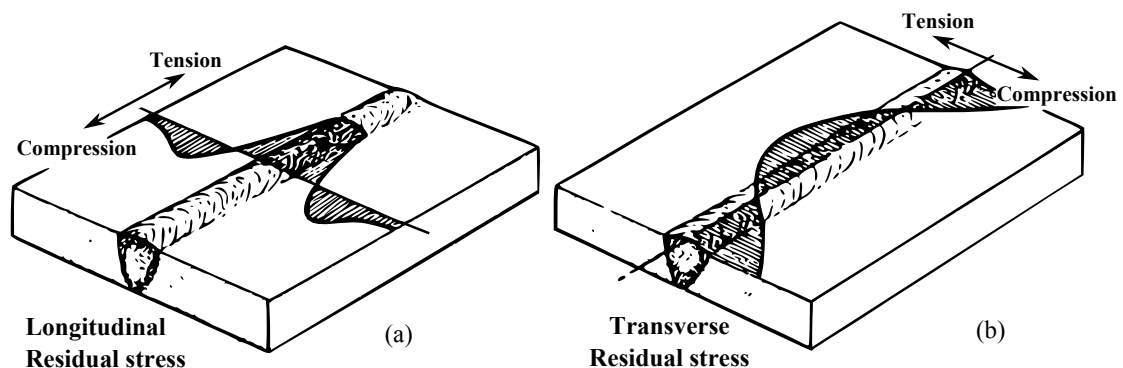


Figure 2.25: Residual stress distribution as a result of welding

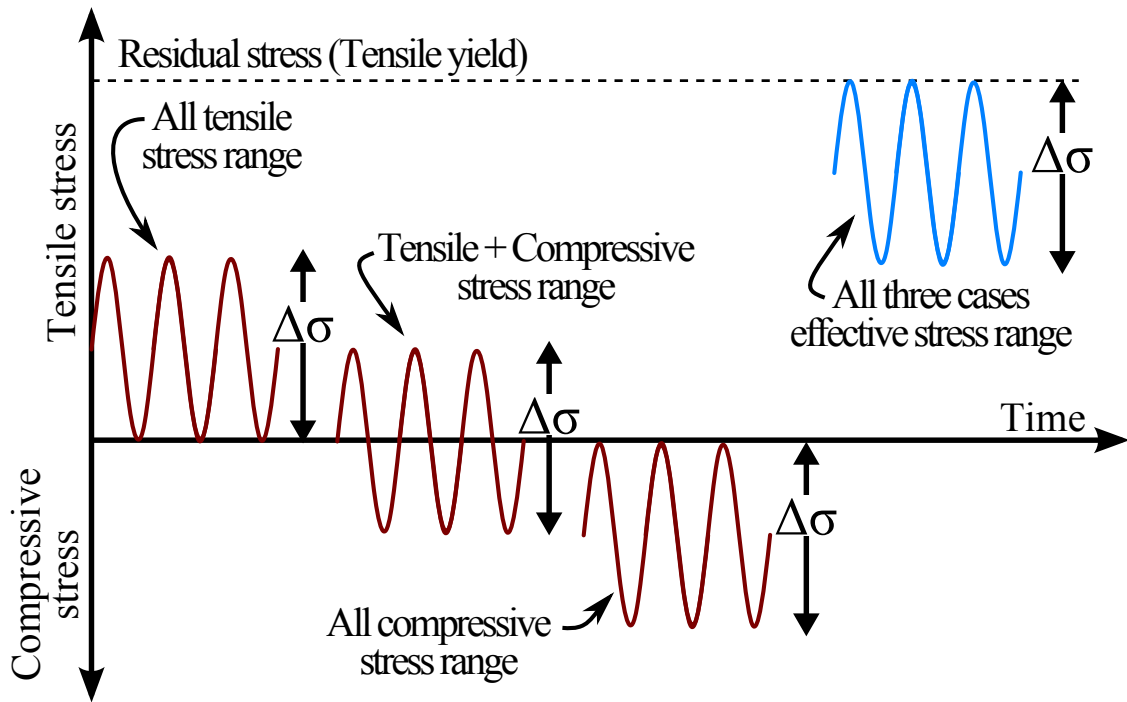


Figure 2.26: *Effect of residual stresses on the stress range*

### 3 Fatigue assessment methods

Any comparison between loads, stresses or strains with their critical values is designated as strength assessment as these values are known to cause a definite deformation, a characterized damage, an incipient crack or total fracture. Similar to the loads that can be composed of moments and forces, stresses and strains can be of different types depending on the extent that the local effects are considered. On the one hand, the stresses and strains are calculated from the loads, generally by means of elasticity and plasticity theory. On the other hand, the critical values are obtained by carrying out various tests. For fatigue strength assessment, the prevalent testing method is to perform the tests at a specified stress range to obtain the fatigue life of the specimen.

Depending on the exploited stress parameters, the strength assessment methods can be divided into two categories:

- Global approaches
- Local approaches

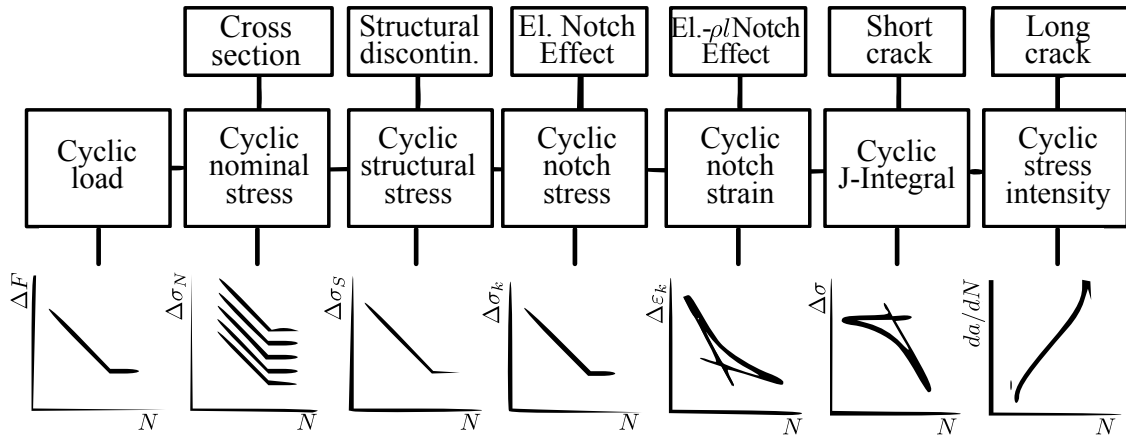
The strength assessments that are derived directly from external loads (forces and moments) or from uniformly distributed stresses at the critical cross section, are described as *global approaches*. The latter stress type which is proceeded by the use of linear elasticity theories, such as Euler-Bernoulli beam theory, is called *nominal stress*. In global approaches, the occurrence of a global phenomena, such as total fracture of the specimen is corresponding to the critical nominal stresses or loads.

The strength assessments that are derived from stresses or strains in the vicinity of the crack initiation location (usually weld toe or weld root) are described as *local approaches*. The local stresses or strains can be obtained from lab measurements or numerical modelings such as FE<sup>2</sup> analysis. In local approaches, the local fatigue damages such as crack initiation, crack propagation and final fracture can be considered.

Several methods have been proposed and elaborated for local analysis of welded structures. Notch stress, notch strain and linear elastic fracture mechanics approaches are examples of local approaches that cover different fatigue damage phases on a local scale. Due to the fact that in welded joints, fatigue cracks generally initiate at the weld toe or weld root, the knowledge of exact weld geometry is the perquisite to a precise strength assessment using the mentioned methods. Weld profile, on the other hand, usually do not imitate a uniform shape along its length. As a result, extra effort has to be employed in order to obtain accurate results according to the local approaches. A method which only accounts for the structure geometry and excludes stress increase due to the weld geometry would consequently require less effort. This method that lies between global and local

---

<sup>2</sup>Finite Element



**Figure 3.1:** Variations of global and local approaches for fatigue strength assessment, after [19]

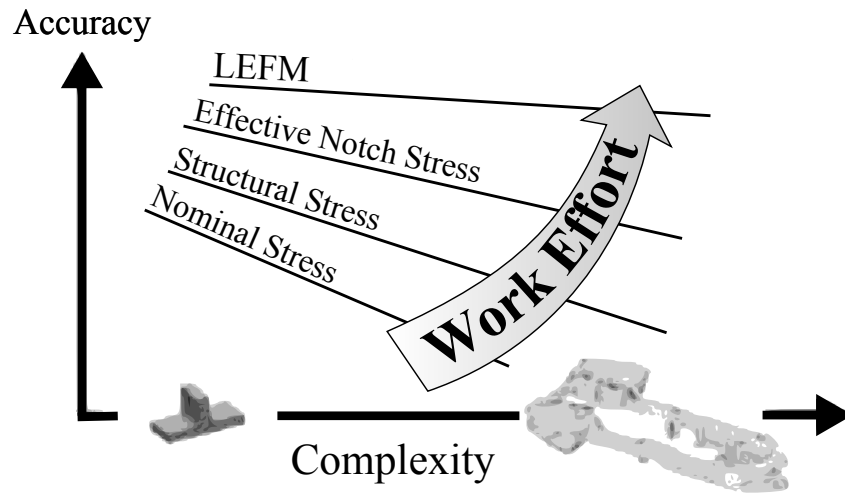
approaches is designated as *Structural stress approach*.

Base upon the stress or strain parameters and the acquainted failure criteria, distinct variations of global and local approaches can be classified as shown in Figure 3.1.

According to [3], fatigue analysis approaches, generally, can be divided into the following categories:

- Nominal stress approach: uses the nominal stress range,  $\Delta\sigma_n$ , which is calculated by the external or internal loads at the relevant cross section according to the elementary theories of structural mechanics.
- Structural or hot-spot stress approach: uses the structural stress range,  $\Delta\sigma_s$ , at the weld toe to account for the stress raise due to the inhomogeneities introduced by changes in the structure's geometry.
- Notch stress and notch intensity approach: uses the elastic notch stress range,  $\Delta\sigma_k$ , or notch intensity factor to consider the stress increase due to both geometry change and notch effect, at the weld toe or weld root.
- Notch strain approach: uses the local elastic-plastic strain range,  $\Delta\varepsilon_k$ , in order to distinguish the relevant fatigue damage process in the material.
- Crack propagation approach: uses special crack growth parameters, such as J-integral or stress intensity range,  $\Delta K$ , to anticipate the crack growth rate,  $da/dN$ , according to the linear elastic fracture mechanics (LEFM), assuming an incipient crack.

Several researchers have done qualitative comparisons in terms of accuracy and work effort of the mentioned approaches. According to [20], [21] and [22], the more time consuming methods, such as the notch stress and LEFM approaches, exhibited better agreement with experimental results than the nominal and structural stress



**Figure 3.2:** *Work effort and accuracy comparison of the different fatigue assessment approaches, after [22]*

methods. If the residual stresses are known, the two former methods, have the capability to determine whether the fatigue crack initiates at the weld toe or weld root. The effective notch stress is the only local approach for root cracking since weld root is embedded and measurements are not possible. Figure 3.2 illustrates a summary of the accuracy and work effort comparisons from several design analysis departments.

In the following sections, the mentioned methods are explicitly discussed. The design concepts and recommendations according to IIW<sup>3</sup> and Eurocode are also described.

---

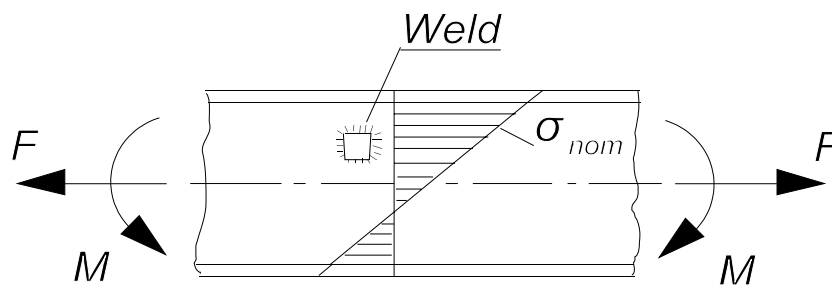
<sup>3</sup>International Institute of Welding

## 3.1 Nominal stress approach

### 3.1.1 Basic concepts

As discussed in the previous section, nominal stress is defined as the stress derived from external loads in the critical cross section in question according to the elementary theories of structural mechanics. The nominal stress excludes any stress raising effect due to welded attachments. Although, the nominal stress can vary as a result of applied loads or macro-geometric changes, the effect of welded attachments, has to be ignored, as it is shown in Figure 3.3. In such a case, the nominal stress can be calculated simply by Navier's equation as follows:

$$\sigma_{nom} = \frac{F}{A} + \frac{M}{I} \cdot z \quad (3.1)$$



**Figure 3.3:** *Nominal stress in a beam-like component* [10]

In some cases where the model is complex or undetermined, finite element modeling can be used to determine the nominal stress magnitude in the desired cross section. Again, care should be given to exclude all the stress raising effects due to the welded attachments. To pursue this goal and find the nominal stress from a finite element model at weld toe, a line should be drawn along a path perpendicular to the toe. This simple rule is on account of the fact that, the abrupt stress gradient in the vicinity of the inhomogeneity (weld toe in this case) becomes zero further away from it, and all that remains is the nominal stress. The implication of this is that the nominal stress at the weld toe can be achieved by extrapolating the stress further away from the toe, inwards. This is shown in Figure 3.4.

### 3.1.2 Design according to the Nominal Stress Approach

The nominal stress is the basis of the classical and most widely used approach for the fatigue assessment of welded joints, i.e. *Nominal stress approach*. The Nominal stress approach has been based upon a huge number of fatigue tests, mainly carried out during 1970s for various welded and not welded joints. The experimental results were used to assign the details to a set of uniform, linearized, parallelized and equally spaced S-N curves corresponding to 97.7% survival probability. As the nominal stress S-N curves are derived from the laboratory tests, they include the



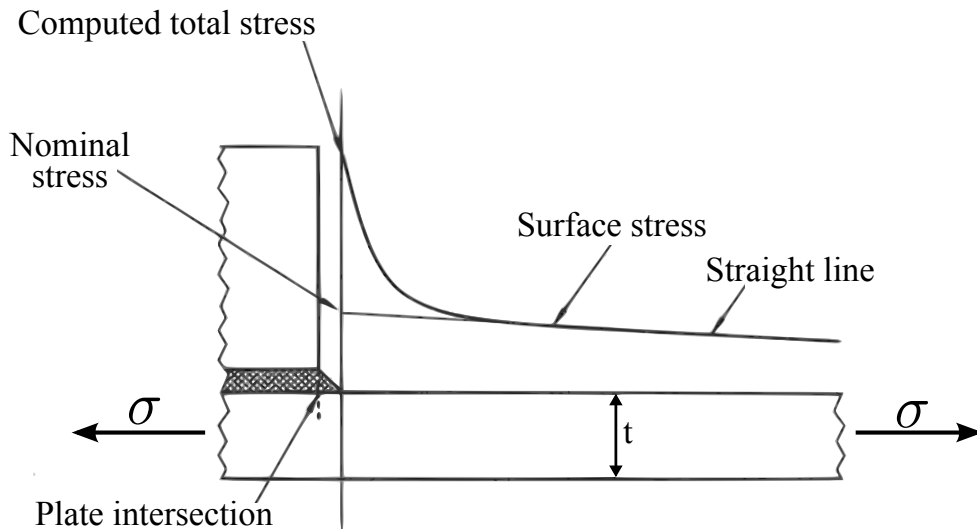


Figure 3.4: Extrapolated nominal stress [23]

effects of geometry, material and weld quality to some extent.

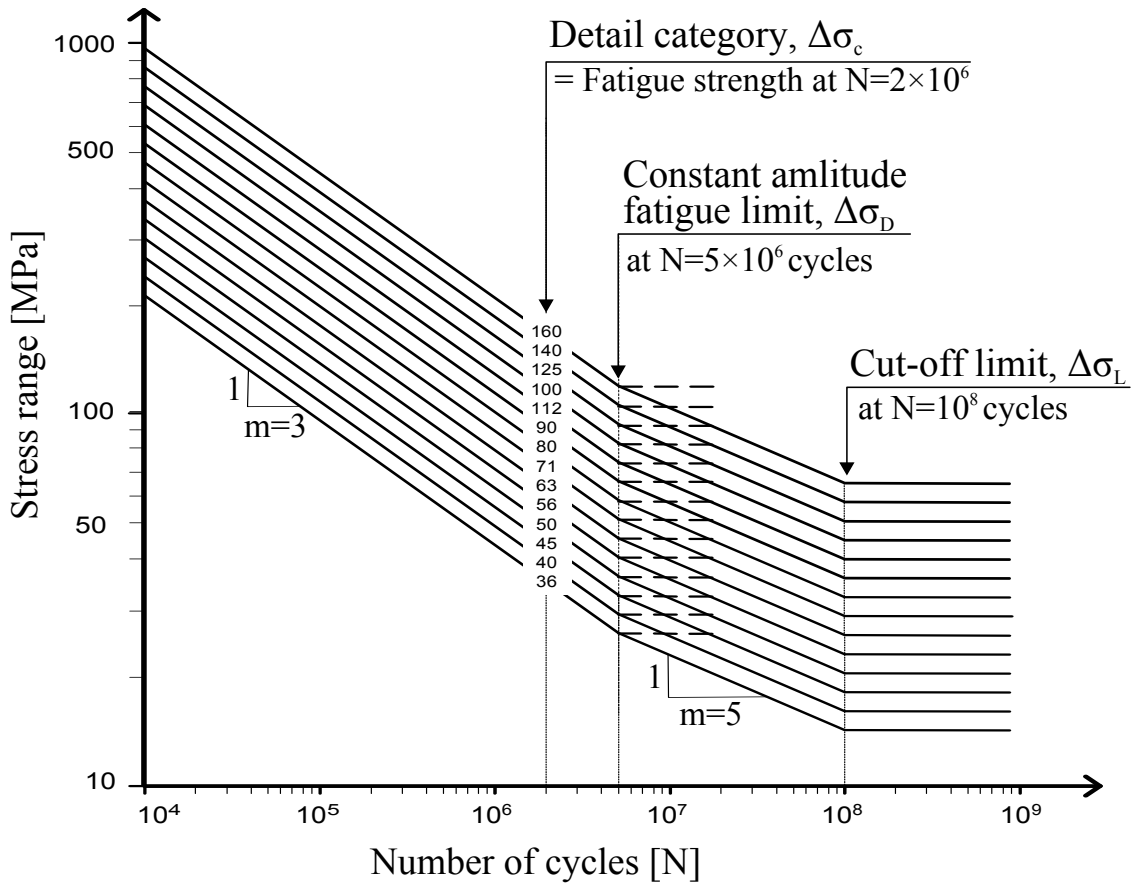
The nominal stress approach is the basic fatigue assessment method of most of the codes and standards, e.g. British standards, German standards, IIW recommendations and Eurocode. The latter two, use a set of 14 nominal stress fatigue strength S-N curves, see Figure 3.5. Each S-N curve is identified by a FAT<sup>4</sup> value which is the characteristic strength at 2 million cycles in MPa.

A change of slope from  $m=3$  to  $m=5$  at 5 million cycles of load application at stress ranges equal to  $\Delta\sigma_D$  is apparent from Figure 3.5. This stress range is known as constant amplitude fatigue limit and implies that the fatigue life of a constant amplitude fatigue loaded detail will be infinite if the stress range does not exceed this limit. However, according to [24], more and more tests of high cycle fatigue resulting up to giga-cycles have revealed a further decline of S-N curve after the knee point. The new IIW recommendations [10], adapted this new finding in their latest guideline and drop the idea of a general fatigue limit for high cycles applications. Consequently, a continuous decline of about 10% per decade in fatigue resistance was assumed. In this new recommendations, the knee point is raised from 5 to 10 million cycles and S-N curves with uniform slope of  $m=3$  for welded joints and  $m=5$  for base metal are specified. Figure 3.6 demonstrates the new IIW nominal stress S-N curves.

Based on the statistical evaluations of the test results, each constructional detail is associated with one or several S-N curves, as illustrated in Figure 3.7.

Design procedure according to the nominal stress approach consists of two distinctive steps:

<sup>4</sup>Abbreviation for the English designation *Fatigue class* or *detail class*



**Figure 3.5:** The nominal stress  $S$ - $N$  curves of steel for normal stress range according to [9]. Numbers on the curves indicate the FAT value.

1. Calculation of the normal or shear stress in the critical section in question as described earlier.
2. Determination of the pertaining detail category from the tables provided by the codes and guidelines.

Once the corresponding detail category is determined, it can be used to establish the appropriate  $S$ - $N$  curve. Comparing the nominal stress in the detail with the  $S$ - $N$  curve can lead to determine the fatigue strength and/or service life of the detail. Alternatively, the  $S$ - $N$  curve equation can be used to determine the fatigue life of the detail ( $N$ ) as follows:

$$N = N_0 \cdot \left( \frac{C}{\sigma_r} \right)^m \quad (3.2)$$

where  $C$  and  $N_0$  are constants corresponding to the fatigue strength and life at a given point on the  $S$ - $N$  curve,  $m$  is the slope of  $S$ - $N$  curve and  $\sigma_r$  is the stress range. In particular case that  $C$  is chosen as the fatigue class of the structural detail at issue, the corresponding fatigue life,  $N_0$ , is 2 million cycles.

For a welded joint that is fatigue loaded with shear stresses, Eurocode-3 recommends 2 equally spaced  $S$ - $N$  curves with constant slope of  $m=5$ . Similar to direct

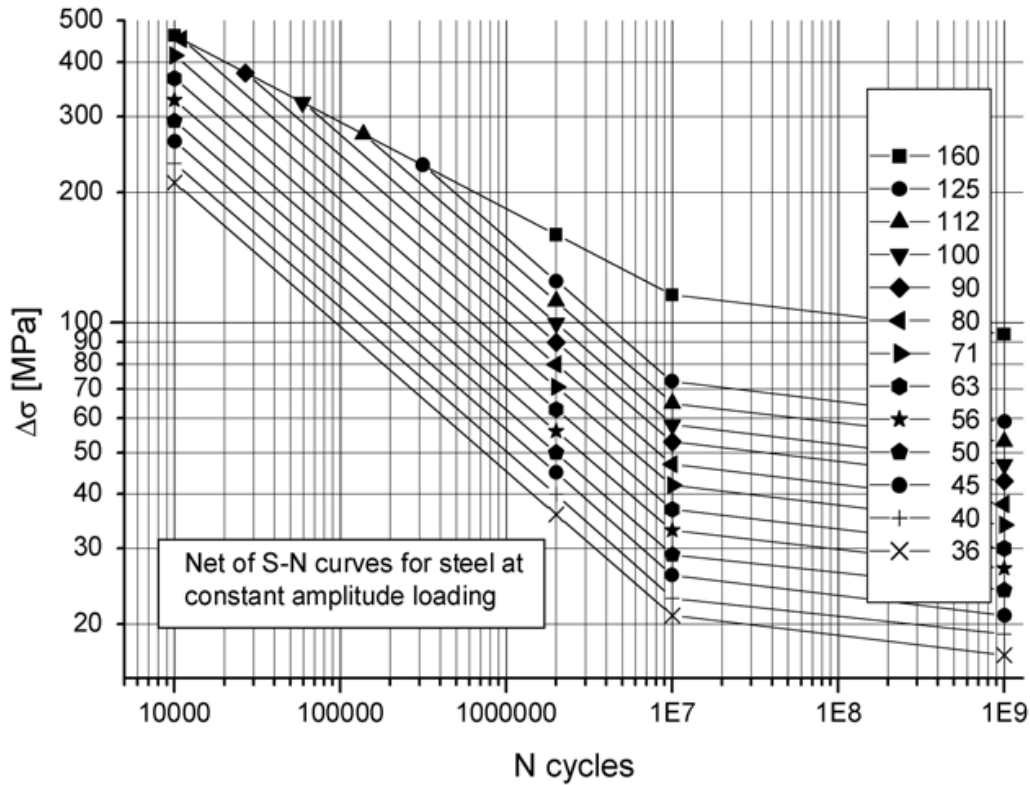


Figure 3.6: The nominal stress S-N curves of steel for normal stress range according to [10].

stresses S-N curves, the detail category ( $\Delta\tau_C$ ) is distinguished as the stress range at 2 million cycles.

Multi-axial loading of welded joints, on the other hand, results in a biaxial stress state with normal stress amplitudes  $\sigma_{\perp a}$  and weld parallel shear stress amplitudes



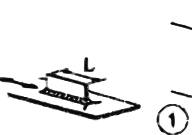
| Detail category | Constructional detail   |   | Description  | Requirements   |
|-----------------|---|---|--|--|
| 125             |  |  | <b>Continuous longitudinal welds:</b><br>1) Automatic butt welds carried out from both sides.<br>2) Automatic fillet welds. Cover plate ends to be checked using detail 6) or 7) in Table 8.5. | <b>Details 1) and 2):</b><br>No stop/start position is permitted except when the repair is performed by a specialist and inspection is carried out to verify the proper execution of the repair. |
| Detail category | Constructional detail   |   | Description  | Requirements   |
| 80              | $L \leq 50\text{mm}$  |  | <b>Longitudinal attachments:</b><br>1) The detail category varies according to the length of the attachment L.   | The thickness of the attachment must be less than its height. If not see Table 8.5, details 5 or 6.  |
| 71              | $50 < L \leq 80\text{mm}$   |   |  |  |
| 63              | $80 < L \leq 100\text{mm}$  |   |  |  |
| 56              | $L > 100\text{mm}$  |   |  |  |

Figure 3.7: Examples of constructional detail classifications and the corresponding FAT values according to [9].

$\tau_{\parallel a}$ . Eurocode 3 and IIW recommendations, propose interaction formulas depending on the loading state.

The maximum principal stress amplitude can be regarded as the fatigue relevant stress factor providing a proportional biaxial constant amplitude loading:

$$\sigma_{eq\ a} = \frac{1}{2} \left( \sigma_{\perp a} + \sqrt{\sigma_{\perp a}^2 + 4\tau_{\parallel a}^2} \right) \quad (3.3)$$

On the other hand, providing a non-proportional biaxial constant amplitude loading, the damages due to the normal and shear stresses have to be assessed separately for each loading state and then similar to the Palmgren-Miner rule, the total damage can be obtained by the summation of individual damages. The resultant equivalent stress amplitude is assumed as the relevant fatigue stress factor:

$$D_{tot} = D_{\sigma} + D_{\tau} \quad (3.4)$$

$$\left( \frac{\sigma_{eq\ a}}{\sigma_{\perp A}} \right) = \left( \frac{\sigma_{\perp a}}{\sigma_{\perp A}} \right)^3 + \left( \frac{\tau_{\parallel a}}{\tau_{\parallel A}} \right)^5 \quad (\sigma_{\perp a} < \sigma_{\perp A}, \tau_{\parallel a} < \tau_{\parallel A}) \quad (3.5)$$

Where  $\sigma_{\perp A}$  and  $\tau_{\parallel A}$  are the permissible stress amplitudes. The fractions of power 3 and 5 stem from the slopes of the S-N curves of normal stress and shear stress, respectively. The total damage ( $D_{tot}$ ) for design purposes, according to IIW and Eurocode 3, has to be kept equal or less than unity for a given number of cycles to failure.

### 3.1.3 Thickness effect

Due to the fact that nominal stress S-N curves have been derived from an extensive number of experimental investigations for each constructional detail, they include the effects of geometric variations to some extent. However, these experimental investigations were generally done on the small scale laboratory specimens with plate thickness in the range of 10 – 30mm. The plate thickness in some bridge details may be considerably larger. Consequently, the consideration of thickness effect in fatigue resistance was first questioned during the 1970s. Gurney [25] performed investigations based on the fracture mechanics and experimental results in which led to the conclusion that plate thickness may have a considerable effect on the fatigue resistance.

Thickness effect as a phenomenon in fatigue of welded joints was first included in fatigue design codes of welded steel structures in 1984, such that the fatigue strength abates as the plate thickness at the crack initiation point increases. Mashiri and Zhao [26] have pointed out the following parameters as the main causes of thickness effect:

- **Statistical size effect:** As mentioned before, fatigue is a highly localized process that nucleate at a location where geometry, defects, material properties and stresses comfort the crack initiation and propagation. Thus, increasing the plate thickness will intensify the probability of the existence of such locations that are highly susceptible to fatigue failures.

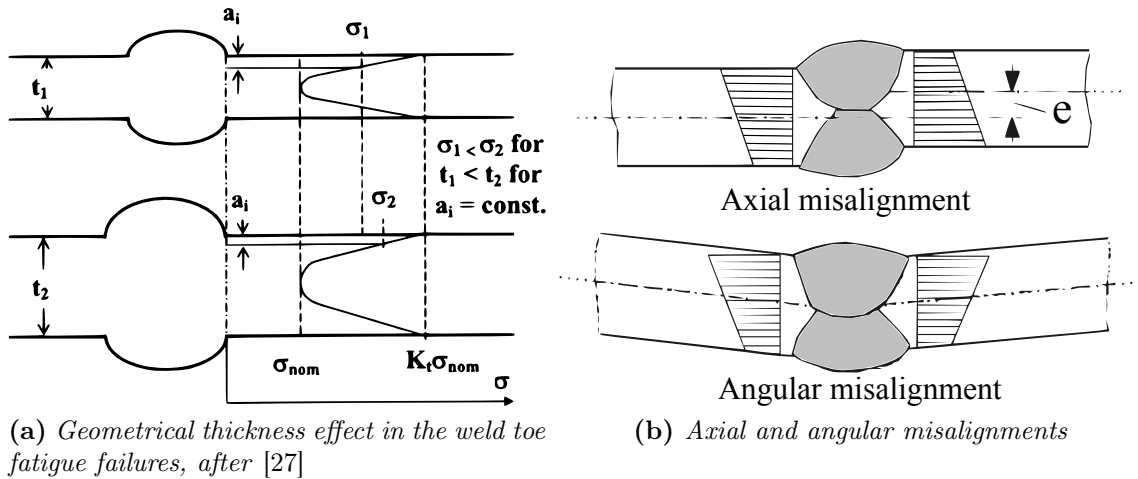


Figure 3.8

- **Technological size effect:** Differences in production parameters, such as rolling reduction ratios or welding induced residual stresses for different plate thicknesses, cause technological size effect.
- **Geometrical size effect:** As it is shown in Figure 3.8a and under the assumption that the initial crack growth conditions are independent of the plate thickness, the initial crack at the weld toe, undergoes higher stresses as the plate thickness increases. This leads to a higher crack growth rate in a thicker plate.

Eurocode 3 and IIW recommendations introduce a strength reduction factor ( $\gamma_t$ ) which has to be considered where the plate thickness ( $t$ ) is larger than the reference thickness ( $t_{ref}$ ).

$$\gamma_t = \left( \frac{t_{ref}}{t} \right)^n \quad t > t_{ref} \quad (3.6)$$

where the exponent  $n$  varies from 0.1 to 0.3 depending on the welded detail and weld toe condition. The reference thickness which is the thickness that is assigned to the S-N curve is  $t_{ref} = 25mm$  according to the aforementioned codes. The FAT class of the constructional detail has to be multiplied by the reduction factor in cases where the incipient crack is likely to commence at the weld toe and the plate thickness exceeds the reference thickness value.

### 3.1.4 Misalignment effect

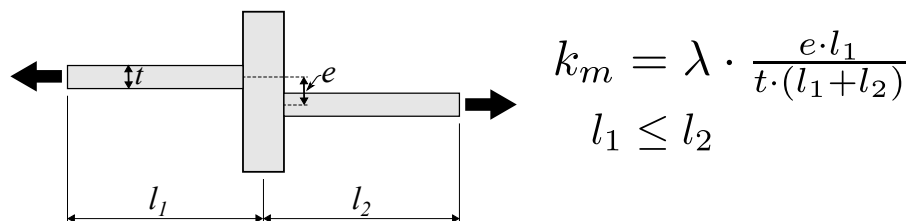
In case of an axially loaded joint, secondary bending stresses as a product of misalignment, give rise to the stresses in the weld joint. Figure 3.8b illustrates two common cases of axial and angular misalignment in a welded joint. Although misalignment induced stresses do not take place in joints subjected to pure bending, they do occur in parts of a component that is loaded in pure bending, where the through thickness stress gradient is trivial, such as beam flanges.

However, as mentioned before, the nominal stress S-N curves have been derived from experimental results which partially include misalignments. Therefore, an allowable misalignment is already comprehended for different constructional details in classified tables. Attention should be paid to the joints with larger misalignments by implementing the stress magnification factor due to misalignment,  $k_m$ , calculated by the formulas or stress analysis. For instance, axial misalignment of cruciform joints with the same thickness and its corresponding stress magnification factor are shown in Figure 3.9.

In cases that the joint include both axial and angular misalignment, the equivalent stress magnification factor should be applied as follows:

$$k_m = 1 + (k_{m,axial} - 1) + (k_{m,angular} - 1) \quad (3.7)$$

The effect of misalignment on the fatigue resistance can be obtained either by multiplying the calculated applied stress or by dividing the pertinent resistance S-N curve by the stress magnification factor.



**Figure 3.9:** Stress magnification factor for axial misalignment of cruciform joints

### 3.1.5 Limitations

The nominal stress approach has been the most widely used fatigue assessment method for decades. This method is generally referred to as the *classic* fatigue assessment method. The ease of use for versatile structural details and the acceptable accuracy, compared to the work effort, are some advantages of this approach. However, the need for more complicated details on the one hand, and the rapid development of computer based analysis tools on the other hand, have caused new limitations for designers to use nominal stress approach. Some of this limitations are:

- The structural detail and load type should fall under one of the design classes that are provided by the code. Nevertheless, not all details are available in the guidelines. Thus, in order to obtain a design class for such details, new laboratory tests should be carried out. After performing statistical analysis of the test results, the data can be consolidated into S-N curves for that detail. This procedure is indeed expensive, time consuming and cumbersome.
- The structure or component should not be very complicated; otherwise the nominal stress will be affected by various macro-geometrical factors. In such a case, it is very difficult or even impossible to define the nominal stress clearly in the section under consideration.
- The increased use of finite element analysis in modern design workflow makes it even vaguer to distinguish the nominal stress in the vicinity of the welded joint. This is due to the fact that, finite element analysis, by definition, determines notch stress and not nominal stress. According to [24], up to now, none of the available codes or guidelines have given concrete instructions of how to determine the nominal stress from FE results. The methods to determine nominal stress from FE results, likewise to the one described earlier in this section, stem from the engineering judgment of the designer.
- The fatigue life of some details depends on the geometrical properties of the joint such as the length of attachment, transition radius, etc. For such details, IIW or Eurocode 3, usually defines several FAT classes for different geometric combinations. The fatigue life, consequently, exhibits a step-wise trend whereas it is, in reality, continuous. This basic limitation of the nominal stress method, makes it in some cases complicated and not design efficient.

## 3.2 Structural stress approach

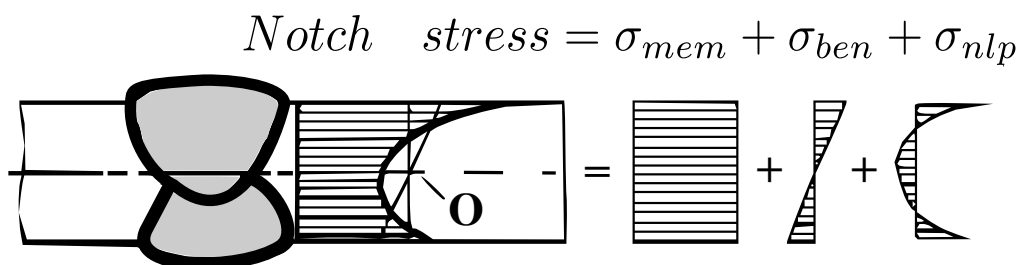
### 3.2.1 Basic concepts

The stress distribution over the plate thickness in the vicinity of a weld toe is non-linear. As shown in Figure 3.10 this non-linearity is due to the notch effect of the weld. The term *Structural stress* designates the basic stress by taking into account the geometrical variations of the detail at the expected fatigue crack initiation area (hot spot) excluding the notch effect. The structural stress, also known as geometric stress, can be measured by strain gages or calculated by engineering stress concentration factor formulas or finite element analysis [19, 28, 29]. The term hot spot stress is referred to the temperature rise due to plastic deformations at the crack initiation location.

The hot spot stress concept was first introduced for the fatigue design of tubular structures in 1960s by Peterson, Manson and Haibach [3, 5]. Over the years, the advantages of this approach compared to the traditional nominal stress method inspired design associations to introduce guidelines and instructions also for fatigue design of plated structures using the hot spot stress. The hot spot stress, by definition, is a fictitious value. Nevertheless, as demonstrated by Radaaj [1], in plate and shell structures it corresponds to the sum of membrane and bending stresses at the weld toe.

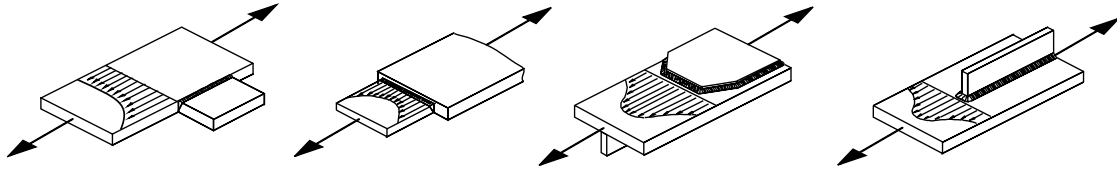
The membrane stress,  $\sigma_{mem}$ , which is constant through the thickness is equal to the average stress through the plate thickness. The shell bending stress,  $\sigma_{ben}$ , has a linear distribution through the thickness and is equal to zero at the mid-plane. The remaining self-equilibrating stress is the non-linear stress peak ( $\sigma_{nlp}$ ). The magnitude of the latter stress depends on the weld toe shape and geometry according to Niemi et al. [11].

Hobbacher [10] suggests that for a given stress distribution  $\sigma(x)$ , the mentioned



**Figure 3.10:** Membrane stress, plate bending stress and non-linear stress peak; The three components of non-linear stress distribution through the plate thickness at the weld toe ([11]).





**Figure 3.11:** *Structural stress in welded structural details*

three components can be calculated according to:

$$\sigma_{mem} = \frac{1}{t} \int_{x=0}^{x=t} \sigma(x) \cdot dx \quad (3.8)$$

$$\sigma_{ben} = \frac{6}{t^2} \int_{x=0}^{x=t} (\sigma(x) - \sigma_{mem}) \cdot \left(\frac{t}{2} - x\right) \cdot dx \quad (3.9)$$

$$\sigma_{nlp}(x) = \sigma(x) - \sigma_{mem} - \left(1 - \frac{2x}{t}\right) \cdot \sigma_{ben} \quad (3.10)$$

The structural hot spot stress (SHSS) disregards the notch effect caused by the weld profile and comprises all other geometric parameters. As pointed out in [1], the suppression of notch stress and the assumption of linear stress distribution through the plate thickness, is a consistent way to define structural stresses at the hot spot because a single-valued solution is achieved. Additionally, as the exact weld profile is not known during the design phase, the exclusion of notch stress appears to be reasonable. The notch effect is indirectly included in design S-N curves as they are obtained from fatigue tests. Some examples of welded structural details and structural stress distribution are shown in Figure 3.11.

As illustrated in Figure 3.12, the perpendicular stress component to the weld increases significantly in the vicinity of a weld toe prone to fatigue cracking. This peculiarity of stress distribution in front of weld toe is primarily attributed to two distinct stress raising factors:

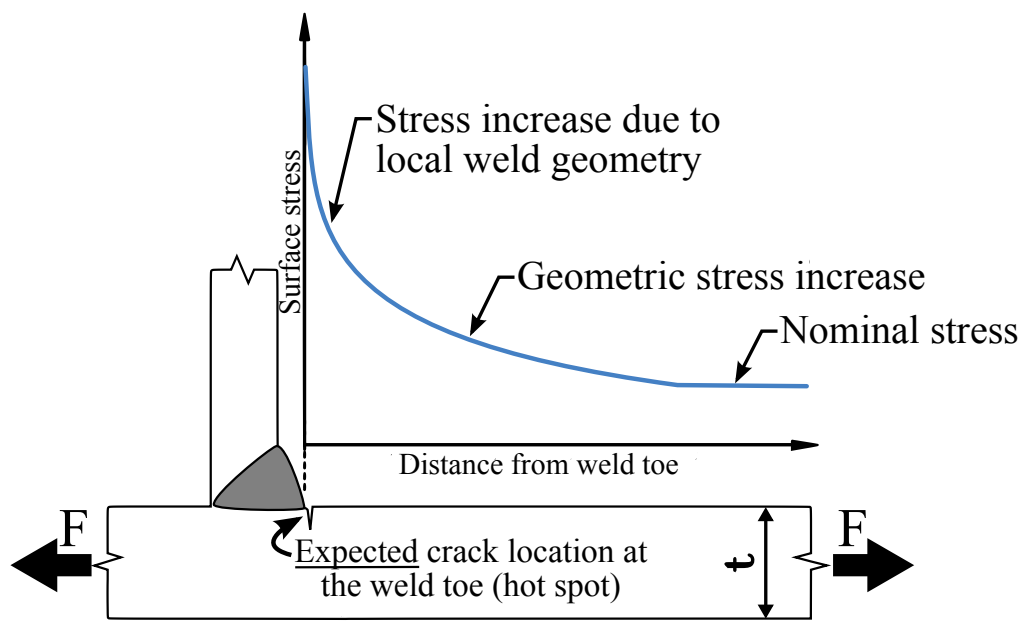
- Macro-Geometric effect
- Weld notch effect

The introduction of local structural variations in welded structures causes the stress in the vicinity of the weld toe to increase. The increase in stress due to macro-geometric variations includes all stress concentration effects except the notch effect induced by weld profile.

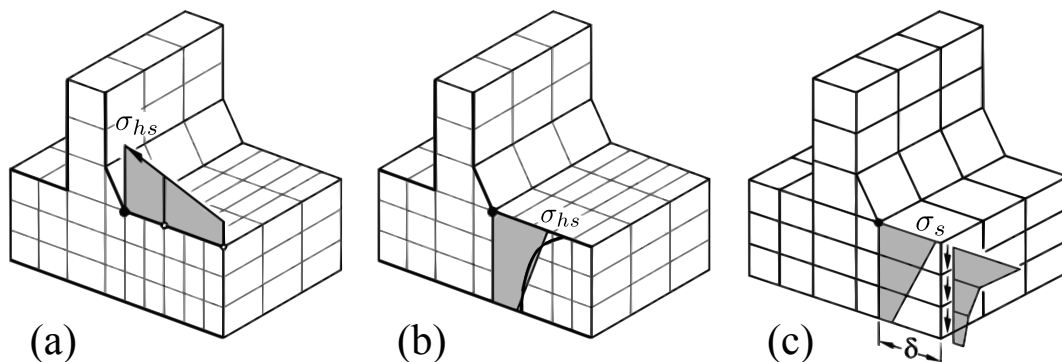
Additionally the stress near the weld toe increases dramatically due to the weld profile. The introduction of a sharp transition at weld toe acts as a local stress raiser that gives rise to a non-linear stress distribution through the plate thickness.

In a welded structure, the stress comprising the macro-geometric effects is designated as *geometric stress*. Structural hot spot stress approach is a local fatigue evaluation method that is based on the geometric stress value at the hot spot. However, the hot spot stress is an imaginary stress obtained by exclusion of the

notch stress from the total stress at the hot spot. The conventional method for the hot spot stress determination is to extrapolate the surface stress at certain reference points to the weld toe. The surface stress can be obtained either from experiment or appropriate finite element modeling. In addition to that, in the recent years by further advancements of computational possibilities, other variants of structural hot spot stress method have been developed. These methods are based on finite element method and often require high computational power. Among these methods, particularly the approaches by Dong [31], Dong et al. [32], Xiao and Yamada [33] and Poutiainen and Marquis [34] are remarkable and will be introduced and discussed in this chapter together with the conventional structural hot-spot stress approaches. Figure 3.13 shows a summary of the most common structural stress calculation approaches.



**Figure 3.12:** *Stress distribution near the weld toe*



**Figure 3.13:** *Alternative methods of SHSS calculation [30]: (a) Surface stress extrapolation, (b) Through thickness stress linearisation, (c) Stress equilibrium at distance  $\delta$  from the weld toe (Dong method)*

The structural hot spot stress concept is yet a research area in progress and a high amount of ongoing researches are aiming to improve this method [24]. IIW recommendations, which is one of the most comprehensive guidelines regarding the structural hot spot stress approach, has undergone substantial revisions in its section dedicated to the structural hot spot stress from 1996 to 2009. This alone can confirm the high amount of research made to improve this method.

### 3.2.2 Applications

The structural hot spot stress approach was first used as a fatigue evaluation method in offshore structures. It has been used for many years to assess the fatigue strength of welded details particularly in tubular structures. However, the implementation of the SHSS approach for other types of structures such as plated details is a work in progress. Several research projects and institutes across the world have been working to adapt this method in their field of application. It was first in 1990 when Radaj [1] summarized the earlier investigations and developed a local concept for geometric stress calculated according to the structural theories used in engineering. He presented applications of the new approach to several welded plated structures.

As early as 1991, Petershagen et al. [35] re-evaluated [1] and concluded a generalized hot spot stress approach for plated structures. Fricke and Petershagen [36] applied the proposed model to complex plated ship details. The method has been in progress since then and has been applied successfully to design of welded plated structures in ships or bridges (e.g. [23, 37–40]) as well as in commercial vehicles (e.g. [41]).

The structural hot spot stress approach is still a relatively new fatigue design method in plated structures. It is not as widely used as the nominal stress method and only a few design codes such as British Standard BS 7608:1993 [42] and Eurocode3 ENV 1993-1-1 [9] have suggested the SHSS approach as an alternative evaluation method. Eurocode 3 refers to the structural hot spot stress as ‘geometric stress’ and was the first general design code to include it. Nevertheless, it is deficient regarding the given instructions for the finite element modeling and the hot spot stress calculation. IIW recommendations [10, 11], on the other hand, provide comprehensive instructions for designers in that regard.

Numerous applications of the structural hot spot stress approach in combination with the finite element analysis, in different industrial fields, have demonstrated the suitability of this method in the following situations:

- Where there is no clear nominal stress definition as a result of complex structure
- Cases where the joint in question is not classified under the standard constructional details in tables provided by the design code. This can be interpreted as either the detail is not available in the code or some of its features do not comply with the code requirement(s). In any of these cases, local approaches

such as the SHSS approach can be alternative evaluation methods.

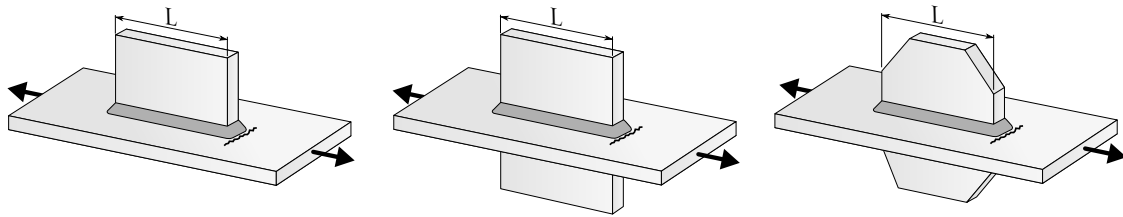
- If the calculation of the nominal stress is not straightforward and requires post-processing, particularly when using a correspondent finite element model. In such cases, it is recommended to use local approaches such as the SHSS method in order to improve the accuracy of the fatigue life estimation of component.
- In case of field or laboratory tests, where the stresses are derived from strain gauge measurements, the SHSS method provides a valuable tool to place an adequate number of strain gauges at appropriate locations and calculate the hot spot stress according to [43].

One advantage of the structural hot spot stress approach over other local approaches such as the effective notch stress method or the LEFM method, is the lower computational requirements and sensitivities of this method. The implementation of the SHSS approach in combination with the finite element analysis requires a rather fine mesh at the weld region. Nevertheless, the mesh size requirements and consequently the demanding computational power is much higher in the other mentioned methods. Moreover, the LEFM method is very susceptible to the initial crack size and material fracture properties and therefore can be mainly used in cases with a known crack size.

Another advantage of this method is the fewer number of required S-N curves than the nominal stress method for fatigue life evaluation. At the time being, IIW recommendations and Eurocode3 have defined only two FAT classes for fatigue evaluation based on the SHSS approach; FAT90 for load carrying and FAT100 for non-load carrying welded attachments. The fewer number of design classes irrespective of the joint geometry is consistent with the hot spot stress principal of including the macro-geometric stress raisers.

Here, in order to distinguish the advantages of the SHSS approach over the nominal stress method, an example of the fatigue life prediction of a structural detail using both methods is presented. In this investigation, the fatigue life of a fillet welded longitudinal non-load carrying attachment is calculated according to both the nominal stress method and the SHSS approach. Figure 3.14 depicts the investigated detail. The fatigue evaluation of this detail is thoroughly discussed in Chapter 4. Both IIW and Eurocode3 define several fatigue classes based on the attachment length ( $L$ ) for this detail. As a result of this step-wise classification, the detail exhibits an intermittent fatigue life whereas, the fatigue strength and consequently fatigue life are continuous functions of the attachment length.

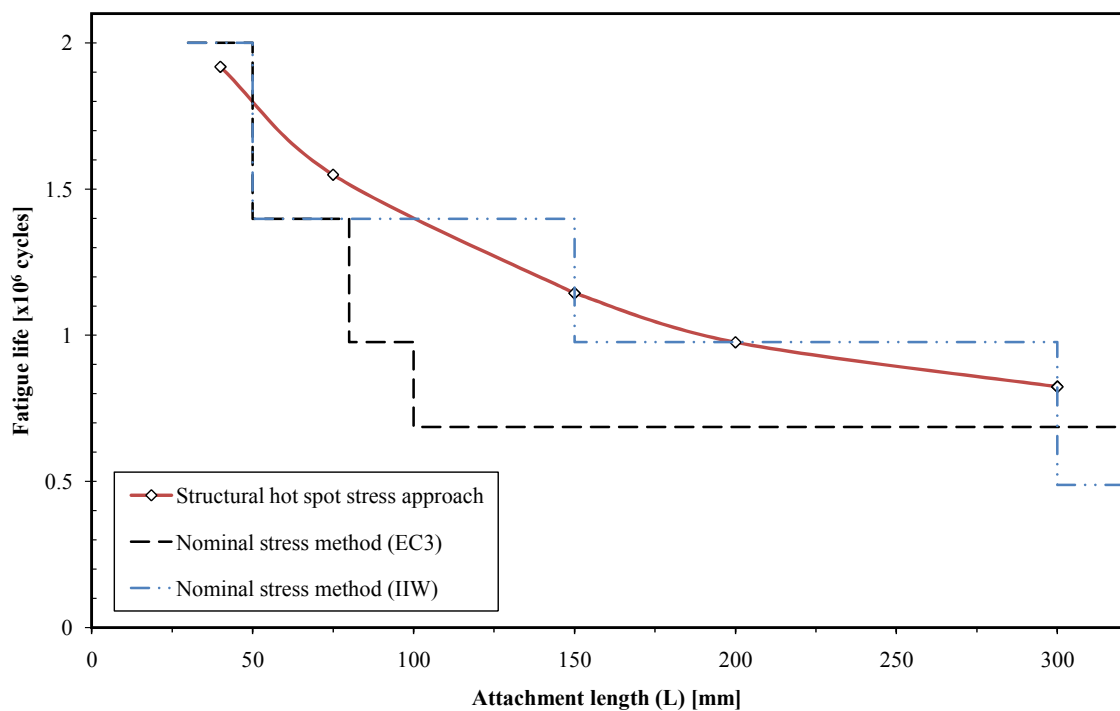
The fragmentizing of fatigue life of such details in codes is due to the fact that the nominal stress method does not account for the geometric variations of a detail. Thereby, codes and guidelines are compelled to subdivide its fatigue life by means of a step function. The structural hot spot stress approach, on the other hand, does not have this limitation and the structural hot spot stress FAT100 is applicable to



**Figure 3.14:** *Longitudinal non-load carrying attachments*

this detail irrespective of its attachment length.

An investigation of longitudinal attachments of 100mm height and 10mm thick plates is reported by Åsa Eriksson et al. [23]. The investigated details were subjected to an axial nominal tensile stress equal to 80 MPa. The structural hot spot stresses were determined using finite element analysis for attachment lengths of 40, 75, 150, 200 and 300mm. Figure 3.15 demonstrates the fatigue life prediction of longitudinal non-load carrying attachments with varying gusset length according to the nominal and the SHSS method using the reported data. It is apparent that the SHSS approach obtains a continuous fatigue life for the specimens with varying attachment lengths. On the contrary, the nominal stress method reveals an step-wise fatigue life for the detail. The discontinuous predicted fatigue life obtained from nominal stress method can lead to either very none-conservative predictions or fatigue lives which are substantially on the safe side. Furthermore,



**Figure 3.15:** *Fatigue life prediction of longitudinal attachments as a function of gusset length (Data partly from [23])*

it is apparent that Eurocode 3 has a different classification for this detail than IIW recommendations. Comparisons of the fatigue test results of non-load carrying longitudinal attachments with different gusset lengths and those predicted by the nominal stress and the SHSS approaches are presented in Chapter 4. Having compared the actual fatigue life of the detail with prediction models, the accuracy and reliability of each method is identified.

Several investigations ([44, 45]) on fatigue cracks initiating from plate edge have shown that for the hot spot stress determination, plate thickness can not be a good reference parameter. Therefore for plate edge fatigue cracks absolute positions for stress evaluation points are recommended [6]. Consequently, in order to codify this, designer's guide to the structural hot-spot stress approach [11] and IIW recommendations [10], classify two types of hot spots in welded details:

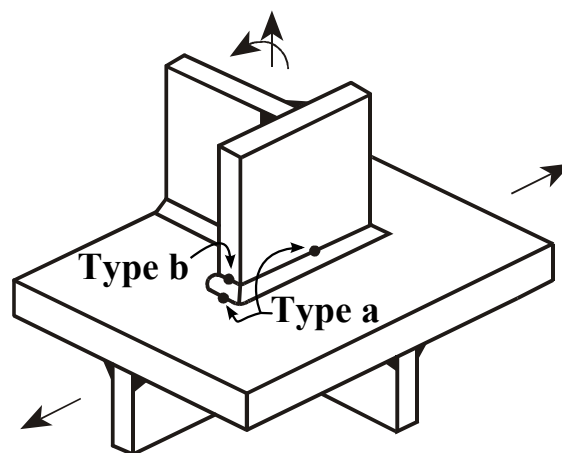
- **Type a** in which the weld is located on plate surface
- **Type b** in which the weld is located at plate edge

Figure 3.16 demonstrates the classification of hot spot types.

### 3.2.3 Experimental evaluation of the SHSS

Generally the stress analysis in the experimental investigations is accomplished by employing strain gauges. The strain gauges are only capable of monitoring the stress state at the surface of the component being tested. Thus, in order to experimentally evaluate the SHSS, surface stress extrapolation would be the most convenient method. The number and arrangement of the strain gauges depends on the magnitude of bending stresses, the plate thickness and the hot spot type. Figure 3.17 illustrates various arrangement of strain gauges for the SHSS derivation.

**Type 'a' hot spots:**



**Figure 3.16:** *Different types of hot spots* [10]

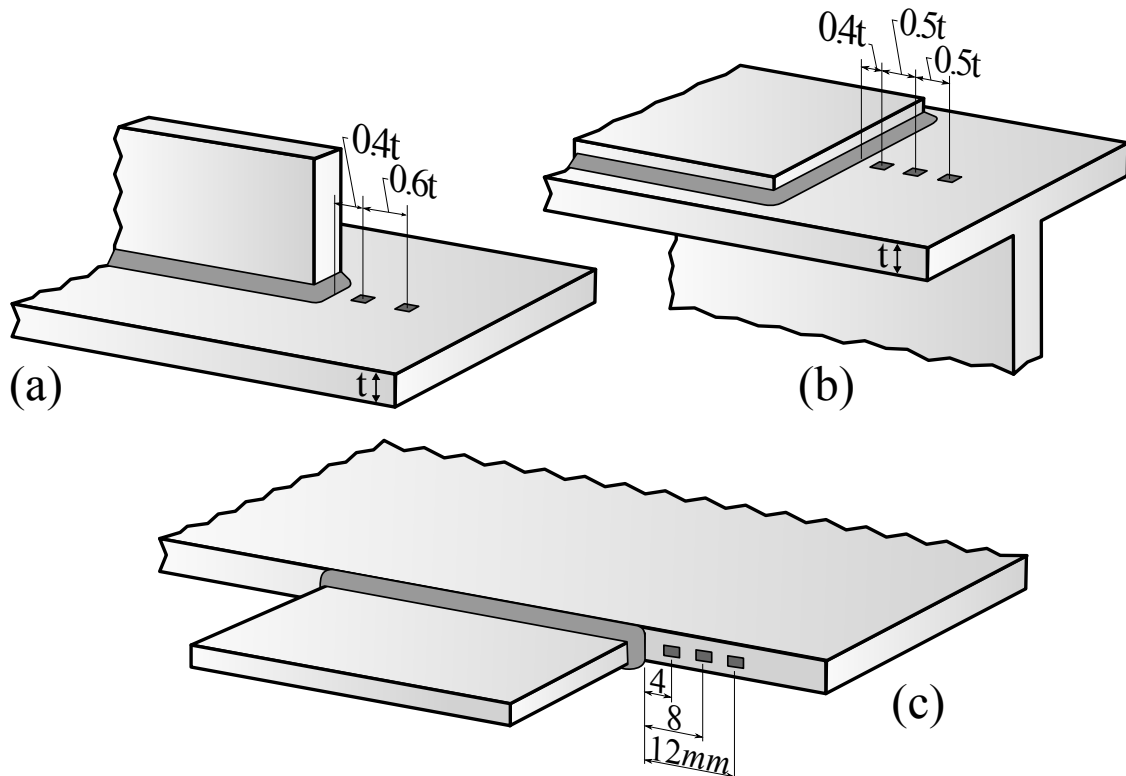
For fatigue cracks initiating from a plate surface (Type a hot spot), previous studies have reported that the area where the stress distribution is influenced by the non-linear notch effect lies within a radius of approximately  $0.3t$  to  $0.4t$  in front of the weld toe on the plate surface. Hence, in order to exclude the non-linear stress peak, the first reference point is defined at  $0.4t$  from the weld toe. For linear extrapolation, the second point is chosen at  $1.0t$  from the weld toe, see Figure 3.17a. Hence, the structural hot spot strain is given by:

$$\varepsilon_{hs} = 1.67\varepsilon_{0.4t} - 0.67\varepsilon_{1.0t} \quad (3.11)$$

Where  $\varepsilon_{0.4t}$  and  $\varepsilon_{1.0t}$  are the measured strains from the strain gauges attached on the plate surface at distances  $0.4t$  and  $1.0t$  from the weld toe, respectively.

In cases of pronounced non-linear structural increase towards the weld toe, linear extrapolation underestimates the actual structural hot spot stress. An example of such circumstances would be where a main plate is resting on a comparatively stiffer support (e.g. welded cover-plate on a beam flange that is supported by the web). Alternatively, a quadratic extrapolation method is suggested in which the strain gauges are placed at  $0.4t$ ,  $0.9t$  and  $1.4t$  as shown in Figure 3.17b. The structural hot spot strain is consequently obtained from:

$$\varepsilon_{hs} = 2.52\varepsilon_{0.4t} - 2.24\varepsilon_{0.9t} + 0.72\varepsilon_{1.4t} \quad (3.12)$$



**Figure 3.17:** Strain gauges arrangement in plated structures in order to obtain the structural hot spot stress: (a) Linear extrapolation of surface stress, (b) Quadratic extrapolation of surface stress, (c) Absolute positioning of strain gauges for quadratic extrapolation in case of plate edge attachments (Type b hot spot)

### Type ‘b’ hot spots:

As mentioned before for type b hot spots, the stress distribution in the vicinity of the weld toe does not depend on the plate thickness. Therefore, IIW recommends absolute positioning of the reference points at distances of 4, 8 and 12mm from the weld toe for implementation of a quadratic extrapolation. Thus, the structural hot spot strain is calculated as follows:

$$\varepsilon_{hs} = 3\varepsilon_{4mm} - 3\varepsilon_{8mm} + \varepsilon_{12mm} \quad (3.13)$$

Eventually, for a uniaxial stress state, the structural hot spot stress for both types ‘a’ and ‘b’ can be estimated from the Hook’s law:

$$\sigma_{hs} = E \cdot \varepsilon_{hs} \quad (3.14)$$

In case of multi-axial stress state, it is recommended to establish the ratio of the longitudinal and transverse strains ( $\varepsilon_y/\varepsilon_x$ ) in order to improve the accuracy. The mentioned ratio can be obtained by using rosette strain gauges or finite element analysis ([11]). The structural hot spot stress can be obtained from:

$$\sigma_{hs} = E \cdot \varepsilon_x \cdot \frac{1 + \nu \frac{\varepsilon_y}{\varepsilon_x}}{1 - \nu^2} \quad (3.15)$$



### 3.2.4 The SHSS evaluation using finite element method

Recent improvements of computational analysis methods along with the development of powerful computers, have paved the way for the application of new fatigue assessment methods. The SHSS approach as a relatively new fatigue evaluation method have shown to yield potentially accurate results in combination with the finite element method. Niemi and Marquis [38] have reported an accuracy range of  $\pm 10\%$  for the results obtained by FEA.

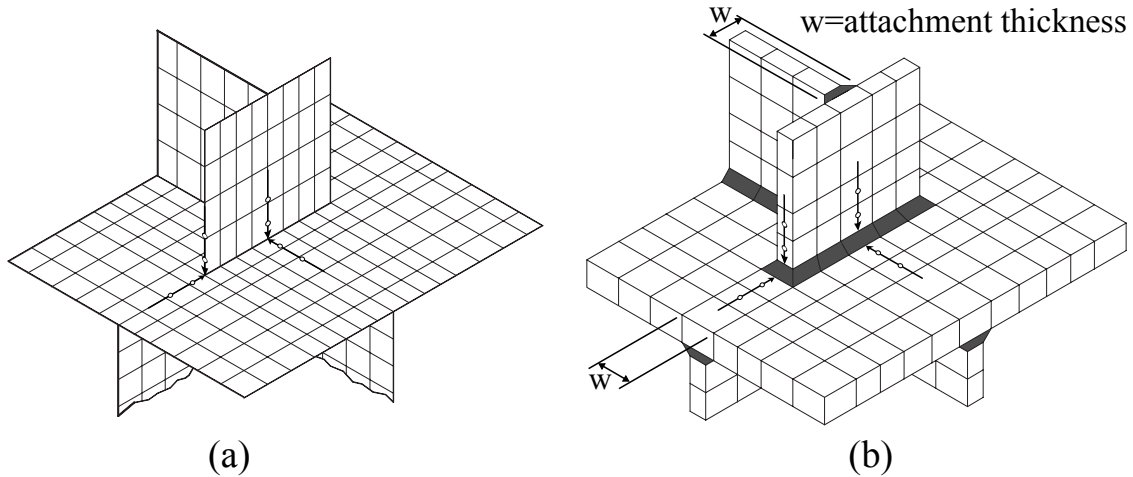
Based on the definition of the SHSS, it should include all the stress raising effects exempting those induced by the weld geometry. Except for very simplified models, this can not be achieved by simple analytical calculations. As an alternative, finite element analysis can be performed to determine it. However, the application of FEA requires relatively more computational effort than the conventional nominal stress method. On the other hand, The FEA results are found to be extremely sensitive to the mesh size and type of finite elements at the weld toe region due to the abrupt stress concentration. Therefore, a comprehensive guideline for the basis of the structural hot spot stress evaluation using finite element method is required.

In 2006, IIW Commission XIII published an updated version of a designer's guide for the structural stress approach to fatigue analysis of welded components [11]. This guide provides detailed instructions on the appropriate application of FEA to evaluate the fatigue life of plate-type structures. In addition to that, Lotsberg [7] has compared the mesh size and element type effect on the calculated SHSS for various plated details. Based on the findings of this study, recommendations are given for the finite element modeling and analysis procedure for such details.

It should be noted that, although currently a high number of sophisticated commercial finite element analysis programs are available, it is still left to the analyst to assess the results, simplify the model, define the suitable boundary conditions and loads, and choose appropriate analysis and element types. It is also the analyst responsibility to always check the creditability of the results by rough calculations.

In practice, there is a high demand for limiting the necessary computational power and effort to determine the SHSS. As a result, relatively simple models and coarse meshes are preferred. On the other hand, the model should be able to catch the formation of steep stress gradients at the hot spot region. Primarily, two types of elements are capable of capturing the plate bending; Shell and Solid element models, see Figure 3.18.

The simplest modeling alternative is offered by shell elements arranged in the mid-plane of the associated plate. Shell elements are the most widely used element types in the engineering applications since they require relatively less modeling effort and computational power. Therefore, as long as it doesn't affect the accuracy of the results, shell elements are the preferred meshing technique for the SHSS determination. Besides, the fact that the modeling procedure occupies the greatest



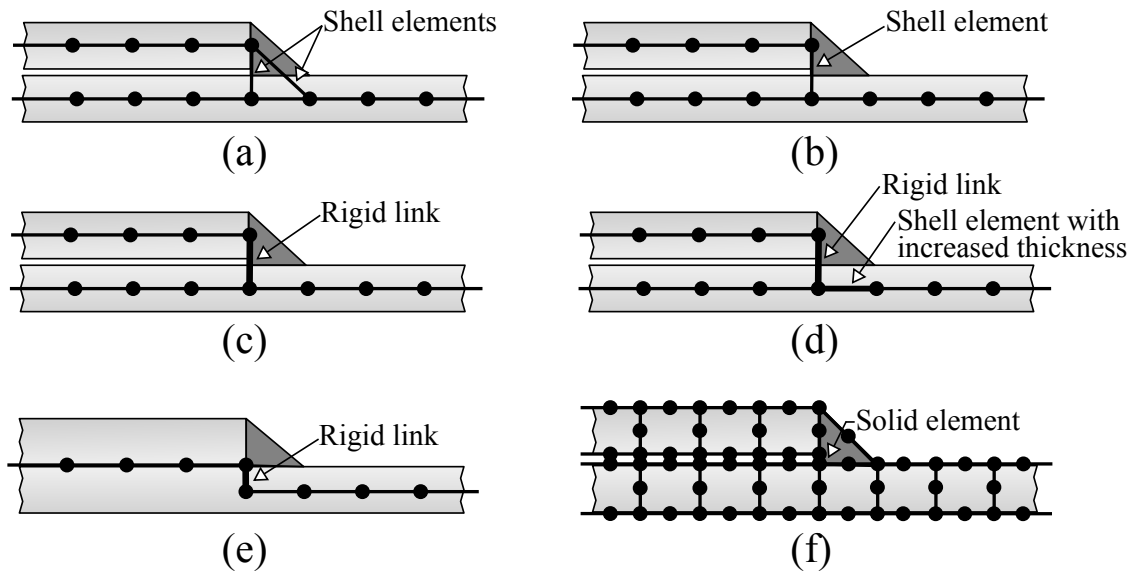
**Figure 3.18:** Typical finite element models for the plate-type welded joints: (a) Shell elements without welds, (b) solid elements

portion of the time required for the SHSS calculation gives additional preferences for the use of shell elements for this purpose.

Two types of shell elements exist; *thin* and *thick* shell elements. The thin shell elements behave according to the Kirchoff plate theory and thus the shear deformation through the element thickness is neglected in these elements. On the contrary, thick shell elements consider shear deformation through the element thickness by assuming the Mindlin plate theory. Accordingly, thin shell elements are best adapted for thin structures where classical shell theory is applicable, whereas, the thick shell elements are better suited for situations where a realistic representation of the plate stiffness is essential. In addition to that, 8-node isoparametric elements are recommended by Fricke [6] for the SHSS analysis based on shell elements.

When using shell elements for evaluation of welded structures, the welds are usually not modeled. Therefore, the plate attachments should be extended to the midplane of the plate. However, this simplification might underestimate the stiffness of the weld. Furthermore, in case of plate offsets (e.g. cover plates), or adjacent welds the weld should be modeled. As illustrated in Figure 3.19, modeling the weld in shell element models can be archived by several alternatives. [28] and [23] have thoroughly investigated different proposals together with their advantages and limitations.

The SHSS can also be obtained by using Solid element models, see Figure 3.18b. Solid elements are particularly recommended in case of complex structures. One layer of isoparametric 20-node elements in thickness direction yields reasonably accurate results due to the quadratic displacement function and linear stress distribution. The linear distribution of stress in thickness facilitates the SHSS determination directly at the weld toe. However, when multi-layer solid element models are used (e.g. when half of the plate thickness is modeled), the stress distribution



**Figure 3.19:** Various alternatives of modeling the weld: (a) modeling the weld with oblique shell elements, (b) modeling the weld with shell elements, (c) modeling the weld with straight rigid link, (d) modeling the weld with straight rigid link and shell elements with increased thickness, (e) modeling the weld with rigid bar, (f) modeling the weld with solid elements

through the thickness becomes non-linear. Subsequently, to obtain the SHSS, the through thickness stress should be linearized or alternative SHSS determination methods should be used. Moreover, using several solid elements through thickness drastically increase the computational model.

When analyzing large structures, modeling the entire structure with solid elements is not often feasible due to the large resulting computational model. Furthermore, except for critical sections such as weld toes or attachment connections, the parabolic shell elements also yield acceptable results in case of models with large areas of thin plates. Additionally, the use of shell elements considerably reduce the computational model size. Therefore, a solution is to use solid elements to merely model the areas in the vicinity of the weld and switch to shell elements for the connecting plates. Care should be given to provide adequate rotational stiffness at the connection point as the shell elements normally can not transfer any moment to the solid elements.

Another problem with solid element models is that by having a fine mesh at the weld toe region the model size increases quickly. *Sub-models* are a good solution to locally increase the mesh density while keeping a relatively coarser mesh for the rest of the structure. In sub-modeling approach, the model with relatively larger mesh is used to calculate the global deformation of the structure. This model is called *Global model*. Having obtained the global stresses, a local model is constructed to model the area in question with an appropriate mesh size needed to obtain the stress accurately. Eventually, the deformations obtained from the global model are used as boundary conditions for the local model (sub-model). Figure 3.20 demon-

strates an example of sub-modeling technique application to compute stresses at the weld toe of a cope-hole detail with an extremely fine mesh.

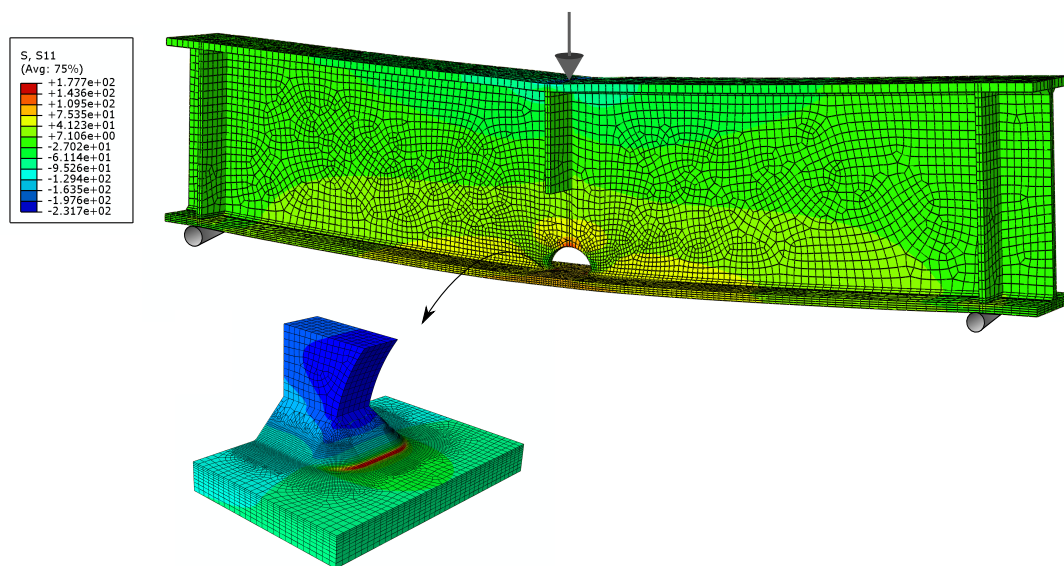
When constructing a solid element model, tetrahedral elements can be used instead of isoparametric elements. Tetrahedral elements, which are often available in CAE (Computer Aided Engineering) softwares, are famous for the easy mesh generation (free meshing technique). This feature dramatically reduces the time required to establish a finite element model. However, the linear tetrahedral elements are not suitable for the SHSS determination. Instead, only higher order tetrahedral elements with sufficiently fine mesh in the vicinity of the weld toe should be used. Additionally, the results should be properly verified by the analyst.

When using solid elements, the weld can be easily modeled with prismatic elements. In addition to that, the gap between two plates is not needed to be modeled as it has little influence on the results. Nevertheless, in case of plate offsets the gap has to be modeled by a relatively small offset between the plates.

Finite element analysis of large structures with several critical points can be conducted in two stages. In the first stage, the entire model can be constructed with a coarse mesh. This way, the potential hot spots can be achieved. In the next stage, either sub-modeling approach can be implemented or the mesh can be refined at the hot spot regions.

The following recommendations should always be noted when using the finite element method for the SHSS evaluation:

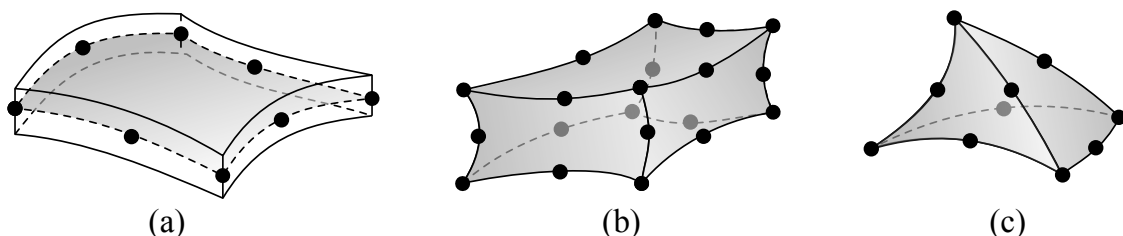
- The element types should be chosen to allow for a linear stress distribution through the thickness. This can be obtained by adapting 8-node shell el-



**Figure 3.20:** *An example of sub-modeling approach to refine the mesh density at the critical section*

elements or one layer of 20-node solid elements with reduced integration. If a multi-layer solid elements are used, the non-linear stress peak should be excluded by one of the available SHSS determination methods. Figure 3.21 depicts the recommended 3D element types for the SHSS determination using FEM.

- In case of shell elements, the weld can be omitted. In such a case, it is recommended to select the structural intersection point as the weld toe representative. This is due to the weld stiffness underestimation as a result of neglecting the weld.
- Linear elastic analysis can be assumed. In addition to that, the weld can be assigned the same mechanical properties as the parent metal.
- The meshing and partitioning procedure of the area close to the weld should be carried out in a way that the stress read out points, for post processing of the results, lie on the elements' integration points or nodal points.
- In case of using the nodal values at the evaluation points, the stress averaging option for the intersecting shell or solid elements should be turned off. An example would be the case of two adjacent elements where one is highly stressed and the other one is not. If the element averaging is exploited, the post processor software uses an average of the two element stresses for the nodal value at the intersection point. This value is not valid and has no practical serviceability. Therefore, it is recommended to only pick the elements of interest in front of the weld toe for further evaluations.
- The ratio of the largest to the smallest element edge must not exceed 3.
- The mesh should be gradually refined at the weld region.
- IIW recommendations and Eurocode 3 advise to use the *maximum principal stress* as the appropriate stress component if it is oriented within  $60^\circ$  of the normal stress. Otherwise, the perpendicular stress component has to be studied.



**Figure 3.21:** *The recommended 3D element types for the SHSS calculation using FEM: (a) 8-node shell elements arranged at the mid plane of the plates, (b) 20-node isoparametric solid elements with reduced integration, (c) 10-node parabolic tetrahedral elements with sufficiently fine mesh at the hot spot*

- If the possible misalignments are not considered in the FE model, the stresses should be magnified by means of an appropriate stress magnification factor provided by codes for different misalignment categories.

### 3.2.5 The SHSS according to surface stress extrapolation

Surface stress extrapolation is the conventional method to exclude the non-linear stress peak from the surface stress and determine the SHSS. In this method the SHSS can be achieved by extrapolating the plate surface stress towards the weld toe at certain reference points located within a reasonable distance from the weld toe where it is not influenced by the weld geometry. Comparative investigations have shown that for the fatigue cracks initiating from the main-plate surface, the reference points are located at distances from weld toe which are fractions of the plate thickness. It is generally accepted that at a distance of  $0.4t$  from the weld toe, the stress is not anymore affected by the weld geometry, see Figure 3.22. However, for attachments welded at a plate edge, plate thickness is not considered a relevant parameter.

Accordingly, the FE results can be applied to the surface stress extrapolation. Nevertheless, systematic stress analysis of various details with different element types and mesh qualities have confirmed that certain rules for the finite element modeling and stress evaluation have to be essentially followed to obtain comparable results [6–8, 11, 46]. It has been observed that in case of two-dimensional FE analysis the surface extrapolation results become insensitive to the mesh size as long as certain limits are met. However, it doesn't always apply for the three-dimensional FE analysis. Therefore, certain meshing recommendations have to be strictly followed in order to have consistent results.

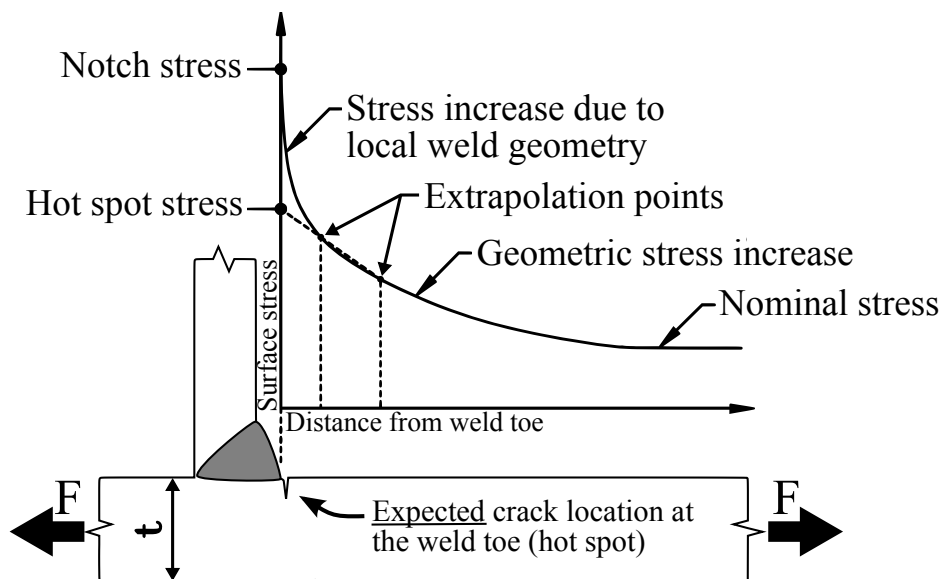


Figure 3.22: Stress distribution near the weld toe

IIW recommendations [10], proposes two meshing densities for shell and solid elements; Fine and coarse mesh. The requirements of the recommended meshing techniques are presented in Table 3.1. Here the specifications and requirements for each of these meshing techniques along with different extrapolation methods are further discussed.

### Fine mesh

It has been confirmed that the finite element models with a fine mesh generally yield more accurate results. Niemi et al. [11] recommends to particularly use a fine mesh for the following:

- Where the stress gradient close to the hot spot is high
- Details with adjacent discontinuities
- Where a comparison between measured data and FEA results is carried out

For type ‘a’ hot spots the first element length should not exceed  $0.4t$  in the loading direction. As nodal stresses are exploited in fine meshes, one of the side edges of the elements in front of the weld toe must lie on the extrapolation path. Thus, the element width should not be more than  $w/2$  ( $w$  being equal to the attachment thickness plus two weld leg lengths as shown in Figure 3.18). For type ‘b’ hot spots the element length for the first three elements should not exceed  $4mm$ . The extrapolation procedures and formulas for various alternatives are given below:

- Linear extrapolation of type ‘a’ hot spots: Evaluation of nodal stresses at reference points  $0.4t$  and  $1.0t$  according to Equation 3.16 as shown in Figure 3.23a.

$$\sigma_{hs} = 1.67 \cdot \sigma_{0.4t} - 0.67 \cdot \sigma_{1.0t} \quad (3.16)$$

- Quadratic extrapolation of type ‘a’ hot spots: Evaluation of nodal stresses at three reference points  $0.4t$ ,  $0.9t$  and  $1.4t$  according to Equation 3.17 as shown in Figure 3.23b. The quadratic extrapolation is recommended in cases of considerable non-linear stress increase at the hot spot, sudden change in the applied force direction or for structures with thick plates.

$$\sigma_{hs} = 2.52 \cdot \sigma_{0.4t} - 2.24 \cdot \sigma_{0.9t} + 0.72 \cdot \sigma_{1.4t} \quad (3.17)$$

- Quadratic extrapolation of type ‘b’ hot spots: Evaluation of nodal stresses at three reference points  $4, 8$  and  $12mm$  according to Equation 3.18 as shown in Figure 3.24a.

$$\sigma_{hs} = 3 \cdot \sigma_{4mm} - 3 \cdot \sigma_{8mm} + \sigma_{12mm} \quad (3.18)$$

### Coarse mesh

A relatively coarse mesh can also be used to determine the SHSS. A finite element model with a relatively coarse mesh requires less computational power and is advantageous over the same model with a fine mesh in this regard. In this method, in case of shell elements the stresses at reference mid points and in case of solid elements

the stresses at reference elements' surface mid side nodes are linearly extrapolated. Due to the singularity at the weld toe, the stress obtained from the first element is slightly exaggerated. This compensates the uncertainty of linear extrapolation of stresses obtained from approximately distant reference points. Thus, when using a coarse mesh, the recommended elements sizes should be strictly followed and no alteration is permitted. Niemi et al. [11] recommends to use a coarse mesh in the following cases:

- The stress gradient close to the hot spot is not severely high
- Details with no other discontinuities close to the hot spot
- 8-node shell elements or 20-node solid elements are being used
- Stresses are obtained at mid points or surface mid side nodes

For type 'b' hot spots the first two element lengths should not exceed 10mm. The extrapolation procedures and formulas for different hot spot types are given below:

- Linear extrapolation of type 'a' hot spots: Evaluation of stresses at mid side nodes of elements with lengths equal to plate thickness at two reference points 0.5t and 1.5t according to Equation 3.19 as shown in Figure 3.23c.

$$\sigma_{hs} = 1.5 \cdot \sigma_{0.5t} - 0.5 \cdot \sigma_{1.5t} \quad (3.19)$$

- linear extrapolation of type 'b' hot spots: Evaluation of stresses at mid side nodes of elements with lengths equal to 10mm at two reference points 5 and 15mm according to Equation 3.20 as shown in Figure 3.24b.

$$\sigma_{hs} = 1.5 \cdot \sigma_{5mm} - 0.5 \cdot \sigma_{15mm} \quad (3.20)$$

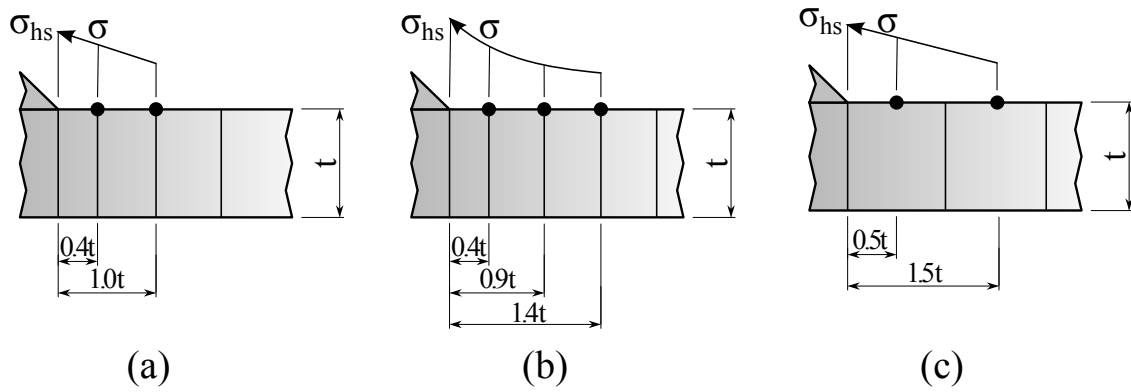
**Table 3.1:** IIW ([10]) Recommended meshing and extrapolation methods for surface stress extrapolation approach as illustrated in Figure 3.23 and 3.24

| Type of model        |       | Relatively coarse mesh                |                               | Relatively fine mesh                              |                              |
|----------------------|-------|---------------------------------------|-------------------------------|---|------------------------------|
|                      |       | Type a                                | Type b                        | Type a  | Type b                       |
| Element size         | Shell | $t \times t$<br>$\max t \times w/2^*$ | $10 \times 10mm$              | $\leq 0.4t \times t$ or<br>$\leq 0.4t \times w/2$ | $\leq 4 \times 4mm$          |
|                      | Solid | $t \times t$<br>$\max t \times w$     | $10 \times 10mm$              | $\leq 0.4t \times t$ or<br>$\leq 0.4t \times w/2$ | $\leq 4 \times 4mm$          |
| Extrapolation points | Shell | 0.5t and 1.5t<br>mid side points**    | 5 and 15mm<br>mid side points | 0.4t and 1.0t<br>nodal points                     | 4,8 and 12mm<br>nodal points |
|                      | Solid | 0.5t and 1.5t<br>surface center       | 5 and 15mm<br>surface center  | 0.4t and 1.0t<br>nodal points                     | 4,8 and 12mm<br>nodal points |

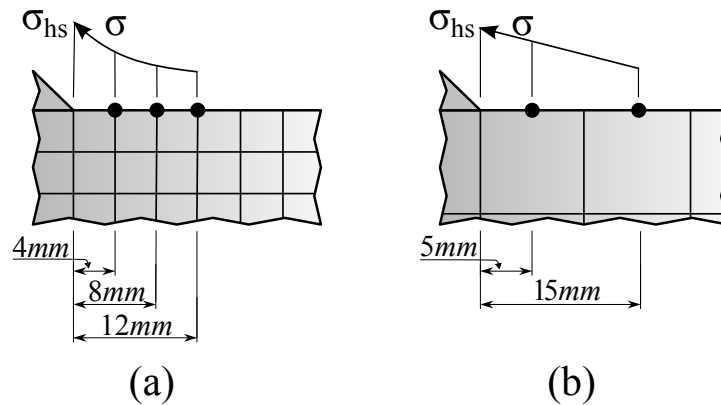
\* w is equal to Attachment thickness plus two weld leg lengths

\*\* Surface center at transverse welds, if the weld below the plate is not modeled





**Figure 3.23:** Hot spot type ‘a’ surface extrapolation method: (a) Linear surface stress extrapolation at nodal points of fine mesh (as shown or finer), (b) Quadratic surface stress extrapolation at nodal points of fine mesh (as shown or finer), (c) Linear surface stress extrapolation at element mid side nodes of coarse mesh (fixed element sizes)



**Figure 3.24:** Hot spot type ‘b’ surface extrapolation method: (a) Quadratic surface stress extrapolation at nodal points of fine mesh (as shown or finer), (b) Linear surface stress extrapolation at element mid side nodes of coarse mesh (fixed element sizes)

Furthermore, care should be given to the design of welded joints with plate thicknesses higher than 25mm as the surface stress extrapolation method is not sensitive to the plate thickness. In such cases, the empirical thickness correction factor that diminishes the fatigue strength has to be considered as follows:

$$\Delta\sigma_{al}(t > 25\text{mm}) = \Delta\sigma_{al}(t_0 = 25\text{mm})(t_0/t)^n \quad (3.21)$$

According to [11], the exponent  $n$  varies between 0.1–0.3 depending on the attachment type such that  $n = 0.1$  for longitudinal edge attachments,  $n = 0.2$  for butt-welded joints and  $n = 0.3$  for fillet welded joints.

### 3.2.6 The SHSS according to through thickness stress linearisation

A linear formulation of the non-linear stress distribution directly at the weld toe is called through thickness stress linearisation, see Figure 3.25. In this method, first, the non-linear stress distribution is integrated over the plate thickness, then, a linear distribution is generated from the outcome. Finally, the integration of the resulting linear distribution produces the bending and membrane stress components. These components can be used to derive the SHSS.

Many finite element analysis softwares, including Abaqus CAE, have the built in post-processor to perform the linearisation procedure automatically. However, as discussed before, the analyst should always ensure the credibility of the results. For instance, when using the through thickness linearisation method, the analyst should only make use of the elements in front of the weld toe while the nodal averaging function is turned off. This can be explained by the fact that the weld metal, due to its extra material, undergoes lower stresses, whereas, the elements immediately in front of the weld toe withstand higher stresses. The nodal averaging procedure, thus, lower the stresses at the weld toe which can result in an underestimation of the computed SHSS. This can be particularly more troublesome in case of FE models with relatively coarse meshes since they are not essentially constructed to capture the stress raise at the sharp weld toe.

Similar to the surface stress extrapolation method, the through thickness linearisation is mesh size dependent. However, according to Poutiainen et al. [46], the through thickness linearisation method is more forgiving when it comes to mesh requirements. When using solid elements to compute the SHSS by the through thickness linearisation, it is recommended to use at least three isoparametric solid elements in the thickness direction to gain an acceptable accuracy in the non-linear stress calculation at the weld toe [23].

In conclusion, when using the trough thickness linearisation method, extra consideration should be given to the nodal averaging. In addition to that, only elements in front of the weld toe should be included in post-processing of the results and the weld element and elements behind the weld toe must be clearly excluded.

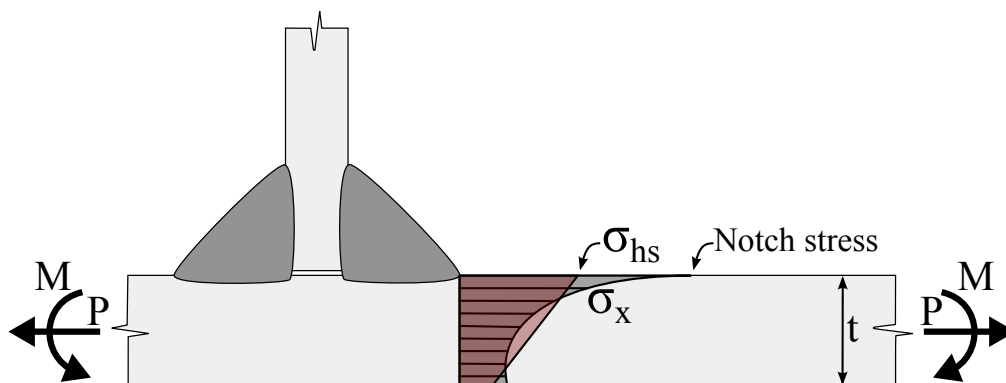


Figure 3.25: Through thickness stress linearisation at weld toe

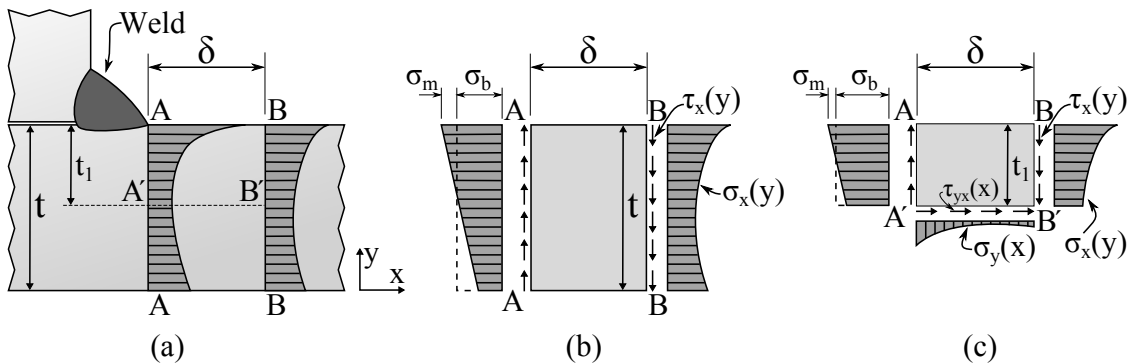
### 3.2.7 The SHSS according to Dong

Dong [31] and Dong et al. [47] have proposed another method for the structural stress calculation similar to the trough thickness linearisation method but at a distance  $\delta$  from the weld toe. As approaching the weld toe, the obtained stress values become affected by the asymptotic singularity caused by the notch. Consequently, the local stresses near the notch are mesh size sensitive. The Dong method is claimed to be mesh insensitive as it makes use of the stresses at a distance  $\delta$  from the weld toe. In this method, the structural stress can be derived by establishing the equilibrium conditions at the weld toe for the normal and shear stresses acting in the distance  $\delta$ , see Figure 3.26. As a result, for a solid model with monotonic through thickness stress distribution (Figure 3.26b), the membrane ( $\sigma_m$ ) and bending  $\sigma_b$  portions of the stress at the weld toe can be obtained from:

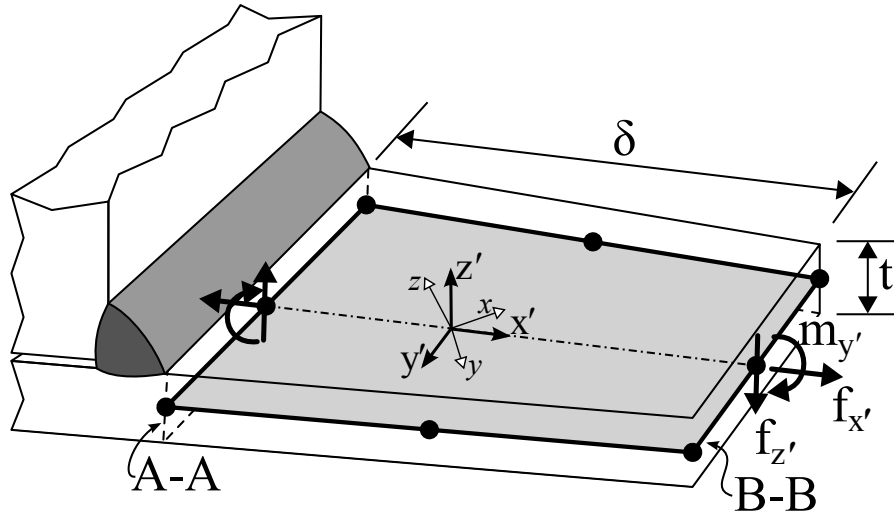
$$\sigma_m = \frac{1}{t} \int_0^t \sigma_x(y) \cdot dy \quad (3.22)$$

$$\sigma_m \cdot \frac{t^2}{2} + \sigma_b \cdot \frac{t^2}{6} = \int_0^t \sigma_x(y) \cdot y \cdot dy + \delta \int_0^t \tau_{xy}(y) \cdot dy \quad (3.23)$$

In case of non-monotonic through thickness stress distribution, such as symmetric fillet welded attachments or thick sections, the linearisation is performed to a finite depth  $t_1 \leq t$ . According to [31], the depth  $t_1$  can be assumed up to a depth where the transverse shear stress changes direction. Four double-sided welded joints subjected to symmetrical loading configurations, the depth  $t_1$  can be substituted by  $t_1 = t/2$ . In addition, since the linearisation is performed partially to the depth  $t_1$  and the lower boundary at this depth is no more a free surface, the stresses acting at the lower area at the depth  $t_1$  have to be included in the equilibrium equations, see Figure 3.26c. Subsequently by imposing equilibrium conditions between sections A-A' and B-B', it can be concluded that the structural stress components must



**Figure 3.26:** *The structural stress according to Dong: (a) Stress distribution trough thickness at weld toe and at distance  $\delta$  from weld toe, (b) Linearized structural stress through plate thickness at weld toe (section A-A) equilibrated by stresses at section B-B, (c) Linearized structural stress through variable thickness ( $t_1$ ) at weld toe (section A-A') equilibrated by stresses at section B-B'*



**Figure 3.27:** *The structural stress according to Dong in case of shell elements*

satisfy the following conditions:

$$\sigma_m = \frac{1}{t_1} \int_0^{t_1} \sigma_x(y) \cdot dy + \frac{1}{t_1} \int_0^\delta \tau_{yx}(x) \cdot dx \quad (3.24)$$

$$\begin{aligned} \sigma_m \cdot \frac{t_1^2}{2} + \sigma_b \cdot \frac{t_1^2}{6} &= \int_0^{t_1} \sigma_x(y) \cdot y \cdot dy + \delta \int_0^{t_1} \tau_{xy}(y) \cdot dy \\ &+ \int_0^\delta \sigma_y(x) \cdot x \cdot dx \end{aligned} \quad (3.25)$$

In case of shell elements, as shown in Figure 3.27, the structural stress calculation procedure consists of transferring the global coordinate system to a local coordinate system in which the local axes  $x'$  and  $y'$  are perpendicular and parallel to the weld toe, respectively. The line forces and moments derived from the nodal forces and moments can consequently be converted to the structural stress components at Section A-A as given below:

$$\sigma_s = \sigma_m + \sigma_b = \frac{f_{x'}}{t} + \frac{6(m_{y'} + \delta \cdot f_{z'})}{t^2} \quad (3.26)$$

Although the Dong method is claimed to be mesh insensitive even for hot spots with steep stress gradients, investigations ([8, 46]) have shown a considerable mesh sensitivity in case of solid elements. Disregarding the influence of the shear stresses acting in the lateral faces of the elements has been found to be the reason for this observation. This causes inaccuracies depending on the element size. Nevertheless, according to [46], at  $\delta = 0.4t$ , the influence of these extra shear forces is negligible.

### 3.2.8 The SHSS according to Xiao and Yamada

Xiao and Yamada [33] have proposed an unconventional structural stress concept based on the calculated stress at depth 1mm below the weld toe. The method is founded on analysis results of a reference structural detail, a non-load carrying cruciform joint with plate thickness of 10mm, see Figure 3.28. Finite element analysis of this reference detail, revealed that irrespective of the weld toe geometry, at one millimeter in depth the through thickness stress value drops to approximately the nominal stress. Moreover, this stress is shown to be correlated with early crack propagation phase.

In order to obtain the structural stress according to Xiao and Yamada, the finite element model should be constructed with a necessarily fine mesh that is capable of providing the stress at 1mm in depth with an acceptable accuracy. The authors have determined 1mm as the maximum allowable element length. In case of shell elements, Doerk et al. [8] have investigated the element size and type effect on calculated 1mm-stress. They reported a surprisingly lower obtained stress for 8-node shell elements compared to 4-node elements, having quadratic and linear displacement functions, respectively. The singularity caused by the notch at the weld toe is seen to be the reason, as it produces increased stresses at the plate edge and consequently decreased stresses at the bottom edge of the element, i.e. 1mm in depth. Thus, it is recommended to use only elements without misdid nodes if the element length is chosen equal to 1mm. Furthermore, in case of hexahedral elements the element length should not exceed the 1mm limit as well.

This concept has been verified by the authors by applying it to several welded joints similar to the reference detail, such as longitudinal and transverse attachments. The fatigue lives obtained from fatigue tests were plotted against the structural stress 1mm in depth. The resulting diagram exhibited a sufficiently narrow scatterband whose lower bound was corresponding to the design class FAT100. Furthermore, Noh et al. [48] have employed this method for fatigue assessment of load-carrying fillet welded cruciform joints and have confirmed its applicability to fatigue assessment of load-carrying attachments.

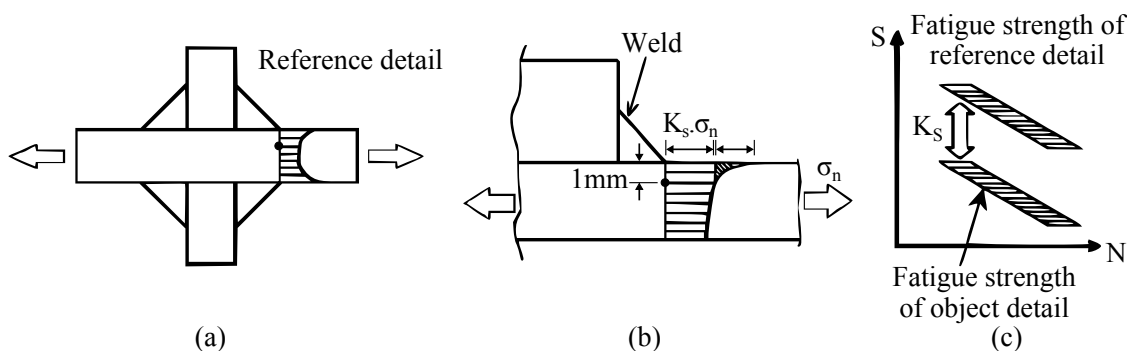


Figure 3.28: Structural stress according to Xiao and Yamada [33]

### 3.2.9 The SHSS according to Poutiainen and Marquis

As it will be discussed in Section 3.2.12, regarding the SHSS design S-N curves, IIW recommendations and Eurocode 3 define alternate fatigue design curves for load carrying and non-load carrying attachments. In addition to that, as it was discussed in Section 3.2.5, the conventional surface stress extrapolation method is not sensitive to plate thickness. In order to obviate these limitations, Poutiainen and Marquis [34] have suggested a multi-linear through thickness stress distribution at the weld toe. The proposed method considers the more severe notch stress concentration in case of load-carrying attachments by increasing the structural stress instead of introducing separate design FAT classes.

Figure 3.29 illustrates how the proposed method superimpose a triangular stress distribution on the linearized through thickness stress distribution at the weld toe. Based on the relation between plate thickness and weld size, two or three linear segments can be formed. The resulting multi-linear stress distribution varies with weld size and can accordingly take the plate thickness and weld size effect into account.

Figure 3.30 demonstrates the linearisation of the through thickness stress according to this concept for two loading cases. As it is apparent, the multi-linear stress distribution can be achieved by first integrating the stress to the depth  $T_1$  and then from  $T_1$  to  $T$ . Thus, the modified structural stress according to Poutiainen and Marquis can be calculated as:

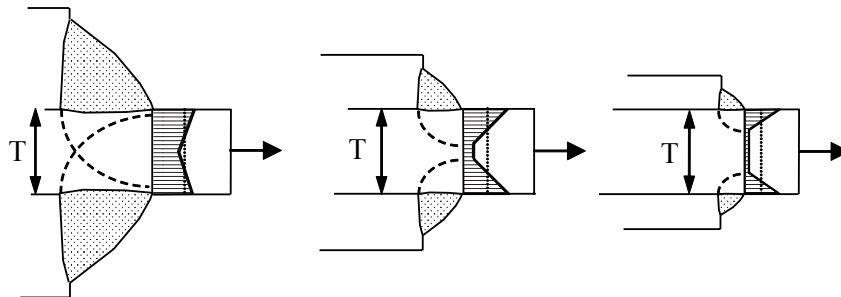
$$\sigma_{sa} = K_{sa} \cdot \sigma_{nom} \quad (3.27)$$

where  $K_{sa}$  is the modified structural stress concentration factor and  $\sigma_{nom}$  is the nominal stress in the base metal. The value  $K_{sa}$  can be easily computed by the following equations:

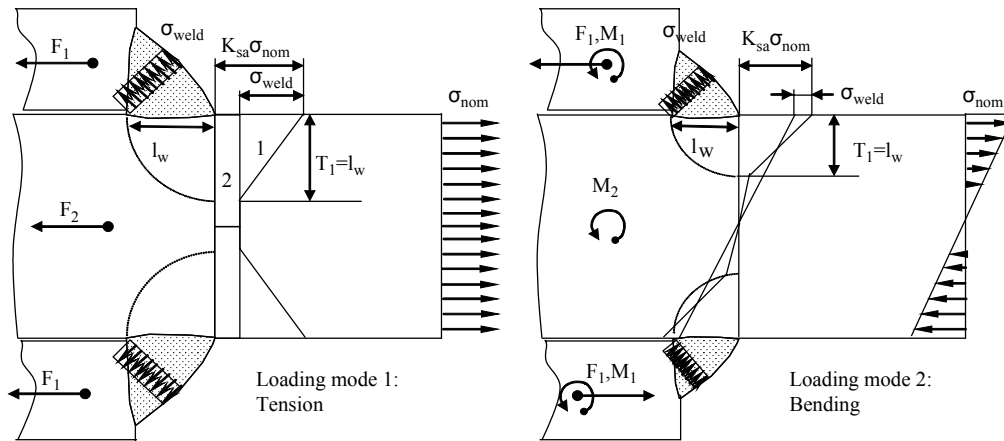
$$K_{sa} = 1 + \frac{\sigma_{weld}}{\sigma_{nom}} \left(1 - \frac{l_w}{T}\right), \quad l_w \leq \frac{T}{2} \quad (3.28)$$

$$K_{sa} = 1 + \frac{\sigma_{weld}}{\sigma_{nom}} \left(\frac{T}{4l_w}\right), \quad l_w \geq \frac{T}{2}$$

Two load cases of tension only and bending only are presented in Figure 3.30. In



**Figure 3.29:** *Structural stress distribution for fully load carrying welds, after [34]*



**Figure 3.30:** *Structural stress according to Poutiainen and Marquis [34]*

addition to that, this method is also applicable to structures subjected to a combination of bending and membrane stresses. For such cases, the  $\sigma_{nom}$  has to be defined as for a bending only loading mode and thereafter Equation 3.28 can be used to obtain  $K_{sa}$  and consequently the modified structural stress. FEM models with relative coarse meshes of plate, shell or solid elements can be constructed for stress analysis.

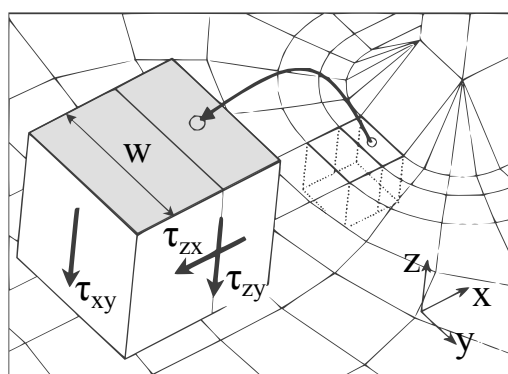
In order to verify the accuracy of this method, the authors have compared the estimated fatigue strengths of fully load-carrying attachments based on linear elastic fracture mechanics (LEFM) and the proposed concept. The results show an excellent correlation for different plate thicknesses and loading modes. Moreover, the method is experimentally verified based on the published fatigue test results.

### 3.2.10 Comparison of different SHSS determination procedures

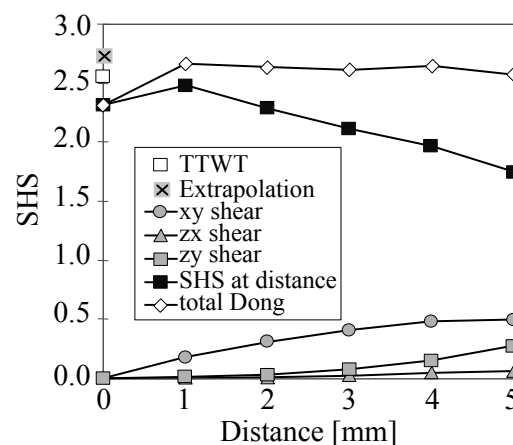
Due to the increasing number of proposed methods for structural stress determination, several researchers have comparatively studied these methods. The comparisons have been mainly focused on the mesh sensitivity, applicability to different welded joints, relative accuracy to estimate the fatigue strength of studied details and the limitations of these approaches. This section aims to provide a summary of some of these investigations.

Doerk et al. [8] compared the calculated structural stress based on the surface stress extrapolation and Dong method for four different structural details. The surface stress extrapolation is applied according to the recommendations for fine and coarse mesh densities and the results appeared to be almost identical provided that certain rules regarding the element types and sizes are followed. The results also confirm the mesh insensitivity claimed by Dong in case of 2D problems. However, in case of 3D models, the results obtained from different mesh densities exhibit a scatter which is anticipated to be as a result of neglecting the transverse shear stresses in the element sides. Eventually, since the SHSS definition suggested by both methods is equivalent, the authors conclude the applicability of the same SHSS design S-N curves irrespective of the adopted calculation method.

Poutiainen et al. [46] implemented through thickness stress linearisation at the weld toe in addition to the methods exploited in the above investigation. In case of 2D elements, the linear surface extrapolation approach is addressed as the most sensitive method to mesh variations. When one element in thickness direction is used, all methods are reported to yield consistent results. Additionally, in case of 3D elements, the authors report a considerable dependency of the results obtained by the Dong and through thickness stress linearisation methods to the element stress determination procedure during post-processing. Nodal averaging, in particular,



(a) The shear stresses acting on the element sides



(b) The effect of  $\delta$  on the calculated Dong structural stress

**Figure 3.31:** The effect of element side shear components on the calculated Dong stress, after [46]



appeared to be a very influential factor when these two methods are used. The effect of neglecting the stresses in the element sides when using Dong method ([8]) is also confirmed in this study, see Figure 3.31. The authors also show that at  $\delta = 0.4t$  this effect is negligible and both trough thickness linearisation at the weld toe and Dong method yield the same results.

In a similar study, Fricke and Kahl [30] utilized the surface stress extrapolation, Dong approach and Xiao and Yamada [33] method to compute the SHSS for several structural details. They observed that the element sizes and properties as well as the weld modeling in shell elements are the main reasons for variations of predicted fatigue lives. However, the fatigue lives predicted by these three methods, which were generally conservative compared to the fatigue tests, are reported to be comparable. Furthermore, the authors have asserted the existing beneficial residual stresses as the main reason for the large differences between predicted fatigue lives and the test results.

Notaro et al. [49] evaluated the fatigue strength of a widely used complex ship detail using the conventional surface stress extrapolation method, the more recent approach proposed by Xiao and Yamada [33] and experimental investigations. Based on comparisons between the fatigue test results and fatigue lives obtained from the two mentioned methods, the authors reported a good agreement between the employed analytical and experimental fatigue evaluation methods.

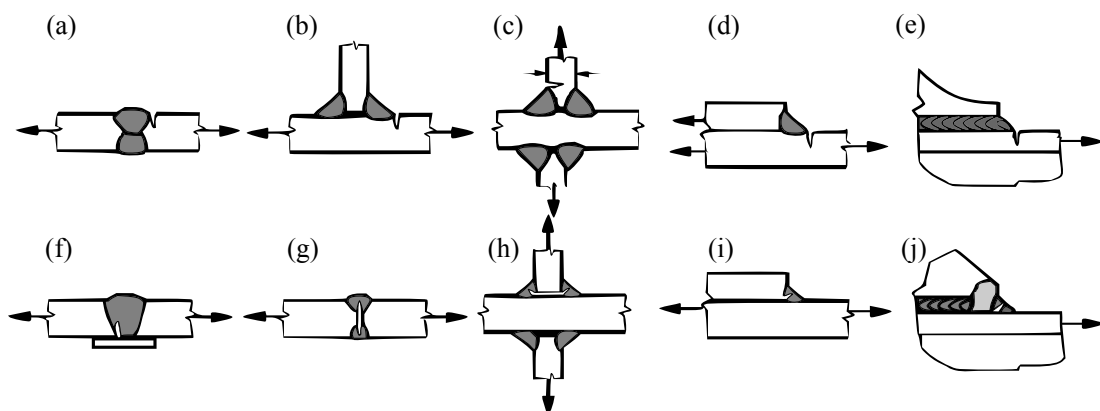
Kim and Kang [50] investigated the application of surface stress extrapolation method and the Dong method for attachments welded to the plate edge i.e. type 'b' attachments. They also experimentally verified the FE analysis by conducting fatigue tests for 12 specimens. The results revealed a lower structural stress obtained from the Dong method compared to the surface stress extrapolation method. Nevertheless, comparatively evaluating, the fatigue life predictions using these methods is reported to be in a better agreement with the test results than the predicted fatigue lives obtained from the nominal stress method. In addition to that, the authors have proposed the use of a thickness correction factor in conjunction with the Dong method to derive more accurate results.

Fricke [51] assessed the fatigue life of partially load-carrying cover-plates and fully load-carrying lap joints using both experimental evaluations and FE-based local approaches. The surface stress extrapolation, Xiao and Yamada [33] method and the method proposed by Poutiainen and Marquis [34] were the approaches exploited by Fricke [51] to determine the SHSS. The analysis results showed that the surface stress extrapolation method yields similar results irrespective of the joint type, although being slightly non-conservative. Moreover, the Xiao and Yamada [33] approach appeared to give more consistent results with reference to the joint type. The conservative results obtained from this method are mentioned to be more reasonable when using the maximum principal stress. Similarly, the method proposed by Poutiainen and Marquis [34] produced conservative results while being more affected by the joint type alteration.

### 3.2.11 Limitations

The structural hot spot stress method as a fatigue assessment method for plated structures is still an inexperienced method compared to the nominal stress method. Some of the most important shortcomings and limitations of this method are presented below:

- As it is depicted in Figure 3.32 fatigue cracks can initiate either from surface at weld toe or from weld root. At the time being, the structural hot spot stress approach is only applicable to fatigue assessments of weld toe cracks, i.e. Figure 3.32a–e. Thus, for cracks initiating from weld root, i.e. Figure 3.32f–j, other assessment methods such as the nominal stress or the effective notch stress methods have to be used. The limitation of the SHSS to only surface failures is considered as the main drawback of this method. It should be noted that several investigations around the world are being performed to adapt the SHSS approach for the weld root assessment as well ([11]). However, this topic is not yet included in any design code.
- The SHSS approach is a suitable fatigue assessment method only where the evaluated stress is acting mainly perpendicular to the weld toe. IIW recommendations [10] proposes to use maximum principal stress acting in range of  $\pm 60^\circ$  with the perpendicular to the weld toe. The assessment of other stresses parallel to the weld or shear stresses should be done using other methods such as the nominal stress method.
- At the moment, only surface stress extrapolation method is included in the design codes and guidelines. As it was discussed earlier, this method of SHSS determination has certain requirements regarding the mesh density. Besides, in order to obtain results with an acceptable accuracy, the welds should be modeled. Thus, the modeling procedure becomes more time-consuming and cumbersome. In short, the uncertainty of the extrapolation procedure is another drawback of the SHSS approach.
- The designer should verify in advance that the detail under investigation will



**Figure 3.32:** *Different locations of crack initiation in the welded details, after [10]*

not fail from the root. This can be achieved by performing preliminary finite element analysis, experimental evaluation of similar details or observation of existing analogous details that have been cracked during their service life.

### 3.2.12 Fatigue design based on the SHSS

In contrast to the nominal stress method, when the design procedure is carried out based on the SHSS approach, standard constructional details are not associated with the design S-N curves. Instead, fatigue design classes (FAT) are attributed to details with reference to the weld type [24]. Table 3.2 represents the classifications based on the weld type according to IIW recommendations [10]. As it is apparent, the extensive number of constructional details defined for the nominal stress method, are replaced with 9 weld types.

As reported by Maddox [39], the choice of appropriate SHSS design S-N curve is considered one of the main issues regarding the SHSS application for plate-type welded joints. At the moment, the relevant SHSS design S-N curves proposed by Eurocode 3 and IIW recommendations are based on comprehensive evaluations of available fatigue test data for fillet-welded cruciform joints and transverse attachment joints [52]. The findings of these studies have led to the implementation of FAT 100 for non-load carrying welds and FAT 90 for load-carrying welds. An exception is the longitudinal edge attachments ( $L > 100mm$ ) for which FAT 90 should be applied. Figure 3.33 demonstrates the recommended SHSS S-N curves and pertinent definitions.

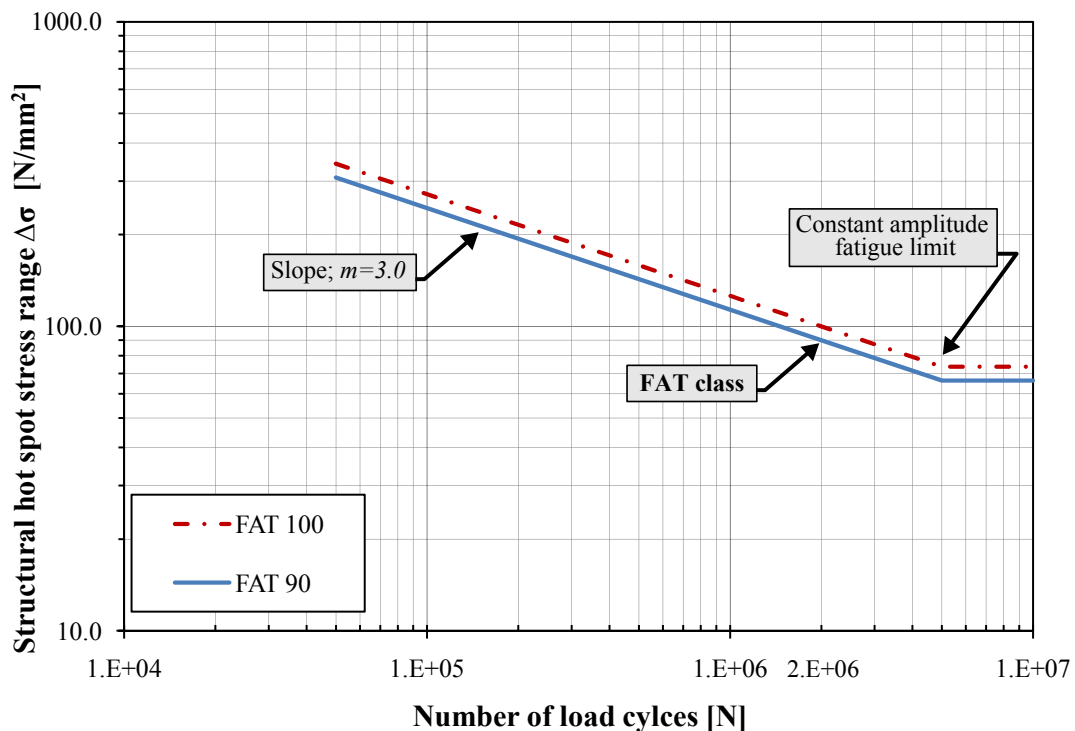

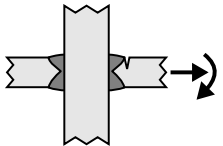
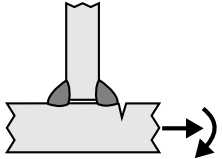
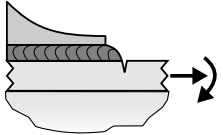
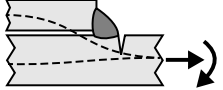
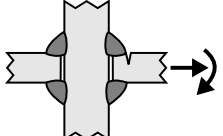
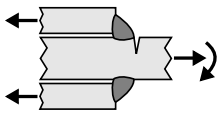
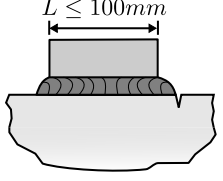
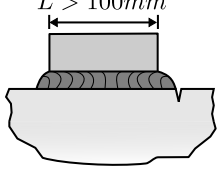


Figure 3.33: Structural hot spot stress design S-N curves

**Table 3.2:** IIW recommendations [10] design categories for steel plated details based on the structural hot spot stress approach

| No. | Weld detail   | Description   | Requirements  | FAT        |
|-----|---|---|---|------------|
| 1   |    | Butt joint  | As welded, NDT  | <b>100</b> |
| 2   |    | Cruciform or T-joint with full penetration K-butt welds | K-butt welds, no lamellar tearing   | <b>100</b> |
| 3   |    | Non load-carrying fillet welds                          | Transverse non-load carrying attachment, not thicker than main plate, as welded | <b>100</b> |
| 4   |    | Bracket ends, ends of longitudinal stiffeners           | Fillet welds welded around or not, as welded                                    | <b>100</b> |
| 5   |  | Cover plate ends and similar joints                     | As welded   | <b>100</b> |
| 6   |  | Cruciform joints with load-carrying fillet welds        | Fillet welds, as welded   | <b>90</b>  |
| 7   |  | Lap joint with load carrying fillet welds               | Fillet welds, as welded   | <b>90</b>  |
| 8   |  | Type 'b' joint with short attachment                    | Fillet or full penetration weld, as welded                                      | <b>100</b> |
| 9   |  | Type 'b' joint with long attachment                     | Fillet or full penetration weld, as welded                                      | <b>90</b>  |

### 3.3 Effective notch stress method

The notch stress is the total stress at a local notch formed by the weld toe or the weld root, based on linear elasticity theory. This stress concept, which includes all the stress raisers effects at the local notch, is consisted of the sum of geometrical stress and non-linear stress peak. Fatigue life assessment based on the notch stress is known as the effective notch stress method. This method, that does not considers the elastic-plastic material behavior at the crack tip, is based on the highest computed elastic stress at the critical points, i.e. weld toe and weld root.

The effective notch stress method was first introduced by Radaj and Sonsino [5], by considering stress averaging in the micro-support theory according to Neuber Rule with a fictitious radius of 1mm for plates thicker than 5mm [10]. As illustrated in Figure 3.34, the reference notch radius is calculated assuming the worst case when the transition radius is absolutely sharp ( $\rho = 0$ ). However, in welded joints, the real notch radius varies widely. When the micro-support length ( $\rho^*$ ) is extended to 0.4mm with the appropriate constraint factor (2.5 for steel members), the final notch radius becomes 1mm [53]. The rounding of the weld root and weld toe based on the effective notch stress method is shown in Figure 3.35.

Fatigue analysis of welded joints using the effective notch stress method is briefly included in the IIW recommendations [10]. As shown in Figure 3.36, FAT225 can be used to design all the structural details irrespective of the loading type and geometry. However, in order for the numerical methods such as the finite element method to be capable of calculating the total stress at the critical sections, a sufficient element density should be maintained. Thus, in order to get accurate results, it is principally important in this method to model the anticipated crack initiation area with an extremely fine mesh. This can be achieved by using 3D solid elements as well as 2D planar elements as long as a certain mesh size is generated.

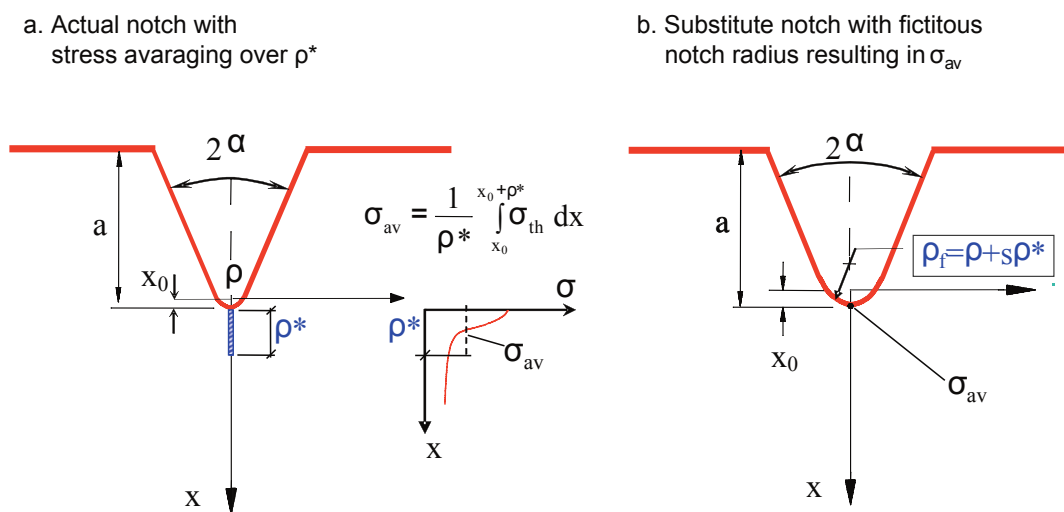
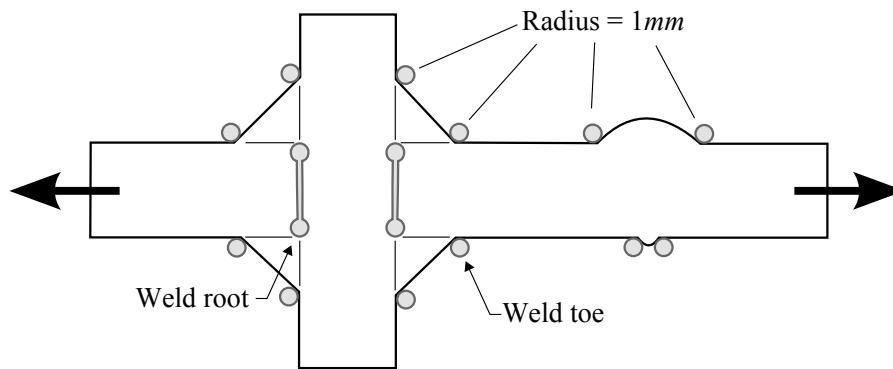
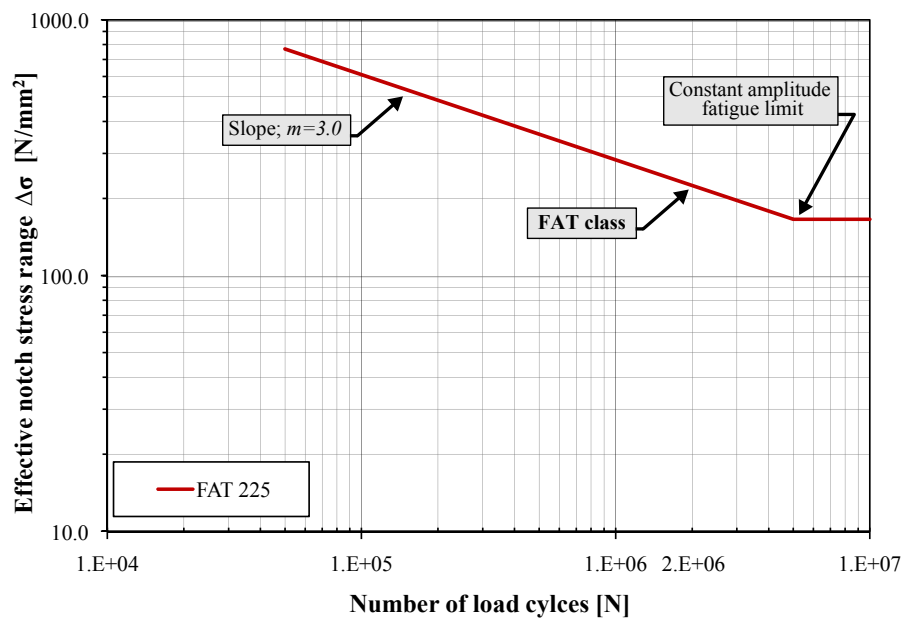


Figure 3.34: Neuber's micro-support concept

Guideline for the fatigue assessment by notch stress analysis for welded structures [54] has recommended the appropriate element sizes for analysis according to this method. It should be noted that, only nodal values are allowed to be used directly for analysis of this kind. In addition to that, maximum principal stress component should be used. Table 3.3 lists the recommended element density for the analysis based on the effective notch stress method.



**Figure 3.35:** Rounding of the weld toe and weld root in the effective notch stress method



**Figure 3.36:** The only proposed fatigue design S-N curve for all structural details

**Table 3.3:** Recommended element sizes for the effective notch stress method application, after Fricke [54]

| Element type | Relative size | size for r=1mm |
|--------------|---------------|----------------|
| Quadratic    | $\leq r/4$    | $\leq 0.25mm$  |
| Linear       | $\leq r/6$    | $\leq 0.15mm$  |

# 4 Fatigue Life Assessment of Longitudinal Non-Load-Carrying Attachments

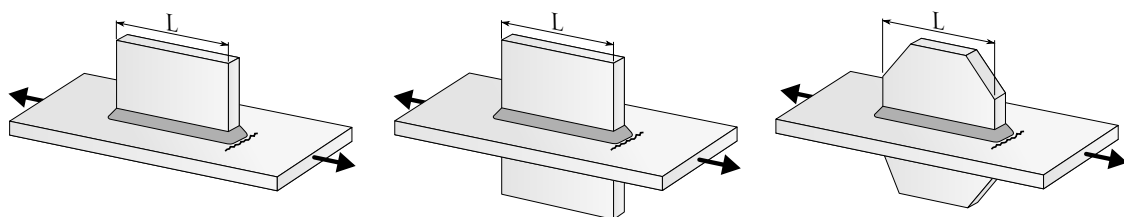
## 4.1 Introduction

Longitudinal non-load-carrying attachments are commonly used in many fatigue loaded structures such as ships, cranes, offshore structures and bridges. The universal use of this type of attachment has made it one of the most frequent fatigue tested details.

In addition to that, it has been observed that the weld terminations often exhibit a very poor fatigue performance. Longitudinal non-load carrying attachments have been frequently employed to investigate this matter. On the one hand, these attachments offer a simple way to create a severe notch of reproducible severity [2] and on the other, since this detail is usually made symmetrical, the weld distortions caused by bending effects can be disregarded. In this study, for simplicity, the longitudinal non-load carrying attachments will be referred to as *longitudinal attachments*. Figure 4.1 demonstrates schematics of the most common type of longitudinal attachments.

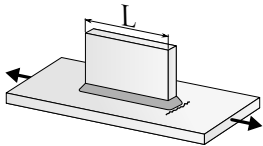
For fatigue assessments based on the nominal stress method, the classification for longitudinal attachments varies according to the attachment length. Nevertheless, IIW recommendations [10] and Eurocode 3 [9] propose dissimilar grouping for this detail. Eurocode 3 groups it into several categories for attachments with lengths less than 100mm, whereas IIW classification covers a wider range of attachment lengths up to 300mm. Tables 4.1 and 4.2 list the instructions given by Eurocode 3 and IIW, respectively.

In this section the credibility of these classifications is investigated. The finite element modeling procedure is comprehensively explained. Moreover, the influencing factors such as the weld size, attachment height, attachment thickness etc. are studied in more detail. Eventually, the findings are summarized and recommendations are given.

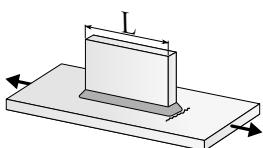


**Figure 4.1:** *Longitudinal non-load carrying attachments*

**Table 4.1:** *Fatigue classification of longitudinal attachments based on the nominal stress method according to Eurocode3 [9]*

| Structural detail   | Description   | Requirements        | FAT       |
|---|---|---------------------|-----------|
|  | Longitudinal attachments:<br>The detail category varies according to the length of the attachment (L) | $L \leq 50mm$       | <b>80</b> |
|   |   | $50 < L \leq 80mm$  | <b>71</b> |
|   |   | $80 < L \leq 100mm$ | <b>63</b> |
|   |   | $L > 100mm$         | <b>56</b> |

**Table 4.2:** *Fatigue classification of longitudinal attachments based on the nominal stress method according to IIW recommendations [10]*

| Structural detail   | Description                                   | Requirements | FAT       |
|---|---|--------------|-----------|
|  | Longitudinal fillet weld gusset with length L | $L < 50mm$   | <b>80</b> |
|   |   | $L < 150mm$  | <b>71</b> |
|   |   | $L < 300mm$  | <b>63</b> |
|   |   | $L > 300mm$  | <b>50</b> |

## 4.2 Test database

Experimental fatigue test results for longitudinal attachments have been collected from the 1950s till present. The test programmes including longitudinal attachments have been performed for various investigations. Evaluation of residual stresses, material strength effect, welding process and material effect, post weld treatment to improve fatigue behavior are some examples of these investigations.

Consequently, not all the test data can be included for further evaluations within the scope of this study. Thus, the test database is re-analyzed and only the test specimens in the as-welded condition are selected. The outcome is a total number of 662 test results.

As a result of the high number of collected tests, a large range of variables are covered by the tests. This can lead to high scatter of the results. Therefore, the available tests were further classified based on different variables such as the attachment length, main plate width and thickness, research programme etc. Additionally, this provides a solid basis for further evaluations of the influencing factors.

The statistical evaluation of the test data was performed according to Eurocode 3 requirements. The mean and characteristic value, respectively equal to 50% and 97.7% safety probability, were calculated for each test series.



### 4.3 Literature review

Smith et al. [55] reported that dissimilar to the transverse attachments in which a 2D finite element analysis is adequate, the determination of Stress Concentration Factor (SCF) in case of longitudinal attachments requires a 3D finite element model. Additionally, Smith and Gurney [56] calculated the Stress Intensity Factor (SIF) in longitudinal attachments using linear elastic fracture mechanics as follows:

$$K_{weld} = M_K \cdot Y \cdot S \cdot \sqrt{\pi a} \quad (4.1)$$

where  $K_{weld}$  is the stress intensity factor for the weldment,  $M_K$  is the weld geometry correction factor,  $Y$  is the geometry correction factor,  $S$  is the applied remote stress and  $a$  is the crack length. Based on the results, the authors suggested that the fatigue life can be improved by:

- Decreasing the attachment length below 152.4mm
- Decreasing the attachment height below 50.8mm
- Decreasing the attachment thickness below 12.7mm
- Increasing the weld leg length
- Decreasing the main plate width below 127mm
- Increasing the main plate thickness

Similarly, Hobbacher [57] derived a relation based on 3D FEA for the weld geometry correction factor ( $M_K$ ) of longitudinal attachments. He addressed the plate thickness, attachment length, plate width and weld angle as the most important fatigue life influencing factors. Dahle and Larsson [58] also investigated the influencing factors on  $M_K$  by including the cold-lap defects in the FEM models.

Huther et al. [59] also performed experimental and analytical investigations on longitudinal attachments with thicknesses between 4 and 20mm. The following conclusions were obtained based on the parametric analysis:

- Length and height of the attachment have little influence on the calculated SCF
- The SCF increases by increasing the attachment thickness
- The stress gradient decreases by reducing the attachment angle
- The stress gradient increases more quickly for symmetrical specimens compared to non-symmetrical specimens (one-sided attachment)

## 4.4 Finite element modeling and analysis

The finite element analysis program ABAQUS software version 6.9-2 [60] was implemented for modeling and processing of the results. This program offers a wide range of modeling possibilities and takes advantage of a comprehensive documentation. In this section, the modeling procedure in the mentioned software is elaborately explained.

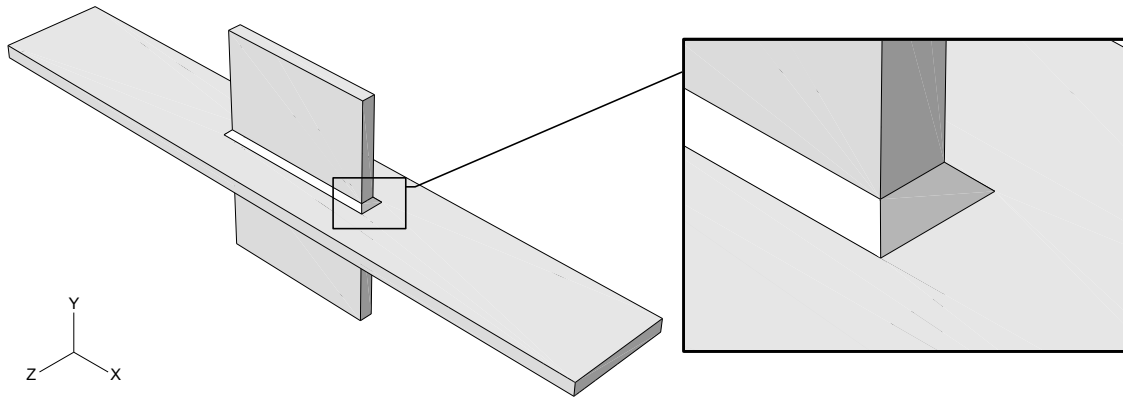
### 4.4.1 Geometry

As it was mentioned in Section 4.3, the fatigue life assessment of longitudinal attachments can be only investigated using 3D FE models. Therefore, shell or solid FE models can be used in this case. The findings of several investigations, studying the accuracy of various modeling techniques, have shown the good agreement of solid element models with experimental measurements [6, 11, 61]. However, the application of these elements with a relatively fine mesh, demands high computational possibilities in addition to the substantial modeling effort. As the aim of this study is not to investigate different modeling techniques, solid element models are employed to construct the FE models. In this way, the inaccuracies attributed to the finite element analysis can be minimized.

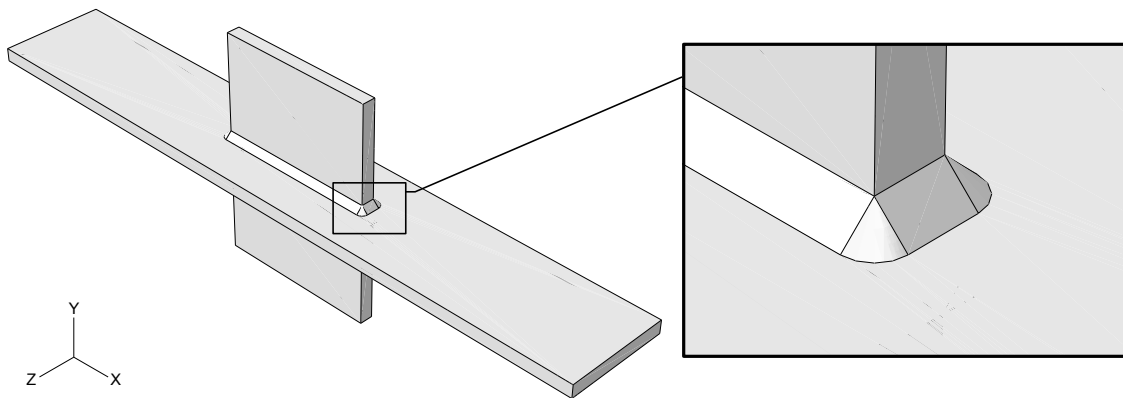
At least one solid element model was created for each test series using the theoretical reported values in the test documentation. Although the ABAQUS software provides the possibility to model only portions of the symmetrical details, the whole model were created in order to avoid possible errors at the boundaries of symmetry. Furthermore, the FE models for this detail are not often huge and modeling the entire structure does not require much higher effort.

When using solid models, the weld has to be included in the FE model. This can be achieved by different techniques. It was previously reported by Akhlaghi [61] that modeling the fillet welds in solid element models by chamfering two intersecting volumes can cause minor problems at the edges. The ‘extrude’, ‘revolve’ and ‘sweep’ features provided by the part module of the software are other possibilities to model the weld volume. Depending on the desired final shape of the weld, any combination of the mentioned features can be used.

Figure 4.2 illustrates a longitudinal attachment geometry in which the weld is modeled by extruding the attachments to the main-plate applying a draft angle of  $45^\circ$ . As it is apparent, the generated weld shape has sharp corners. By definition, as long as the weld stiffness is included in the model, the weld shape does not have considerable effect on the calculated SHSS. However, as the surface stress extrapolation method is employed to determine the SHSS, the severity of the notch can affect the nodal stresses close to the weld and consequently the SHSS. A more realistic weld shape can be generated by using a combination of extrude and revolve features as shown in Figure 4.3. The demonstrated weld volume has been



**Figure 4.2:** *Modeling the weld with sharp corners in longitudinal attachments*

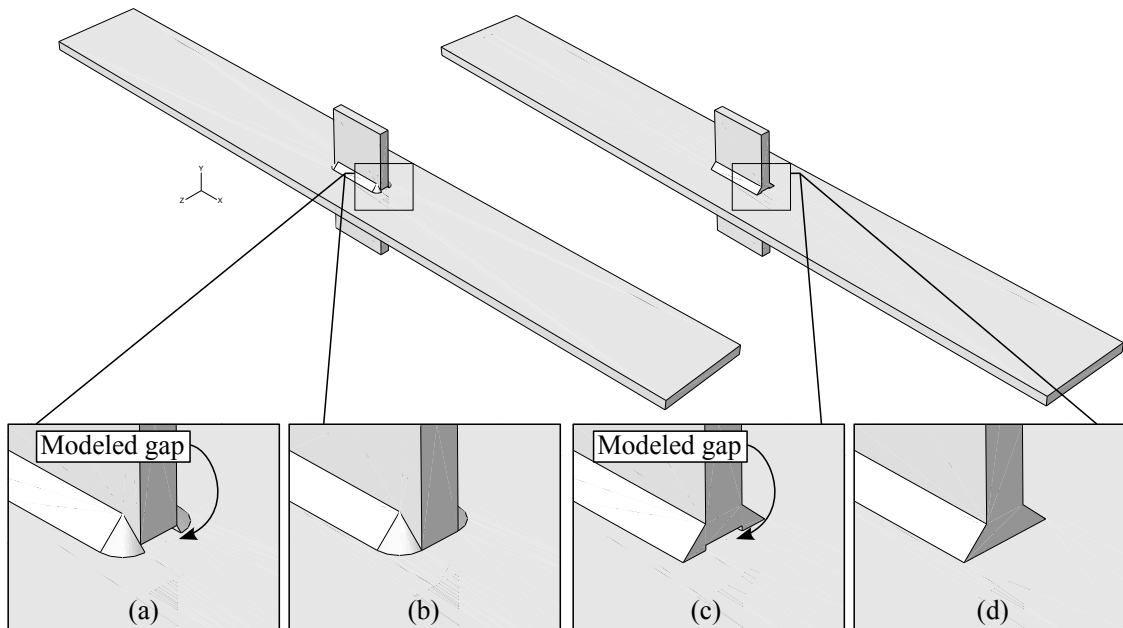


**Figure 4.3:** *Modeling the weld with round corners in longitudinal attachments*

generated by extruding the weld parallel to the attachment edges and revolve it  $90^\circ$  around the attachment corners. Although, the latter procedure for weld generation is more time-consuming and cumbersome, it is believed to yield more accurate results. Thus, in this study, welds with round corners have been generated for the longitudinal attachments with end welds. Moreover, the gap between the attachment and the main-plate is not modeled.

For the case of longitudinal attachments without end welds, modeling the weld end is more controversial. Up to date, there is no explicit recommendation of how to model a weld end for the SHSS determination. In addition to that, when omitting the end welds during the welding procedure, the welder does not have full control over the finished weld end angle. Therefore, several alternatives of modeling the weld in attachments without end welds are investigated.

Figure 4.4 depicts the studied weld end FE models. The results revealed a variation of 11% for the determined structural hot spot stresses based on the different models. It was observed that when the gap is modeled (Figure 4.4a and c), the computed SHSS is underestimated. Additionally, when the weld end is modeled according to Figure 4.4d, no clear extrapolation path can be selected for the SHSS



**Figure 4.4:** *Different techniques to model the weld end for the case of longitudinal attachments with omitted end welds*

determination. This is a result of the abrupt introduction of the weld end at the intersection point. Hence, with reference to the above discussion, the weld ends for the case of longitudinal attachments with omitted end welds were modeled as shown in Figure 4.4b.

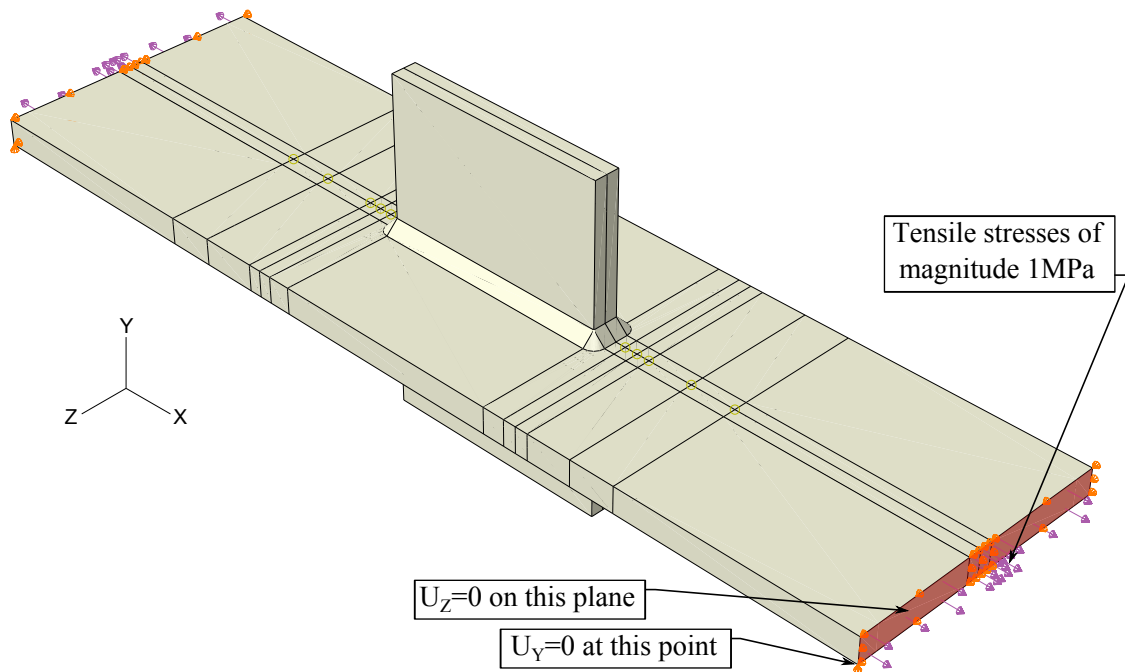
#### 4.4.2 Material properties

A typical steel with elastic modulus of  $E = 210GPa$  and Poisson's ratio of  $\nu = 0.3$  was defined and assigned to the entire geometry including the welds. It should be mentioned that, since elastic material behavior can be assumed for the fatigue analysis of this kind, only elastic material properties are needed to be defined.

#### 4.4.3 Loading and boundary conditions

As mentioned, elastic material behavior is assumed. Therefore, a linear elastic analysis with stresses linearly proportional to the applied load can be defined. For the sake of simplicity, two unit stresses equal to  $1MPa$  were applied on both sides of the specimens. As a result, the actual stresses for each specimen and each loading level can be obtained by multiplying the analysis results by the actual applied stresses.

Furthermore, boundary conditions are chosen in such way to simulate the real applied boundaries during testing. In addition to that, boundary conditions should be chosen to avoid stability and singularity issues in the FE model. Therefore, min-

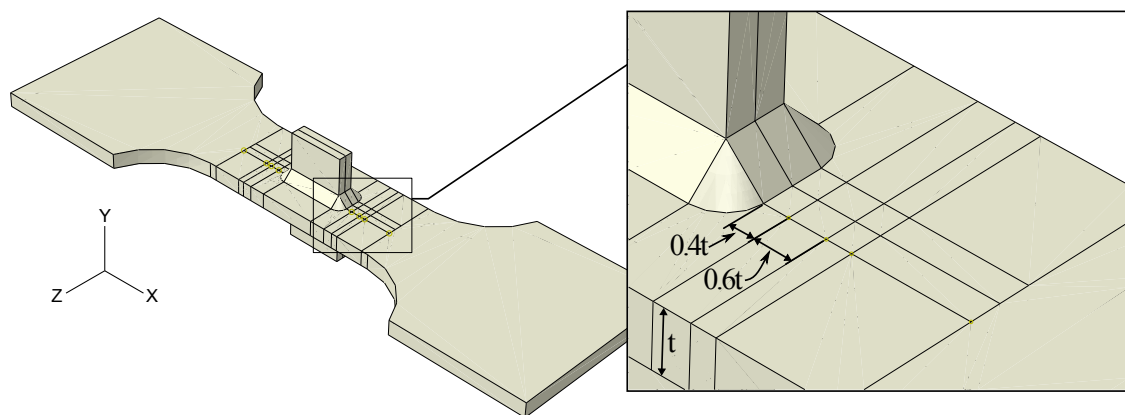


**Figure 4.5:** Loading and boundary conditions for the FE models; Identical for both ends

imum translational restrains in directions other than the load application direction should be provided. Figure 4.5 demonstrates the applied loading and boundary conditions for the FE models. It should be noted that, the boundary conditions are identical for both ends of the specimens.

#### 4.4.4 Partitioning, meshing and element types

The fatigue crack in longitudinal attachments initiates from the plate surface at the weld toe. Therefore the hot spot can be classified under hot spots type ‘a’.

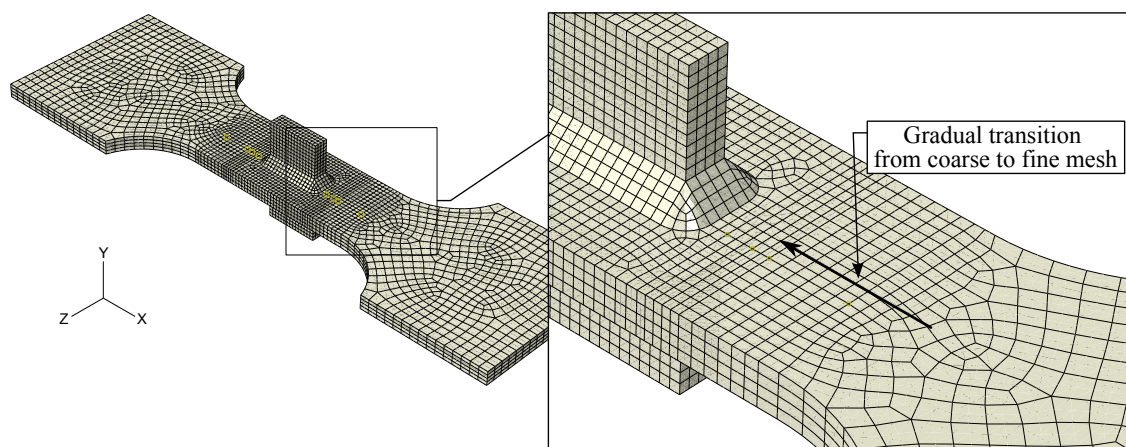


**Figure 4.6:** Partitioned area in front of the weld toe to allow for linear stress extrapolation

As it was discussed earlier, both linear and quadratic extrapolation methods can be applied for this kind of hot spot providing that a fine mesh is constructed. In this study both methods are implemented. Consequently, as for the SHSS determination the nodal stresses are recommended to be used, the geometry should be partitioned in an appropriate way. The edges of the partitions should intersect at the desired extrapolation nodes to facilitate the formation of element's corners at these points. Figure 4.6 demonstrates a partitioned geometry utilized to calculate the SHSS using a linear extrapolation.

The next step is to mesh the partitioned geometry to comply with the minimum requirements of the mesh density at the hot spot area. The mesh size at areas far from the hot spot does not need to be as fine as in the hot spot area. Thus, a coarser mesh can be constructed in these areas. However, the transition from a coarse mesh to a fine mesh should be gradual. This can be achieved by dividing the transition area to several sub-partitions and gradually change the mesh density. Another alternative is to define element nodes proportionally along the longitudinal edges in the geometry such that more element nodes are attributed to regions closer to the hot spot. Figure 4.7 illustrates the meshed model of the partitioned geometry shown in Figure 4.6. As can be seen in this figures, a gradual transition from coarse to fine mesh has been obtained by dividing the geometry to several sub-partitions.

20-node isoparametric solid elements with reduced integration (C3D20R) are used for all the models. In order to have more control over the element nodes, 'Structured meshes' are generated at the areas close to the hot spot. However 'Hex-dominated meshes' can be used for other areas further form the hot spot as this option provides more flexible nodal placements. This will lead to a reduction in the total number of constructed elements and reduce the model size considerably in some cases.



**Figure 4.7:** *The meshed model of the partitioned geometry shown in Figure 4.6*

#### 4.4.5 Post-processing of the results

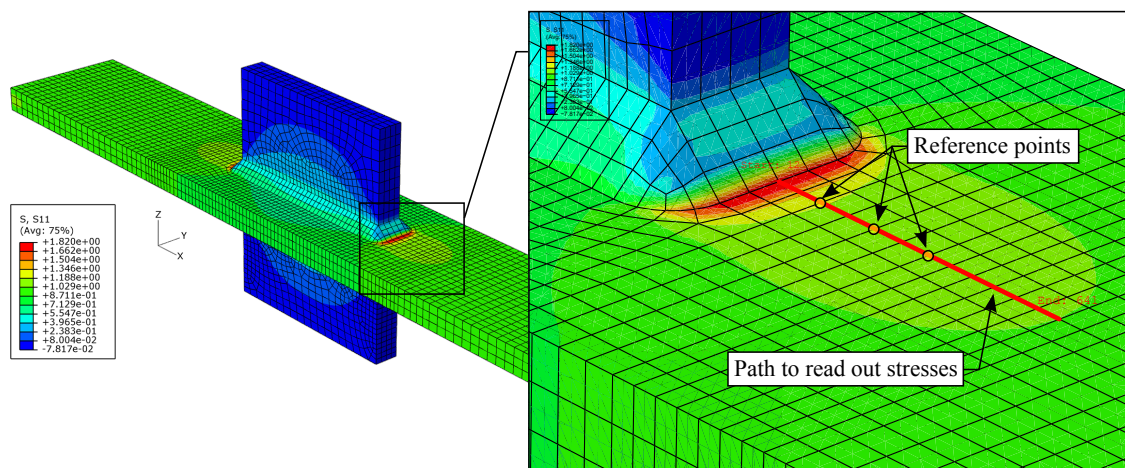
In order to calculate the hot spot stress by extrapolating the surface stress values at certain reference points, the stress profile in front of the hot spot, i.e. weld toe, has to be obtained. This can be archived by defining a path perpendicular to the weld toe and extracting the stress field results. Figure 4.8 demonstrates an example of a defined path in order to obtain the surface stress profile at the weld toe.

Having the stress profile obtained, the nodal stress values at the reference points can be adopted to calculate the hot spot stress according to Equations 3.16–3.20. It should be noted that Niemi et al. [11] have recommended to extract the stress values while the stress averaging function of the post-processing software is turned off. However, it has been confirmed by [61] that the averaging function mainly affects the stresses at the weld toe itself and does not affect the calculated SHSS. Therefore, in this study, the aforementioned feature was kept active.

Furthermore, since a unit stress (1MPa) was applied to the FE models, the output was interpreted as the structural hot spot stress concentration factor ( $K_{hs}$ ). Subsequently, the equivalent hot spot stress ( $\sigma_{Hotspot}$ ) corresponding to the actual test stress range ( $\sigma_{Nominal}$ ) were obtained as follows:

$$\sigma_{Hotspot} = K_{hs} \cdot \sigma_{Nominal} \quad (4.2)$$

Eventually, the corresponding SHSS S-N curve was plotted by replacing the nominal stress with the calculated hot spot stress. The same procedure can also be applied to obtain the effective notch stress S-N curves.



**Figure 4.8:** A path defined along the extrapolation points to extract the stress data

## 4.5 Influencing factors

The collected fatigue test data for this detail dates back to 1950. As a result, good documentations of the tests were missing in most cases. For instance, the weld leg length is one of the parameters that were missing in most of the tests. Therefore, since the whole geometry including the welds had to be modeled, the effect of different parameters on the stress concentration factor is investigated. This way, in case of a missing parameter in the test description, a reasonable assumption can be made providing that its effect is proved to be negligible.

Moreover, by determining the effect of different parameters, the accuracy of the proposed fatigue assessment classifications can be investigated. For example, fatigue design regulations regarding both double-sided and one-sided longitudinal attachments is identical according to IIW recommendations and Eurocode 3. Hence, in order to check the reliability of this recommendation, finite element analysis have been carried out to investigate the effect of detail symmetry. The effect of weld size variation, attachment height, attachment thickness, chamfer angle, main-plate width and thickness, and attachment length are other influencing factors that are presented in this section.

### 4.5.1 Weld size effect

Weld size is one of the parameters that was often missing in the test documentations. However, due to practical considerations, the variation range of this parameter is limited. In order to investigate this issue, a typical double-sided longitudinal attachment with  $L=150\text{mm}$  and  $t=16\text{mm}$  were modeled using several weld throat thicknesses within the practical range. The stress distribution in front of the weld toe and the linearly extrapolated SHSS for different cases are plotted in Figure 4.9. The results confirm that varying the weld throat thickness from 3.5 to 7 mm alters the calculated structural stress concentration factor with less than 5%. Therefore, the effect of varying this parameter within the range of practicality can be assumed insignificant.

Nevertheless, IIW recommendations [10] has defined a minimum weld throat thickness equal to one third of the main plate thickness. Thus, the defined minimum weld throat thickness is assumed in case of an unknown weld throat thickness.

### 4.5.2 Attachment thickness effect

Similar to the weld size, there is a lack of information in a majority of the reported tests for attachment thickness. Thus, the possible effects of varying the attachment thickness was also investigated. The finite element analysis results of longitudinal attachments with different attachment thicknesses are shown in Figure 4.10. It is apparent that the calculated SHSS deviates less than 2% for different attachment thicknesses and therefore the effect of this parameter on the structural hot spot stress can be considered negligible.



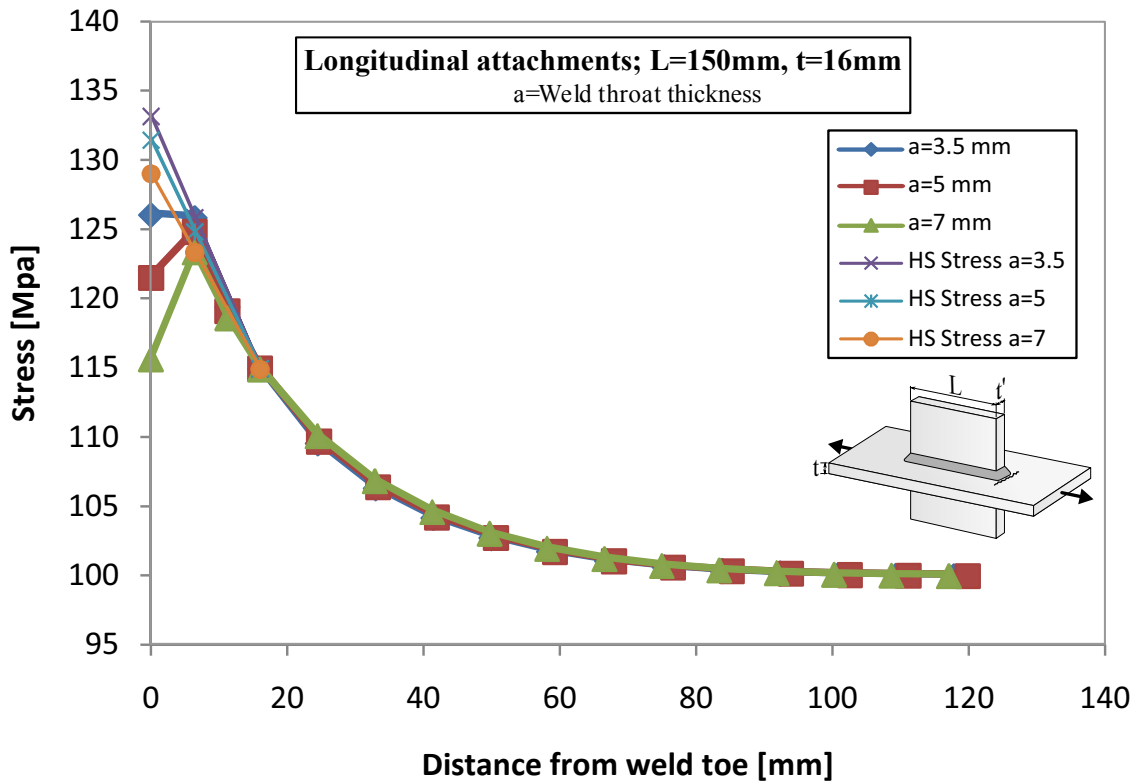


Figure 4.9: Stress distribution and extrapolated SHSS paths for longitudinal attachments with various weld throat thicknesses

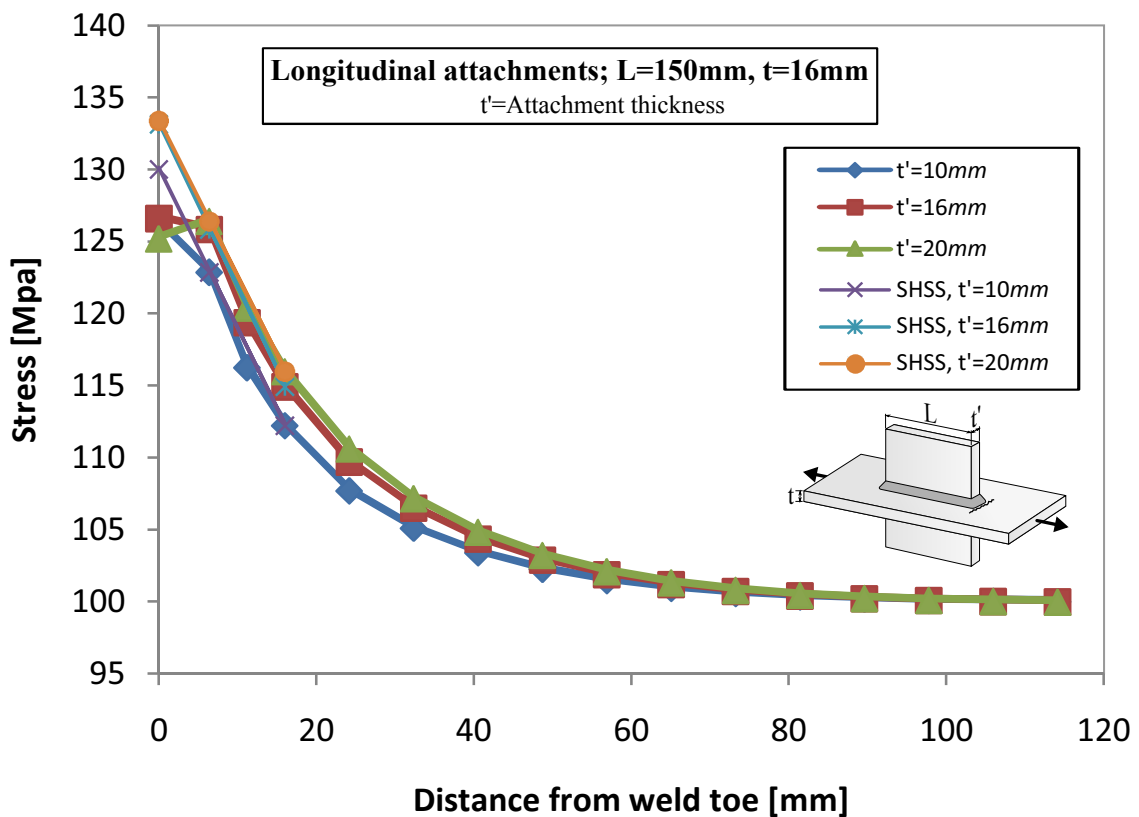


Figure 4.10: Stress distribution and extrapolated SHSS paths for longitudinal attachments with various attachment thicknesses

In the current study, in case of unknown gusset thickness, the same thickness as the main-plate was considered.

### 4.5.3 Chamfer angle effect

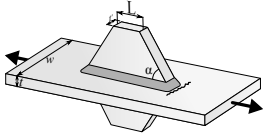
In case of chamfered longitudinal attachments,  $L > 100mm$ , with a chamfer angle ( $\alpha$ ) less than  $45^\circ$ , Eurocode 3 upgrades the recommended fatigue class from 56 to 71, see Table 4.3. In this section, the possible effects of chamfering the longitudinal attachments are investigated.

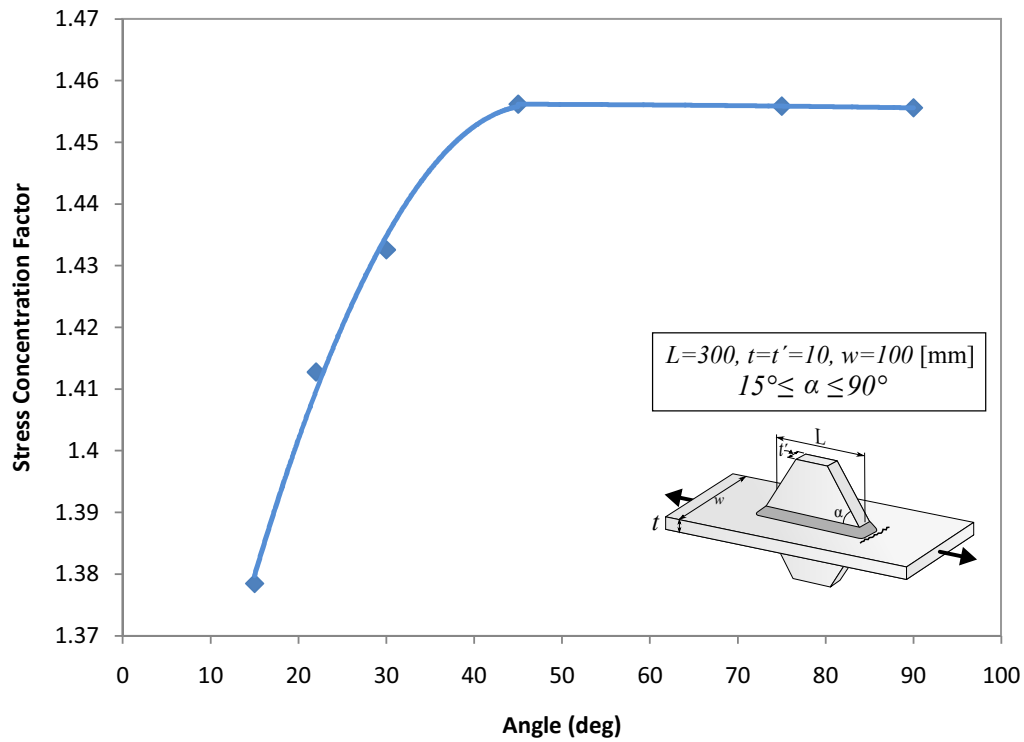
In a case study, longitudinal stiffeners with attachment angles varying from  $15^\circ$  to  $90^\circ$  were investigated by means of finite element analysis. All other parameters were kept constant to eliminate further variations. As it is shown in Figure 4.11, when plotting the SHSS concentration factor for different angles, the effect of chamfering the angle vanishes for attachments with angles greater than  $45^\circ$ . However, those with a sharper angle exhibit an abrupt decrease in the stress concentration factor. Therefore, it can be concluded that a possible enhancing effect can be expected from attachments with chamfer angles less than  $45^\circ$ .

In order to experimentally confirm this phenomenon, the test results of longitudinal attachments with variable chamfer angles were collected. Unfortunately, no test results with chamfered angles less than  $45^\circ$  could be found. However, the results of a group of tests ([62]), in which the author investigates the influence of shape for longitudinal attachments with two chamfer angles of  $45^\circ$  and  $90^\circ$ , were re-analyzed using both the nominal stress and hot spot stress methods. The findings are plotted in Figure 4.12 and 8.11a, respectively. It is apparent that chamfering the corners with a  $45^\circ$  has not improved the fatigue life of the detail. This observation is consistent with the finite element analysis results plotted in Figure 4.11.

Further evaluations of the finite element analysis results showed that the corners of attachments are only slightly stressed. As a result, by chamfering this area and taking away the corners, the stress would not redistribute and the change in the stress concentration factor would therefore be negligible. Nevertheless, removal of the corners with a sharper angle redistributes the local stresses so that a smaller

**Table 4.3:** *Fatigue classification of chamfered longitudinal attachments based on the nominal stress method according to Eurocode3 [9]*

| Structural detail   | Description                        | Requirements                       | FAT |
|---|------------------------------------|------------------------------------|-----|
|  | Chamfered longitudinal attachments | $L > 100mm$<br>$\alpha < 45^\circ$ | 71  |



**Figure 4.11:** Structural hot spot stress concentration factor for chamfered longitudinal attachments as a function of chamfer angle

portion of the applied load would be transferred to the attachment and the stress concentration factor associated to the joint becomes less severe. Therefore, the upgrade of the design class for these attachments seems to be reasonable.

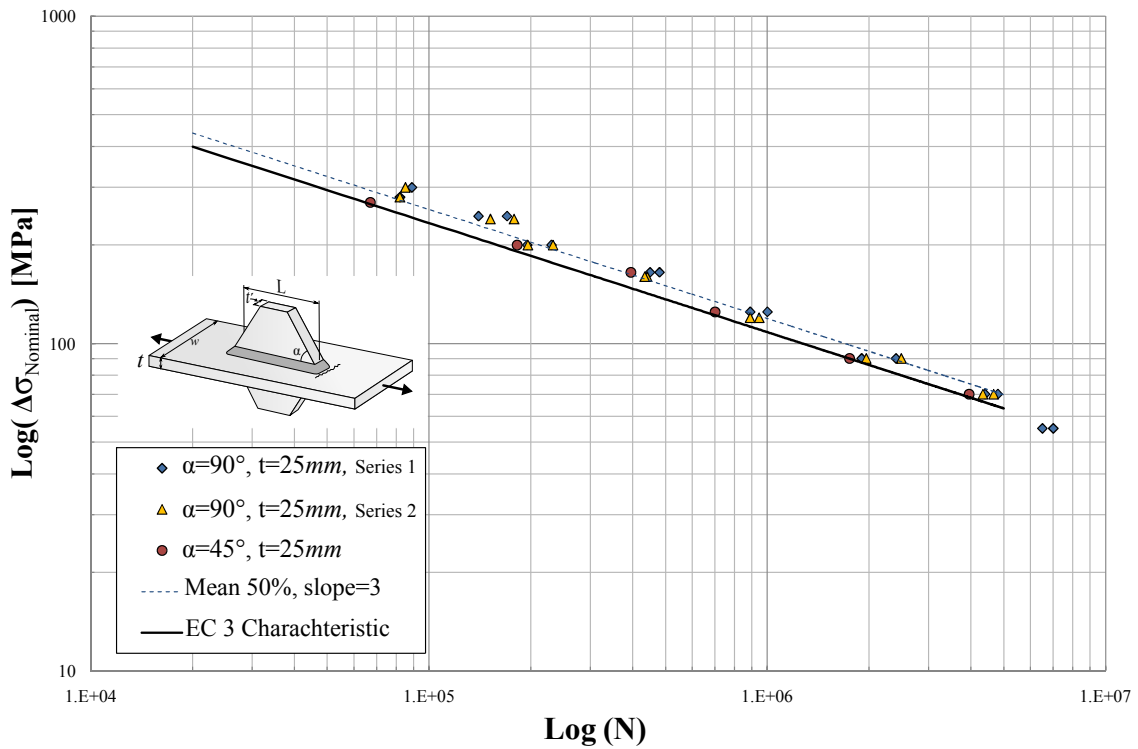


Figure 4.12: Fatigue test results for longitudinal attachments according to the nominal stress approach

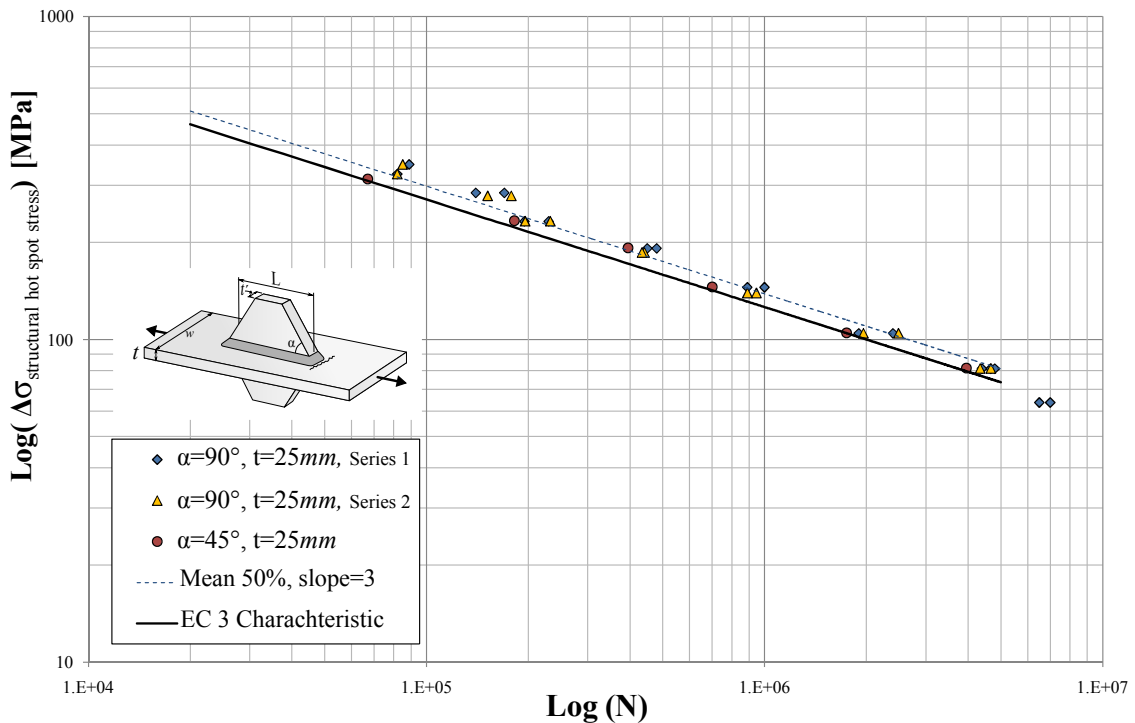


Figure 4.13: Fatigue test results for longitudinal attachments according to the structural hot spot stress approach

#### 4.5.4 Weld end effect

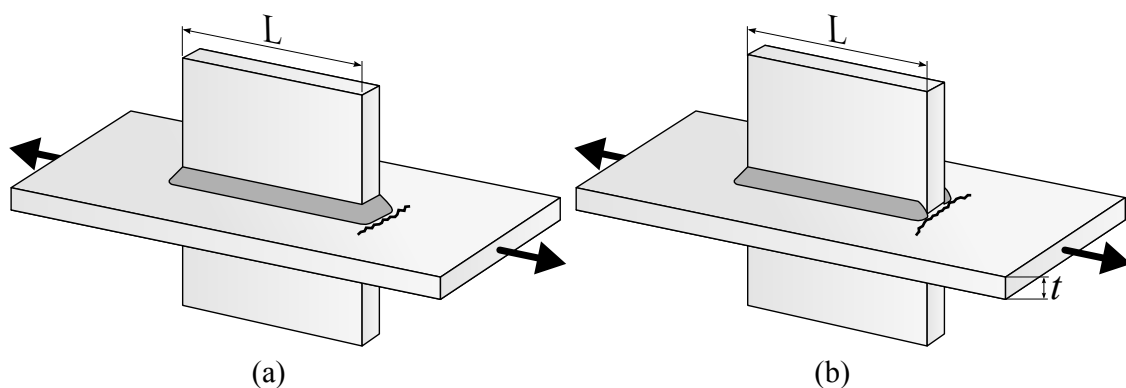
As it is depicted in Figure 4.14, the collected test data for this detail were consisted of two different attachment end configurations:

1. Attachments welded around ends (Figure 4.14a)
2. Attachments not-welded around ends (Figure 4.14b)

Eurocode 3 disregards the effect of end weld variation and suggests identical design classifications for both configurations. Similar to the previous investigations, in order to examine the credibility of this presumption, a case study was performed. Finite element models of longitudinal attachments with different end weld configurations were constructed and analyzed. The effect of modeling the gap between attachment and main-plate was also investigated by assembling the plates with and without the gap.

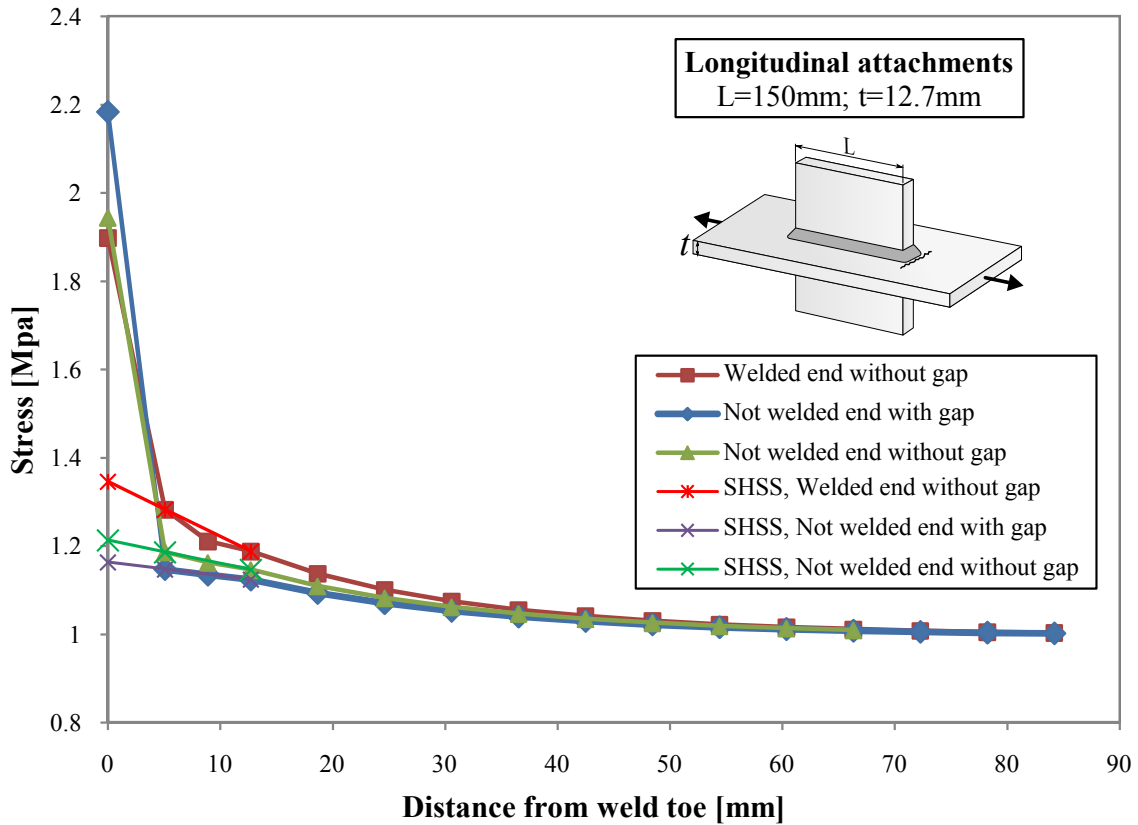
Figure 4.15 illustrates the analysis results in which a perceptible change in the calculated SHSS for different end weld types is apparent. It is clear that the stress gradient and the stress concentration factor is higher in case of attachments with continued welds around ends. In addition to that, it seems that modeling the gap has hardly influenced the calculated structural hot spot stress. This observation is consistent with the IIW recommendations that suggests to disregard the existent gap in the modeling procedure for details of this type. Figure 4.16 demonstrates a finite element model of a not-welded end attachment in which the gap is omitted.

The findings of the statistical evaluations of the test data are summarized in Table 8.5. The re-analysis of the test data confirms the lower fatigue life of welded round end details. However, as it was expected, the difference is not huge and both test series can be assigned to the same design classification. Thus, it can be concluded that omitting the end welds would not result in a significant variation of the fatigue life of this detail. Consequently, the identical classification of longitudinal attachments irrespective of the end weld configuration seems to be



**Figure 4.14:** *Different weld end configurations of longitudinal attachments: (a) Welded round ends, (b) Not-welded round ends*

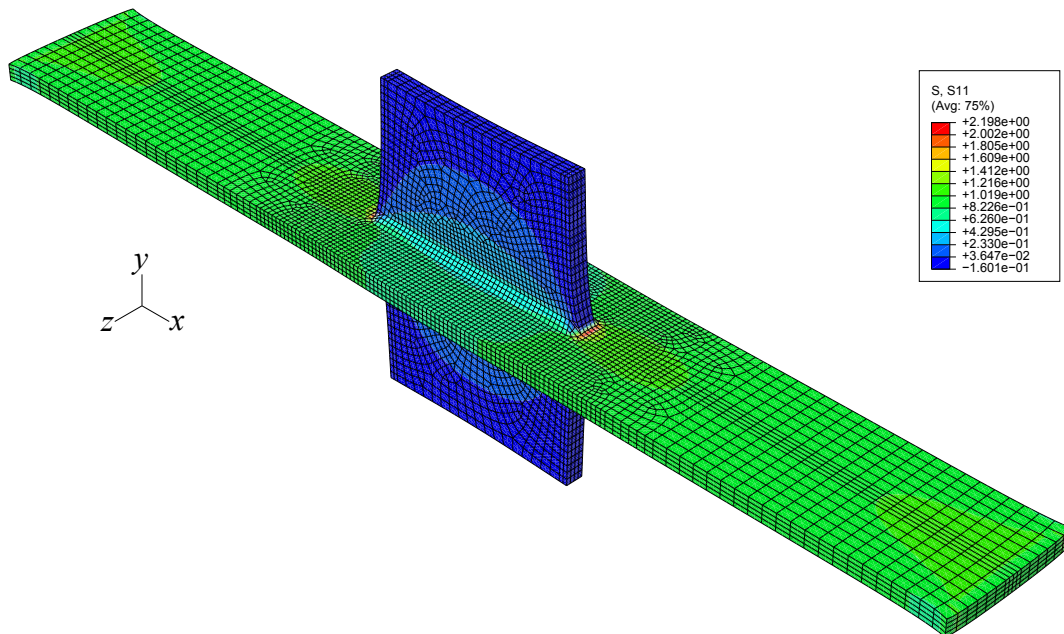
reasonable. Figure 4.17 and Figure 4.18 present the fatigue test results of welded and not-welded end attachments, respectively.



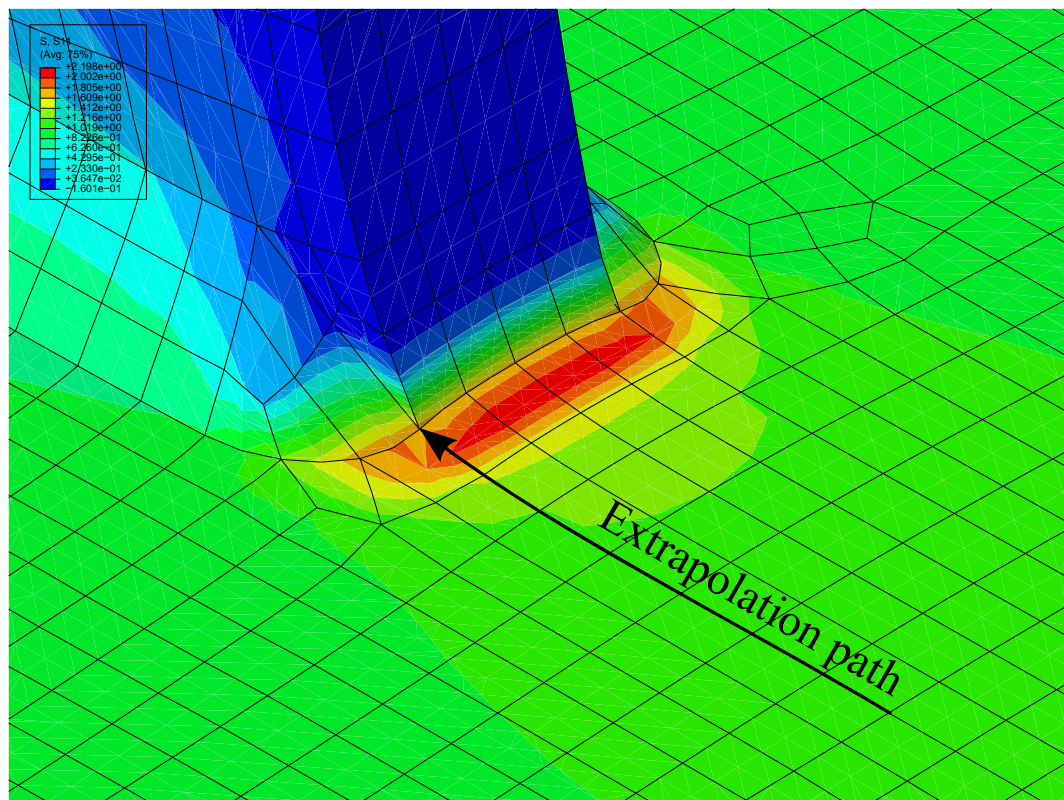
**Figure 4.15:** Stress distribution and extrapolated SHSS paths for longitudinal attachments with various end weld configurations

**Table 4.4:** Statistical evaluation of the test results of longitudinal attachments with and without end welds

| Detail type     | $L[mm]$ | $t[mm]$ | Tests No. | Standard deviation | Mean value [MPa] | Characteristic value [MPa] |
|-----------------|---------|---------|-----------|--------------------|------------------|----------------------------|
| Welded ends     | 150     | 12.7    | 35        | 0.152              | 89.56            | 70.95                      |
| Not welded ends | 150     | 12.7    | 68        | 0.099              | 90.35            | 77.59                      |



(a) 3D deformed finite element model of a longitudinal attachment without weld ends



(b) Close-up of the mesh at the hot spot

**Figure 4.16:** The normal stress component plot, 3D solid element model of a longitudinal attachment without weld ends

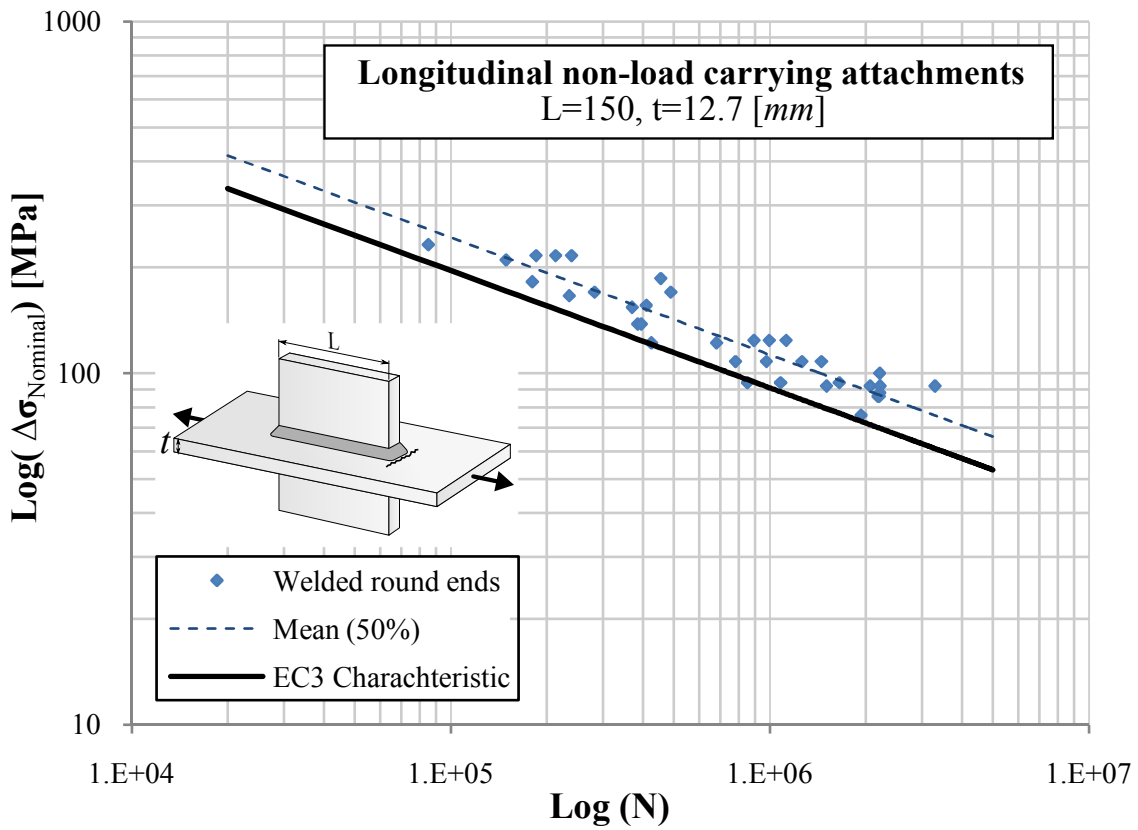


Figure 4.17: Fatigue test results for longitudinal attachments welded round ends

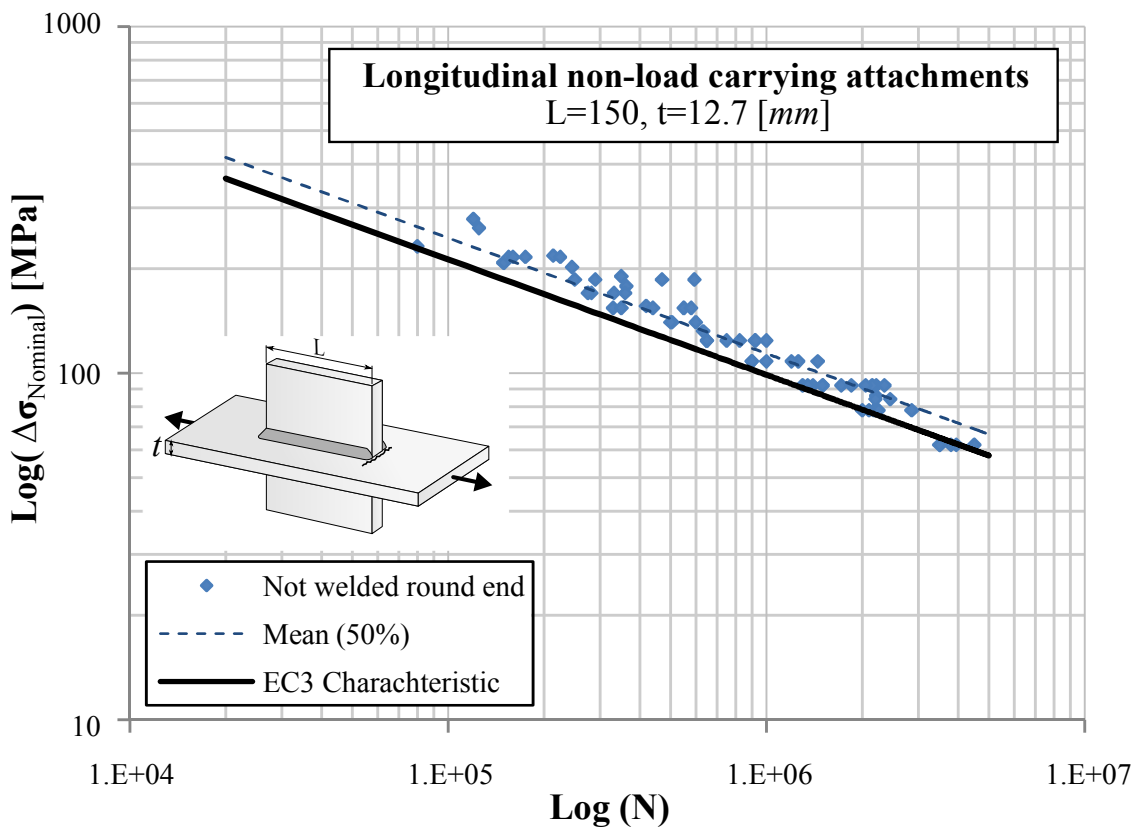


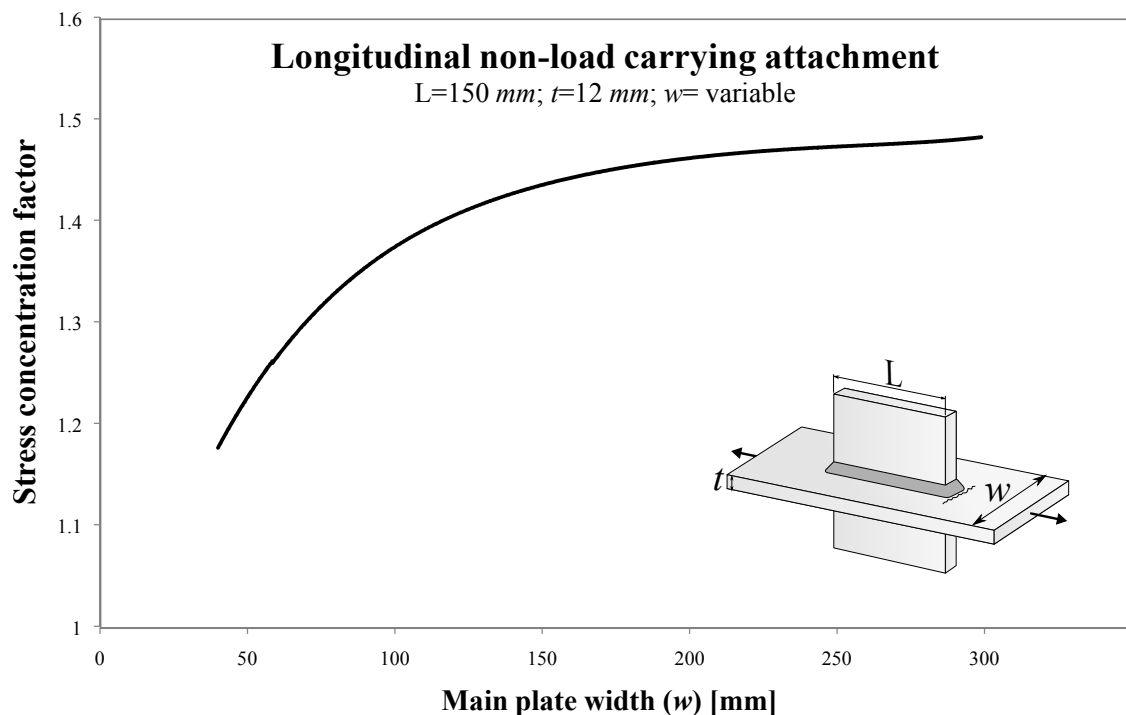
Figure 4.18: Fatigue test results for longitudinal attachments not-welded round ends



#### 4.5.5 Width effect

As it was mentioned in Section 4.3, Smith and Gurney [56] have reported a possible effect of the main-plate thickness on the stress concentration factor derived from the linear elastic fracture mechanics analysis. In this section the effect of altering the main-plate width on the fatigue behavior of longitudinal attachments is analyzed by adopting a case study approach. A number of finite element models of longitudinal attachments with main-plate widths varying from 40mm to 300mm were created whereas the attachment length and all plate thicknesses were constantly kept equal to 150mm and 12mm, respectively.

The resulting fitted curve in terms of the structural hot spot stress concentration factor as a function of the plate width is plotted in Figure 4.19. The figure indicates clearly that as the main plate becomes wider, the stress concentration factor increases. This effect is more pronounced for plates with the width of 50 to 150mm. Since most of the tests have a plate width in the mentioned range, it is recommended to also consider this parameter for evaluations based on the nominal stress method.



**Figure 4.19:** Structural hot spot stress concentration factor for longitudinal attachments as a function of main plate width

#### 4.5.6 Thickness effect

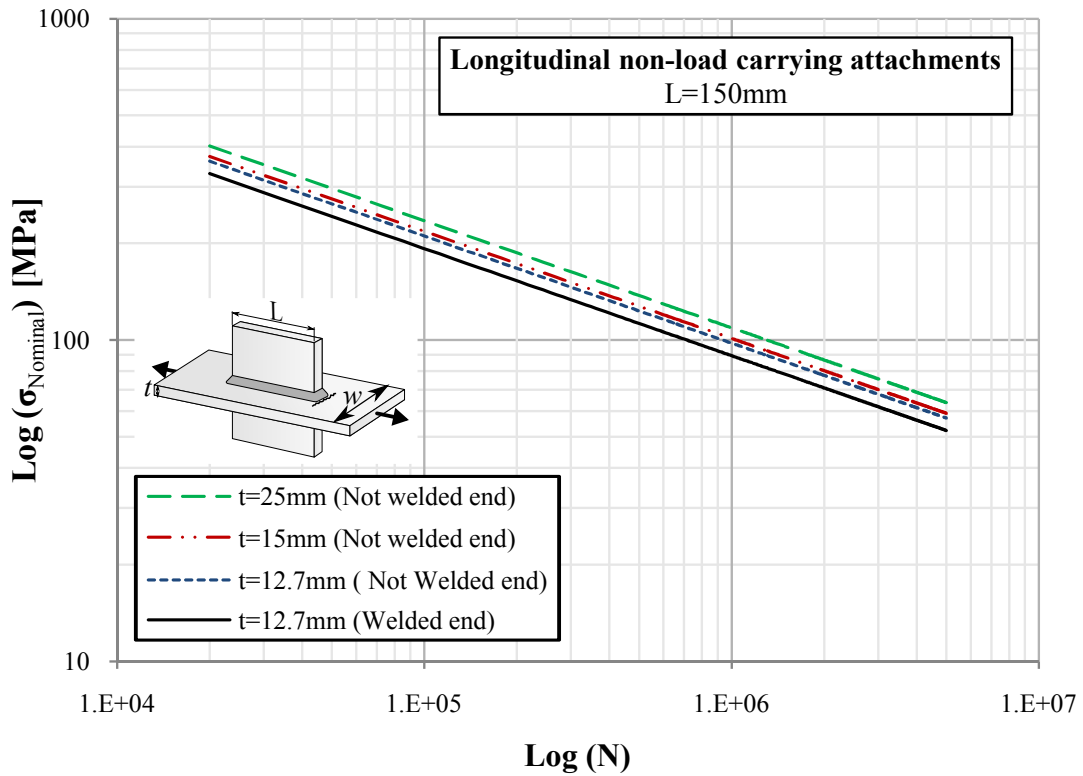
The effect of thickness on the fatigue behavior of welded details were discussed in Section 3.1.3. It was concluded that as the plate thickness increases, the fatigue life decreases. However, as mentioned in Section 4.3, Smith and Gurney [56] determined a higher fatigue life for longitudinal attachments with thicker plates. In order to clarify this contradiction, fatigue test results of longitudinal attachments with 150mm gusset length and variable main-plate thicknesses were collected and their characteristic design curves (mean curve minus two standard deviation) were plotted in Figure 4.20. Additionally, the corresponding SHSS for the investigated specimens were determined and plotted in Figure 4.21. Table 4.5 presents a summary of the statistical evaluation results of the test data based on both the nominal stress method and the structural hot spot stress approach.

The statistical evaluations of the test results confirm the findings reported by Smith and Gurney [56]. It is shown that, when using the nominal stress method, the design value for joints with plate thicknesses from 12.7mm to 25mm deviate from 70.95 MPa to 96.82 MPa. Nevertheless, when the SHSS method is applied, the scatter reduces significantly and almost one design curve can be associated to all details with different thicknesses. This observation is consistent with Eurocode 3 and IIW recommendations regarding the consideration of the thickness effect in the SHSS approach for plate thicknesses less than 25mm.

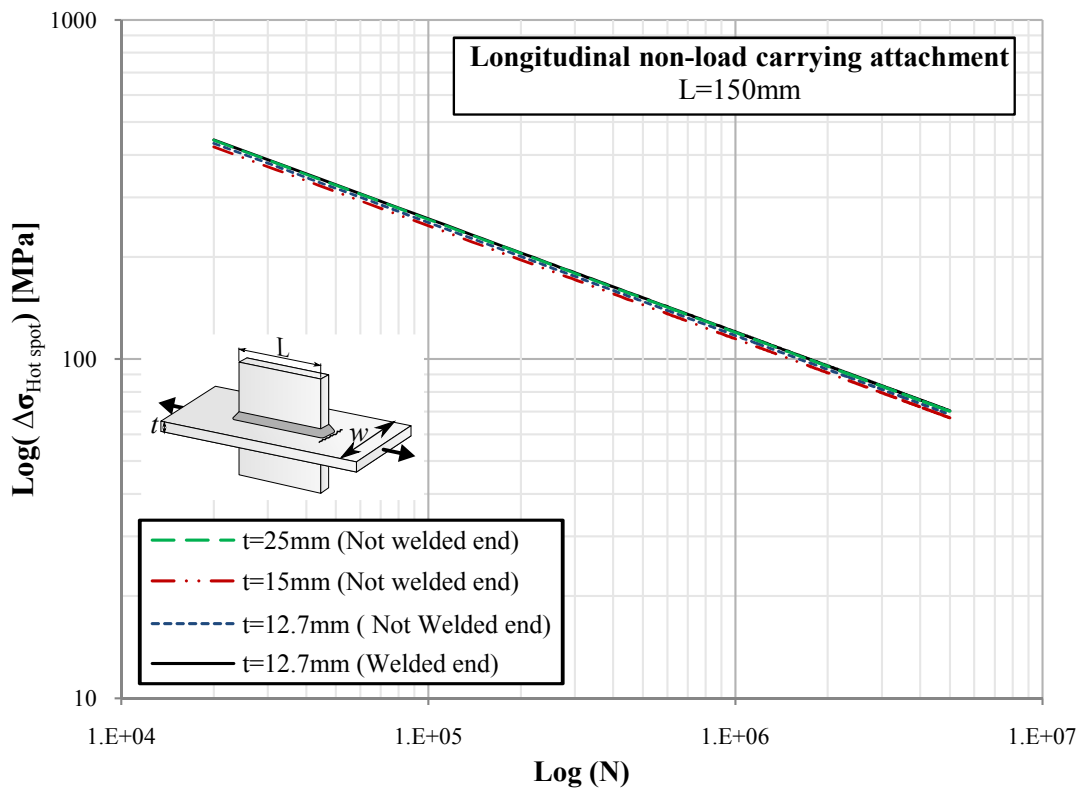
Furthermore, a set of finite element models of longitudinal attachments were constructed to derive a relationship between the plate thickness and the SHSS stress concentration factor. Accordingly, the plate thickness was the variable parameter while other factors were set constant. The analysis results along with an exponentially fitted curve are shown in Figure 4.22. It is apparent that a thicker plate would result in a higher stress concentration factor. However, this effect vanishes gradually for plates thicker than 16mm so that the SHSS concentration factor becomes almost constant for plates thicker than 20mm.

**Table 4.5:** *Statistical evaluation of the test results of longitudinal attachments with various plate thicknesses*

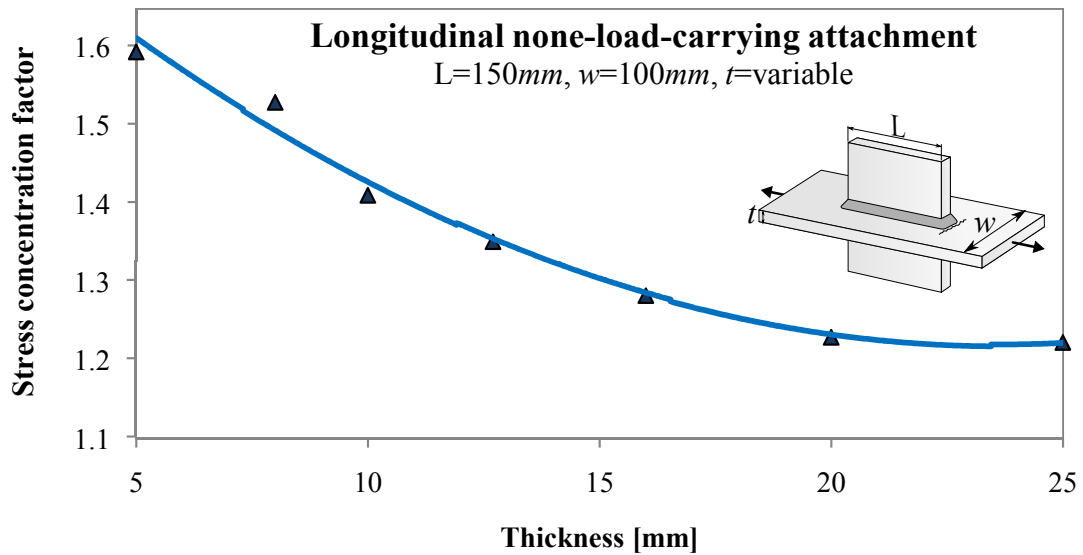
| Detail type     | Dimensions |      | Data | St.D. | Nominal stress        |                  | SHSS                  |                  |
|-----------------|------------|------|------|-------|-----------------------|------------------|-----------------------|------------------|
|                 | $L$        | $t$  |      |       | $\Delta\sigma_{mean}$ | $\Delta\sigma_C$ | $\Delta\sigma_{mean}$ | $\Delta\sigma_C$ |
| Welded ends     | 150        | 12.7 | 35   | 0.152 | 89.56                 | 70.95            | 120.52                | 95.48            |
| Not welded ends | 150        | 12.7 | 68   | 0.099 | 90.35                 | 77.59            | 108.81                | 93.12            |
| Not welded ends | 150        | 15   | 30   | 0.142 | 99.82                 | 80.27            | 113.2                 | 91.03            |
| Not welded ends | 150        | 25   | 22   | 0.072 | 96.82                 | 86.64            | 96.12                 | 89.01            |



**Figure 4.20:** Fatigue characteristic design values for longitudinal attachments with various thicknesses according to the nominal stress approach



**Figure 4.21:** Fatigue characteristic design values for longitudinal attachments with various thicknesses according to the structural hot spot stress approach



**Figure 4.22:** *Structural hot spot stress concentration factor for longitudinal attachments as a function of main plate thickness*

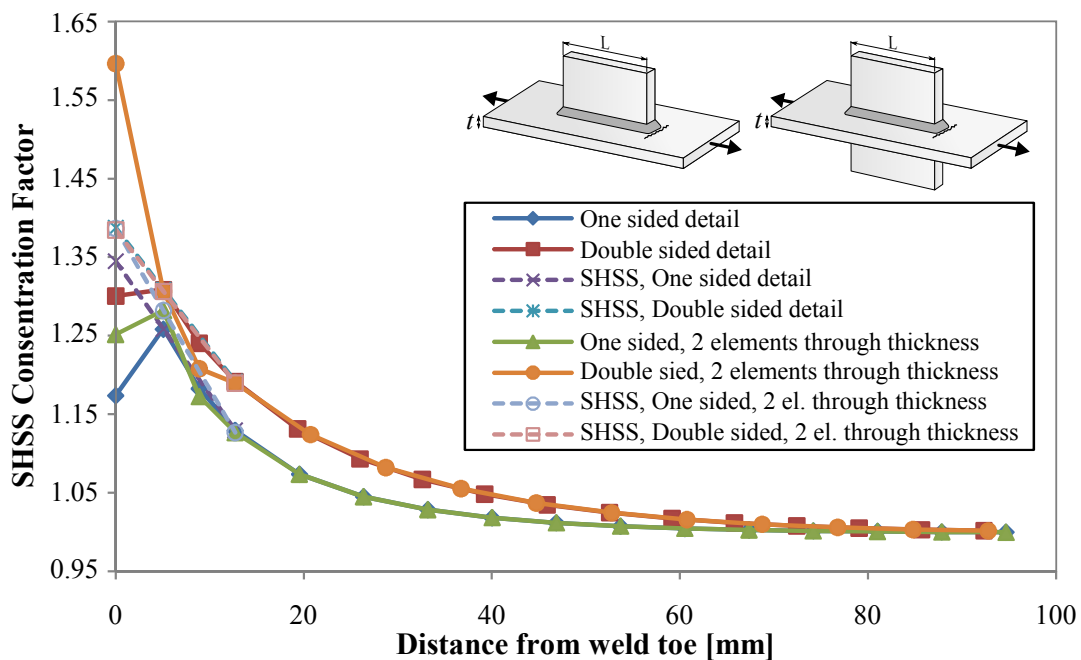
As a conclusion, based on the two findings discussed above, the fatigue life of longitudinal attachments increases as the plate thickness increases. The fatigue life variation due to thickness effect is considerable and several distinct design classes can be assigned to identical longitudinal attachments with variable thicknesses. On the contrary, when exploiting the structural hot spot stress approach, this phenomenon is accounted for and subsequently the scatter of the test results reduces. However, this is only valid for plate thicknesses less than 25mm and as recommended by most of the codes, a thickness correction factor has to be applied in case of thicker plates.

#### 4.5.7 Detail symmetry effect

Longitudinal attachment can be welded on either both sides or one side of the main plate. In order to see the possible effects of this variation, a case study including longitudinal attachments of 150mm long and 12.7mm thick was performed. The attachments were welded on one side only or both sides of the main-plate. As can be seen in Figure 4.23, although the surface stress gradient is higher in case of one-sided attachments, the final SHSS concentration factor is identical for both cases. This finding is consistent with the conclusion drawn by Huther et al. [59] regarding the influence of detail symmetry.

Furthermore, since two types of finite element meshes with either one or two elements through thickness were generated, mesh sensitivity of the analysis results can also be investigated. The results are evident that as long as the mesh density satisfies the requirements of a fine mesh, increasing the element numbers at the hot spot region would not affect the calculated structural hot spot stress.

From the discussion made here, it can be concluded that welding the longitudinal attachments on both sides or one side of the main-plate does not affect the fatigue life of the detail. However, it should be noted that, this conclusion is only valid when severe out of plane deformations are prevented in case of one sided attachments.



**Figure 4.23:** Stress distribution and extrapolated SHSS paths for double-sided and one-side longitudinal attachments with  $L=150\text{mm}$  and  $t=12.7\text{mm}$

#### 4.5.8 Length effect

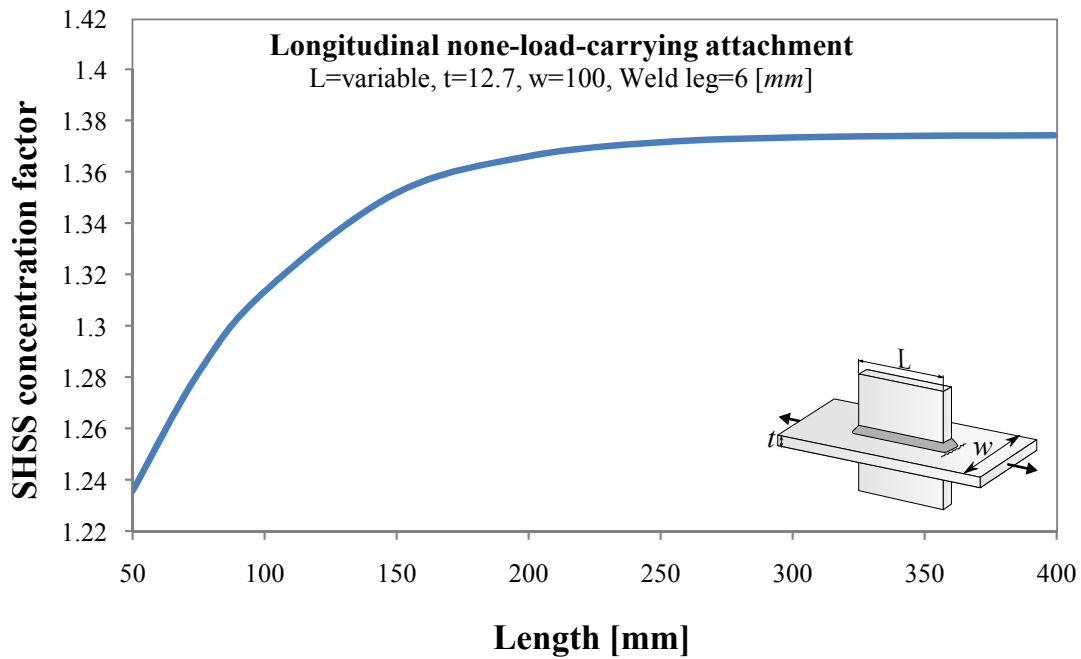
Length of the welded attachment is the only variable parameter that is included in the fatigue design classification of longitudinal attachments based on the nominal stress method according to Eurocode 3. Therefore, it is anticipated that the stress concentration factor would deviate remarkably due to varying the attachment length.

Similar to previous investigations, finite element models of longitudinal attachments with varying attachment length were constructed to evaluate the SHSS concentration factor. In addition to that, the effective notch stress analysis were also conducted to obtain the effective notch stress concentration factor as a function of gusset length. Since an extremely fine mesh is required for the latter analysis, sub-modeling technique were implemented. It should be noted that, although only a small portion of the weld toe were sub-modeled, analysis could not be performed using ordinary desktop computers. As a result, the model were submitted to a super computer (cluster) for analysis. Details regarding the sub-modeling technique and its application are elaborately discussed in Section 6.4. Figures 4.26 and 4.27 show an example of the analyzed models.

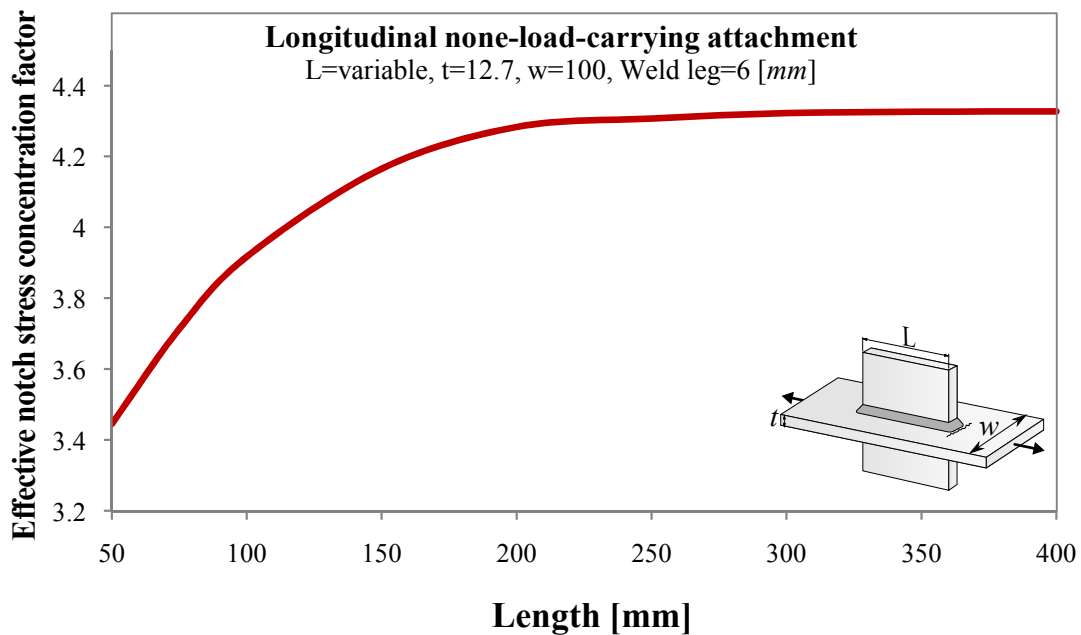
The investigated finite element models as well as the analysis results are presented in Table 4.6. Moreover, representative fitted curves of the obtained values are plotted in Figures 4.24 and 4.25. As can be seen, by increasing the length of the attachments, the stress concentration factor, based on both the SHSS approach and effective notch stress method, increases. It is apparent that the SCF rises sharply by increasing the attachment length from 50 to 150mm. Afterwards, by further attachment enlargement, the SCF increase rate gradually descends such that it becomes almost steady for attachments longer than 250mm.

**Table 4.6:** *Investigated finite element models and the analysis outcomes for length effect investigation of longitudinal attachments; all dimensions are in mm.*

| Attachment |           | Main plate |           | Weld leg length | Stress concentration factor |                        |
|------------|-----------|------------|-----------|-----------------|-----------------------------|------------------------|
| Length     | Thickness | Width      | Thickness |                 | SHSS                        | Effective notch stress |
| 50         | 12.7      | 100        | 12.7      | 6               | 1.235                       | 3.445                  |
| 75         | 12.7      | 100        | 12.7      | 6               | 1.282                       | 3.713                  |
| 100        | 12.7      | 100        | 12.7      | 6               | 1.313                       | 3.917                  |
| 150        | 12.7      | 100        | 12.7      | 6               | 1.352                       | 4.165                  |
| 200        | 12.7      | 100        | 12.7      | 6               | 1.366                       | 4.283                  |
| 250        | 12.7      | 100        | 12.7      | 6               | 1.372                       | 4.307                  |
| 300        | 12.7      | 100        | 12.7      | 6               | 1.373                       | 4.322                  |
| 350        | 12.7      | 100        | 12.7      | 6               | 1.374                       | 4.326                  |
| 400        | 12.7      | 100        | 12.7      | 6               | 1.374                       | 4.327                  |

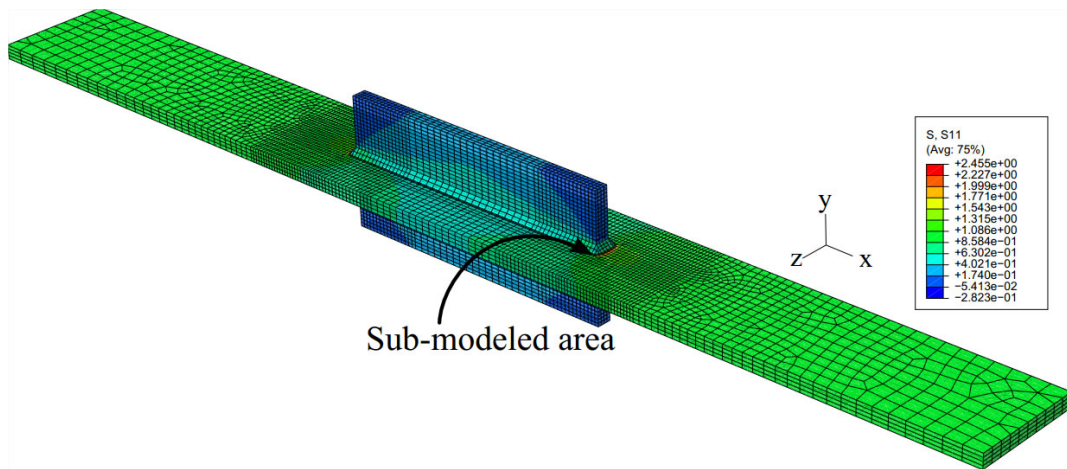


**Figure 4.24:** *The structural hot spot stress concentration factor for longitudinal attachments as a function of attachment length*

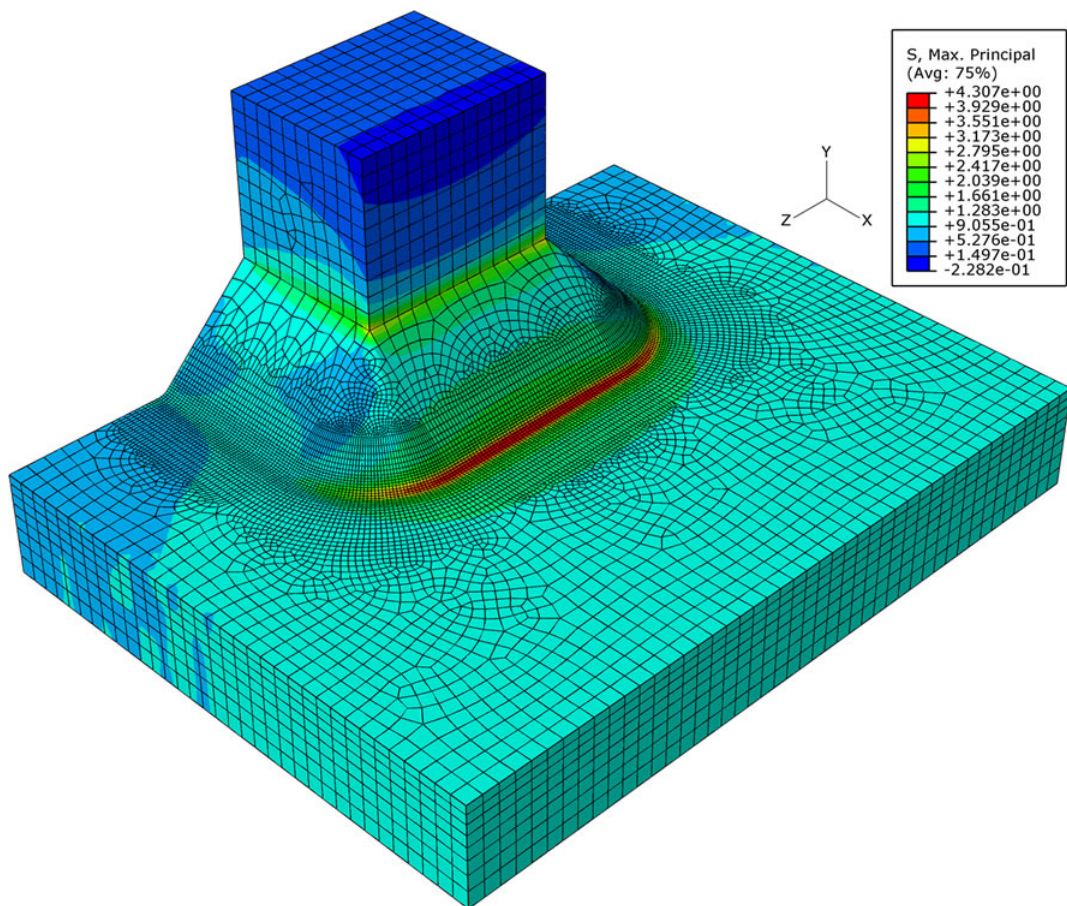


**Figure 4.25:** *The effective notch stress concentration factor for longitudinal attachments as a function of attachment length*

Based on the above discussion, it can be concluded that the investigated length effect disappears after exceeding an attachment length of 250mm. However, it varies significantly for smaller attachments. As a result, any fatigue design classification of longitudinal attachments based on the nominal stress method has to specifically consider the length effect for joints with attachments smaller than 250mm.



**Figure 4.26:** 3D solid global model constructed for length effect investigation of longitudinal attachments



**Figure 4.27:** 3D solid sub-model constructed for length effect investigation of longitudinal attachments



## 4.6 Evaluation according to the nominal stress method

After a preliminary evaluation of the extensive number of collected fatigue test results for longitudinal attachments, a total number of 286 specimens were selected for further evaluations. In the initial evaluation phase, inappropriate test data such as tests with post-weld treatment, unusual ambient temperatures, negative stress ratios etc. were excluded. Table 4.7 lists a summary of the approved fatigue test series.

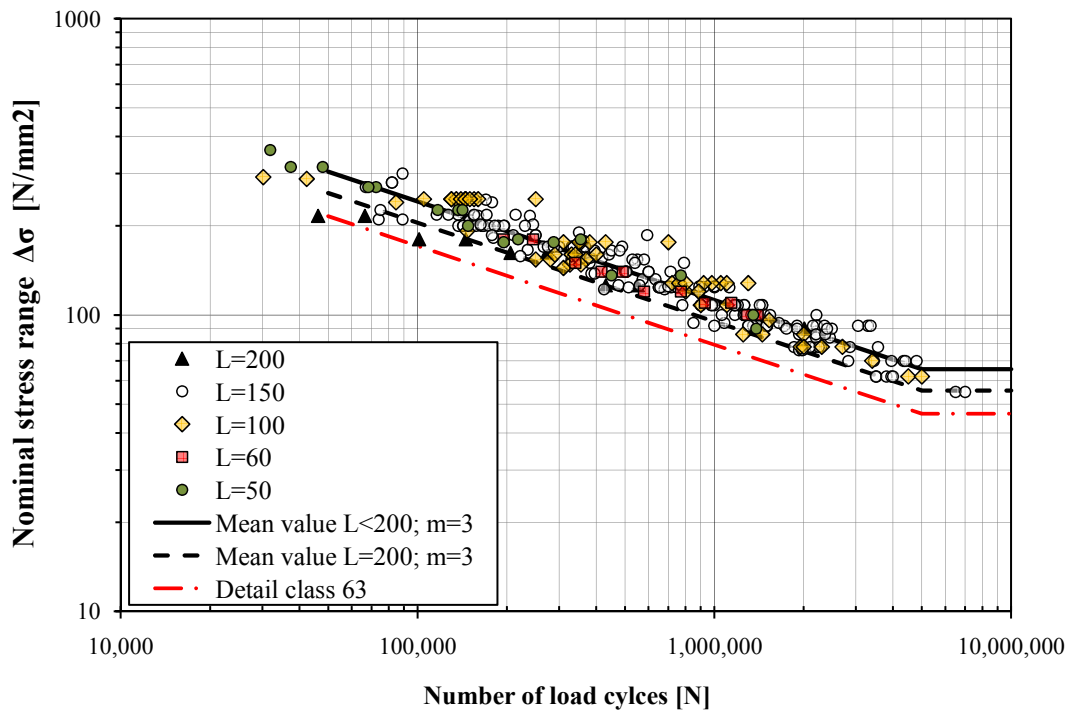
The results from evaluating the test results based on the nominal stress method are presented in Table 4.8. It is clear that for specimens with attachment plates having a length up to 150mm, FAT71 seems to provide a good representation for the fatigue strength of the detail. This complies very well with the recommendations in IIW. For test data with L=200, the evaluated fatigue strength at 2 million cycles is below the recommended fatigue category 63. Nevertheless, this category is only composed of one test series in which the main plate is very thin. Therefore, it is anticipated that by including more test data the characteristic value may improve. However, according to the tests evaluated in this study, the recommended FAT class of 63 seems to be unreliable. The test data are plotted in Figure 4.28.

**Table 4.7:** *Dimensions and quantity of the evaluated fatigue test specimens for longitudinal attachments; all dimensions are in mm.*

| Attachment length | Test data | Main plate |          | Attachment |        |
|-------------------|-----------|------------|----------|------------|--------|
|                   |           | Thickness  | Width    | Thickness  | Length |
| L=200             | 10        | 4          | 100      | 4          | 200    |
| L=150             | 193       | 4.8–25.4   | 75–100   | 4.8–25.4   | 150    |
| L=100             | 55        | 10–25      | 80–152.4 | 10–25      | 100    |
| L=60              | 11        | 16         | 90       | 16         | 60     |
| L=50              | 17        | 8          | 80       | 8          | 50     |

**Table 4.8:** *Statistical evaluation of the test results of longitudinal attachments based on the nominal stress method*

| Configuration | Test data | $\Delta\sigma_{mean}$ [MPa] | $\Delta\sigma_C$ [MPa] | St.D. |
|---------------|-----------|-----------------------------|------------------------|-------|
| L=200         | 10        | 75.4                        | 56.9                   | 0.157 |
| L=150         | 193       | 88.7                        | 75.9                   | 0.123 |
| L=100         | 55        | 91.3                        | 73.6                   | 0.164 |
| L=60          | 11        | 85.8                        | 77.9                   | 0.056 |
| L=50          | 17        | 88.6                        | 77.3                   | 0.088 |

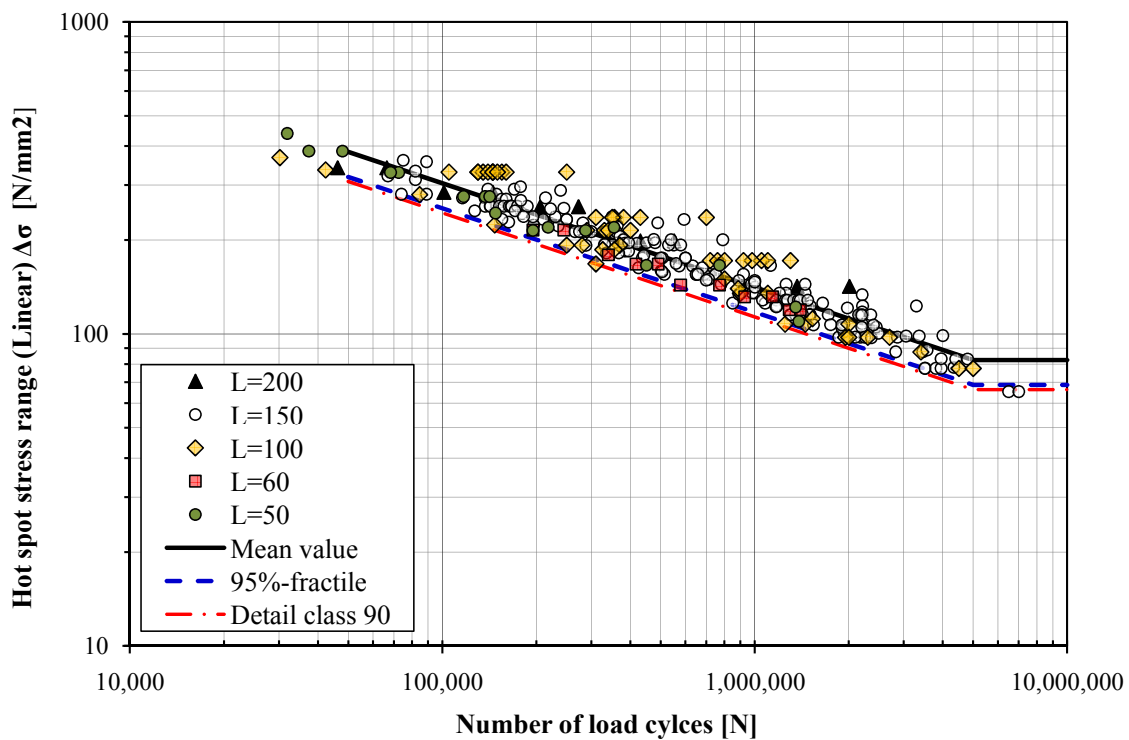


**Figure 4.28:** Fatigue test results for longitudinal attachments according to the nominal stress approach

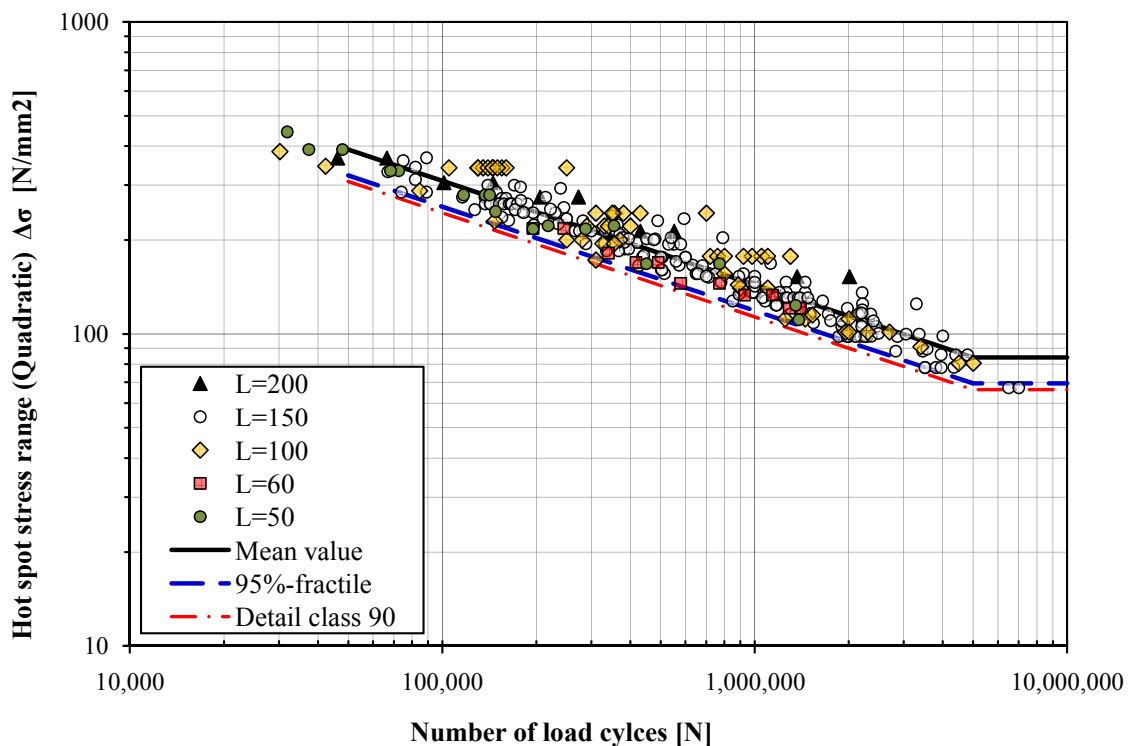
## 4.7 Evaluation according to the hot spot stress approach

The test results according to the structural hot spot stress approach are listed in Table 4.9. In addition to that, Figure 4.29 depicts the test results according to the SHSS approach obtained from both linear and quadratic extrapolation methods. As can be seen, the test data associated to the joints with an attachment length of 200mm have shifted upwards and now lie within the scatter band. This observation is confirmed numerically based on the results presented in Table 4.9 where nearly the same characteristic value has been obtained for all details irrespective of geometric variations.

When using the quadratic extrapolation, the standard deviation is 0.138 and the slope 2.67 evaluated with free linear regression. The characteristic strength is 88.8 MPa. With a fixed slope of 3 the standard deviation becomes 0.150 and the characteristic fatigue strength is 94.2 MPa. Linear extrapolation was also examined for this detail, giving a standard deviation of 0.150 and characteristic fatigue strength of 93.1 MPa. Considering the results in Figure 4.29 it seems that FAT-category 90 should be used for this detail instead of the FAT100 which is recommended by the IIW.



(a) SHSS derived from the linear surface extrapolation method



(b) SHSS derived from the quadratic surface extrapolation method

**Figure 4.29:** Fatigue test results for longitudinal attachments according to the structural hot spot stress approach

**Table 4.9:** *Statistical evaluation of the test results of longitudinal attachments based on the structural hot spot stress approach, stresses are in MPa.*

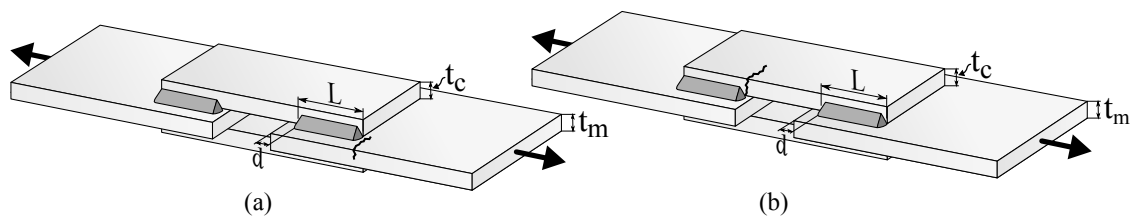
| Configuration | Test data | Linear extrapolation  |                  |       | Quadratic extrapolation |                  |       |
|---------------|-----------|-----------------------|------------------|-------|-------------------------|------------------|-------|
|               |           | $\Delta\sigma_{mean}$ | $\Delta\sigma_C$ | St.D. | $\Delta\sigma_{mean}$   | $\Delta\sigma_C$ | St.D. |
| L=200         | 10        | 119.2                 | 89.9             | 0.157 | 128.0                   | 96.6             | 0.157 |
| L=150         | 193       | 110.9                 | 95.3             | 0.119 | 112.2                   | 96.3             | 0.120 |
| L=100         | 55        | 117.7                 | 88.9             | 0.214 | 121.8                   | 92.3             | 0.211 |
| L=60          | 11        | 102.6                 | 93.2             | 0.056 | 103.8                   | 94.3             | 0.056 |
| L=50          | 17        | 108.1                 | 94.3             | 0.088 | 109.4                   | 95.5             | 0.088 |

# 5 Fatigue Life Assessment of Over-Lapped Joints

## 5.1 Introduction

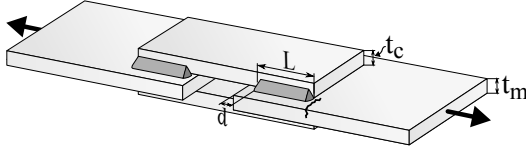
Longitudinally loaded over-lapped joints with side welds are usually used in fatigue loaded structures to join different sections to a gusset plate. As depicted in Figure 5.1, two possible failure modes exist for the longitudinally welded over-lapped joints; failure from the weld toe at the main plate and failure from the weld end at the cover plate.

The Eurocode 3 fatigue design classifications of this detail with reference to the mentioned failure modes are listed in Tables 5.1 and 5.2. As can be seen, for longitudinally welded over-lapped joints cracked at the main plate, the classifications are rather comprehensive. Depending on the length of the longitudinal welds and the main plate thickness a wide range of detail categories varying from FAT40 to FAT80 are associated to this detail. On the other hand, for the joints cracked at the cover plate only one design category, FAT45, is proposed. Moreover since the weld is load-carrying, irrespective of the failure mode, FAT90 is recommended for

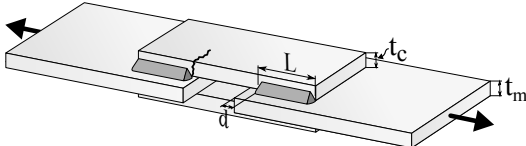


**Figure 5.1:** Fillet welded over-lapped attachments; (a) Cracked at the main-plate, (b) Cracked at the cover-plate

**Table 5.1:** Fatigue classification of over-lapped joints failed at the main plate based on the nominal stress method according to Eurocode3 [9]

| Structural detail   | Requirements       | FAT                |           |
|---|--------------------|--------------------|-----------|
|  <p>Fillet welded over-lapped joints with crack at the main plate; <math>\Delta\sigma</math> in the main plate</p> | $L < 50mm$         | all $t_m$          | <b>80</b> |
|   | $50 < L \leq 80$   | all $t_m$          | <b>71</b> |
|   | $80 < L \leq 100$  | all $t_m$          | <b>63</b> |
|   | $100 < L \leq 120$ | all $t_m$          | <b>56</b> |
|   | $L > 120$          | $t_m \leq 20$      | <b>56</b> |
|   | $120 < L \leq 200$ | $t_m > 20$         | <b>50</b> |
|   | $L > 200$          | $20 < t_m \leq 30$ |           |
|   | $200 < L \leq 300$ | $t_m > 30$         | <b>45</b> |
|   | $L > 300$          | $30 < t_m \leq 50$ |           |
|   | $L > 300$          | $t_m > 50$         | <b>40</b> |

**Table 5.2:** *Fatigue classification of over-lapped joints failed at the cover plate based on the nominal stress method according to Eurocode3 [9]*

| Structural detail   | Description   | FAT       |
|---|---|-----------|
|  | Fillet welded over-lapped joints with crack at the cover plate; $\Delta\sigma$ in the cover plate | <b>45</b> |

assessments based on the structural hot spot stress method.

It is also noteworthy that Eurocode 3 limits the extent of the weld to a distance  $d = 10\text{mm}$  from the plate edges. This recommendation stems from the high probability of the formation of weld defects such as undercuts or the melt away of the plate edges. This is mainly due to the material deficiency at the plate edge to conduct away the weld heat.

In this section, the appropriate finite element modeling recommendations regarding the longitudinally welded over-lapped joints is given. Next, the credibility of the recommended classifications is investigated using both the nominal and hot spot stress methods. The structural Dong stress is also calculated to obtain the S-N curve pertaining to the joints cracked at the main plate. In the following sections, for the sake of simplicity, longitudinally welded over-lapped joints will be referred to as *over-lapped joints*.

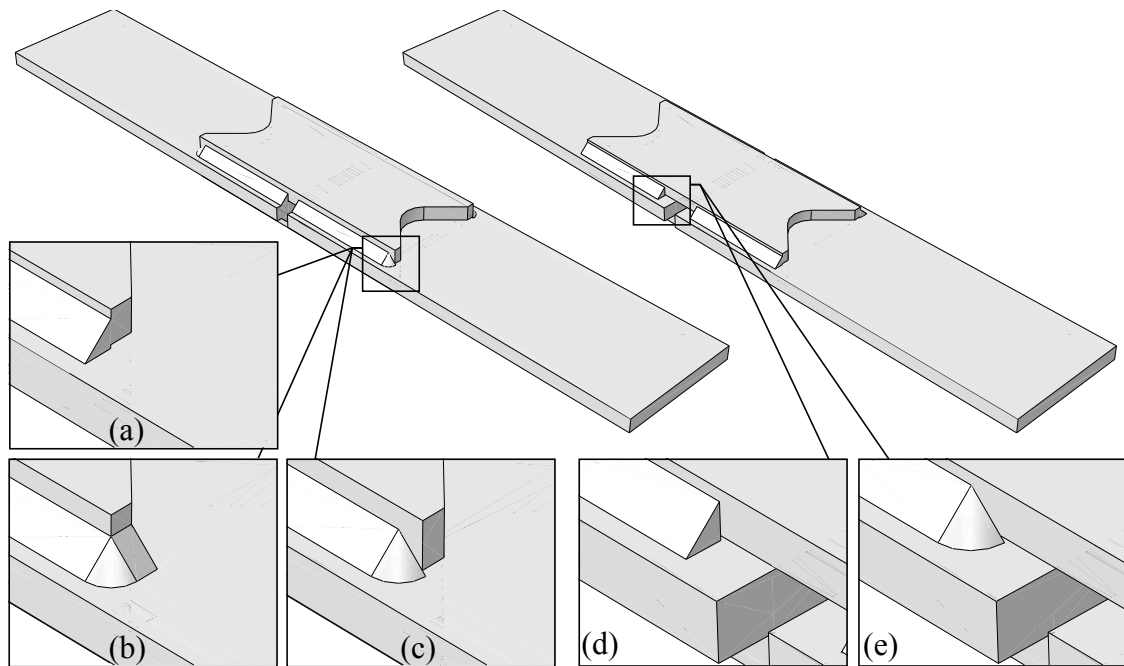
## 5.2 Finite element modeling and analysis

Similar to the longitudinal attachments, 3D solid element models with a relatively fine mesh were constructed to study the fatigue performance of the over-lapped joints. As the general employed modeling techniques are similar to those discussed in Section 4.4, only the distinct modeling procedures of over-lapped joints will be presented in this section.

### 5.2.1 Geometry

The geometry of the over-lapped joints were constructed according to the theoretical reported dimensions. However, no information was generally provided regarding the weld termination shape. This parameter is important since in both failure modes of this detail, the crack has been initiated from the weld terminations. In addition to that, as mentioned in Section 4.4.1, the codes have not yet provided any guideline regarding the weld end modeling.

Figure 5.2 shows the investigated models to obtain the most suitable weld termination modeling procedure. The preliminary studies revealed that in case of an over-lapped joint cracked from the main plate, the weld end can be modeled in three different ways as depicted in Figures 5.2a–c. Figures 5.2d–e illustrate the possible modeling alternatives in case of an over-lapped joint cracked from the cover plate. In order to find the most suitable modeling alternative, finite element models of an over-lapped joint with different weld terminations were constructed and analyzed. The findings indicated that despite the negligible difference of the calculated SHSS based on different techniques, modeling the weld end according

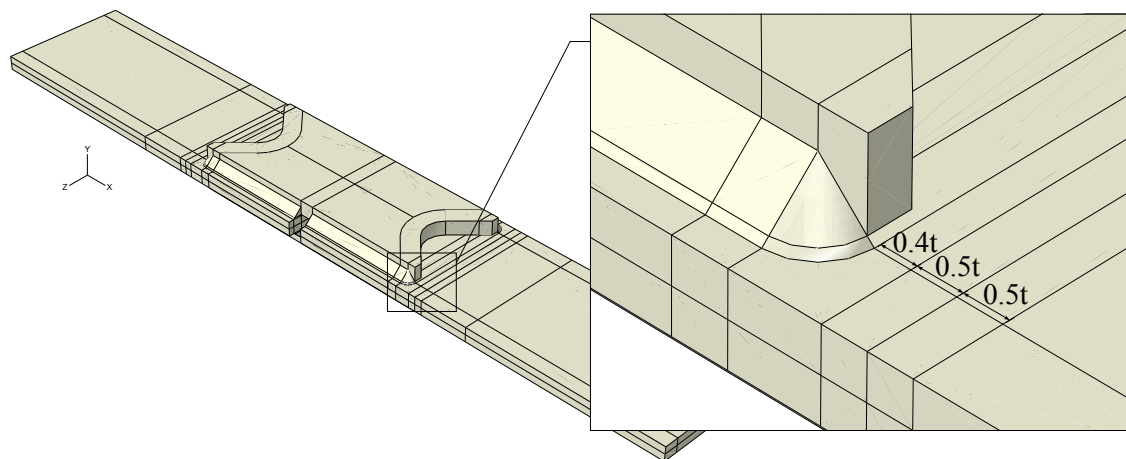


**Figure 5.2:** *Different techniques to model the weld terminations of longitudinally welded over-lapped joints*

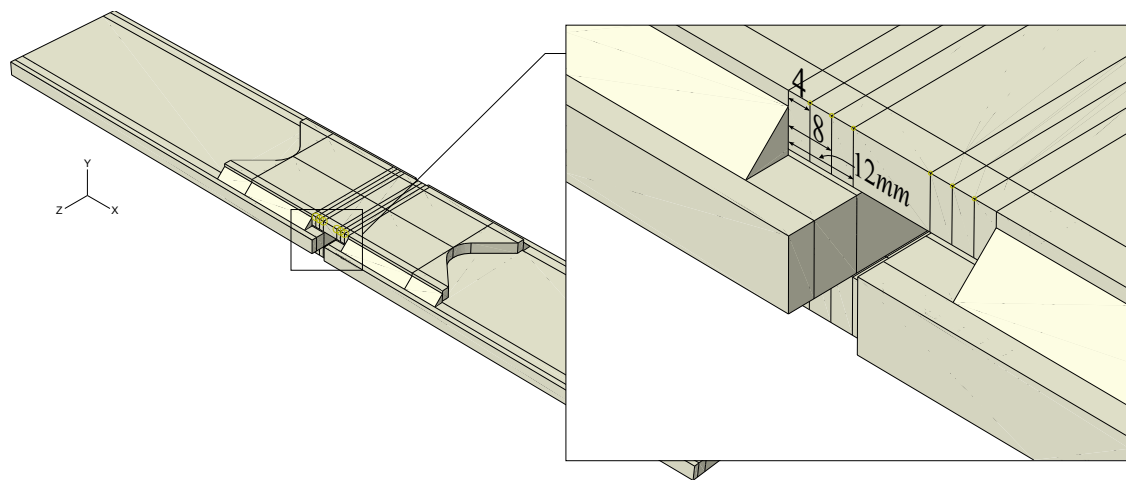
to Figure 5.2c in case of failure at the main plate and Figure 5.2d in case of failure at the cover plate yields more acceptable results. It was observed that if the weld end geometry is modeled as shown in Figure 5.2b and e, the obtained SHSS value would be underestimated. On the contrary, modeling the weld termination as shown in Figure 5.2a would cause the resulting SHSS to be overestimated. It should be also mentioned that, in contrast to the longitudinal attachments, the gap between the main and cover plates has to be modeled in case of over-lapped joints.

### 5.2.2 Partitioning and post-processing of the results

As discussed before, over-lapped joints can fail either at the main plate or at the cover plate. Subsequently, the hot spot would be of type 'a' and type 'b', respectively. The constructed geometry should therefore be partitioned accordingly in any of these cases. Figure 5.3 demonstrates a partitioned geometry that facilitates for the quadratic type 'a' hot spot stress determination, whereas, Figure 5.4 shows



**Figure 5.3:** *Fillet welded over-lapped joint model partitioned at the weld toe for type 'a' hot spot stress determination*

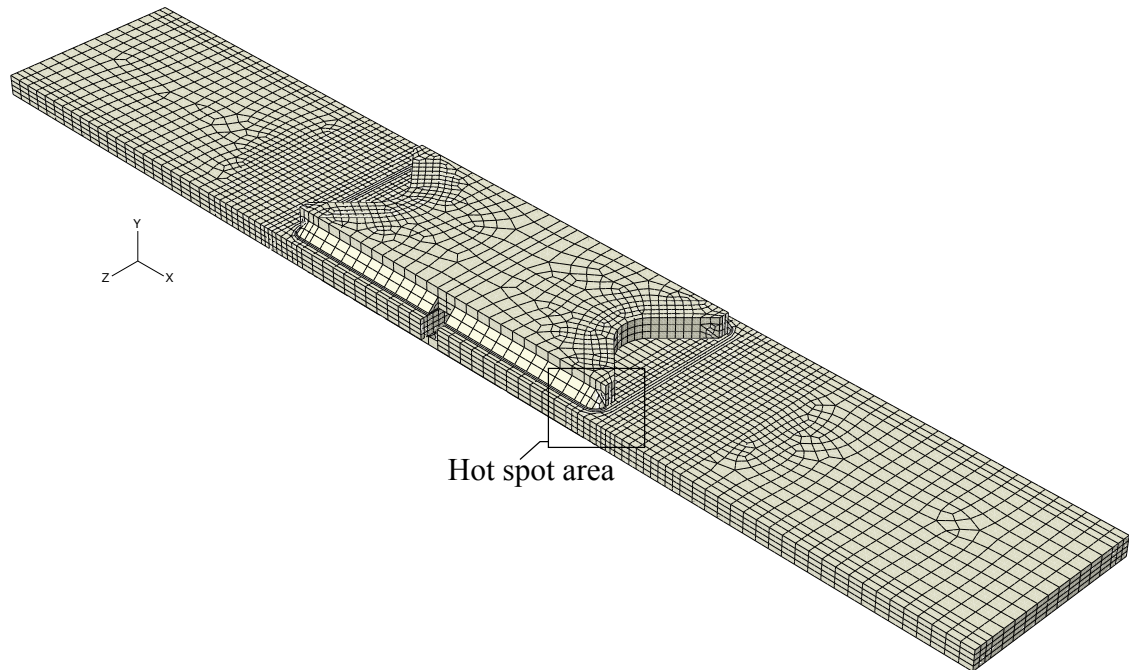


**Figure 5.4:** *Fillet welded over-lapped joint model partitioned at the plate edge for type 'b' hot spot stress determination*

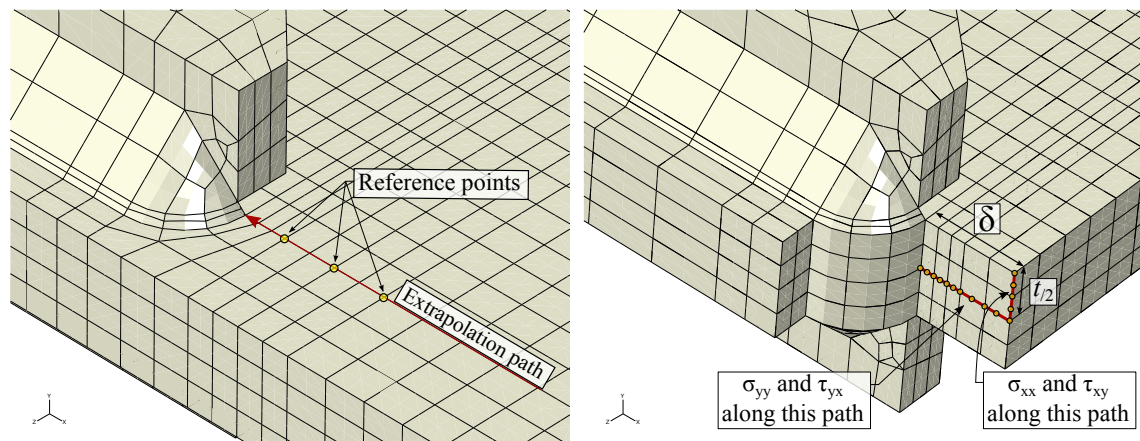


the appropriate partitioning for the type 'b' hot spot stress calculation.

Once the partitioned geometry is meshed, it can be submitted for static analysis. Since the models were partitioned along the extrapolation pathes and reference points, the nodal values of the perpendicular stress component can be extracted to obtain the SHSS. Figure 5.5 shows the meshed geometry of an over-lapped joint failed from the weld end at the main plate. As can be seen in Figure 5.5b, the stresses along the defined path at the reference points can be determined to obtain the SHSS according to Equation 3.17. Figure 5.5c demonstrates the defined paths

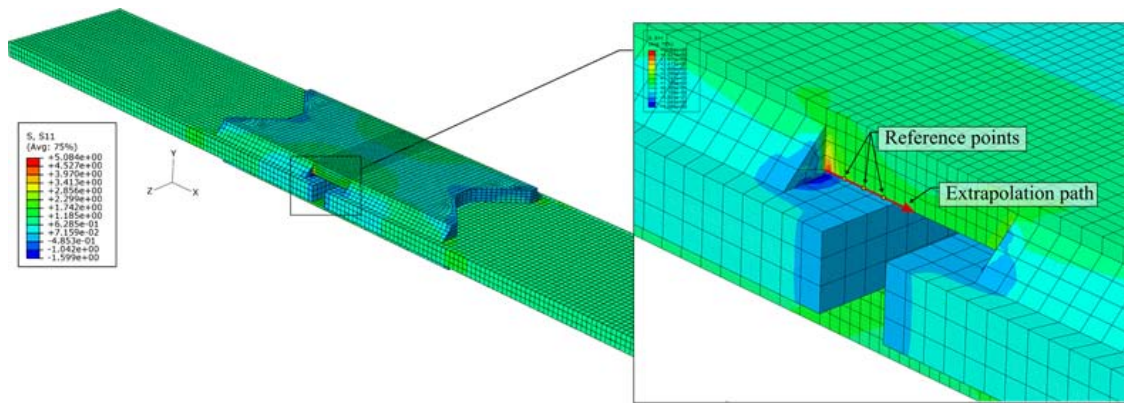


(a) The meshed model of the partitioned geometry shown in Figure 5.3



(b) Close-up of the mesh at the hot spot and the path and reference points used for the SHSS determination according to the quadratic extrapolation method (c) Extracted mesh at the hot spot and the paths and stress components used for the SHSS determination according to the Dong method

**Figure 5.5:** 3D solid element model of an over-lapped joint failed from the weld end at the main-plate



**Figure 5.6:** Contour plot of  $\sigma_{xx}$  distribution as well as the extrapolation path and reference points for the type 'b' hot spot stress determination

to read out the through thickness stresses in order to calculate the structural stress according to Dong as discussed in Section 3.2.7. An example of the Dong stress calculation is presented in Appendix I.

Figure 5.6 shows the defined path and reference points used to evaluate the hot spot stress for an over-lapped joint failed at the cover plate edge. The figure shows also a contour plot of the perpendicular stress ( $\sigma_{xx}$ ) as the appropriate stress component for the SHSS calculation. Once the stress results are extracted, Equation 3.18 can be used to determine the corresponding SHSS value.

### 5.3 Evaluation according to the nominal stress method

The evaluation of fillet welded overlapped joints included 19 test specimens of which 10 failed in the main-plate and 9 in one of the cover-plates [63]. The geometrical parameters that are considered for this detail are given in Table 5.3.

In case of failure at the main plate, as shown in Figure 5.7, the fatigue strength of over-lapped specimens with longer cover plates (OM2) is slightly higher than the specimens in series OM1. The dependency of the fatigue life on the weld length has been recognized by Eurocode 3 as well. In addition to that, the lower fatigue resistance of OM1 specimens can be a result of extending the welds all the way to the plate edges. As it was discussed earlier, extending the welds to the plate edge can be destructive by forming weld defects such as undercuts. Statistical analysis of the test results reveals mean values of 73.4MPa for detail OM1 and 82.9MPa for detail OM2. The characteristic value of all the test data according to the nominal stress method is 61.8MPa with a standard deviation of 0.135. The obtained value is consistent with FAT56 recommended by Eurocode.

The fatigue test results of over-lapped joints cracked at the cover plate are plotted in Figure 5.8. Similar to the case with crack at the main plate, the longer plates exhibit an insignificant higher fatigue life. The standard deviation when all the tests are considered is 0.151 when performing a linear regression analysis with a

free slope, giving a mean value of 57.3MPa and a characteristic value of 46.4MPa. With a fixed slope of 3, the characteristic value is calculated to 41.1MPa with a standard deviation increasing to 0.169. It is worth mentioning that both Eurocode and IIW neglect the plate length effect and recommend design classes 45 and 50, respectively. While Eurocode recommendation appears to be a good representation, the IIW suggested FAT class seems to be optimistic, when the tests at hand are evaluated.

Table 5.4 presents the statistical evaluation of the fatigue test results of all over-lapped joints with a fixed slope of 3.

**Table 5.3:** *Dimensions and quantity of the evaluated fatigue test specimens for over-lapped joints; all dimensions are in mm.*

| Detail                     | Test data | Main plate | Cover plate |       | $d$  |       |      |
|----------------------------|-----------|------------|-------------|-------|------|-------|------|
|                            |           |            | Thickness   | Width |      |       |      |
| Cracked at the main plate  | OM1       | 5          | 12.7        | 114.3 | 12.7 | 108   | 0    |
|                            | OM2       | 5          | 12.7        | 114.3 | 12.7 | 171.5 | 12.7 |
| Cracked at the cover plate | OC1       | 4          | 12.7        | 114.3 | 9.5  | 95.25 | 0    |
|                            | OC2       | 5          | 12.7        | 114.3 | 9.5  | 171.5 | 12.7 |

**Table 5.4:** *Statistical evaluation of the fatigue test results of over-lapped joints based on the nominal stress method with a fixed slope of 3*

| Detail                     | Test data | $\Delta\sigma_{mean}$ [MPa] | $\Delta\sigma_C$ [MPa] | St.D. |       |
|----------------------------|-----------|-----------------------------|------------------------|-------|-------|
| Cracked at the main plate  | OM1       | 5                           | 73.4                   | 48.9  | 0.161 |
|                            | OM2       | 5                           | 82.9                   | 75.1  | 0.040 |
| Cracked at the cover plate | OC1       | 4                           | 49.7                   | 29.0  | 0.187 |
|                            | OC2       | 5                           | 58.1                   | 45.3  | 0.113 |

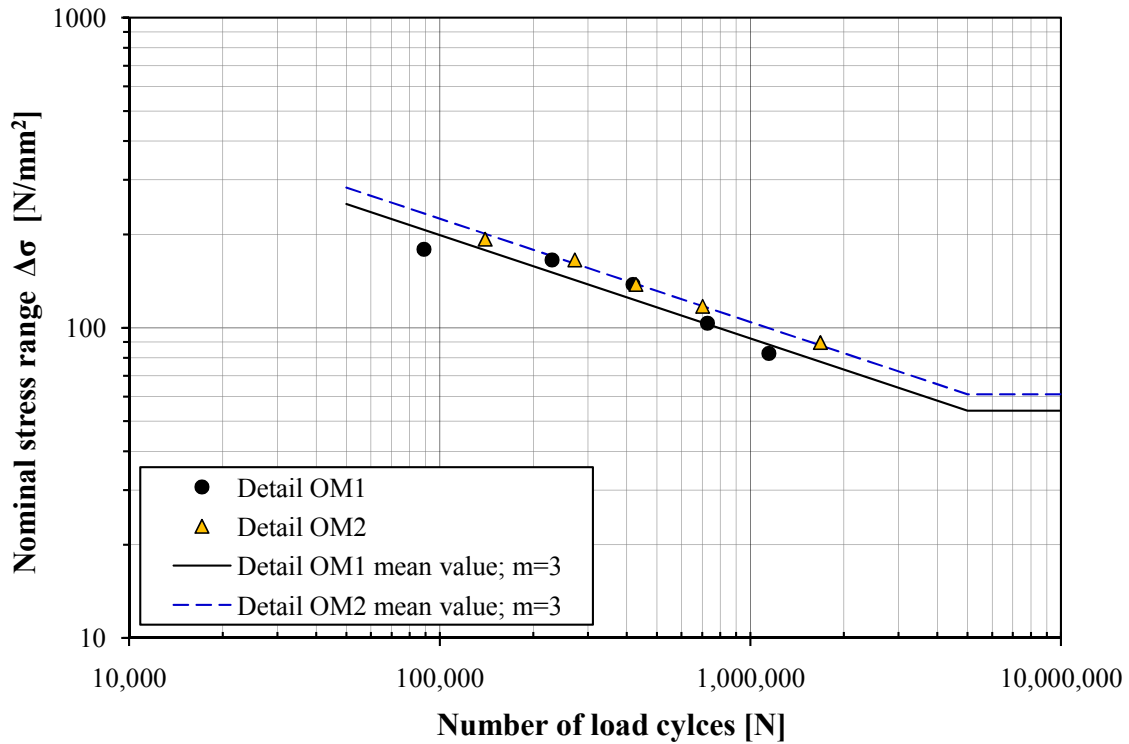


Figure 5.7: Fatigue test results of over-lapped joints failed from the main-plate according to the nominal stress approach

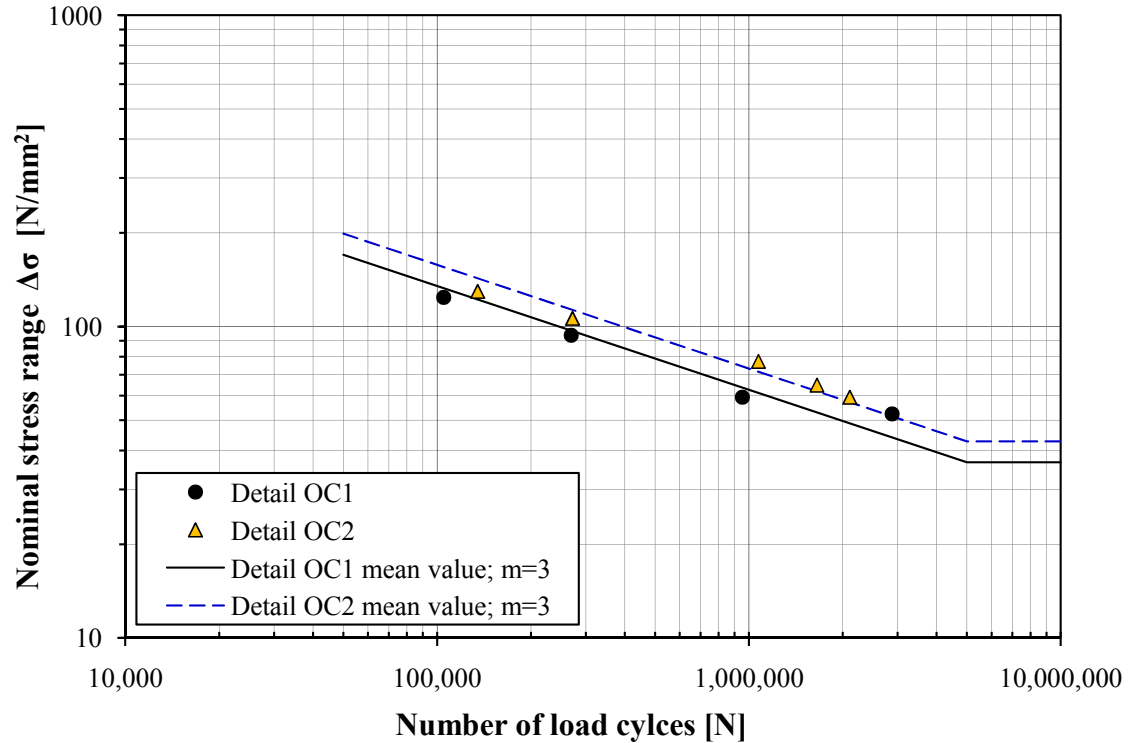


Figure 5.8: Fatigue test results of over-lapped joints failed from the cover-plate according to the nominal stress approach

## 5.4 Evaluation according to the hot spot stress approach

The hot spot stress S-N curve for over-lapped joints with crack at main plate are plotted in Figure 5.9. A linear regression analysis affirms a reduced standard deviation to 0.120 for all the data in this case. The characteristic value for fatigue strength is 80.3MPa which is lower than the recommended FAT90 strength in the IIW. The number of available tests is of course rather limited to question the credibility of this recommendation. Quadratic extrapolation is recommended for this detail as the stress increases very rapidly at the crack initiation point.

In case of over-lapped joints cracked at the cover plate, as it is shown in Figure 5.10, the scatter of the test data seems to be reduced when the hot spot stress is used, compared with the nominal stress method, and the two test groups lie within a narrow scatter band. Linear regression analysis reveals a meaningful reduction of standard deviation to 0.109 when using a free slope. With a fixed slope of 3 the characteristic value becomes 98.9MPa. As mentioned before, since the welds are load-carrying, fatigue detail category 90 can be assigned to this detail. Considering the evaluated tests in this study, FAT100 appears to give good representation. However, more test data on similar details with various configurations of different lengths and thicknesses are needed before a firm conclusion regarding upgrading the current detail category can be made.

In conclusion, the recommended SHSS detail category 90 for over-lapped joints with crack at the main plate seems to be incautious, whereas it is on the safe side for over-lapped joints failed at the cover plate. In the next section, the former over-lapped joints will be assessed based on the structural stress approach as proposed by Dong [31]. The findings from this investigation will help to determine the credibility of the proposed design category based on a hot spot stress calculation procedure other than the conventional surface stress extrapolation method.

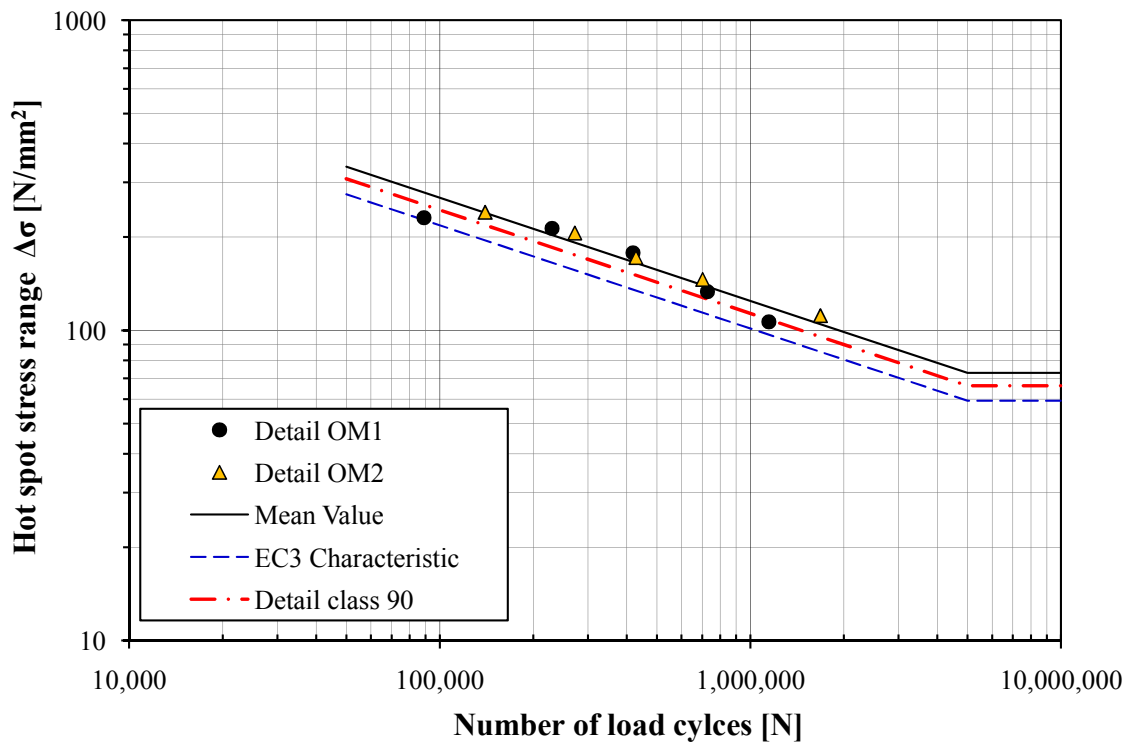


Figure 5.9: Fatigue test results of over-lapped joints failed from the main-plate according to the structural hot spot stress approach

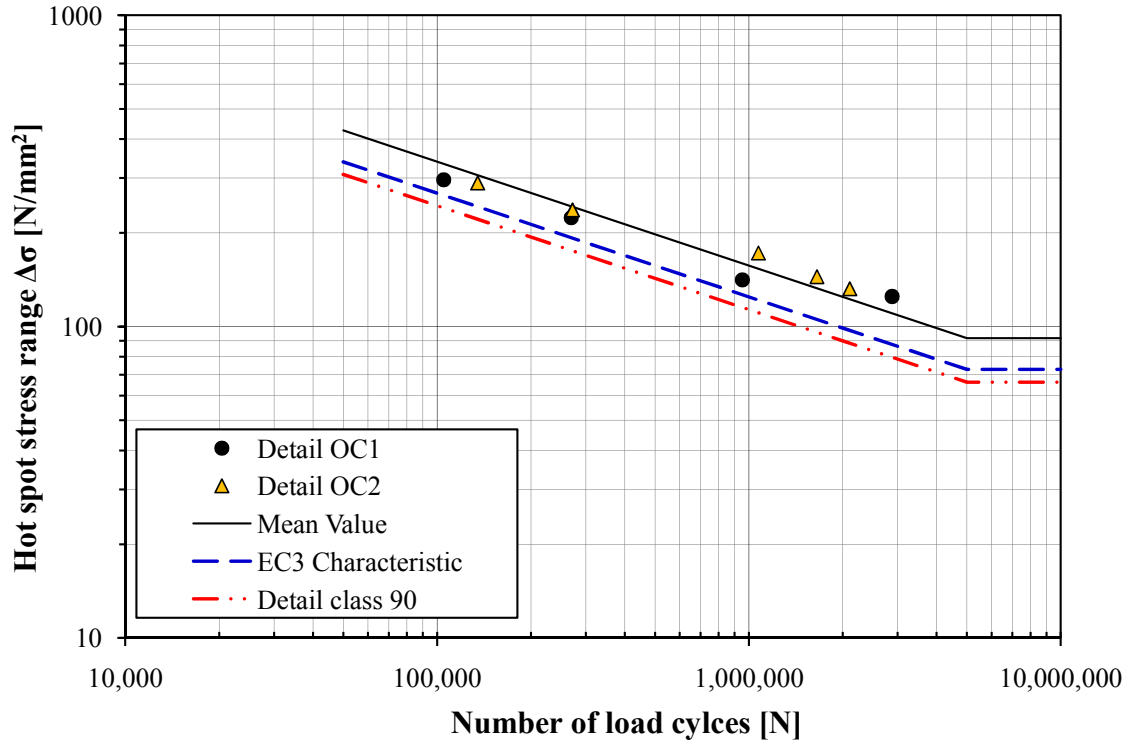


Figure 5.10: Fatigue test results of over-lapped joints failed from the cover-plate according to the structural hot spot stress approach

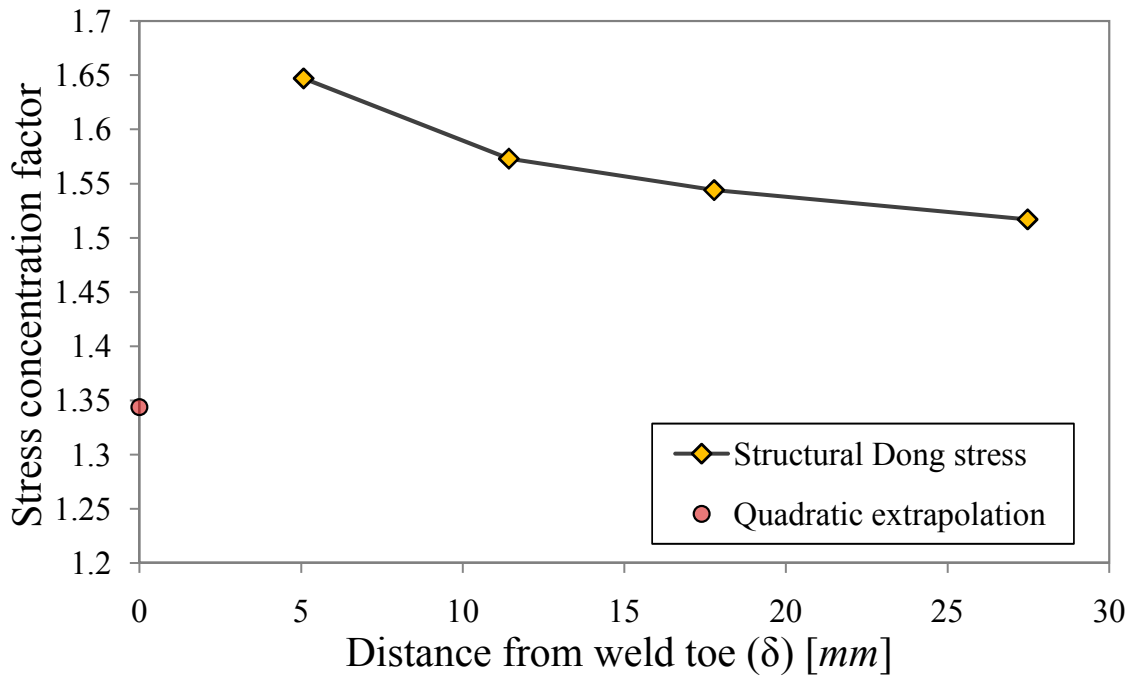
## 5.5 Evaluation according to the Dong stress method

It was discussed in the previous section that the characteristic fatigue strength of over-lapped joints with crack at the main plate, based on the SHSS approach, is below the recommended FAT90. In this section, the hot spot stress according to Dong [31] is implemented to derive the characteristic fatigue strength of the mentioned detail.

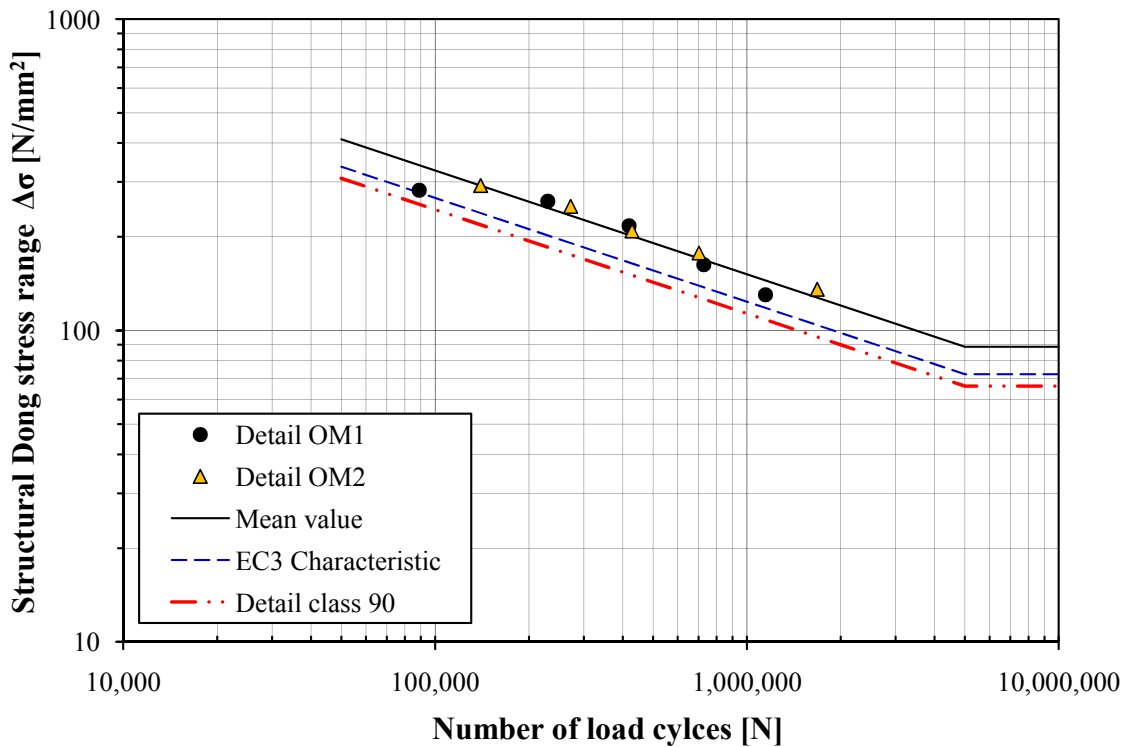
In the performed case study, the Dong stress was calculated for detail OM1 at several various distances from the weld toe ( $\delta$ ). The results in terms of stress concentration factor are plotted in Figure 5.11. It is apparent that the obtained Dong stress concentration factors decline as  $\delta$  increases. This observation is consistent with those reported by Doerk et al. [8] and Poutiainen et al. [46]. In addition to that, it is clear that the first obtained value at distance  $\delta = 0.4 \cdot t_m$  drops sharply as getting further away from the weld toe, while, the value obtained at  $\delta = 0.9 \cdot t_m$  seems to be stabilized. Figure 5.5c demonstrates the employed pathes to extract the appropriate nodal stress values for Dong stress calculation as explained in Appendix I.

Thus, the structural Dong stress concentration factors of over-lapped joints with crack at the main plate were calculated at  $\delta = 0.9 \cdot t_m$ . Figure 5.12 demonstrates the corresponding structural Dong stress S-N curve for this detail. The statistical evaluation of the results reveals a mean value equal to 120.2MPa followed by a characteristic fatigue design value of 98.1MPa. The standard deviation of all test data is equal to 0.118 which is slightly less than 0.120 in which was derived based on the surface stress extrapolation method.

Subsequently, it can be concluded that the recommended hot spot stress FAT90 for over-lapped joints failed at the main plate is reliable provided that the structural stress is derived according to the Dong method. In addition to that, it is recommended to calculate the Dong stress at a distance equal to  $\delta = 0.9 \cdot t_m$ .



**Figure 5.11:** Stress concentration factor for detail OM1 according to different SHSS calculation procedures



**Figure 5.12:** Fatigue test results of over-lapped joints failed from the main-plate according to the structural Dong stress approach

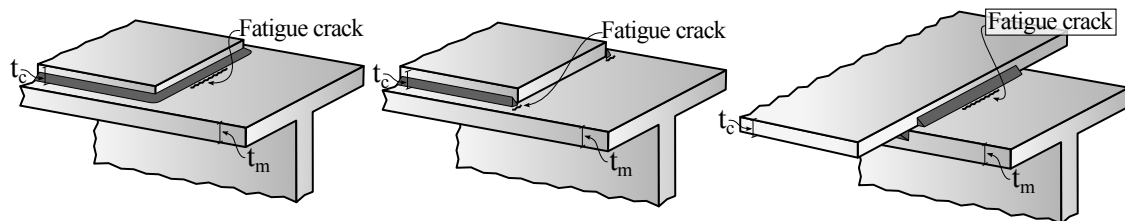


## 6 Fatigue Life Assessment of Cover-Plates

### 6.1 Introduction

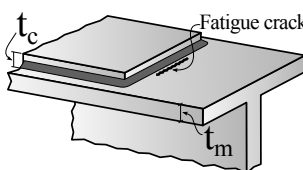
Partial-length cover-plates are usually welded to the flanges of steel bridge girders in order to increase the moment capacity and consequently the allowable traffic load and span of the bridge. Numerous studies [64–66] have shown that the cover-plate end zones have a very low fatigue resistance, see Figure 6.1. According to the most well-known fatigue design codes and guidelines, the cover-plate end is the most severe of all details. Tables 6.1 and 6.2 list the fatigue design classifications of cover-plate ends according to Eurocode 3 and IIW recommendations, respectively. Both design codes, categorize the cover-plate ends based on the relative thickness of the cover-plate to the main-plate i.e. flange. It is interesting to note that, except for the cover-plates wider than the flange, the transverse end welds can be omitted.

In this section, firstly, the literature related to the cover-plate details are reviewed and a comprehensive test database is built up. Afterwards, the advanced 3D finite element techniques, used to study the fatigue behavior of cover-plate ends are explicitly explained. Next, the effects of changing cover-plate ends are investigated. Eventually, the fatigue strength of cover-plate ends is investigated according to the structural hot spot stress and the effective notch stress approaches.

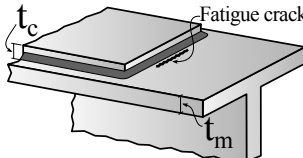


**Figure 6.1:** Schematics of cover plates with and without transverse end welds

**Table 6.1:** Fatigue classification of cover-plate details welded on I beams based on the nominal stress method according to Eurocode3 [9]

| Structural detail   | Description   | Requirements       |                    | FAT       |
|---|---|--------------------|--------------------|-----------|
|   |   | $t_c/t_m < 1$      | $t_c/t_m \geq 1$   |           |
|  | Cover plates in beams and plate girders; Single or multiple welded cover plates with or without transverse end weld | $t_m \leq 20mm$    | -                  | <b>56</b> |
|   |   | $20 < t_m \leq 30$ | $t_m \leq 20mm$    | <b>50</b> |
|   |   | $30 < t_m \leq 50$ | $20 < t_m \leq 30$ | <b>45</b> |
|   |   | $t_m > 50$         | $30 < t_m \leq 50$ | <b>40</b> |
|   |   | -                  | $t_m > 50$         | <b>36</b> |

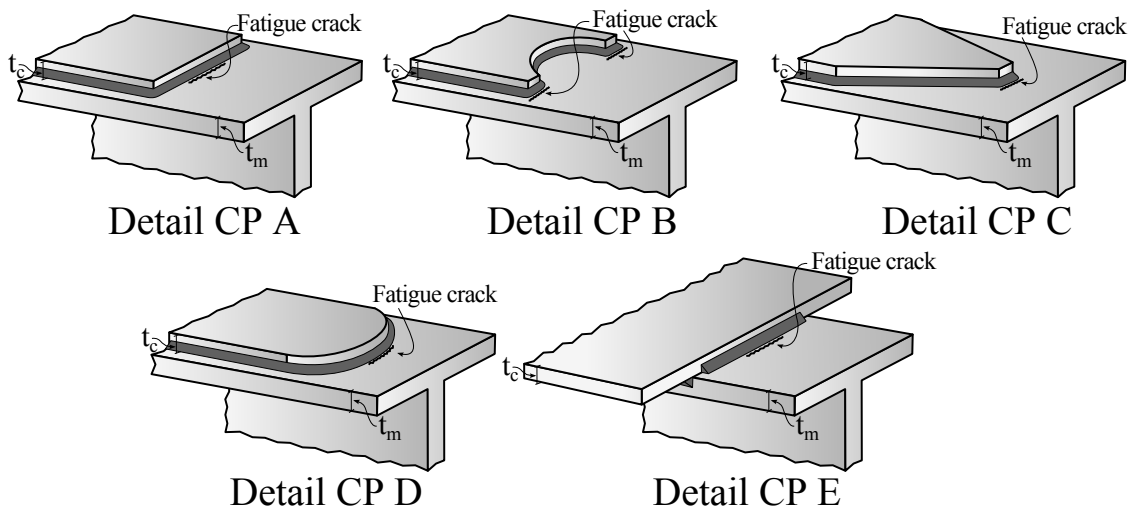
**Table 6.2:** Fatigue classification of cover-plate details welded on I beams based on the nominal stress method according to the IIW recommendations

| Structural detail   | Description   | Requirements             | FAT       |
|---|---|--------------------------|-----------|
|  | End zones of single or multiple welded cover plates with or without transverse end weld | $t_c/t_m \leq 0.8$       | <b>56</b> |
|   |   | $0.8 < t_c/t_m \leq 1.5$ | <b>50</b> |
|   |   | $t_c/t_m > 1.5$          | <b>45</b> |

## 6.2 Test database

The constant amplitude fatigue test results of 183 cover-plate specimens have been collected [64, 65]. The specimens accommodate a wide range of geometric variations such as the cover-plate to main plate thickness ratio ( $t_c/t_m$ ) and the cover-plate end shape; see Figure 6.2 and Table 6.3.

As it will be discussed in the next section, the majority of test programmes investigating the fatigue behavior of as-welded cover-plate details were conducted before 1980. Since then, the conducted researches were mainly focused on the fatigue life enhancement of cover-plate details by post-weld improvement techniques such as grinding and peening. Therefore, as the assessment of post-weld treated specimens is not within the scope of this study, the latter group of tests was excluded.



**Figure 6.2:** Different cover-plate test configurations

**Table 6.3:** *Dimensions and number of evaluated fatigue test specimens for cover-plate details; all dimensions are in mm*

| Detail | Test | Main plate |       | Cover plate |       | $t_c/t_m$ |
|--------|------|------------|-------|-------------|-------|-----------|
|        |      | Thickness  | Width | Thickness   | Width |           |
| CP A1  | 30   | 9.525      | 171   | 19.05       | 114   | 2         |
| CP A2  | 102  | 9.525      | 171   | 14.3        | 114   | 1.5       |
| CP A3  | 5    | 19.05      | 127   | 12.7        | 101.6 | 0.67      |
| CP B   | 5    | 19.05      | 127   | 12.7        | 101.6 | 0.67      |
| CP C   | 6    | 19.05      | 127   | 12.7        | 101.6 | 0.67      |
| CP D   | 5    | 19.05      | 127   | 12.7        | 101.6 | 0.67      |
| CP E   | 30   | 9.525      | 171   | 14.3        | 229   | 1.5       |

### 6.3 Literature review

Munse and Stallmeyer [67] performed a series of fatigue tests at the University of Illinois to investigate the effect of detail geometry on the fatigue behavior of flexural welded members such as cover-plates. With respect to beams with partial length cover-plates, the authors concluded the followings:

- Tapered partial length cover-plates have greater life than square ended cover plates. However, the difference is insignificant.
- Omitting transverse end welds increases the fatigue life by a small percentage.
- A gradual transition in thickness or width of flanges is the most effective way of increasing the fatigue strength.

A review of the early work, which was mostly done at the University of Illinois, was reported by the Task Committee on Flexural Members (1967). The main finding was that changing the cover plate end shape results in comparable fatigue lives.

Fisher et al. [65] tested 193 beams with various square-ended cover-plates that were made of three different steel types and subjected to various stress ranges. This study specified the stress range and the detail type as the fatigue strength determining factors. It was also found that the following variations of cover-plates does not influence the fatigue life:

- Cover-plates with or without transverse end welds
- Cover-plates wider or narrower than the flange
- Cover-plates up to 19mm thick
- Single or multiple cover-plates

The only exception was the not-welded end cover-plates wider than the flange which exhibited a much shorter fatigue life.

## 6.4 Finite element modeling techniques

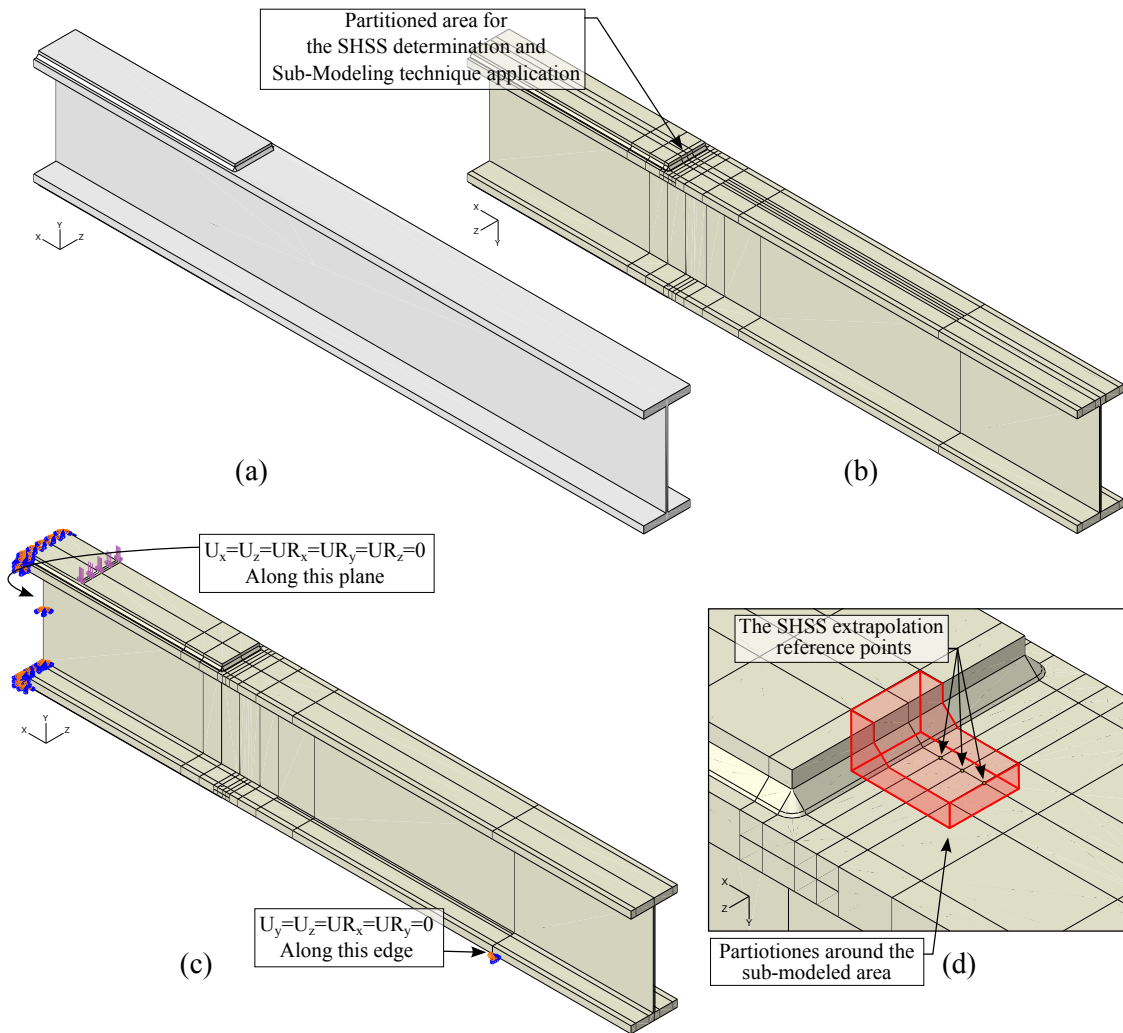
Welded cover-plate details on I beams are more complex in terms of the finite element modeling than the previous studied details. The constructed model is often very big which makes it difficult to maintain the mesh quality requirements. Moreover, cover-plate details are also assessed based on the effective notch stress method. As it was discussed in Section 3.3, this approach requires an extremely fine mesh in which meshing the entire model according to that will lead to a drastically large model. Thus, sub-modeling technique is used for the effective notch stress analysis. In addition to that, loading and boundary conditions should be defined in such a way to be compatible with the performed tests. In this section, the peculiarities of the finite element modeling of welded cover-plate details according to both the structural hot spot stress approach and the effective notch stress method are thoroughly discussed.

### 6.4.1 Global model

In order to calculate the SHSS, a global model is constructed for each test series. Furthermore, since the cover-plate details are also assessed according to the effective notch stress method, this model is used to obtain the displacements along the boundaries of the correspondent sub-model. As it is shown in Figure 6.3, due to the symmetrical nature of the conducted tests, only half of the tested specimens is modeled. Similar to the over-lapped joints, a symbolic one millimeter gap is modeled between the cover-plate and the flange. On the one hand, since the model size is still relatively large, it needs to be divided into small portions in order to allow for a gradual refinement of the mesh size at the critical locations. On the other hand, since the displacements along the boundaries of the sub-model have to be calculated, partitions should be created around the entire periphery of the sub-modeled region. Figure 6.3d illustrates the partitioned area at the weld toe of a square-ended cover-plate that facilitates the sub-modeling application.

Figure 6.3c demonstrates the applied boundary conditions and loads. As can be seen, symmetric boundary conditions with respect to the 'x axis' are defined along the symmetry plane of the beam. Additionally, boundary conditions corresponding to a roller restraint are defined along the support edge. Further, since linear elastic analysis can be assumed, the beam is loaded with an arbitrary pressure load at the load application surface. The hand calculations of the resulting displacements and stresses at the mid-section of the beam are compared with the analysis results in order to verify the model.

Similar to the performed 3D analysis in the previous sections, 20-node isoparametric elements are used. Moreover, due to the sharp stress gradient at the cover-plate end zone, quadratic surface stress extrapolation is performed to calculate the SHSS. These extrapolation points are distinguished in Figure 6.3d.



**Figure 6.3:** 3D finite element model of an I beam with welded cover-plates: (a) Modeled geometry, (b) Partitioned model, (c) Applied loads and boundary conditions, (d) Partitioned cover-plate weld toe area accommodating the SHSS calculation and the sub modeling application

#### 6.4.2 Sub model

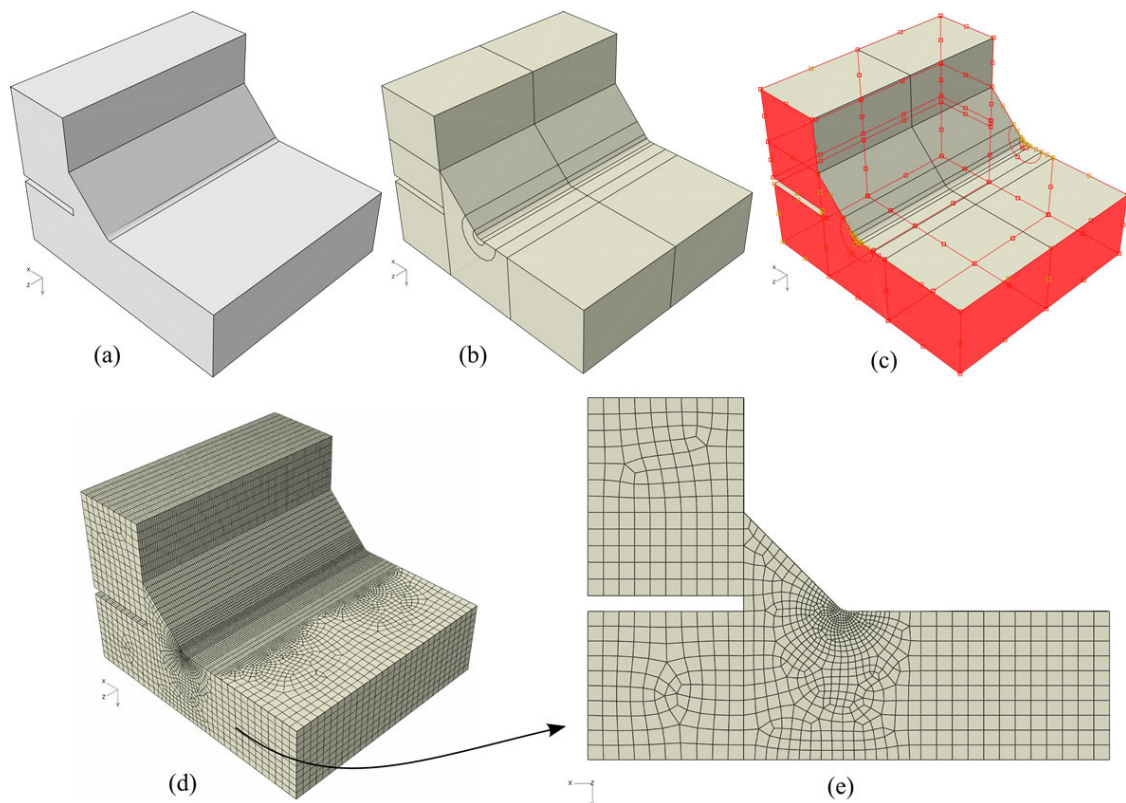
As discussed before, in order to maintain the extremely fine mesh required for the effective notch stress method, sub-modeling technique is used. This section aims to provide a short and general guideline regarding the application of 3D sub-modeling technique.

A sub-model uses the displacements obtained from the global model as the boundary conditions. Therefore, the nodal coordinates of a sub-model must be identical to its coordinates as a part of the global model. The sub-model can be constructed separately or obtained by cutting away the excessive parts of the global model surrounding the sub-modeled area. If the latter is used to obtain the sub-model, its nodal coordinates would be automatically properly placed. Otherwise, the sub-

model should be transferred to the correspondent position. Figure 6.4a shows the sub-model pertaining to the weld toe region shown in Figure 6.4d.

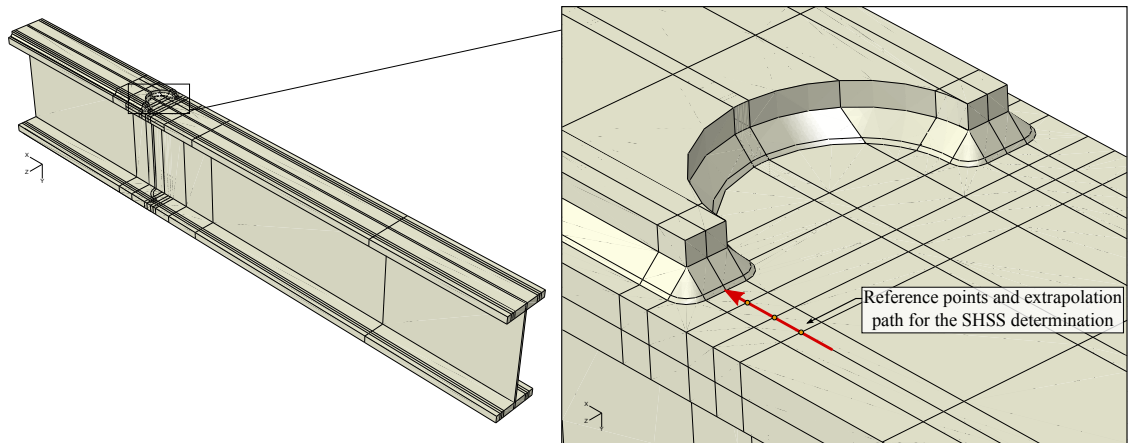
Once a sub-model geometry is constructed, the critical areas at the weld toe should be modified in accordance to the effective notch stress method. For the detail in question, the weld toe has been reported as the crack initiation area. Thus, the weld toe of the sub-model is rounded with a 1mm radius. Furthermore, the sub-model needs to be partitioned into smaller divisions to allow for a gradual transition from a coarse to a fine mesh at the weld toe region. A method to achieve this mesh quality is illustrated in Figure 6.4b.

The next step is to assign the proper boundary conditions to the relevant surfaces of the sub-model. As previously mentioned, a sub-model uses the displacements of its global model as the boundary conditions. Hence, on this basis it may be inferred that, the boundary conditions have to be applied along the sub-model's faces which are connected to the global model. In addition to that, since 3D solid elements are used, the boundaries has to be restrained for all three degrees of freedom. This type of boundary condition resembles the continuity of a sub-model as a part of a global model. Figure 6.4c shows the selected surfaces of the sub-model to assign proper boundary conditions.

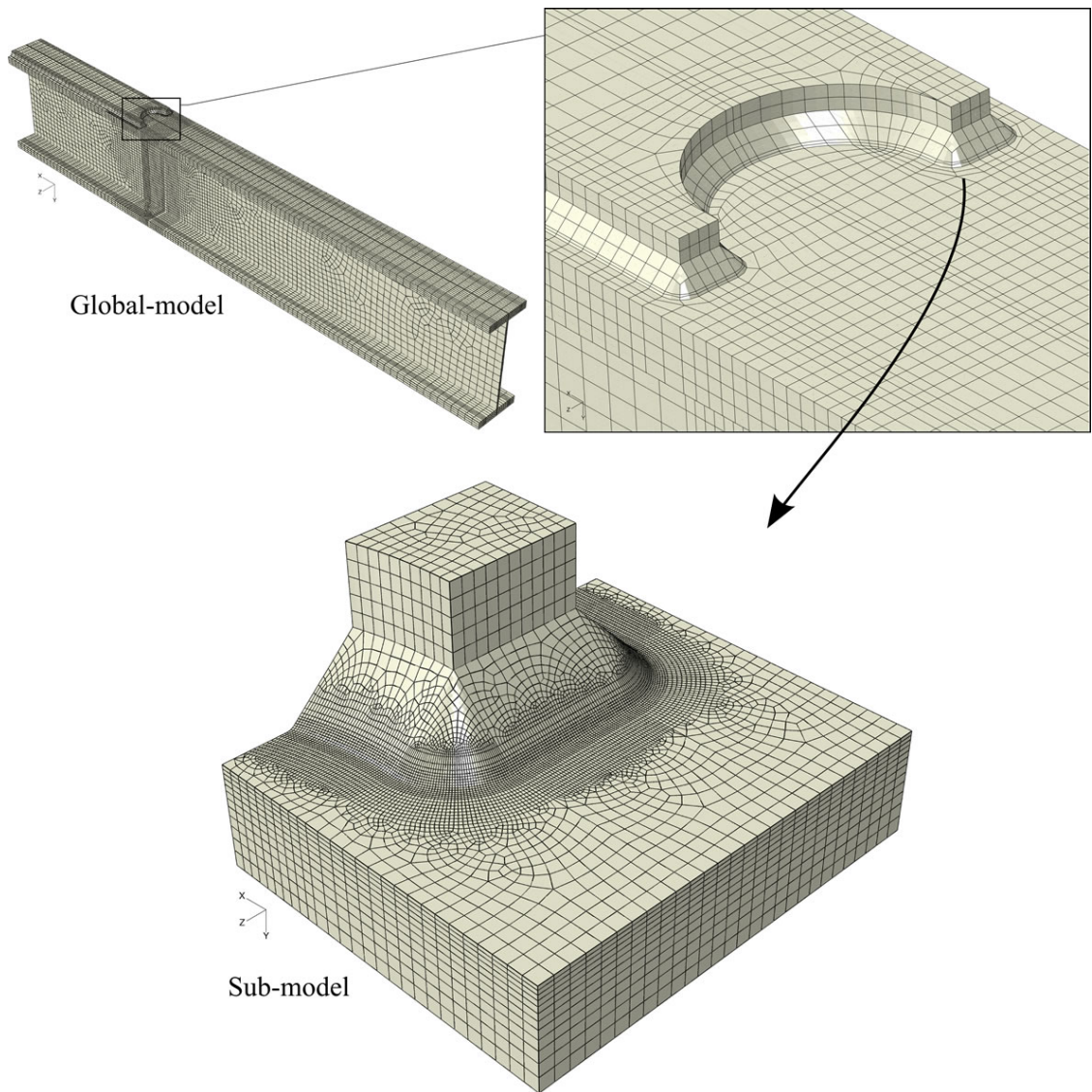


**Figure 6.4:** *Sub-modeling technique*





**Figure 6.5:** *Finite element model of a semicircular concave-ended cover-plate detail and the SHSS extrapolation path and reference points*



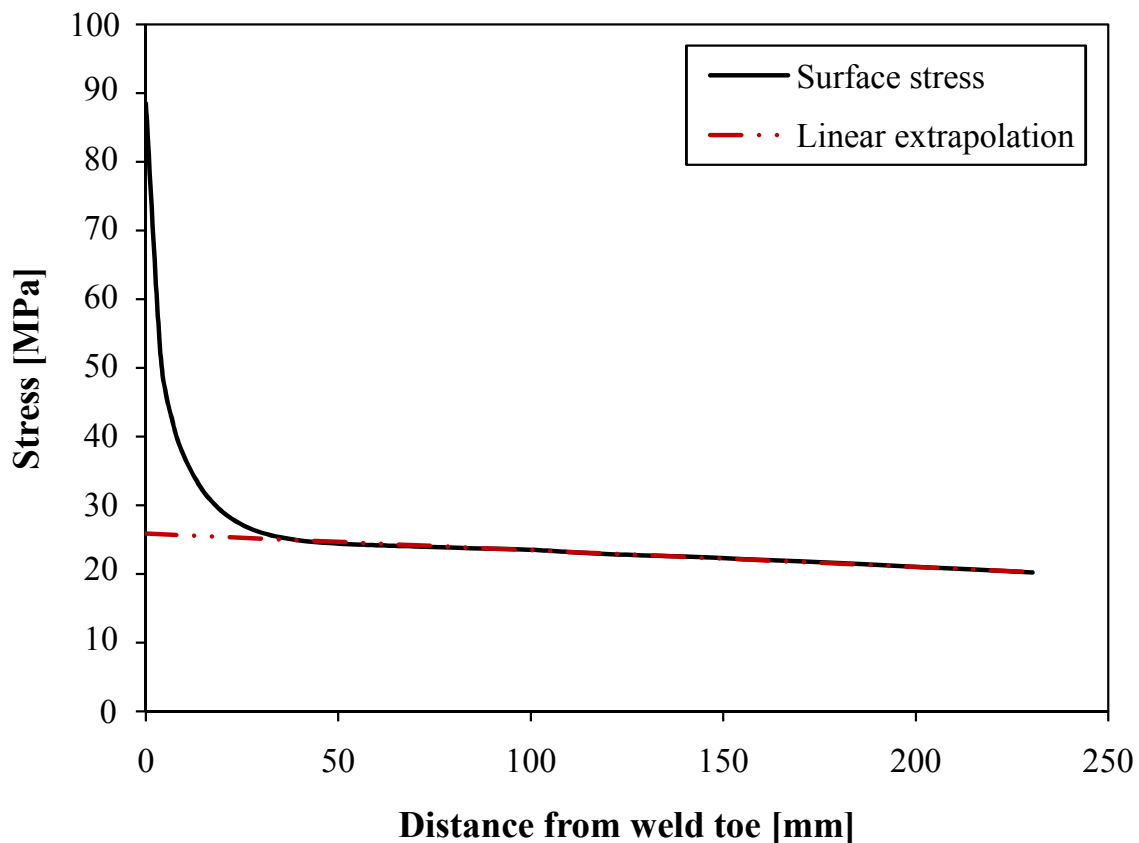
**Figure 6.6:** *Meshed global model and weld toe sub-model of a semicircular concave-ended cover-plate detail*

Eventually, a suitable mesh has to be generated for the prepared sub-model. In order to obtain a more flexible mesh with better element aspect ratios, a ‘hex-dominated sweep’ mesh is recommended. Moreover, by using the Abaqus ‘redefine sweep path’ feature and setting appropriate meshing pathes, a better mesh quality can be achieved. A generated mesh using the above mentioned recommendations are shown in Figure 6.4d and e.

Figures 6.5 and 6.6 demonstrate the finite element models of a semicircular concave-ended cover-plate detail.

### 6.4.3 The nominal stress calculation

In order to calculate the hot spot stress, the nominal stress at the outer most fiber of the flange should be calculated. This can be done by using either simple elastic beam calculations or by linear extrapolation of the stress distribution at a distance from the weld toe which is not affected by the local stress raiser i.e. weld. An example of the latter method is shown in Figure 6.7.



**Figure 6.7:** *The nominal stress calculation from the FEA output by linear extrapolation of the surface stress distribution in front of the weld toe*



## 6.5 Cover plate end shape effect

As it was mentioned in Section 6.3, several research programmes have shown that altering the cover-plate end shape yields comparable results. However, as plotted in Figure 6.10, the exhibited fatigue lives of the cover-plate details illustrated in Figure 6.8, slightly differs. The SHSS analysis results of the investigated cover-plate end configurations are plotted in Figure 6.9. As it is apparent, Type F end configuration has the lowest stress concentration factor. This observation is consistent with the test results in which the mentioned cover-plate end configuration has shown the highest fatigue life. The fatigue test results according to the SHSS are plotted in Figure 6.11.

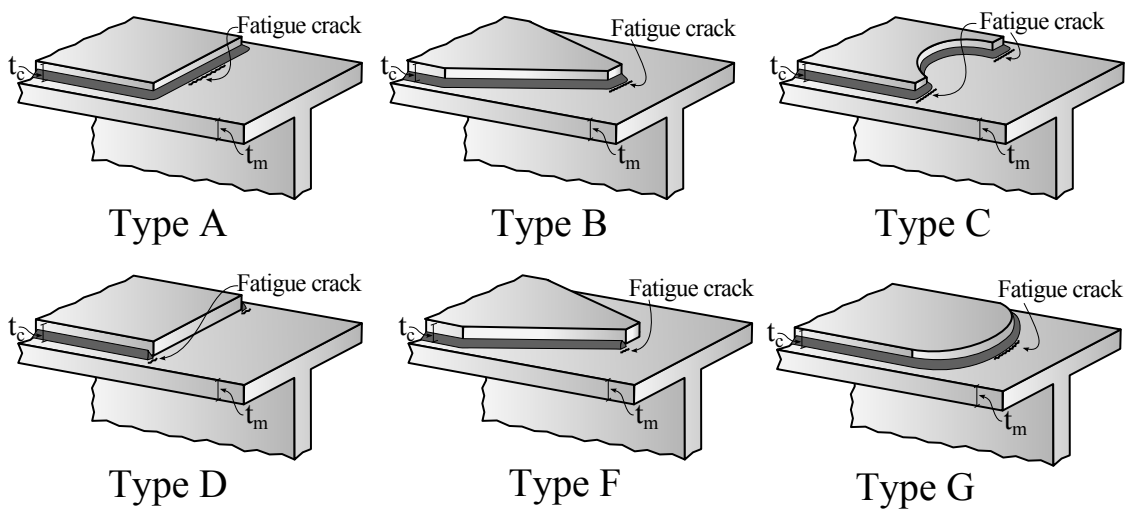


Figure 6.8: Various configurations of cover-plate end shapes

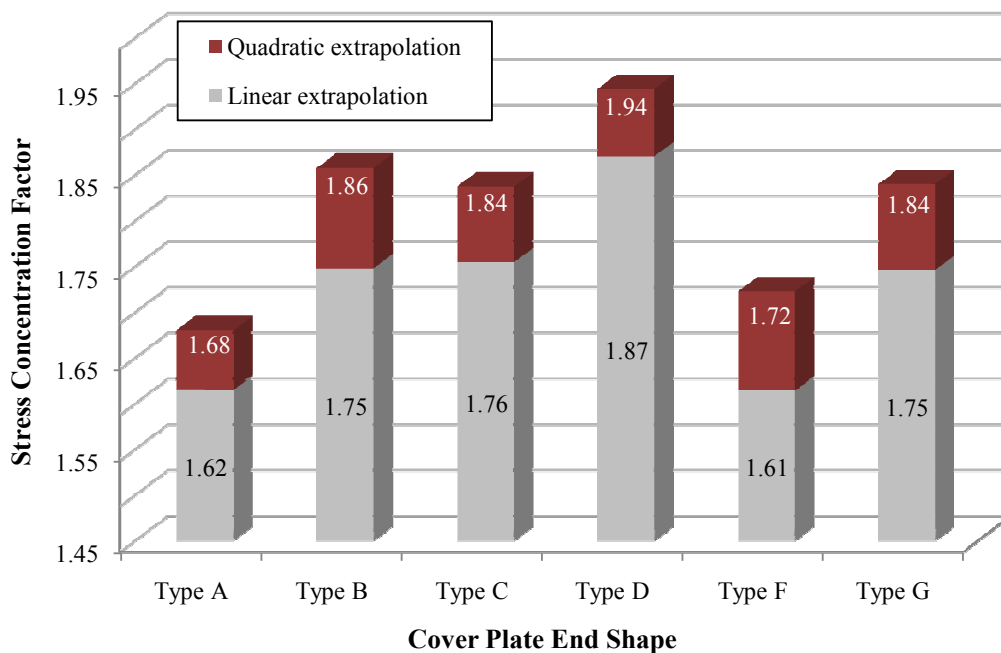


Figure 6.9: Various configurations of cover-plate end shapes

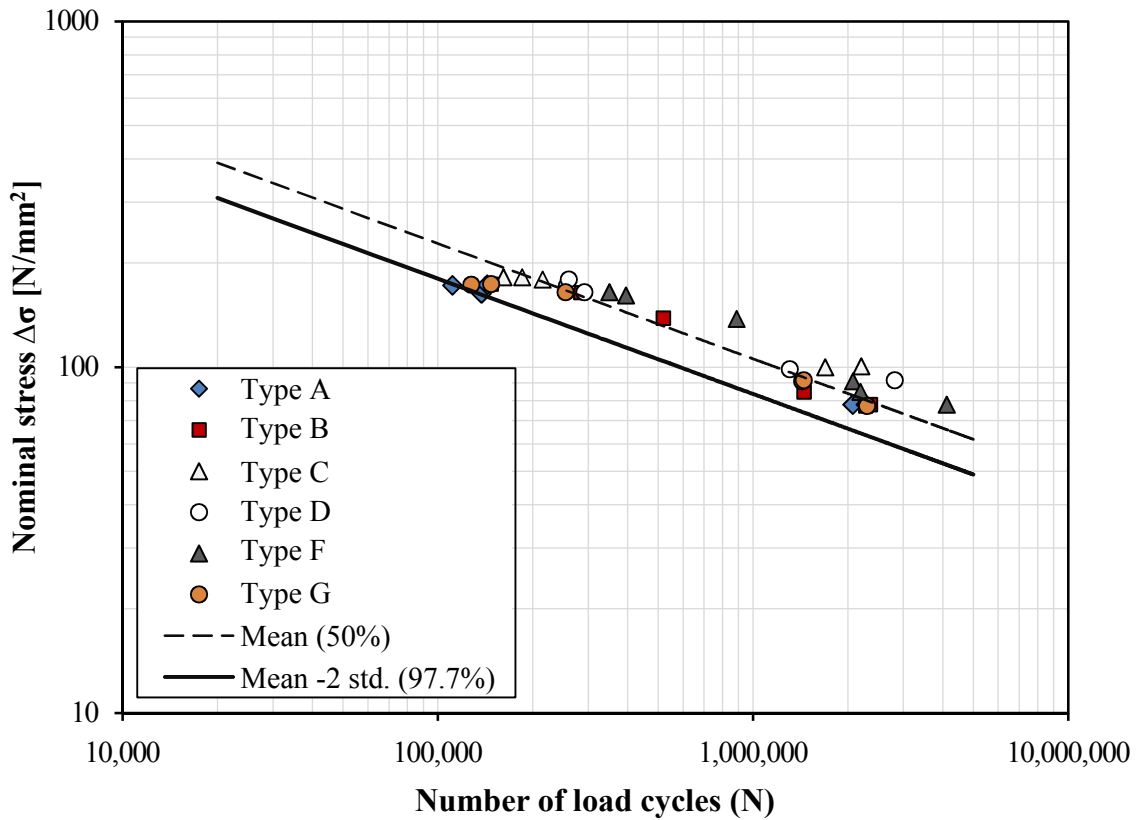


Figure 6.10: Fatigue test results of cover-plate details with different end shapes according to the nominal stress method

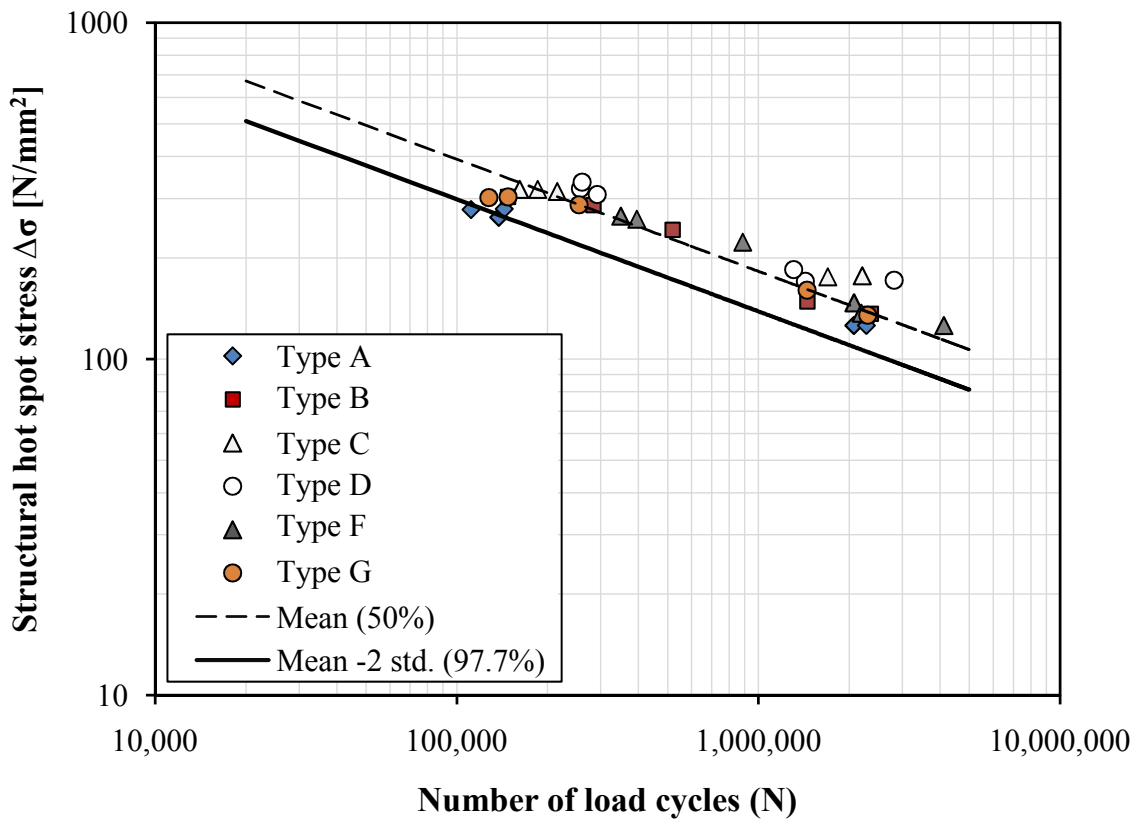


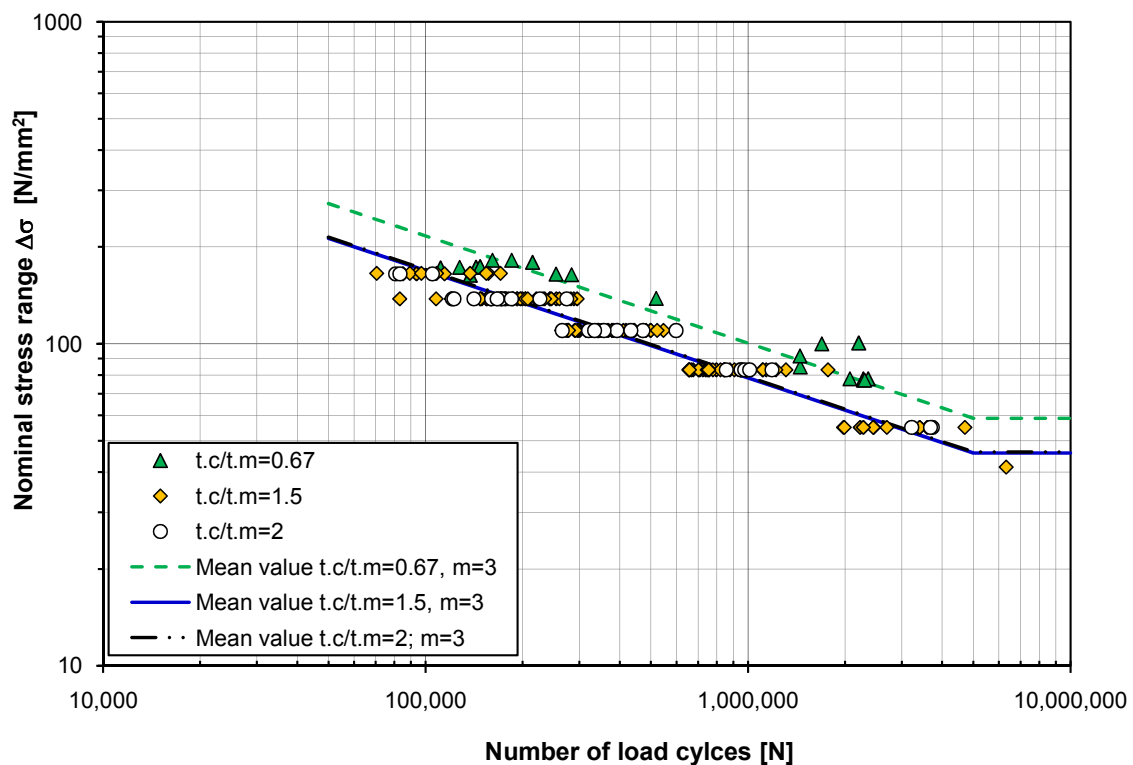
Figure 6.11: Fatigue test results of cover-plate details with different end shapes according to the structural hot spot stress approach

## 6.6 Evaluation according to the nominal stress method

Conforming to the data shown in Figure 8.3 and Table 8.4, the fatigue strength of cover plates seems to be particularly affected by the ratio  $t_c/t_m$ . It is apparent that cover plates with the lowest  $t_c/t_m$  ratio exhibit the highest fatigue strength. However, this effect disappears for details with  $t_c/t_m > 1$ . These details demonstrate the same fatigue strength. Moreover, as the fatigue test results of cover plates with various end shapes lie latently within the same scatter band, it can be concluded that changing the cover plate end shape does not affect the fatigue strength of cover plate details. While Eurocode has limited the effect of  $t_c/t_m$  to ratios only less than and higher than one, IIW considers several intervals. Consequently, considering the evaluated data in this study, Eurocode 3 recommendations appear to be more consistent.

**Table 6.4:** Statistical evaluation of the cover-plate test results using linear regression analysis with a fixed slope of 3

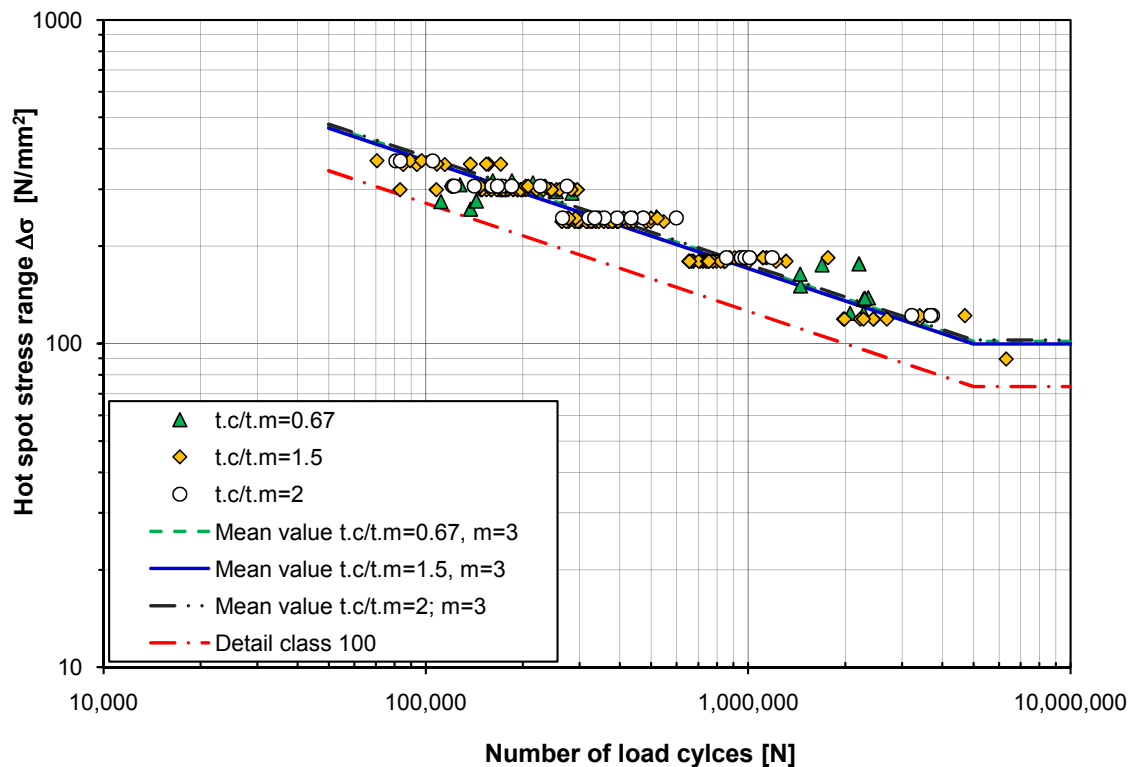
| Configuration    | Test data | $\Delta\sigma_{mean}$ [MPa] | $\Delta\sigma_C$ [MPa] | St.D. |
|------------------|-----------|-----------------------------|------------------------|-------|
| $t_c/t_m = 0.67$ | 21        | 79.7                        | 64.8                   | 0.147 |
| $t_c/t_m = 1.5$  | 132       | 62.2                        | 54.4                   | 0.104 |
| $t_c/t_m = 2$    | 30        | 62.7                        | 54.3                   | 0.103 |



**Figure 6.12:** Fatigue test results of overlapped joints failed from the main-plate according to the nominal stress method

## 6.7 Evaluation according to the hot spot stress approach

The test results of all cover-plate details evaluated using the structural hot spot stress approach are shown in Figure 6.13. As it was expected, the geometrical effects of different shapes and configurations are implicitly accounted for by the hot spot stress approach and all the data lie within one scatter band. This observation is supported by the statistical analysis as well. The standard deviation of all test data decreases significantly from 0.149 in the nominal stress approach to 0.116 for the hot spot stress approach. The recommended FAT100 seems also to be a reasonable representation for the fatigue strength of this detail.

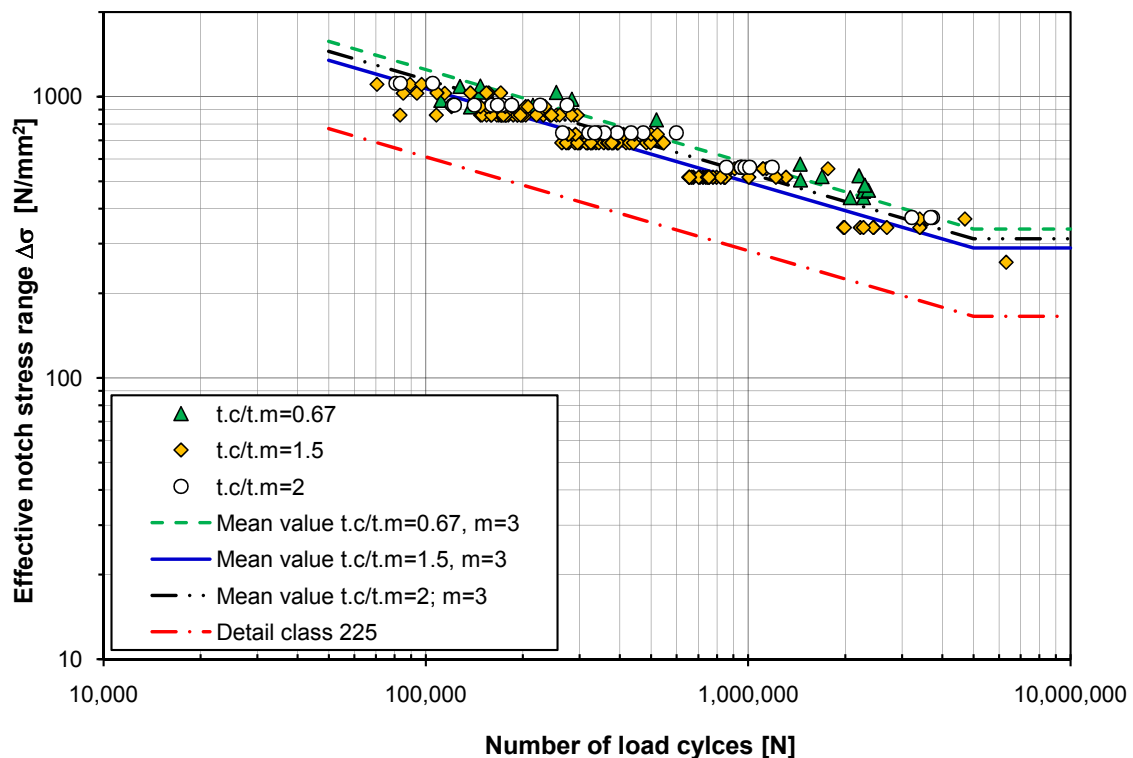


**Figure 6.13:** Fatigue test results of over-lapped joints failed from the main-plate according to the structural hot spot stress approach

## 6.8 Evaluation according to the effective notch stress method

The test results according to the effective notch stress approach are shown in Figure 6.14. It is apparent that although the scatter of the test data is reduced compared to the nominal stress method, they don't lie within one scatter band. The reason for this anomalous observation is assumed to stem from the fact that, when using effective notch stress method, the exact weld geometry should be modeled in order to obtain accurate results. However, the precise weld geometry is often unknown when assessing the test data or in the design phase.

The statistical comparison between the three investigated evaluation methods is listed in Table 6.5. FAT225 based on the effective notch stress approach seems to be in a good agreement with the evaluated test data for this detail.



**Figure 6.14:** Fatigue test results of over-lapped joints failed from the main-plate according to the effective notch stress approach

**Table 6.5:** Statistical evaluation of the cover-plate details according to different evaluation methods using linear regression analysis with a fixed slope of 3

| Evaluation method             | $\Delta\sigma_{mean}$ [MPa] | $\Delta\sigma_C$ [MPa] | St.D. |
|-------------------------------|-----------------------------|------------------------|-------|
| Nominal stress method         | 64.2                        | 53.0                   | 0.149 |
| Hot spot stress approach      | 136.5                       | 117.6                  | 0.116 |
| Effective notch stress method | 289.7                       | 230.3                  | 0.135 |



## 7 Fatigue Life Assessment of Cruciform Joints

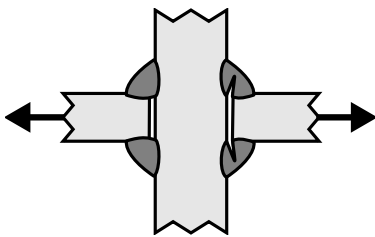
### 7.1 Introduction

As presented in Table 7.1, the assessment of root failure of cruciform or tee joints based on the nominal stress method, is categorized under the fatigue design class FAT36 irrespective of the joint geometry and the code. IIW recommendations propose an increase of FAT class 40 for the joints with  $a/t \leq 1/3$ , where  $a$  is the throat thickness of the weld and  $t$  is the thickness of the load carrying plate. It should be noted that the misalignment of the load-carrying plates should not exceed 15% of the thickness of the intermediate plate.

When it comes to local stress approaches, since the root cracking cannot be investigated by the structural hot spot stress approach, the effective notch stress method is proposed as an appropriate substitute. In this method the fatigue design class FAT225 is claimed to be applicable to all details provided that the maximum principal stress is used.

In this section, after building up a large test database, various influencing factors on the fatigue life of load-carrying cruciform joints with root failure are investigated. In addition to that, specific recommendations regarding the finite element modeling and analysis of load-carrying cruciform details is given. The credibility of the current design categories based on the nominal and the effective notch stress approach is investigated. Eventually, the capability of the effective notch stress method to predict the crack initiation and propagation path is examined through a case study.

**Table 7.1:** *Fatigue classification of the weld root cracks based on the nominal stress method*

| Structural detail   | Description  | FAT       |
|---|--|-----------|
|  | Root failure in fillet welded load-carrying cruciform joints | <b>36</b> |

## 7.2 Test database

A great number of tests have been carried out for this detail. However, a good documentation of the tests is not available for most of them. Therefore, in the test selection procedure, tests with more details and better documentation have given a higher priority to be included. Figure 7.1 shows a summary of all the 25 selected test series. The selected test series are consisted of a total number of 317 fatigue test data and cover a wide range of miscellaneous specimens [68–76].

In order to facilitate further references, based on the dimensions of the tested specimen an ID is assigned to its test group. For instance, a test group designated as M9M25C6L5 has been performed on specimens made of 9mm and 25mm thick plates as the main loaded plates on sides of the joint and a 6mm thick intermediate plate welded with a weld leg length of 5mm. In case of joints with equally thick side plates, the repetitive variable is dismissed.



| Performer             | ID         | Stress Ratio (R)                               | Weld geometry |                   |         |  | Residual stresses | Test data |
|-----------------------|------------|--|---------------|-------------------|---------|--|-------------------|-----------|
|                       |            |  | Leg Length    | Penetration depth | Angle   | Welding method                                 |                   |           |
| Kainuma et al 2005    | M14M14C14  | 0  | 6             | 0.5 - 3.2         | 45      | CO2 gas metal arc welding                      | Eliminated        | 7         |
| Kainuma et al 2005    | M9M14C14   | 0  | 6             | 0.5 - 3.2         | 45      | CO2 gas metal arc welding                      | Eliminated        | 9         |
| Kainuma et al 2005    | M9M14C6    | 0  | 6             | 0.5 - 3.2         | 45      | CO2 gas metal arc welding                      | Eliminated        | 9         |
| Kainuma et al 2005    | M9M25C6    | 0  | 6             | 0.5 - 3.2         | 45      | CO2 gas metal arc welding                      | Eliminated        | 10        |
| Kainuma et al 2006    | M16L7 - I  | 0  | 7             | n/a               | 45      | CO2 gas metal arc welding                      | Eliminated        | 3         |
| Kainuma et al 2006    | M16L7 - S1 | 0  | V7H14         | n/a               | Scalene | CO2 gas metal arc welding                      | Eliminated        | 3         |
| Kainuma et al 2006    | M16L7 - S2 | 0  | V14H7         | n/a               | Scalene | CO2 gas metal arc welding                      | Eliminated        | 3         |
| Kainuma et al 2006    | M16L7 - CV | 0  | 7             | n/a               | Convex  | CO2 gas metal arc welding                      | Eliminated        | 3         |
| N.N. 1980             | M25L19     | 0  | 19            | n/a               | 45      | Manual arc welding                             | Preheated         | 5         |
| N.N. 1980             | M25L22     | 0  | 22            | n/a               | 45      | Manual arc welding                             | Preheated         | 3         |
| N.N. 1980             | M38L24     | 0  | 24            | n/a               | 45      | Manual arc welding                             | Preheated         | 5         |
| N.N. 1980             | M38L33     | 0  | 33            | n/a               | 45      | Manual arc welding                             | Preheated         | 7         |
| N.N. 1980             | M25L21     | 0  | 21            | n/a               | 45      | Manual arc welding                             | Preheated         | 5         |
| Neumann A. 1958       | M15L10     | 0.3  | 10            | n/a               | 45      | Manual arc welding                             | n/a               | 11        |
| Neumann A. 1958       | M15L10     | 0.3  | 10            | n/a               | 45      | Semi-automatic submerged arc welding           | n/a               | 8         |
| Neumann A. 1958       | M15L10     | 0.3  | 10            | n/a               | 45      | Automatic submerged arc welding                | n/a               | 7         |
| Neumann A. 1966       | M12L11.3   | 0.26<br>0.32<br>0.12<br>0.09<br>-0.72<br>-0.39 | 11.3          | n/a               | 45      | Low-hydrogen electrode manual arc welding      | n/a               | 27        |
| Macfarlane D.S. 1965  | M12.7L8C32 | 0  | 7.9           | n/a               | 45      | Rutile electrode manual arc welding            | n/a               | 8         |
| Haibach E. 1966       | M10L8.5    | -1.0<br>0                                      | 8.5           | n/a               | 45      | Rutile electrode manual arc welding            | n/a               | 17        |
| Haibach E. 1966       | M10L8.5    | 0  | 8.5           | n/a               | 45      | Rutile electrode manual arc welding            | Stress relieved   | 7         |
| Haibach E. 1966       | M10L8.5    | 0  | 8.5           | n/a               | 45      | Rutile electrode manual arc welding            | Stress relieved   | 7         |
| Haibach E. 1966       | M10L5.7    | -1.0<br>0                                      | 5.7           | n/a               | 45      | Rutile electrode manual arc welding one pass   | n/a               | 25        |
| Haibach E. 1966       | M10L8.5    | 0.57<br>0.33<br>0.67                           | 8.5           | n/a               | 45      | Rutile electrode manual arc welding two passes | n/a               | 36        |
| Haibach E. et al 1968 | M10L8.5    | -1.0<br>0                                      | 8.5           | n/a               | 45      | Rutile electrode manual arc welding two passes | n/a               | 81        |
| Latzin K. 1974        | M14L6.3    | -1.0   | 6.3           | n/a               | 45      | Manual arc welding                             | n/a               | 11        |

Figure 7.1: Summary of the selected tests of the root failure of load-carrying cruciform joints

## 7.3 Finite element modeling and analysis

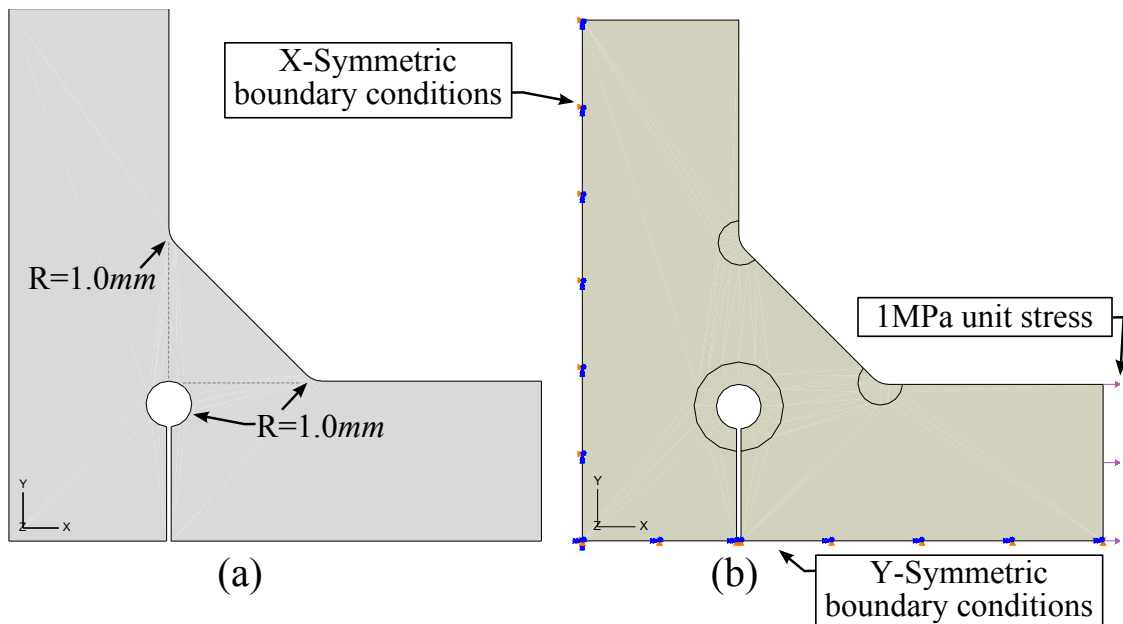
As discussed earlier, the structural hot spot stress approach is not applicable in case of root failures. Therefore, the effective notch stress method is implemented to assess the fatigue performance of load-carrying cruciform joints. Due to the constant cross section of the detail through the depth, a 2D analysis is sufficient. This section aims to describe the finite element modeling and analysis procedure of load-carrying cruciform joints using the effective notch stress method.

### 7.3.1 Geometry and partitioning

Load-carrying cruciform joints are usually symmetrical with respect to both or one axis. Therefore, it is often satisfactory to model one quarter or half of the detail. Additionally, as mentioned above, the detail geometry is uniform through the depth and a 2D analysis is sufficient.

In this study, the theoretical reported values are used to model the geometries. Afterwards, the required modifications according to the effective notch stress concept are applied to the FE models. The sharp transitions from the plate to the weld toes are replaced with smooth transitions with 1.0mm radius. Also, a 1mm radius notch is introduced at the weld root such that the tip of the radius touches the root of the real notch. Figure 7.2a demonstrates an example FE model of a load-carrying cruciform joint prepared for the effective notch stress analysis.

In order to mesh the modeled geometry according to the effective notch stress



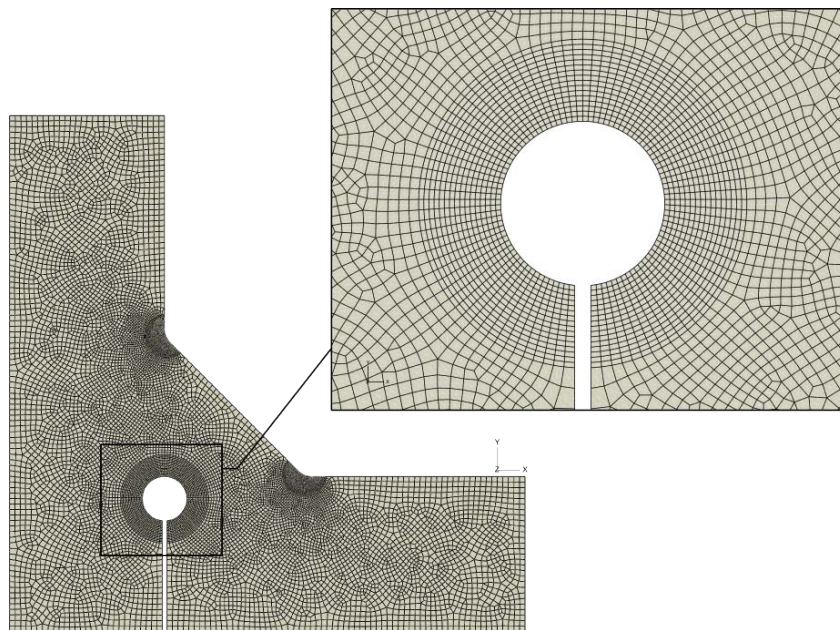
**Figure 7.2:** 2D finite element model of a load-carrying cruciform joint : (a) Modeled geometry with respect to the effective notch stress requirements, (b) Loading and boundary conditions applied on the partitioned model

requirements, it has to be partitioned in several smaller regions. In another words, since an extremely fine mesh is required at the crack initiation sites, the model should be divided into partitions to allow for a gradual transition from a coarse to a fine mesh at the mentioned areas. Figure 7.2b shows a partitioned model as well as the applied loading and boundary conditions. Similar to the previous analysis, a unit tensile stress is applied on the pertaining boundary of the model. The boundary conditions are also defined along the symmetry planes as illustrated in Figure 7.2b.

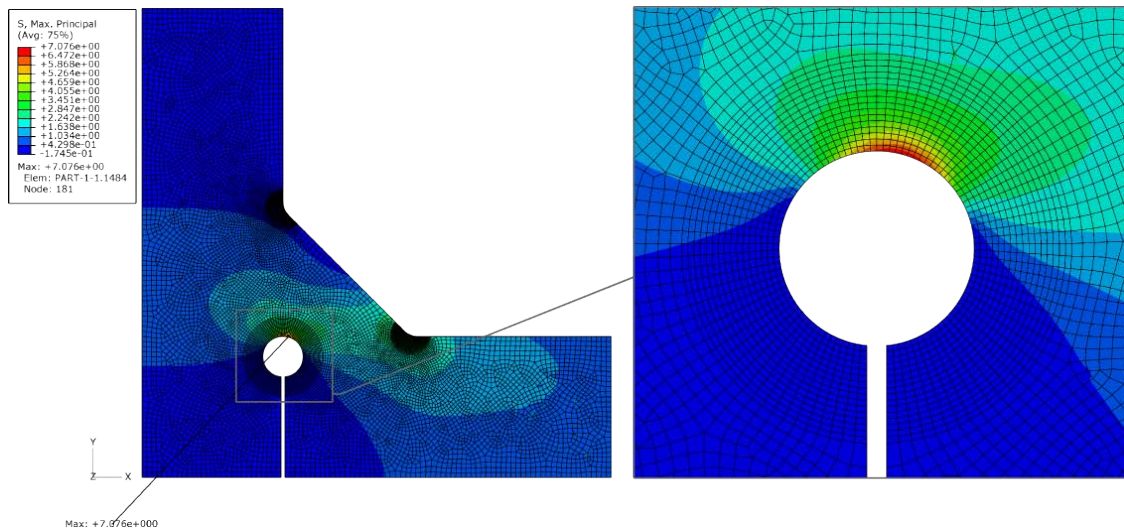
### 7.3.2 Meshing, Element type and analysis procedure

Figure 7.3 shows a typical generated mesh for the discussed detail. As can be seen, for increased accuracy, a finer mesh than that proposed by the IIW recommendations is constructed at the weld root. In order to obtain the exact desired mesh, 'structured mesh' is generated at the critical areas while the rest of the model is meshed using 'Quad-dominated' free mesh control.

As recommended by Fricke [54] quadratic plain strain shell elements are chosen as the appropriate element type for the analysis of this detail. Once the model is analyzed using a static analysis procedure, the maximum principal stress as the pertinent stress component can be directly exploited. For the analysis of the detail in question, the maximum obtained stress value at the weld root is considered as the effective notch stress. Since a unit nominal stress is applied, the obtained value is regarded as the effective notch stress concentration factor. Figure 7.4 shows the maximum principal stress contour plot for a sample detail.



**Figure 7.3:** 2D meshed finite element model of a load-carrying cruciform joint with special consideration given to the weld root as the crack initiation area



**Figure 7.4:** *Maximum principal stress contour plot of a load-carrying cruciform joint*

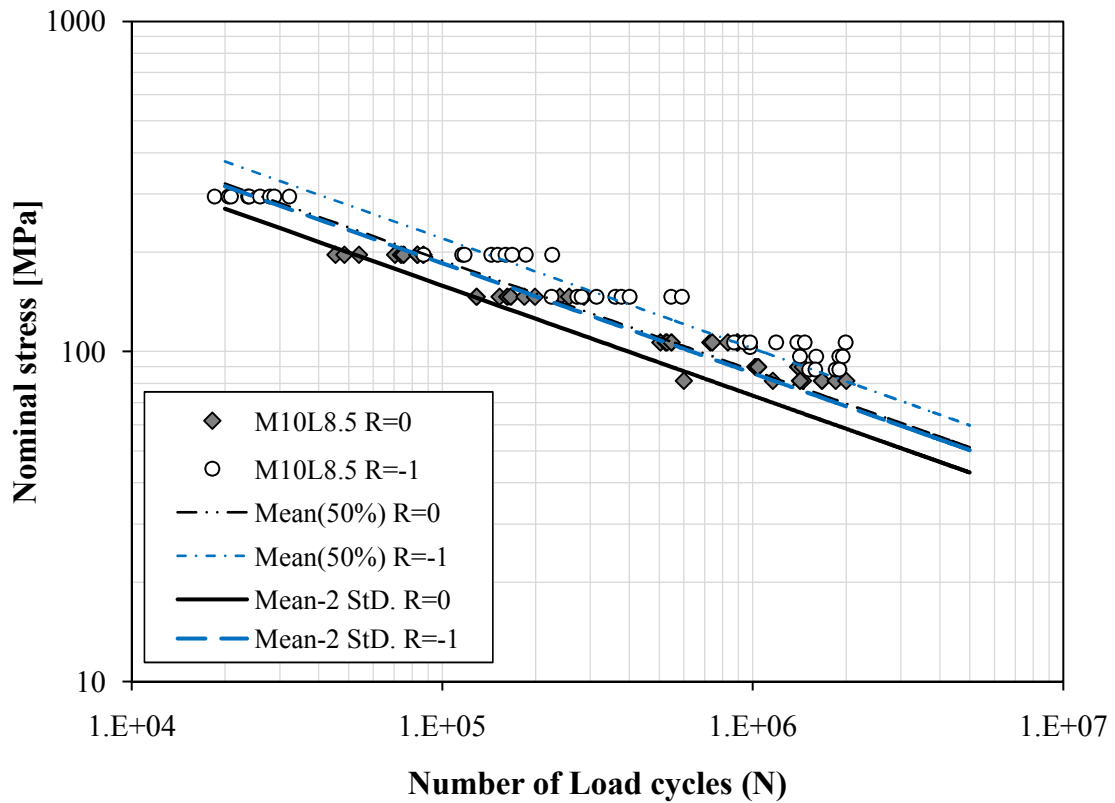
## 7.4 Influencing factors

In this chapter several factors which can affect the fatigue life of load-carrying cruciform joints will be studied in more details. However, the investigated parameters are limited to those which can be assessed by the available fatigue analysis approaches and have been provided with adequate information via the test reports.

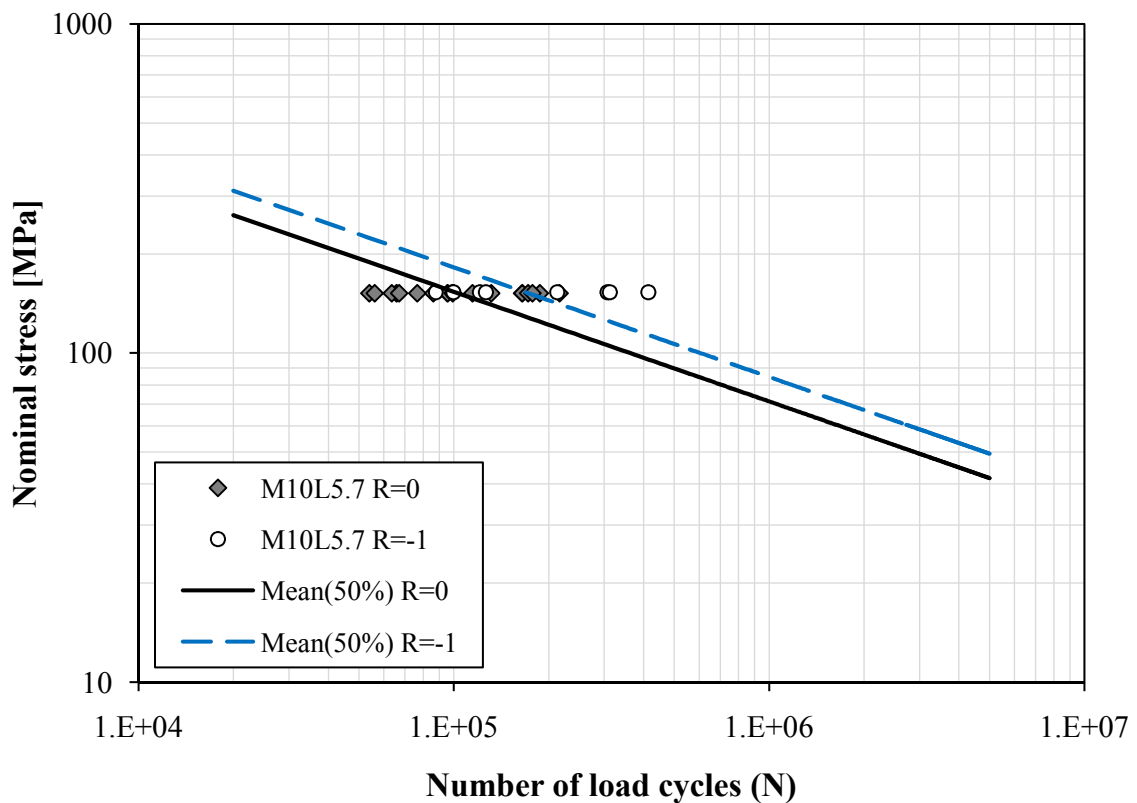
### 7.4.1 Stress ratio (R) effect

In order to investigate the effect of stress ratio on the fatigue life of this detail, the tests which were carried out by different R ratios were used to produce S-N curves of the test results. In cases that the stress was provided in the plate section, the equal stress at the throat section is calculated and replaced, see Section 7.4.4.

It is shown in Figures 7.5 and 7.6 that the stress ratio has a significant effect on the fatigue life of the specimens. It is apparent that the tests with a negative stress ratio have generally exhibited a higher fatigue life than those tested with  $R=0$ . As the effect of stress ratio can not be accounted for when using the effective notch stress approach, only the tests with a positive stress ratio have been considered in this study.



**Figure 7.5:** *Fatigue test results of identical load-carrying cruciform joints tested with different stress ratios*

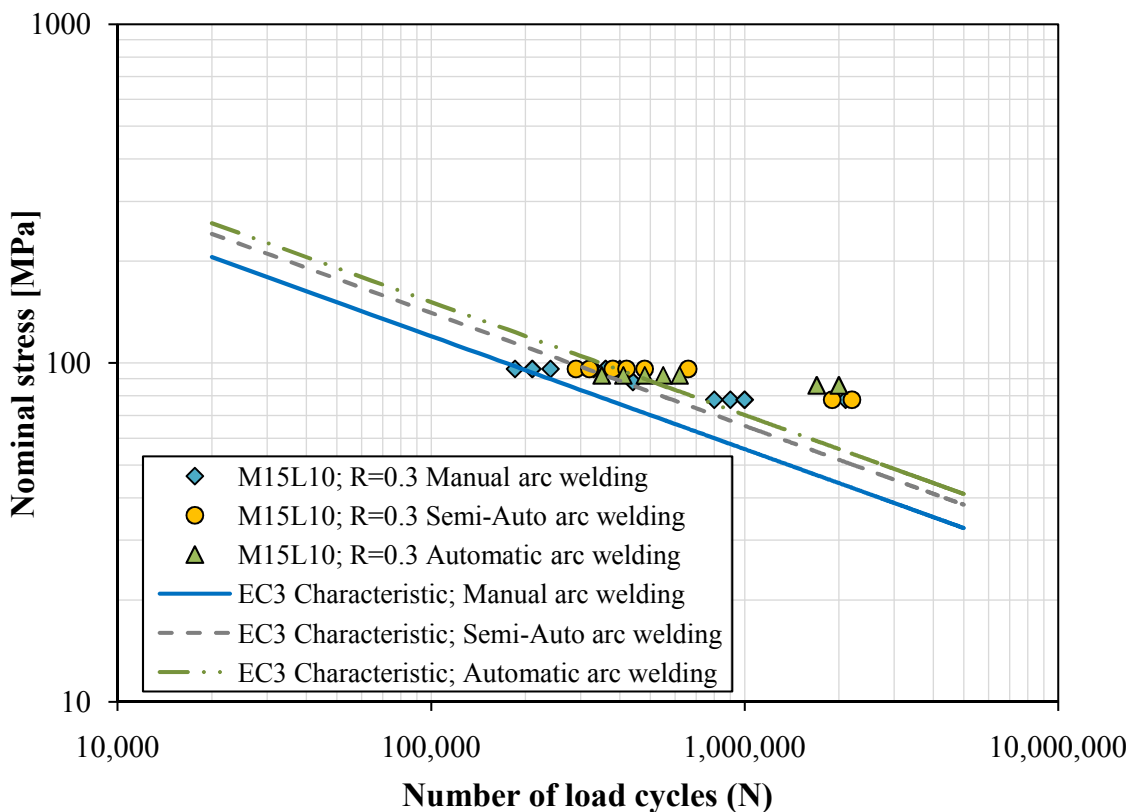


**Figure 7.6:** *Fatigue test results of identical load-carrying cruciform joints tested with different stress ratios*

## 7.4.2 Welding method effect

Figure 7.7 demonstrates the effect of welding method on the fatigue life of geometrically identical details but welded with different techniques. It is apparent that the welding method can affect the results such that the manually welded details reveal a significantly lower fatigue resistance than the other cases. Thus, it can be concluded that, the welding technique should be considered as an effective factor in comparisons of the test results.

It is interesting to note that, none of the fatigue assessment methods including the nominal and the effective notch stress approaches, consider this effect. Therefore, similar to the stress ratio effect, only details made with the same welding technique have been studied.

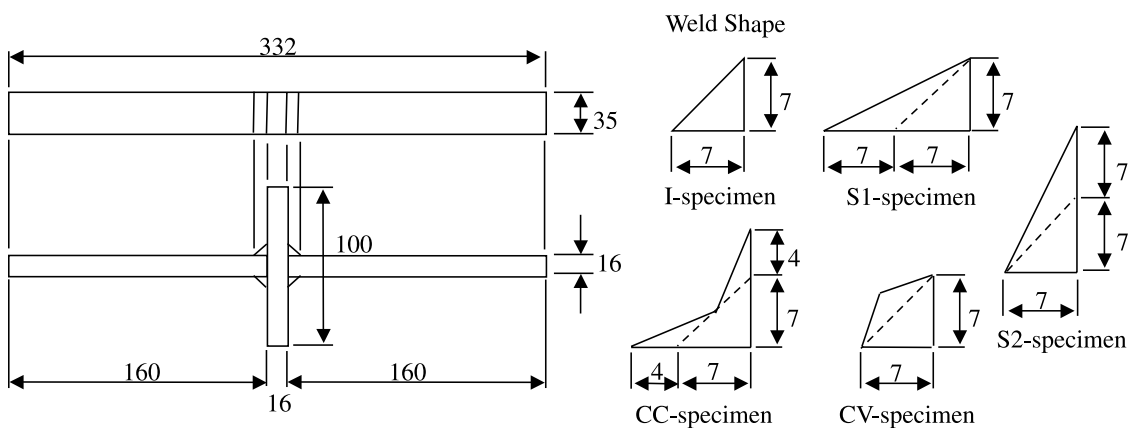


**Figure 7.7:** Fatigue test results of geometrically identical load-carrying cruciform joints welded with different techniques

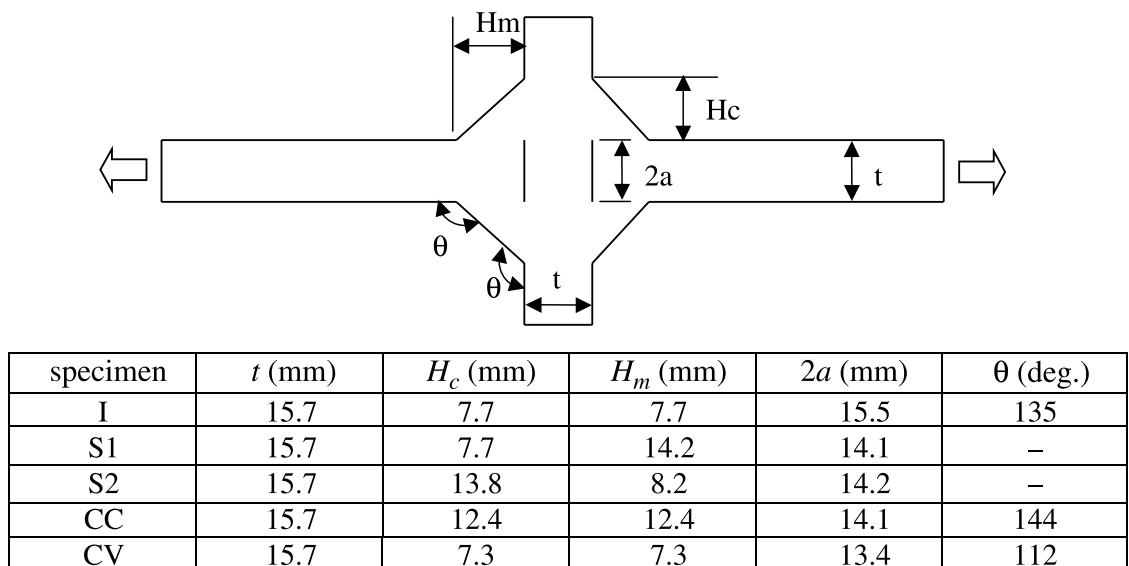
### 7.4.3 Weld shape effect

Fricke et al. [77] have reported an effect of the modeled weld geometry using the effective notch stress method. Since the weld geometry is precisely modeled for analysis based on this method, it is of great interest to assess the capability of this method to reduce any possible scatter of the test results caused by the variations of the measured weld shapes. Therefore, a group of tests performed by Kainuma and Mori [69] on specimens with the same plate thickness but different weld shapes were selected, see Figure 7.8. The authors have also measured the fabricated specimens and reported the mean measured values as can be seen in Figure 7.9.

The test results are plotted in Figure 7.16. It is apparent that as long as the weld leg length in the direction of the load application is constant, the shape of the weld is almost ineffective. On the contrary, increasing the leg length in the load

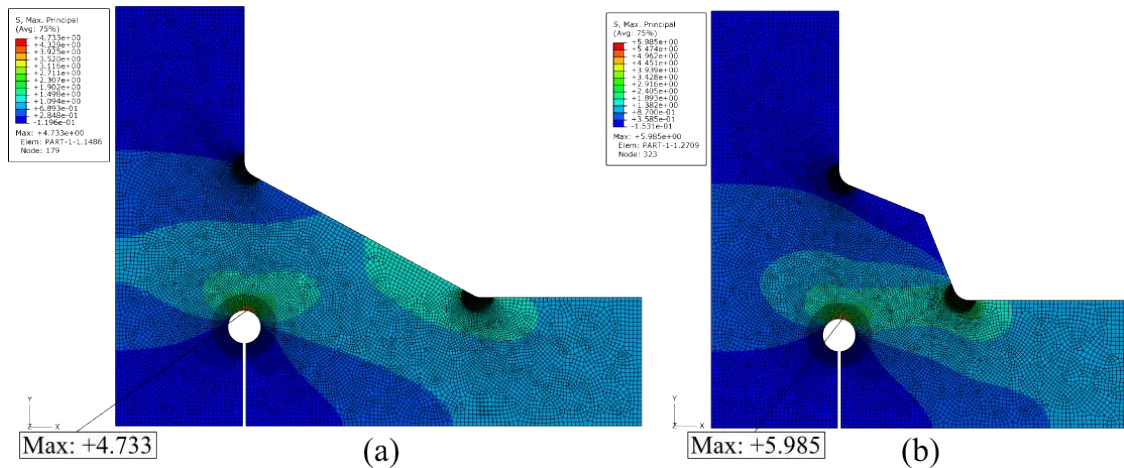


**Figure 7.8:** Fatigue tested load-carrying specimens with different weld shapes, after [69]



**Figure 7.9:** Shapes and dimensions of the analytical models, after Kainuma and Mori [69]



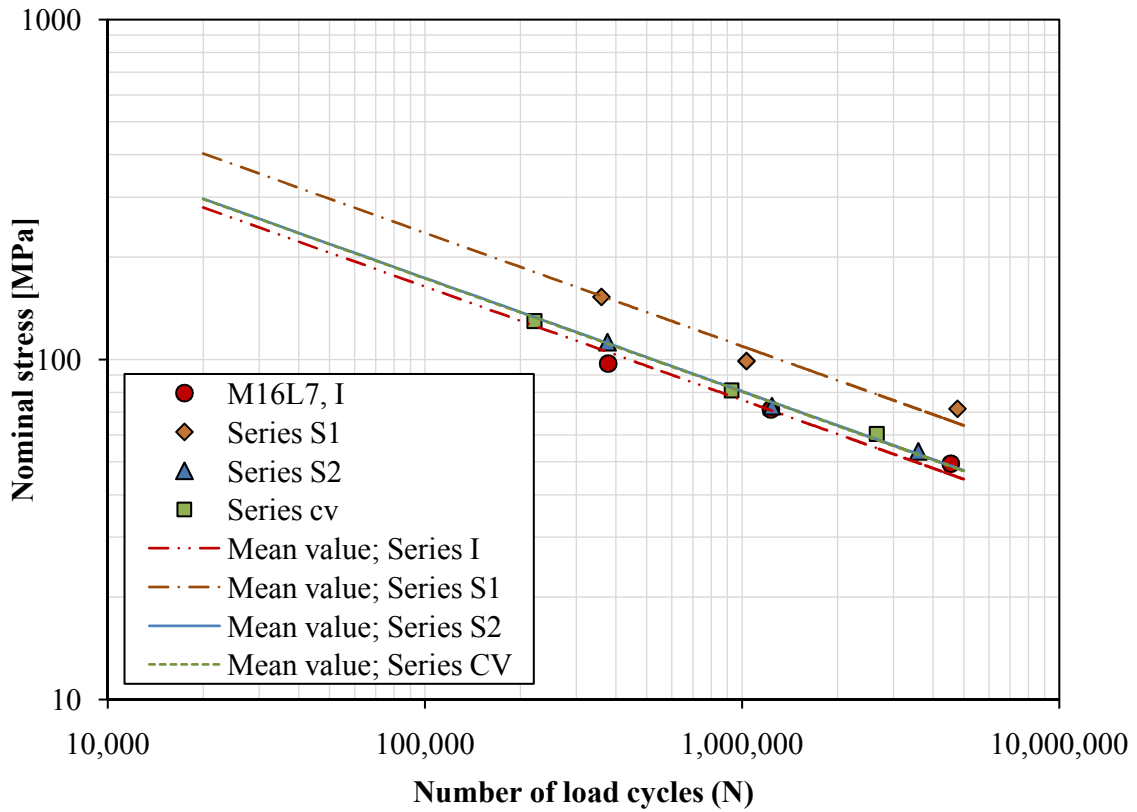


**Figure 7.10:** 2D finite element models of load-carrying cruciform details with different weld shapes: (a) Test series S1, (b) Test series CV

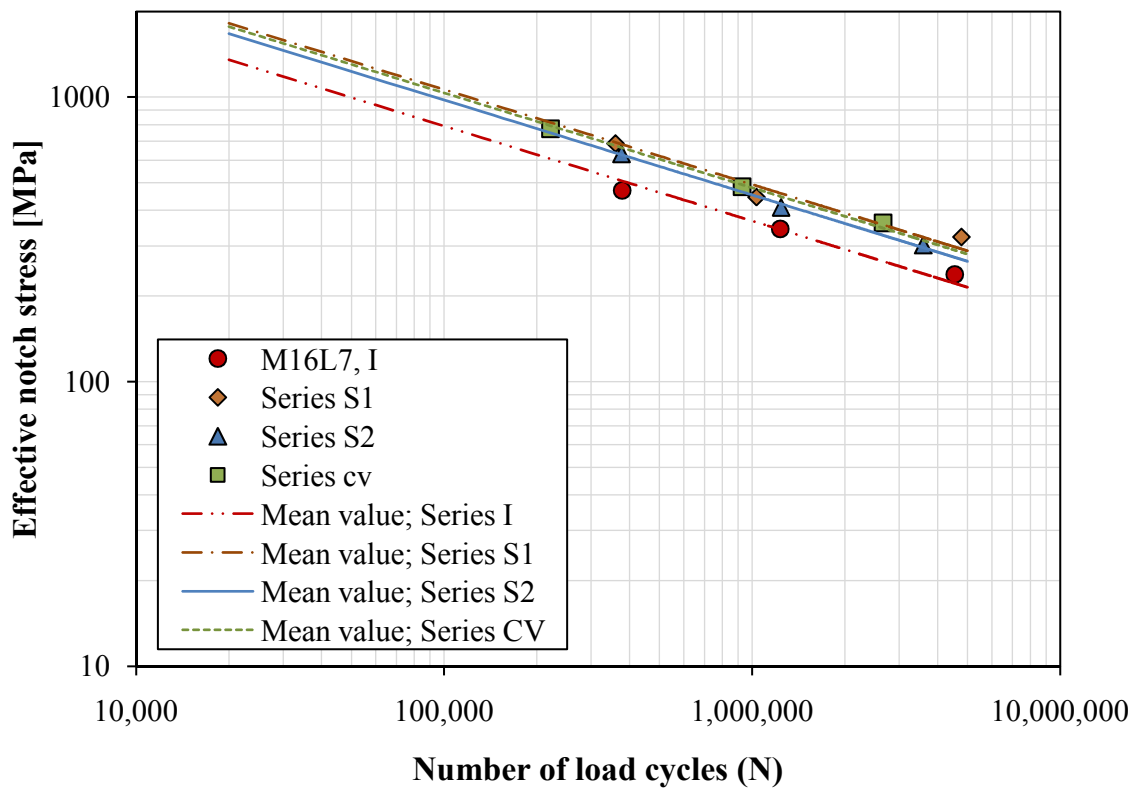
application direction has resulted a higher fatigue life. As the effective notch stress method claims to be shape independent, the discussed scatter of the test results is expected to diminish provided that the exact weld geometry is modeled. Subsequently, having mentioned that the authoress have reported the mean measured dimensions of the fabricated specimens, these values have been used to construct the finite element models. Figures 7.10a and b, depict the analyzed FE models of the test series S1 and CV, respectively. As it can be seen, the obtained effective notch stress value for the CV-specimen is considerably larger than that for the S1-specimen. This observation is consistent with the test results where the S1-specimen exhibited a distinguishable higher fatigue life than the other specimens including the CV-specimen.

Eventually, the re-analyzed fatigue test results according to the effective notch stress approach are plotted in Figure 7.17. It is apparent that the existing scatter of the test results is clearly reduced and all the test data lie within a uniform scatter band. Thus, it can be concluded that a single effective notch stress design curve can be assigned to similar specimens with different weld shapes provided that the exact weld geometry is known. In another words, the effective notch stress method is capable of reducing the scatter caused by varying the weld geometry. This conclusion makes the effective notch stress method a suitable fatigue assessment approach for the existing structures in which the precise specimen dimensions are known.





**Figure 7.11:** Fatigue test results of similar load carrying cruciform joints with various weld shapes according to the nominal stress method; all dimensions are in mm



**Figure 7.12:** Fatigue test results of similar load carrying cruciform joints with various weld shapes according to the effective notch stress approach

#### 7.4.4 Stress calculation effect

The stress used to produce the nominal stress S-N curves could be either the stress in the plate or in the weld throat section. The majority of the tests tabulated in Figure 7.1 have been documented using the stress in the plate section. However, Eurocode 3 and IIW explicitly request to base the analysis on the stress at the weld throat section. The effective notch stress method also makes use of the stress at the weld throat section as the corresponding nominal stress to obtain the stress concentration factor. In this study, in case of reported stress values at the plate section, the stresses are re-calculated at the weld throat section as follows:

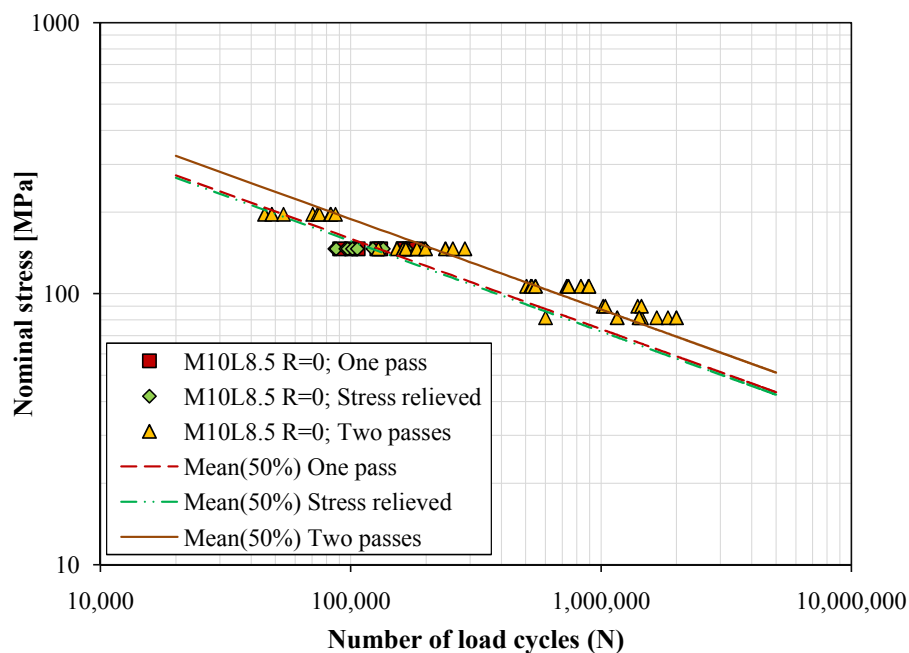
$$a_w = (s + P_w) \cdot \cos(\theta)$$

$$\sigma_w = \frac{F}{\Sigma(a_w \cdot l)}$$

where  $a_w$ , weld throat thickness;  $s$ , weld leg length;  $P_w$ , weld penetration depth;  $\theta$ , weld toe angle;  $\sigma_w$ , stress at the weld throat;  $F$ , applied force and  $l$  length of the weld.

#### 7.4.5 Residual stresses effect

The measurements of residual stress distribution in the cruciform details indicate the existence of favorable compressive residual stresses at the weld root. Therefore, evaluating the test results without considering this effect could lead to an overestimation of the fatigue life. Figure 7.13 affirms that even for a specimen with a small weld size, eliminating the residual stresses can result in a lower fatigue life. It should be noted that a higher profitable residual tensile stresses is expected for



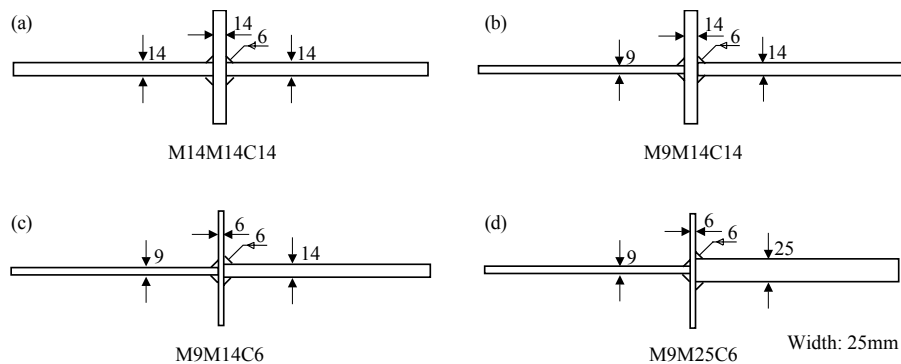
**Figure 7.13:** *Fatigue test results of analogous load-carrying cruciform details with different residual stresses*

the details with thicker weld throats. Therefore, it is recommended to investigate the test results with eliminated residual stresses in order to obtain reliable findings.

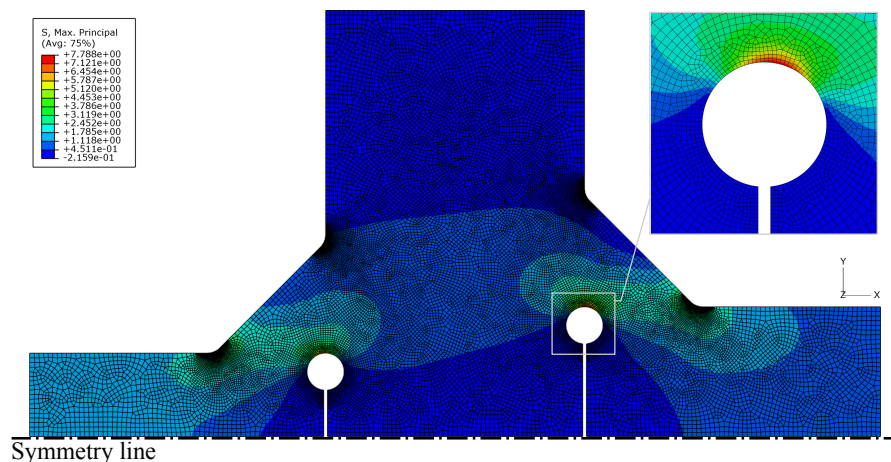
#### 7.4.6 Detail configuration effect

Kainuma and Mori [69] tested load-carrying cruciform joints with different plate thicknesses as shown in Figure 7.14. The minimum stress level of the conducted tests was set higher than the minimum required for opening the weld root gap. As a result, the effect of residual stresses on root crack propagation was eliminated. As can be seen in Figure 7.16, the plotted fatigue test results exhibit a noticeably large scatter.

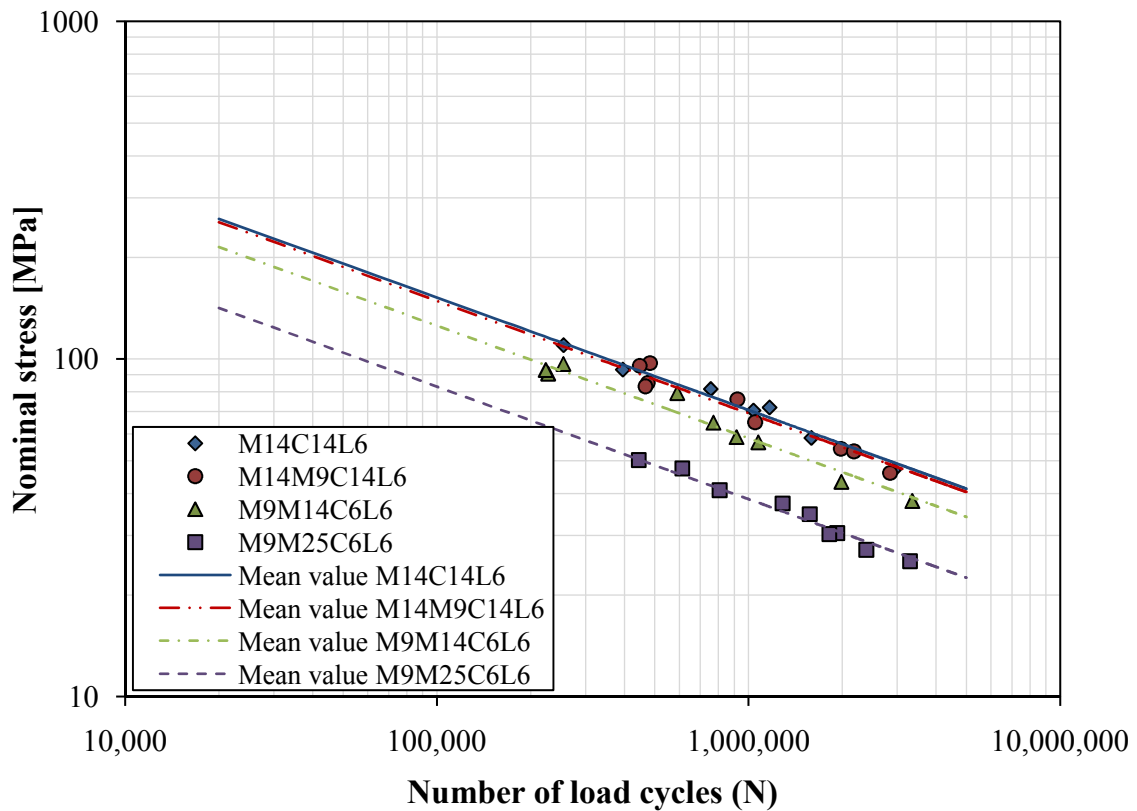
Figure 7.15 demonstrates an analyzed finite element model of one of the tested specimens. Only half of the detail is modeled due to its symmetry with respect to the horizontal axis. It was observed that in all the analyzed models, the maximum effective notch stress appeared at the side with thicker plate. This finding is supported by the reported failure locations of the actual test specimens. The fatigue test results of the load-carrying cruciform joints with different detail configurations according to the effective notch stress approach are plotted in Figure 7.17. As can be seen, the scatter of the test results is meaningfully reduced so that one



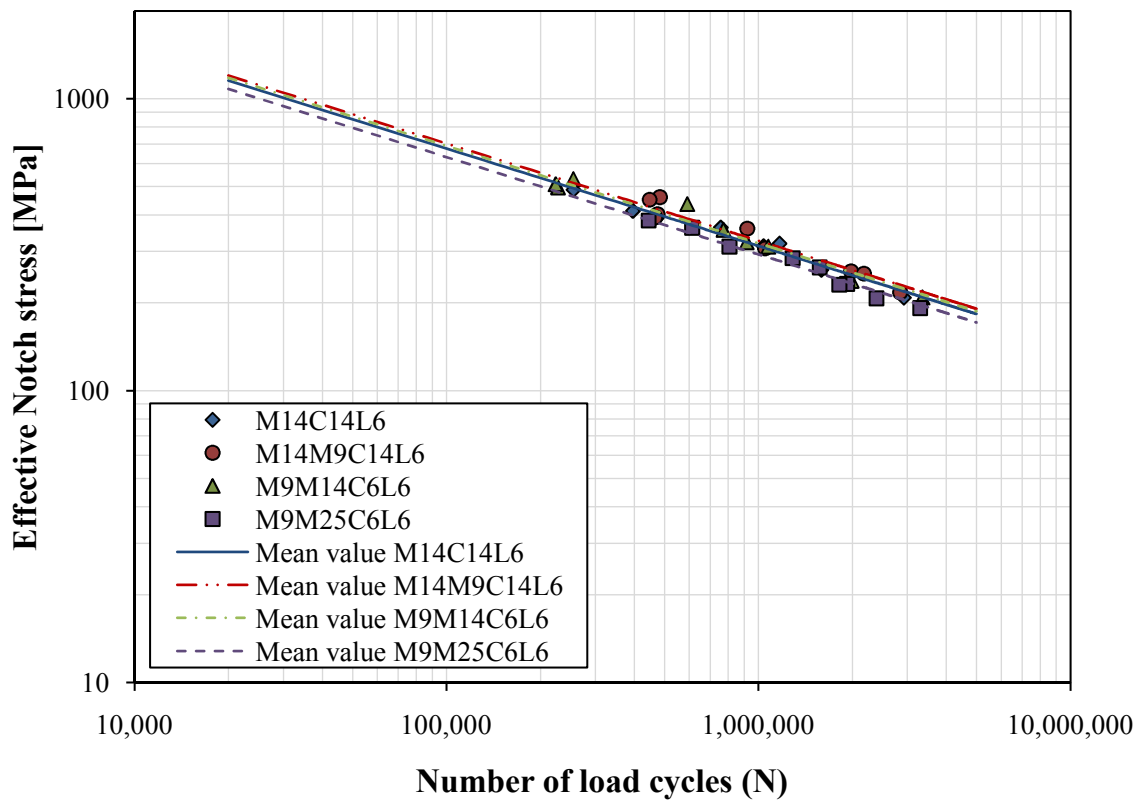
**Figure 7.14:** *Fatigue test specimen configurations, after Kainuma and Kim [68]*



**Figure 7.15:** *The analyzed finite element model of detail M9M14C14*



**Figure 7.16:** Fatigue test results of the load carrying cruciform joints with various detail configurations according to the nominal stress approach



**Figure 7.17:** Fatigue test results of the load carrying cruciform joints with various detail configurations according to the effective notch stress approach

design category can be assigned to all the details irrespective of their miscellaneous configurations.

## 7.5 Evaluation according to the nominal stress method

As it was discussed in the beginning of this chapter, both Eurocode 3 and IIW recommendations, propose the nominal stress fatigue design category 36 for root failures of any kind. In this section, the credibility of this recommendation is questioned by means of evaluating the collected fatigue test results of load-carrying cruciform joints. Considering the findings of the investigated influencing factors, the collected test data were refined to exclude the irrelevant test series. Subsequently, only the tests conducted with positive stress ratios were included for further investigations.

The corresponding fatigue test results, evaluated according to the nominal stress method, are plotted in Figure 7.18. As the characteristic value of the evaluated tests is higher than the suggested design category, it can be concluded that FAT36 seems to be a good representative for this detail. Nevertheless, the test data exhibit a large scatter which may be mainly due to the stochastic nature of the root failures. In addition to that, as the higher band of the test results is consisted of specimens with relatively thick welds, the discussed effect of residual stresses may be another reason for the large present scatter. As a conclusion, although FAT36 can be a good representative of the majority of the test results, it may be on the unsafe side for specimens with severe configurations e.g. test series M9M25C6.

## 7.6 Evaluation according to the effective notch stress method

Figure 7.19 shows the fatigue test results of this detail evaluated according to the effective notch stress method. It is apparent that the test series which exhibited low fatigue strengths, have shifted up to the main scatter band. Although the obtained characteristic design value is lower than the proposed FAT225, it appears to be an acceptable design category for this detail based on a visual assessment of the re-analyzed data.

Moreover, similar to the evaluation according to the nominal stress method, the specimens with relatively thick welds show a considerably higher fatigue life based on the effective notch stress method. As discussed in the previous section, this observation may be due to the favorable compressive residual stresses at the weld root. Thus, a considerable reduction in the scatter of the test results by excluding these test series is anticipated. Eventually, it is concluded that the effective notch stress method can reduce the scatter of the test data in case of the root failure of load-carrying cruciform joints provided that the scatter is caused by geometrical variations. As a result, a single fatigue design category, FAT225, can be assigned to these details irrespective of the detail geometry.

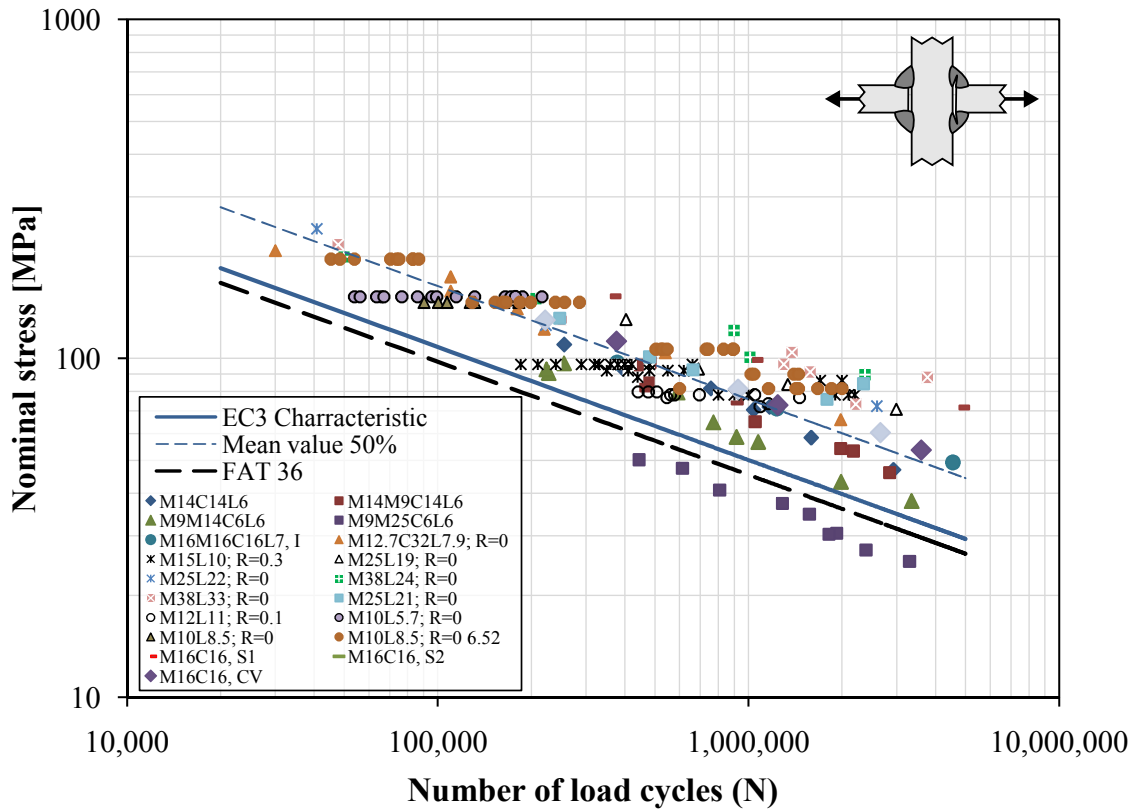


Figure 7.18: Fatigue test results of the load carrying cruciform joints according to the nominal stress method

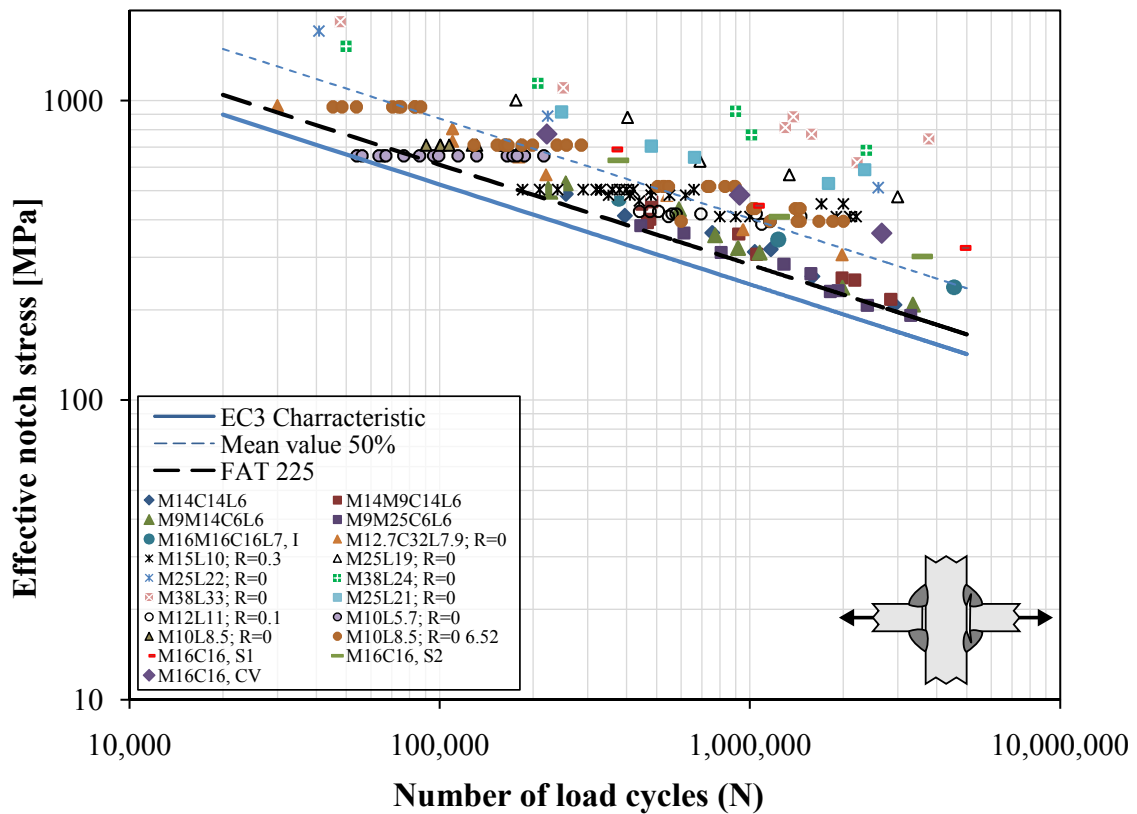
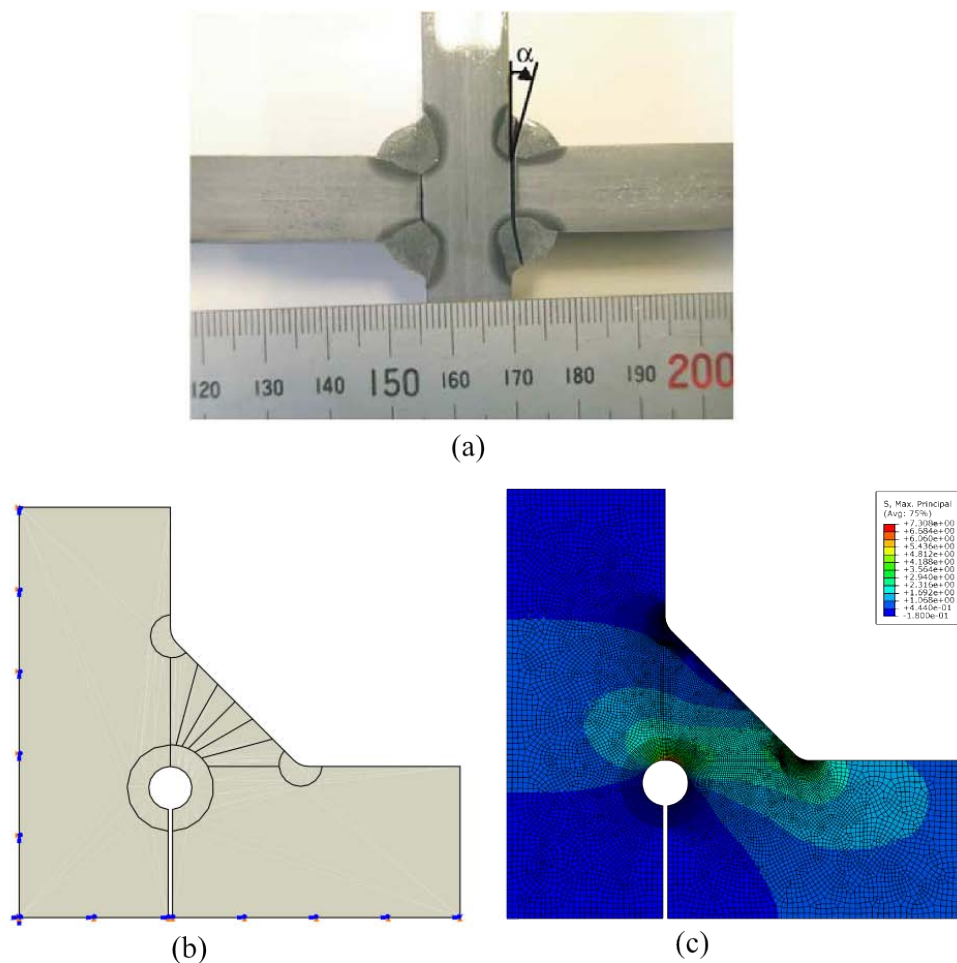


Figure 7.19: Fatigue test results of the load carrying cruciform joints according to the effective notch stress approach

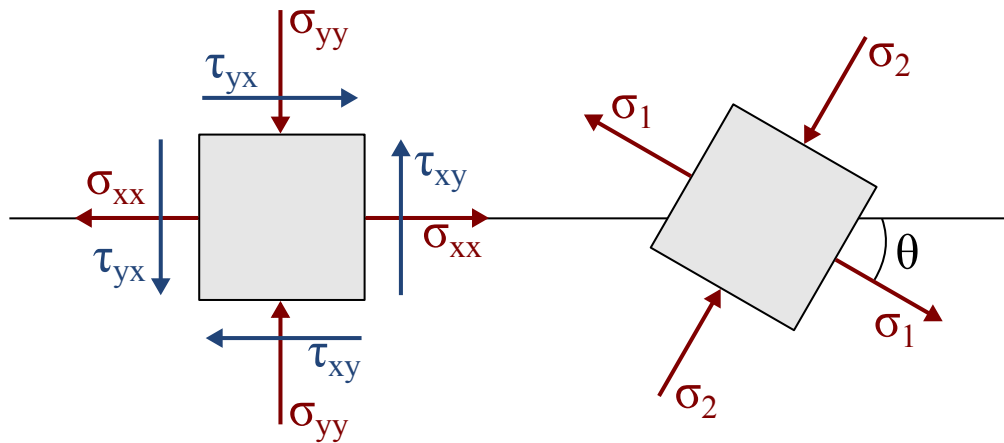
## 7.7 An investigation of crack propagation path

It is a well established fact that the fatigue cracks start and propagate perpendicular to the stress direction. Taking this general rule into account, this section aims to investigate the applicability of the effective notch stress method to predict the crack initiation and propagation path. This is achieved by comparing the calculations with the experimental results. Figure 7.20a depicts the tested specimen by Kainuma and Mori [69] in which the authors have reported an angle between 10 to 15 degrees for the crack propagation path.

In order to investigate the crack propagation path by means of finite element analysis, a corresponding finite element model as shown in Figure 7.20b was constructed and partitioned. The partitions were created in a way to divide the weld geometry to small portions distributed every  $15^\circ$ . Figure 7.20c shows the maximum principal stress contour plot of the analyzed model.



**Figure 7.20:** The investigation of crack propagation path: (a) A root failed specimen, after Kainuma and Mori [69], (b) Partitioned 2D finite element model, (c) Maximum principal stress contour plot



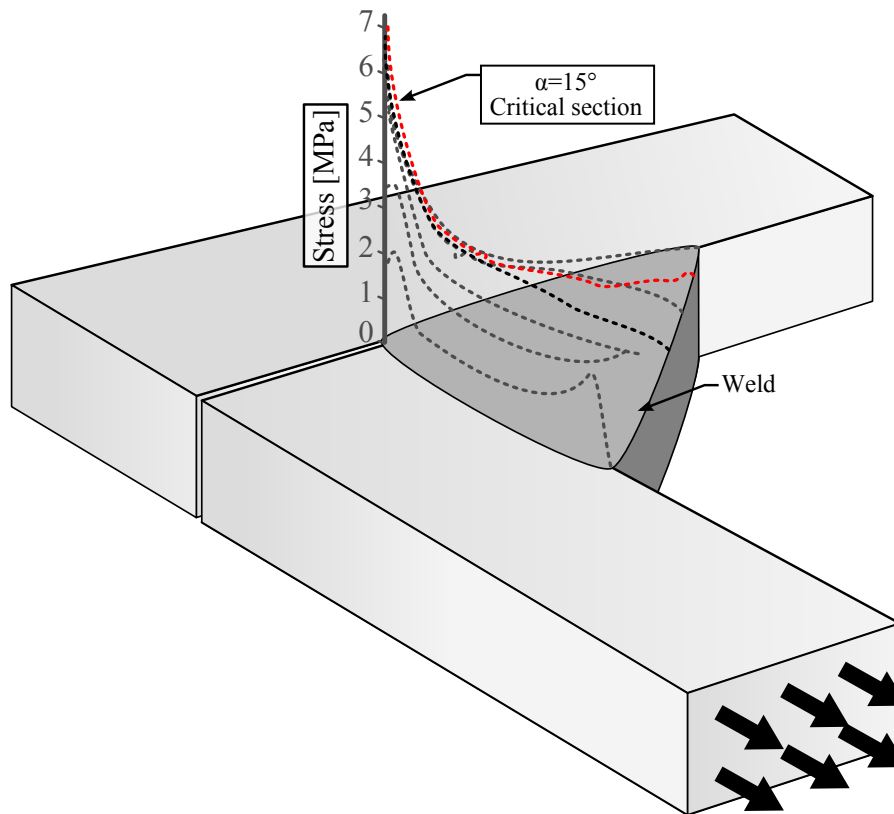
**Figure 7.21:** *The transformation to the maximum principal stress directions*

Due to the fact that the crack propagation is a function of both the stress direction and magnitude, the maximum principal stress value is not merely helpful. Hence, in order to calculate the direction of the stress,  $S_{11}$ ,  $S_{22}$  and  $S_{12}$  are measured along each partition. The maximum principal stress direction ( $\theta$ ), as illustrated in Figure 7.21, can be calculated as follows:

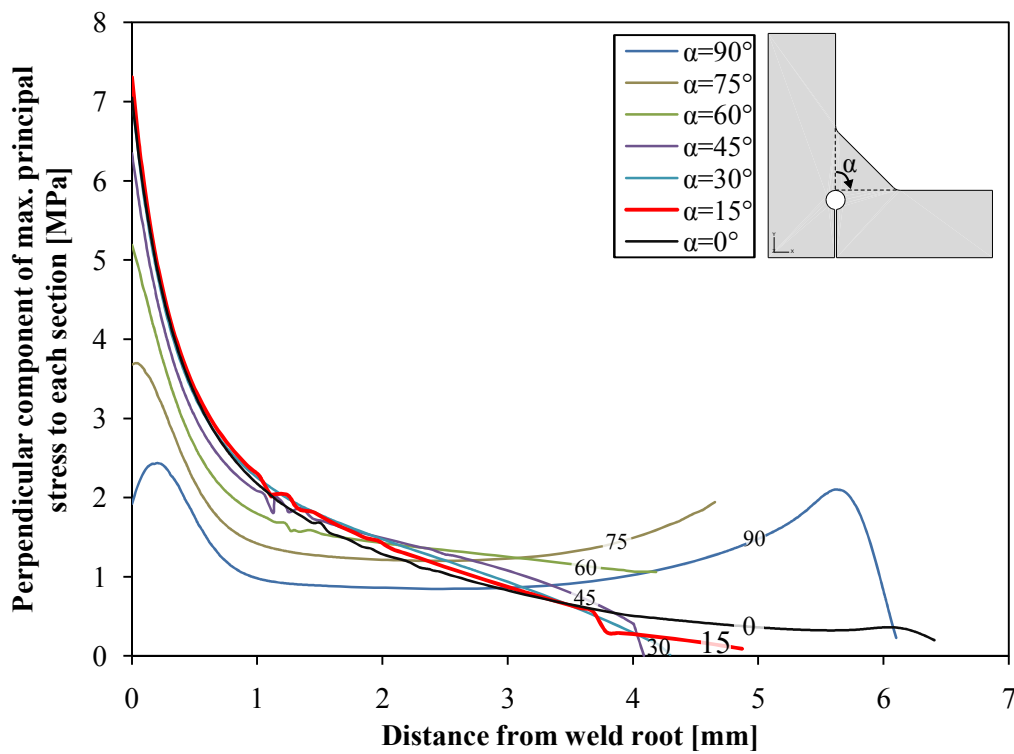
$$2\theta = \arctan\left(\frac{2 \cdot \tau_{xy}}{\sigma_{xx} - \sigma_{yy}}\right) = \arctan\left(\frac{2 \cdot S_{12}}{S_{11} - S_{22}}\right) \quad (7.1)$$

Eventually, having calculated the maximum principal stress direction, the perpendicular component of it to each partition can be simply calculated. Figures 7.22 and 7.23 demonstrate the distribution of the calculated stress component along each partition in the weld section. As can be seen, the section oriented at an angle of  $15^\circ$  is the critical one and the crack is anticipated to initiate and propagate along this section. As this observation is consistent with the experimental results, the effective notch stress method is believed to be capable of predicting the crack propagation path. It should be noted that extra consideration should be given to the exploited stress components.





**Figure 7.22:** 3D scatter diagram of the perpendicular component of maximum principal stress to each partition



**Figure 7.23:** The distribution of perpendicular component of maximum principal stress to each partition



# 8 Fatigue Life Assessment of Cope-Hole Details

## 8.1 Introduction

Large span bridges made of steel girders are generally fabricated in several splices due to transportation limitations and section variations. Consequently, the bridge splices have to be joined together in the field with welded or riveted connections. When welded connections are used, and in order to facilitate for the transversal butt welds in the flanges and avoid weld crossing, cope-holes are introduced in the girder web, see Figure 8.1. As a result, the risk of incomplete weld penetration at the intersection of web and flanges would be reduced. Additionally, cope-holes give access for the application of non-destructive testings to ensure the weld quality. However, the recent advancements of welding technologies have eliminated the necessity of cope-holes in such connections by improving the welding process and material. Nevertheless, bridge construction companies in some countries such as Sweden yet prefer to use cope-holes in welded girder splices for practical and safety considerations.

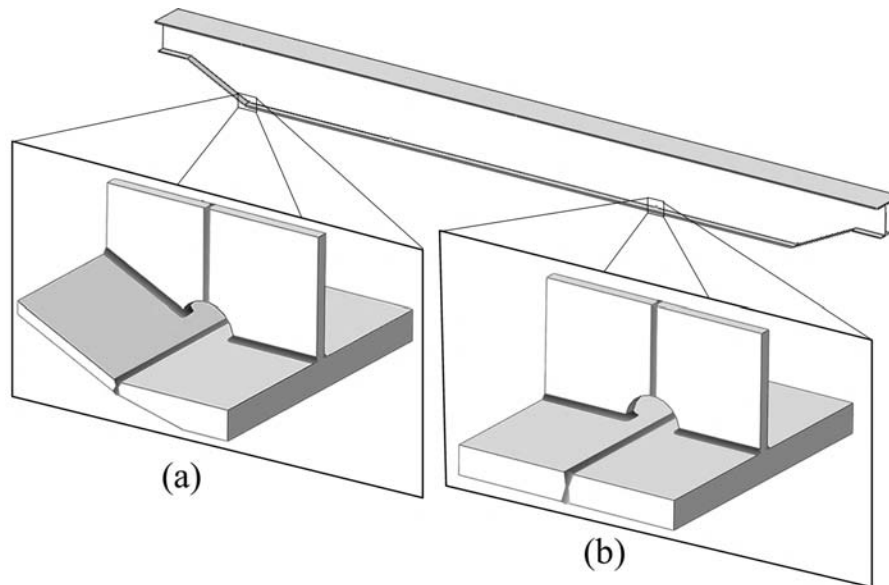
From a structural point of view, the existence of cope-holes results in an abrupt reduction of the stiffness of the section which causes high stress concentration areas mainly at the weld toes. This will lead to a relatively lower fatigue strength of this detail compared to the other constructional details in a bridge girder. Table 8.1 represents the considerable reduction of fatigue life of beams with cope-holes.

Eurocode-3 [9] recommends fatigue design class FAT71 for welded joints with cope-holes in which the design stress is considered based on the stress in the flange, see Table 9.1. This design criteria for cope-holes is comparatively lower than the same for stiffeners and other common welded joints in girders. Subsequently the design stress for cope-holes will govern the design of the section at a low stress level which is not economical. Therefore, an increase in fatigue design class of cope-holes is of great interest of bridge designers.

The available fatigue tests for this detail are limited [40, 78–80]. Further fatigue tests are carried out in this study in order to evaluate the recommended fatigue

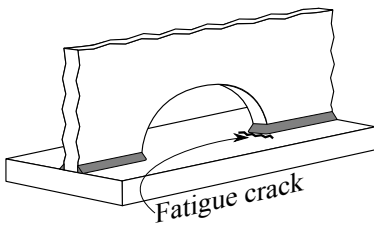
**Table 8.1:** *Fatigue behavior comparison of several spliced beams, after Stallmeyer and Fisher [78].*

| Splice type                  | Average cycles for failure $\times 10^3$ | Crack initiation area                                      | Fatigue life percentage |
|------------------------------|--|--|-------------------------|
| Beams without splices        | 1315.2                                   | Root of fillet weld in the region of a change of electrode | 100%                    |
| Beams with cope-holes only   | 428.8                                    | Initiated at the top of cope-hole                          | 32.6%                   |
| Beams with welded cope-holes | 217.4                                    | At the edge of cope-hole in the flange base material       | 16.5%                   |



**Figure 8.1:** Application of cope-holes in a bridge girder: (a) Cope-hole at a splice due to section change, (b) Cope-hole at a splice due to transportation limitations

**Table 8.2:** Fatigue classification of the cope-hole details based on the nominal stress method according to Eurocode 3

| Structural detail   | Description  | FAT       |
|---|--|-----------|
|  | Cope-hole details: $\Delta\sigma$ based on direct stress in the flange | <b>71</b> |

design class of cope-holes. Moreover, structural hot spot stress approach and effective notch stress method have employed to investigate the validity of recommended design classes based on these approaches. As the mentioned methods require finite element analysis, the well known IIW recommendations [10] are adapted in order for the results to be comparable with previous studies and recommendations [10, 81]. The evaluation of the current fatigue test data reveals a noticeable dependency of the fatigue life to the available amount of shear stresses at the cope-hole section. This phenomenon was previously addressed in [40] as well. However, this finding has been criticized not to be a good representative for bridge girders by virtue of the cope-holes being placed in sections with high shear and small bending stresses. This loading condition is very unlikely to be experienced by splices in real bridge girders. Moreover, the bridge girders have generally a stiffer section than those tested in laboratories. For this reason, the shear deflections and consequently additional stresses may not be considerable. In the current study, several existing bridge girders are further analyzed to investigate the effect of shear stresses on the fatigue life of splices with cope-holes in full scale bridge sections.

Furthermore, an influence of altering the cope-hole shape on the fatigue life has been reported in [37]. Cope-holes with different shapes redistribute the stresses at the weld toe differently which leads to a change in the stress concentration factor. This effect in conjunction with different loading modes is thoroughly investigated by means of finite element analysis. In conclusion, the effectiveness of reshaping the cope-hole is examined by comparisons of fatigue lives.

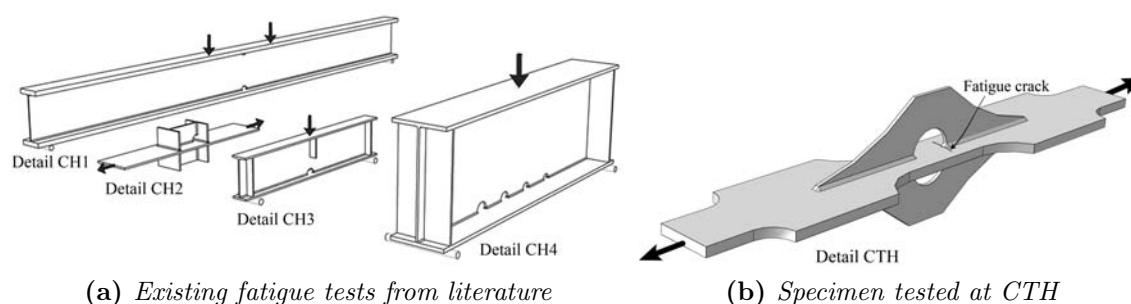
Eventually, the effect of post-weld treatment on the fatigue life enhancement of cope-holes is investigated analytically and experimentally. Burr grinding and ultrasonic impact treatment methods are compared and the application instructions are given. Conclusively, a new fatigue design class for post-weld treated cope-hole details is proposed.

## 8.2 Existing fatigue tests

The number of available fatigue tests for cope-hole details is limited. However, a total number of 29 constant amplitude fatigue test results of as-welded specimens from 4 different sources [40, 78–80] are collected to evaluate fatigue strength of this detail. In addition to the existing fatigue tests, a new test series on axially loaded specimens with cope-holes was conducted. The test program was aimed to verify the current available guidelines regarding cope-holes and was carried out at Chalmers University of Technology (CTH). Table 8.3 represents a detailed overview of various test configurations as illustrated in Figure 8.2.

As listed in Table 8.4, the fatigue strength of the evaluated cope-hole details is very inconsistent. A closer look at the results in Figure 8.3 reveals that despite the conspicuous geometrical variation of details CH1, CH2 and CTH, they exhibit almost identical fatigue strength. However, detail CH4 which is more similar to CH1 shows a dramatic fall in terms of fatigue strength. A more thorough assessment of the tests, reveals a pronounced dependency of fatigue life of cope-hole details on the ratio of shear stress to normal stress in the specimens ( $\tau_a/\sigma_m$ ), see Figure 8.3. It is clear that the relatively low fatigue strength of details in the test series CH4 is due to the presence of considerable shear stresses in the web at the intersection of flange and web at the weld toe of cope-hole.

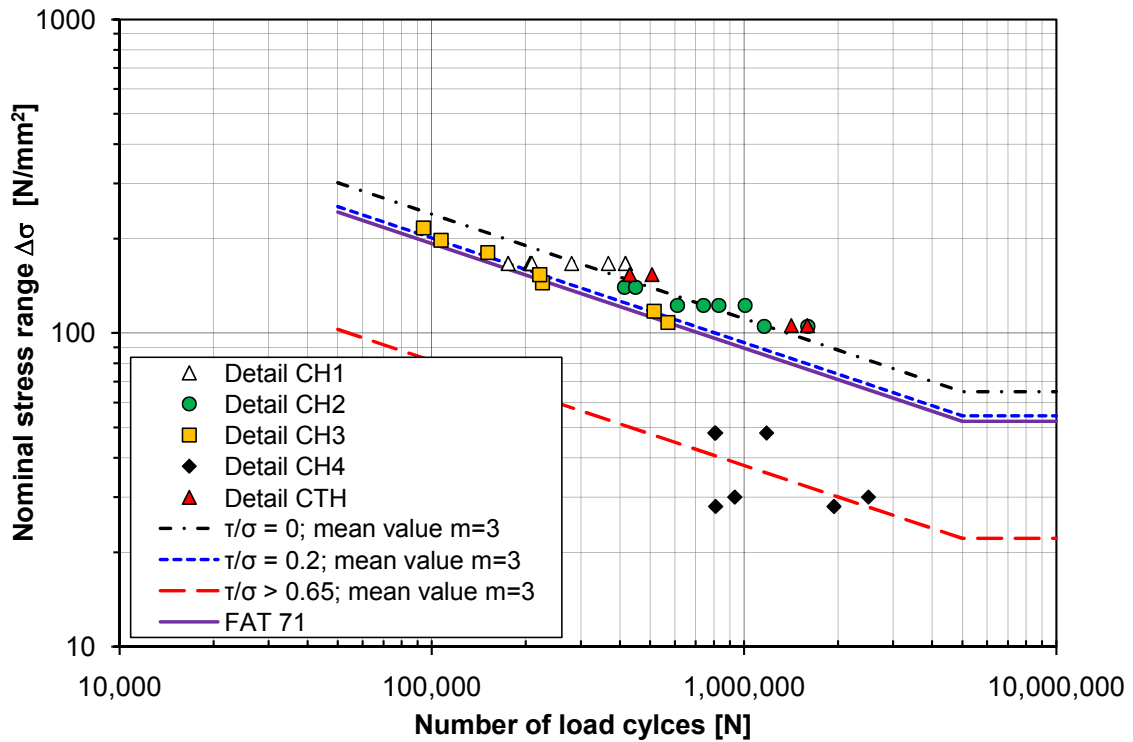
The destructive effect of shear stresses on the fatigue life of cope-hole details has been previously confirmed in [40]. Therefore, evaluation of the test results, based on the nominal stress in these details, should consider the ratio  $\tau_a/\sigma_m$  as an important



**Figure 8.2:** Schematics of various cope-hole test configurations

**Table 8.3:** Dimensions and quantity of the evaluated fatigue test specimens for cope-holes; all dimensions are in mm.

| Detail | Test data | Main plate |       | Attachment |        | $\tau_a/\sigma_m$ | Ref. |
|--------|-----------|------------|-------|------------|--------|-------------------|------|
|        |           | Thickness  | Width | Thickness  | Radius |                   |      |
| CH1    | 7         | 25.4       | 127   | 4.8        | 25.4   | 0                 | [78] |
| CH2    | 8         | 9          | 200   | 9          | 35     | 0                 | [80] |
| CH3    | 7         | 8          | 80    | 6          | 26     | 0.2               | [79] |
| CH4    | 7         | 16         | 50    | 9          | 25-40  | 0.7-1             | [40] |
| CTH    | 4         | 20         | 100   | 8          | 50     | 0                 | -    |



**Figure 8.3:** Fatigue test results of cope-hole details distinguished by the shear to normal stress ratio

**Table 8.4:** Statistical evaluation of the cope-hole test results using linear regression analysis with a fixed slope of 3.

| Detail | $\Delta\sigma_{mean}$<br>$N/mm^2$ | $\Delta\sigma_C$<br>$N/mm^2$ | Standard Deviation |
|--------|-----------------------------------|------------------------------|--------------------|
| CH1*   | 83.8                              | –                            | –                  |
| CH2    | 88.9                              | 71.9                         | 0.093              |
| CH3    | 74                                | 64.7                         | 0.055              |
| CH4    | 30                                | 16.7                         | 0.345              |
| CTH    | 95.2                              | 82.7                         | 0.044              |

\* Statistical evaluation is not possible due to only one stress level.

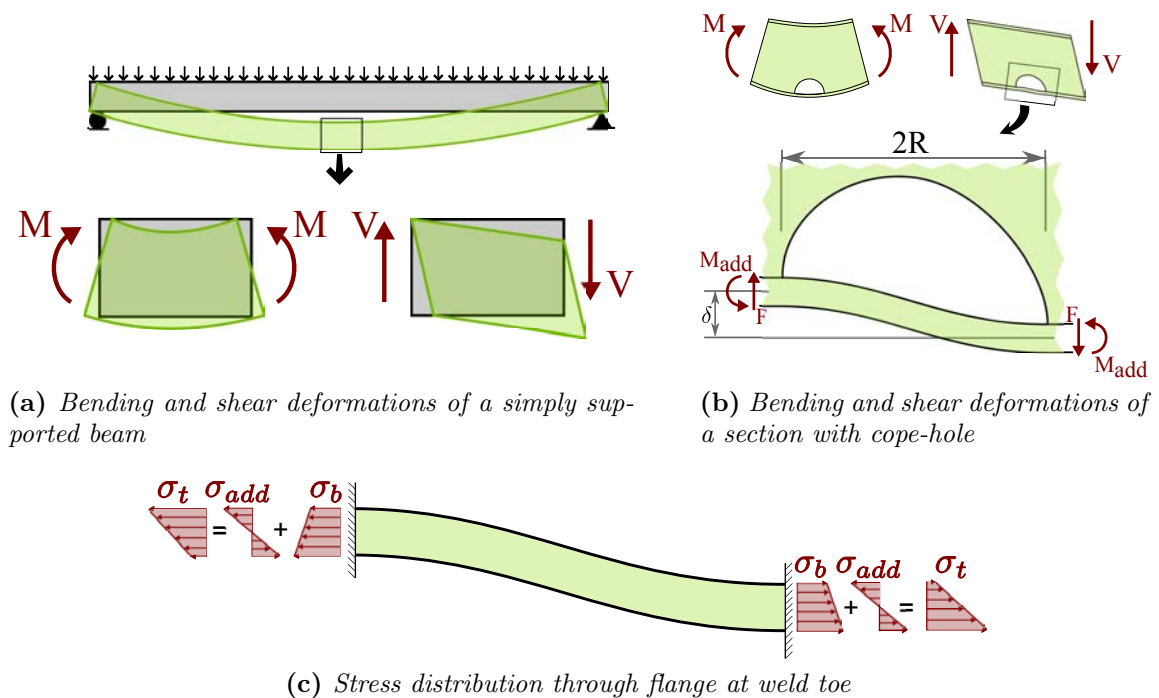
parameter that affects the fatigue strength of cope-hole details. While this has been recognized in IIW, the Eurocode 1993-1-9 assigns detail category 71 to cope-hole details irrespective of the ratio  $\tau_a/\sigma_m$ .

## 8.3 Influencing factors

### 8.3.1 load effect

The discussion in this section aims to illuminate the damaging effects of shear stresses on fatigue strength of cope-holes. According to structural mechanics principals, total displacement of a section along a beam which is subjected to an arbitrary loading, is composed of displacements due to normal and shear stresses (Figure 8.4a). Although, it has been argued that the deflection due to shear can be generally neglected in long span beams, the local effects of such deformations may be prominent. To illustrate the point clearly, the deformations of a beam section with cope-holes are further studied, see Figure 8.4b. It is apparent that as a result of the presence of shear, a relative displacement ( $\delta$ ) is induced between the sections before and after the cope-hole. Furthermore, considering that the lateral support of flange provided by web is no longer available in this section, the flange undergoes an additional deformation. In this instance, the flange plate is analogous to a beam with both ends fixed enduring an additional moment ( $M_{add}$ ) due to the relative displacement of the two ends ( $\delta$ ).

As demonstrated in Figure 8.4c, the additional moment introduces secondary bending stresses ( $\sigma_{add}$ ) through the depth so that the total stress ( $\sigma_t$ ) at the inner surface of the flange at weld toe undergoes abrupt variations. The total stresses at the cope-hole weld toe on the inner surface of a flange at the tension side increases at one end and decreases on the other end. This peculiarity of stress state at a cope-hole section instigates the weld to experience higher stresses than the anticipated design ones.



**Figure 8.4:** Schematic model for beam deformations



To enlighten the importance of stress variations at cope-hole sections due to shear deformations, the discussed model is investigated numerically. The relative deformation of beam ends can be obtained by subtracting the shear deflections of sections before and after the cope-hole. For a cope-hole with radius  $R_{cp}$  located at  $x = L_1$  it yields

$$\delta = \omega_S(L_1 + R_{cp}) - \omega_S(L_1 - R_{cp}) \quad (8.1)$$

where

$$\omega_S(x) = \frac{V(x)}{GA_s} \quad (8.2)$$

and the shear area ( $A_s$ ) for an arbitrary section can be calculated based upon the conservation of energy law as follows

$$\frac{1}{2} \frac{V^2}{GA_s} = \frac{1}{2} \int \frac{\tau^2}{G} dA \quad (8.3)$$

Having obtained  $\delta$ , the additional moment can be calculated using Euler-Bernoulli beam theory:

$$M_{add} = \frac{6EI_f \delta}{(2R_{cp})^2} \quad (8.4)$$

However, further investigations have confirmed that the  $2R_{cp}/t_f$  and the  $\tau_a/\sigma_m$  ratios have also a considerable effect on stress redistributions through the flange depth. In order to consider the secondary stress redistribution, further finite element analysis of a satisfactory number of cope-hole details were performed. According to the results, the additional stress at the edges of the beam with a normalized cope-hole detail with  $R_{Ref} = 25mm$ , can be obtained from:

$$\sigma_{add} = \frac{M_{add} t_f}{2I_f} \frac{\tau_a}{\sigma_m} \frac{2R_{cp}}{t_f R_{ref}} \quad (8.5)$$

As can be seen, by introducing a normalized cope-hole radius, the results can be linearly extrapolated for any other cope-hole detail geometry. However, as also mentioned by Eurocode 3, the cope-hole radius has to be limited to less than 60mm. From Equations 8.4 and 8.5, the additional stress at the inner edge of the flange at the weld toes is given by

$$\sigma_{add} = \frac{3}{4} \frac{Et_f \delta}{R_{cp}^2} \frac{\tau_a}{\sigma_m} \frac{2R_{cp}}{t_f R_{ref}} \quad (8.6)$$

Eventually, the total utilized stress at the weld toes of cope-hole is obtained through superposition:

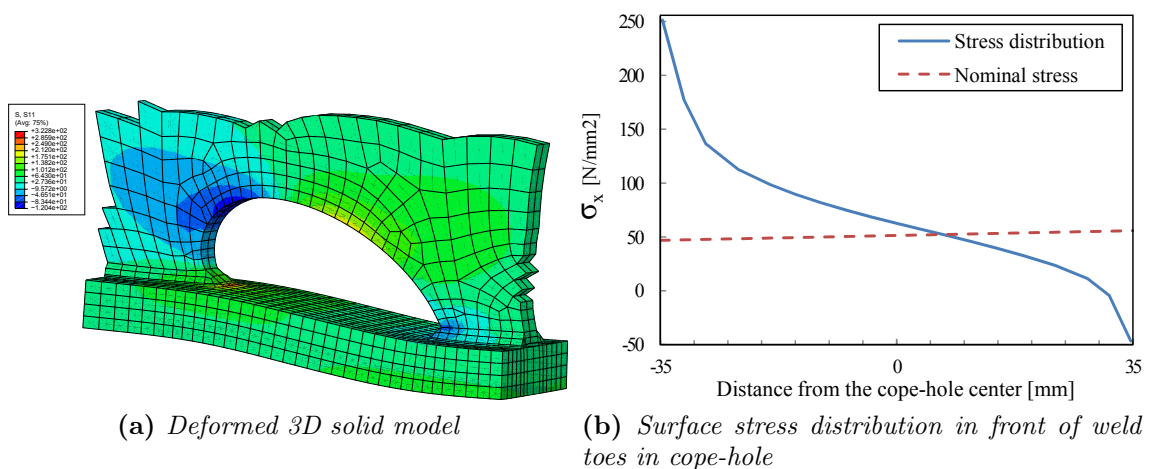
$$\sigma_t = \sigma_b \pm \sigma_{add} \quad (8.7)$$

In order to further evaluate the proposed model, finite element analysis of several beams with cope-holes are performed. Figure 8.5 shows the FEA results of a cope-hole subjected to high shear stresses. It is apparent that the introduced shear deformation model is valid and stresses at weld toes have undergone significant

changes.

Evaluating the findings of load effects, it is anticipated that by modifying the nominal stress according to Equation 8.7 for specimens where cope-hole experiences high shear stresses, the destructive shear effect should be implicitly covered. In order to highlight this issue, the previously discussed tests reported by [40] are implemented. The mentioned test specimens were tested under severe shear stresses and consequently exhibited absolutely poor fatigue strength. However, as plotted in Figure 8.6, when modifying nominal stress, the data lie within the scatter band of all tests, cf. Figure 8.3. This observation confirms the fact that when using modified nominal stress for cope-holes a single design FAT class can be used for various loading conditions. Furthermore the fact that calculated modified nominal stresses for this test series are up to three times larger than the conventional nominal stresses, is an evidence of the significance of stresses induced by shear deformations.

On the other hand, bridge girders have generally stiffer cross sections than those tested in laboratories. Thus, it is of great interest to assess the participation of additional stresses induced by shear deformations to total stresses at such stiff sections. Likewise, investigating the criteria used by designers to place splices along a beam and accordingly the loading experienced by cope-holes can shed light on the severity of load effects in bridges. A survey, including a railway and a traffic bridge, is conducted to illuminate the ambiguities of load effects in existing bridges. The results of this study, which are presented in Appendix III and Appendix IV, appear to reaffirm the proposed model for additional stress calculation. Figure 8.7 shows the finite element model of the investigated composite bridge based on the effective notch stress method. Moreover, as there is no conclusive criterion regarding the splices location, cope-holes are prone to endure high  $\tau_a/\sigma_m$  ratios e.g. splices close to mid support in multi-span bridges. In conclusion, the shear effect must be recognized and considered in fatigue design of bridges with cope-hole details.



**Figure 8.5:** FEA results of a cope-hole subjected to high shear stresses

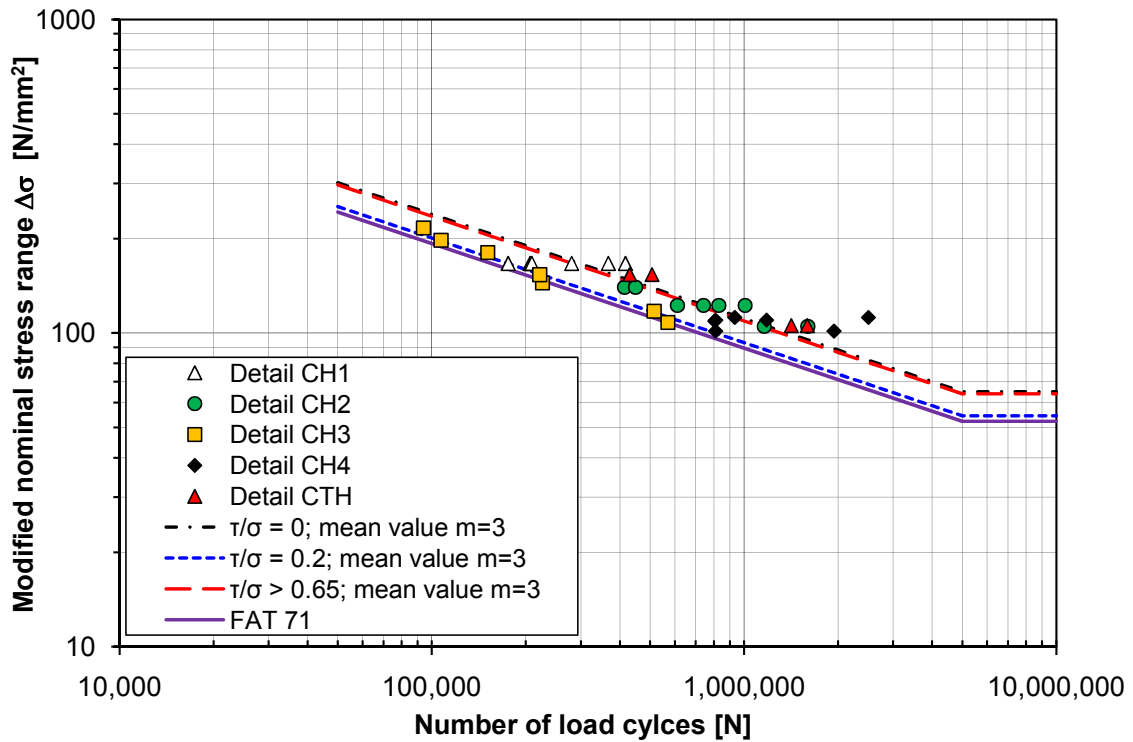


Figure 8.6: Fatigue test results of cope-hole details according to the modified nominal stress

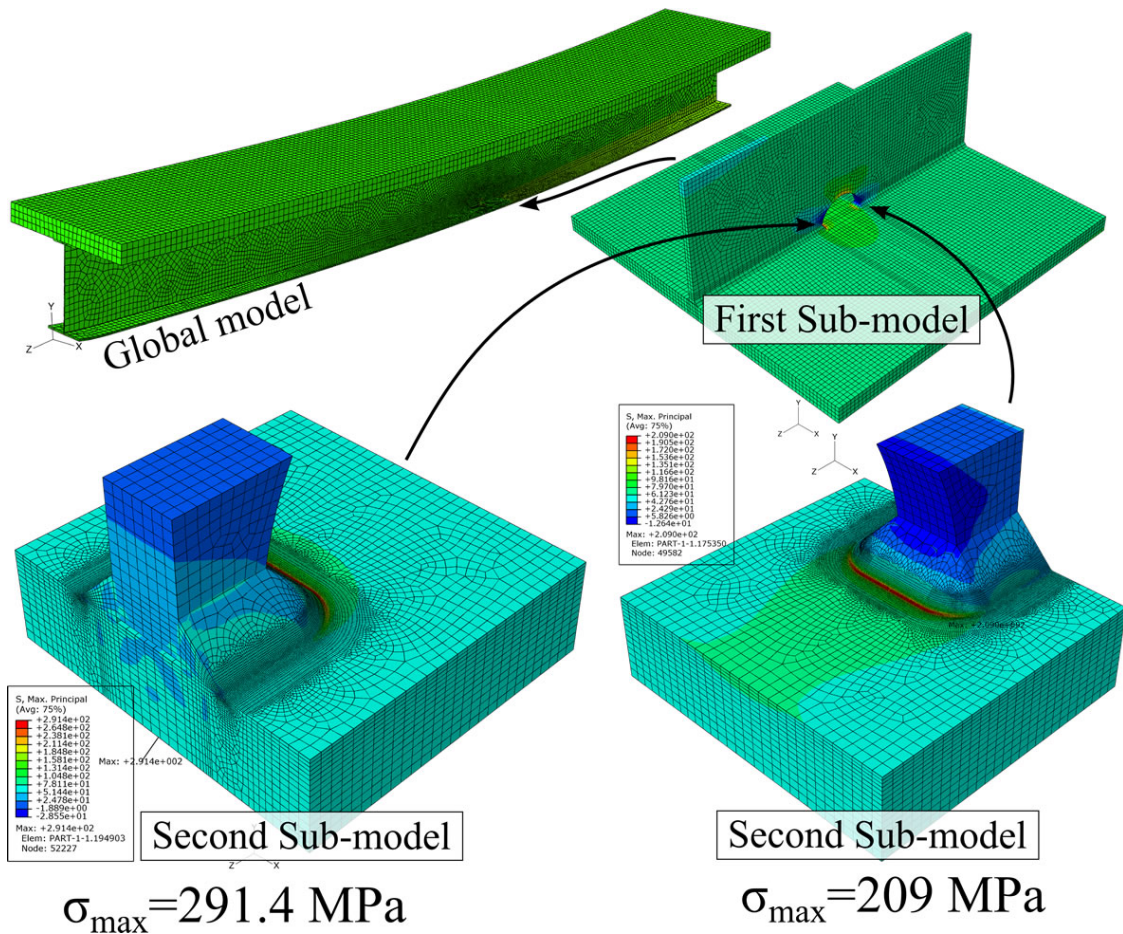


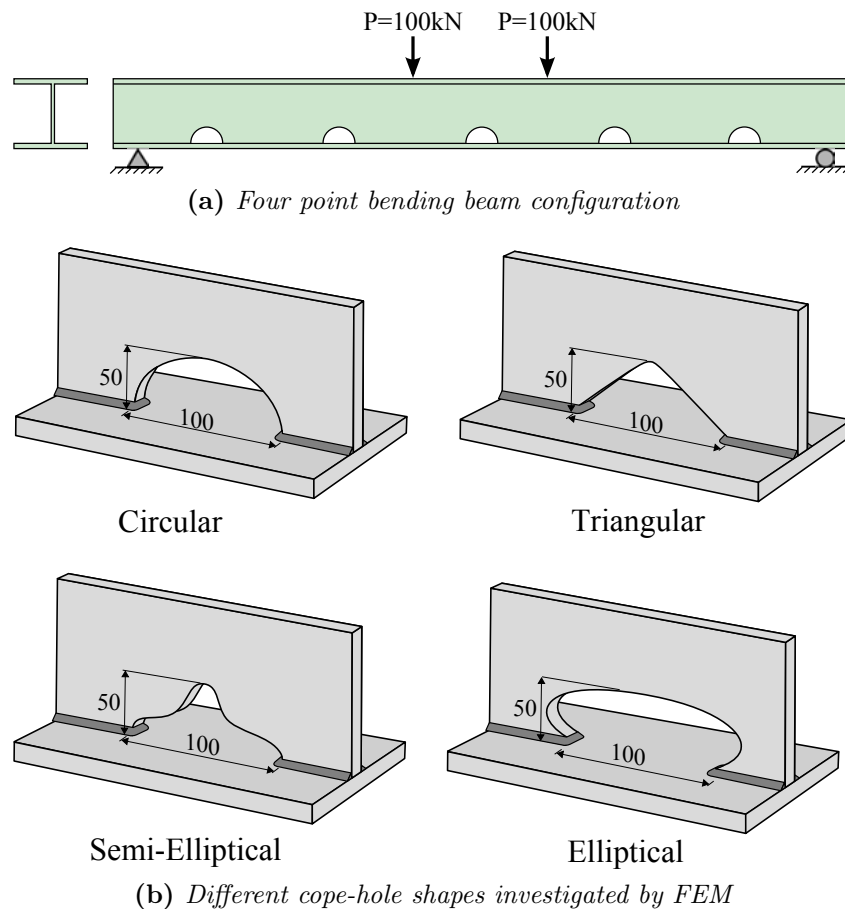
Figure 8.7: The finite element model of an investigated existing composite bridge based on the effective notch stress method

### 8.3.2 shape effect

Finite element analysis of specimens with cope-holes has revealed that the weld toes at introduced gap undergo severe stress concentrations. Therefore, it is anticipated that by altering the cope-hole shape and consequently the local stress distribution around it, an enhancement in fatigue strength would be achieved. In order to investigate the local stress distribution of cope-holes with different shapes, FEM analysis has been carried out for beams with four disparate cope-hole shapes as shown in Figure 8.8.

As a result of the applied loading configuration, the cope-hole in the middle experiences merely bending stresses, whereas the side holes undergo a combination of shear and bending stresses. The  $\tau_a/\sigma_m$  ratio is the highest for the cope-holes closest to the support.

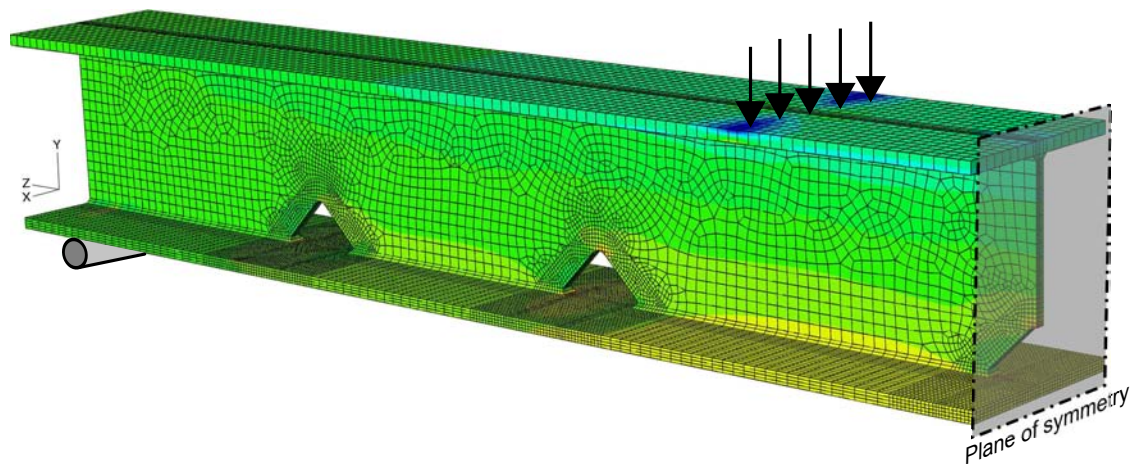
As it is apparent from Figure 8.10a, for the cope-holes located in shear-present regions, the normal stress derived from FEM notably rises on the side of cope-hole closer to the support and drops on the other side. On the other hand, the center cope-hole endures a symmetric stress distribution with stress peaks at the weld toes.



**Figure 8.8:** Cope-hole shape effect investigated models; All dimensions in mm.

Figure 8.10b illustrates the stress distribution in front of second cope-hole for different shapes. A quadratic extrapolation of the stresses according to IIW recommendations [10] has been done to obtain structural hot spot stress at the weld toe as an acceptable criterion to compare different shapes. It is apparent that the triangular cope-hole exhibits the lowest hot spot stress while the highest stress belongs to the elliptical cope-hole. The higher hot spot stress for elliptical shape is a result of the more reduction in the cross section stiffness at cope-hole ends which consequently causes a higher additional stress.

Table 8.5 represents a comparison of hot spot stress concentration factors (SCF) for different cope hole shapes. The presented data confirms the unfavorable effect of using elliptical cope-holes, whereas the lowest SCF is obtained for triangular cope-holes. Further analysis reveals that an increase of 31.2% in fatigue life can be obtained by using triangular cope-holes instead of conventional circular ones. However, due to the fact that fatigue tests are usually accompanied by a large scatter, it is anticipated that the achieved improvement would be negligible.

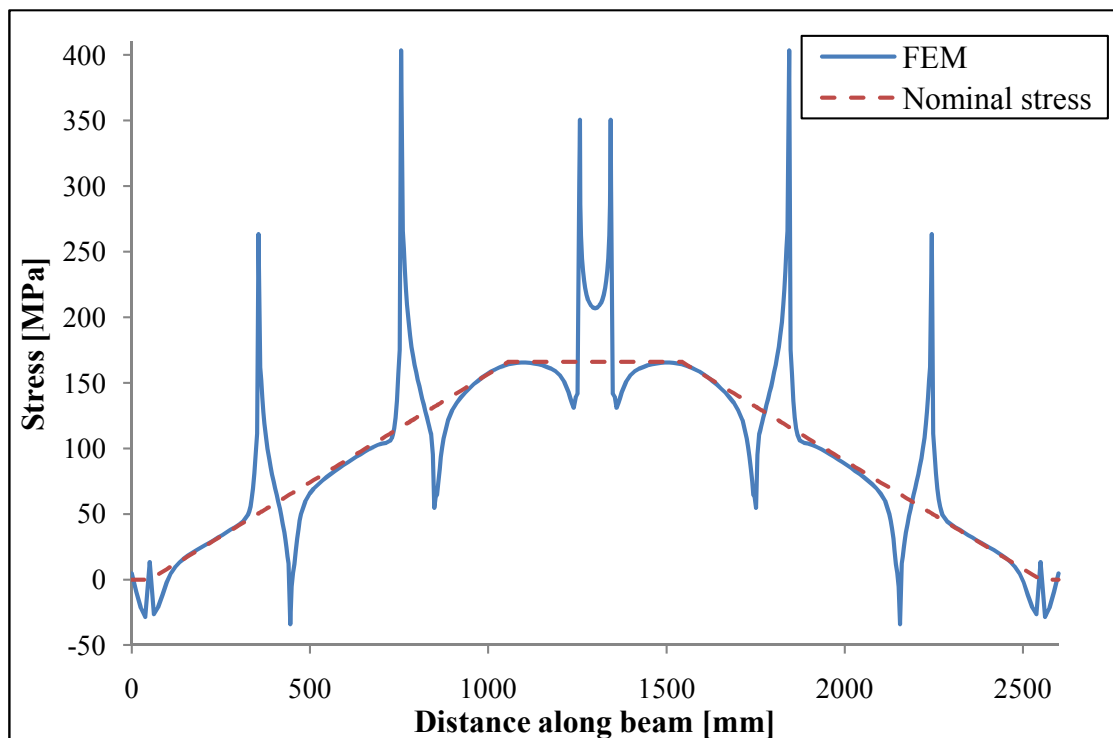


**Figure 8.9:** 3D Solid finite element model of a beam with triangular cope-holes

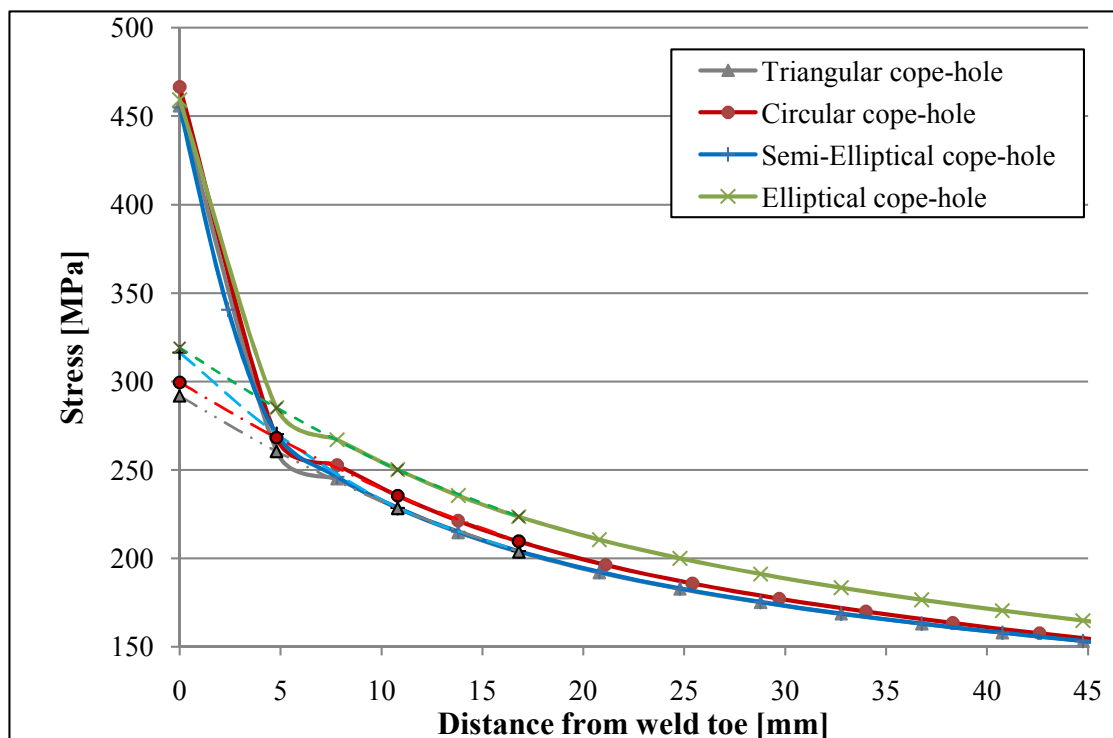
**Table 8.5:** Comparison of fatigue strength for cope-holes with disparate shapes

| Cope-hole shape | Hot spot SCF |             |             | Fatigue life variation |             |             |
|-----------------|--------------|-------------|-------------|------------------------|-------------|-------------|
|                 | First hole   | Second hole | Center hole | First hole             | Second hole | Center hole |
| Circular        | 3.24         | 2.42        | 1.79        | –                      | –           | –           |
| Triangular      | 3.15         | 2.36        | 1.63        | +9%                    | +8.1%       | +31.2%      |
| Semi-Elliptical | 3.43         | 2.56        | 1.73        | -15.4%                 | -15.2%      | +11.2%      |
| Elliptical      | 3.42         | 2.58        | 1.89        | -14.5%                 | -17.3%      | -14.6%      |





(a) Stress distribution along the beam with circular cope-holes



(b) Stress distribution and extrapolated hot spot stress in front of second cope-hole for different cope-hole shapes

**Figure 8.10:** Influence of loading and shape type on stress distribution

## 8.4 Evaluation according to the hot spot stress approach

The test results of all cope-hole details evaluated based on the hot spot stresses are plotted in Figure 8.11a. It is apparent that although the test data do not lie in one group, the scatter of the results, compared to the nominal stress method, is decreased. Linear regression analysis with a fixed slope of 3 gives a standard deviation of 0,281 compared with the value of 0.614 obtained from the nominal stress method. However, the calculated characteristic fatigue strength of 70.6MPa is considerably lower than what is specified in IIW and Eurocode(FAT 90). If the results from detail 4D which undergoes the highest  $\tau_a/\sigma_m$  ratio are excluded, FAT100 appears to be a reasonable representation.

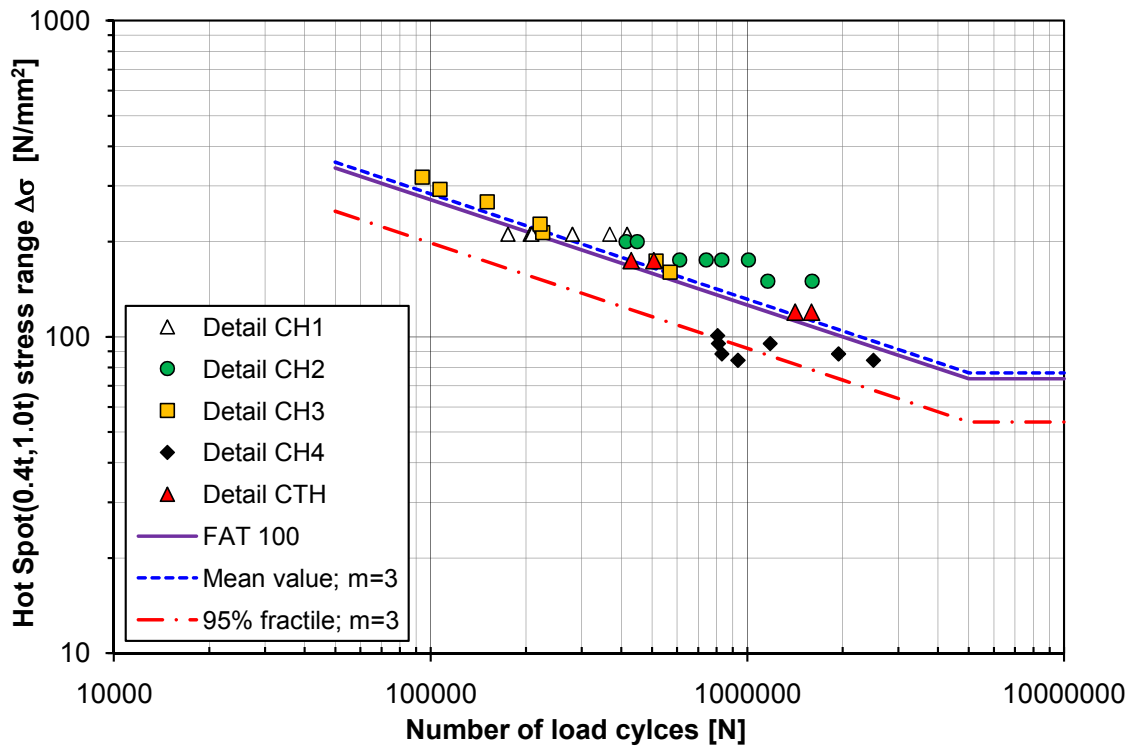
The low hot spot stress value obtained for the detail 4D is assumed to be because of the presence of high amount of shear stresses in the web which causes the weld to become load carrying. In such a case, the weld at the cope-hole transfers the existing shear stresses in addition to the normal stresses caused by the bending of the beam. Thus, in order to account for such severe loading conditions, it is recommended to use another assessment method such as the nominal stress method or the effective notch stress method.

It is noteworthy that for Detail 4C which the surface stress extrapolation according to IIW recommendation was not feasible due to the small radius of the cope-hole in relation to the flange thickness, hot spot stress is calculated as  $1.12 \cdot \sigma_{0.5t}$  according to Lotsberg and Sigurdsson [29]. Moreover, in order to calculate the hot spot stress concentration factor, the nominal stress for beam specimens is calculated as the stress in the mid section of the cope hole using the net cross section and the simple beam theory formula.

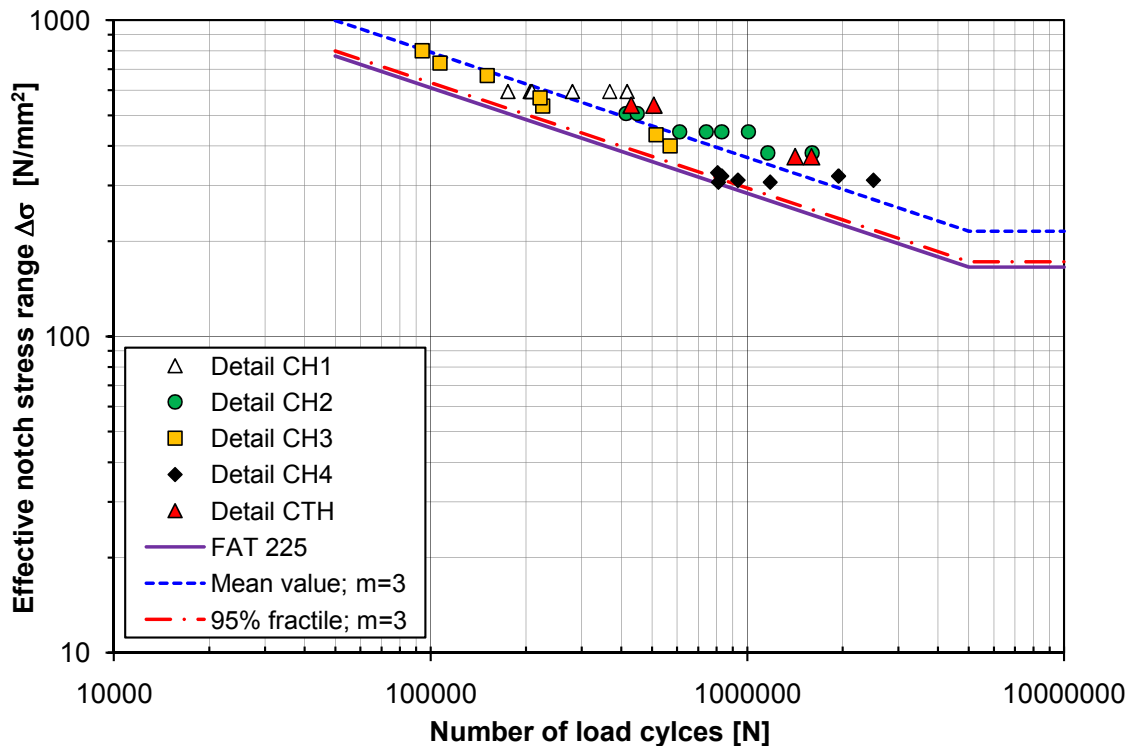
## 8.5 Evaluation according to the effective notch stress method

Considering Figure 8.11b, in which the fatigue test data are evaluated with the effective notch stress method, the scatter of the test data are noticeably reduced. All test data lie within the same narrow scatter band. Moreover, linear regression analysis reveals a slope of 2.74 accompanying by the characteristic value of 216.1MPa and standard deviation of 0.162, which is the lowest obtained standard deviation for this detail based on different evaluation methods.

Eventually, the IIW recommended FAT class 225 based on effective notch stress method, appears to be in acceptable agreement with the evaluated cope hole details in this study.



(a) Fatigue test results of cope-hole details according to the structural hot spot stress approach



(b) Fatigue test results of cope-hole details according to the effective notch stress method

**Figure 8.11:** Fatigue test results of cope-hole details according to the local approaches



## 8.6 Experimental study

This chapter aims to present the information regarding the experimental study conducted at Chalmers University of Technology Structural Engineering Laboratory. To begin with, the test specimens geometry and treatment methods are introduced. Afterwards, the test configuration and procedure are discussed. Finally, the test results and observations are presented.

### 8.6.1 Test specimen

Cope-hole test specimens were fabricated from hot-rolled (EN 10025-2) S355J0 general structural steel. 20mm thick plate were used for the main plate while the attachment thickness was chosen to be 8mm. Overall specimen length was 1200mm and the gripping section had a width of 120 mm. The gripping section width was increased gradually to 220mm with a radius of 50mm. The 600mm long attachments were welded on both sides by means of fillet welds with leg length of 7mm. The specimen width was gradually narrowed down to 100mm in the middle where the cope-holes of radius 50mm were placed. The test specimen geometry and dimensions are illustrated in Figure 8.12. Table 8.6 and Table 8.7 represent chemical and mechanical properties of S355J0 steel respectively.

In order for the specimen to be an appropriate representative of cope-holes, it has to fail as a result of crack initiation and propagation at the cope-hole weld toe. However, the implemented longitudinal attachments that accommodate cope-holes have a fatigue design class identical to cope-hole details i.e. FAT71. Therefore, measures should be taken to enhance the longitudinal attachments weld toe conditions. Reducing the applied perpendicular stresses, introducing a transition radius in longitudinal attachment and post-weld treatment of longitudinal attachment weld toe are some methods that are capable of increasing the fatigue life of this critical section.

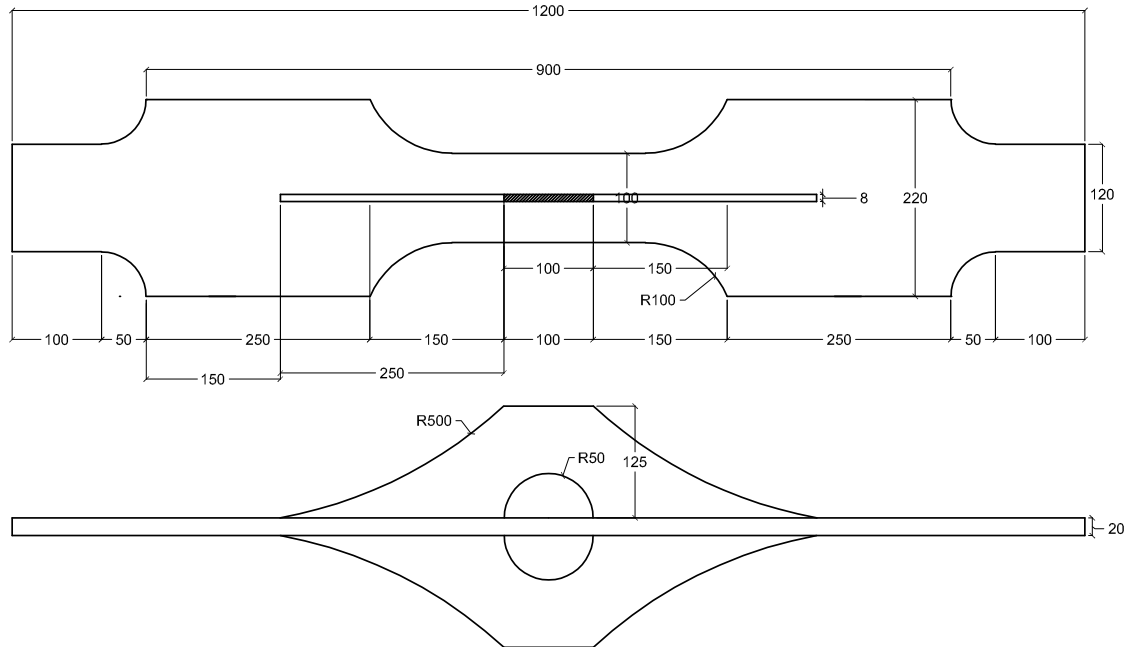
Thereby, as it was crucial to limit the probable fatigue crack locations to cope-hole weld toes, all the above methods were implemented. The section in which longitudinal attachment starts were widened to reduce the experienced stresses by the weld toe. A transition radius of 500mm were introduced in the attachment and the weld toes were BG treated. In addition to that, as a portion of the applied load will be taken by the attachments on both sides, the main plate width were imperceptibly narrowed down to 100mm in the middle where cope-holes are located. By this means, the stresses at cope-hole weld toes will additionally increase and compensate the load carried by attachments. Figure 8.13 shows a 3D model of the tested specimen.

**Table 8.6:** *Chemical analysis of material S355J0 (%), after [82]*

| C     | Si   | Mn   | Al    | Nb    | S     | P      |
|-------|------|------|-------|-------|-------|--------|
| <0.18 | <0.5 | <1.6 | >0.02 | <0.05 | <0.02 | <0.025 |

**Table 8.7:** Mechanical properties of material S355J0, after [82]

| Yield strength<br>$R_e$ [MPa] | Ultimate strength<br>$R_m$ [MPa] | Elongation<br>$A_5$ [%] | Impact ductility<br>KV [J] 0°C |
|-------------------------------|----------------------------------|-------------------------|--------------------------------|
| 355                           | 490–630                          | 20                      | 27                             |



**Figure 8.12:** Cope-Hole test specimen of structural steel S355 tested at CTH; all dimensions are in mm.

In total 12 test specimen were fabricated for the first phase of the study from which four were kept in the AS-Welded condition, four were BG<sup>5</sup> treated and four were UIT<sup>6</sup> treated. All test specimens were BG treated at the longitudinal attachments weld toes.

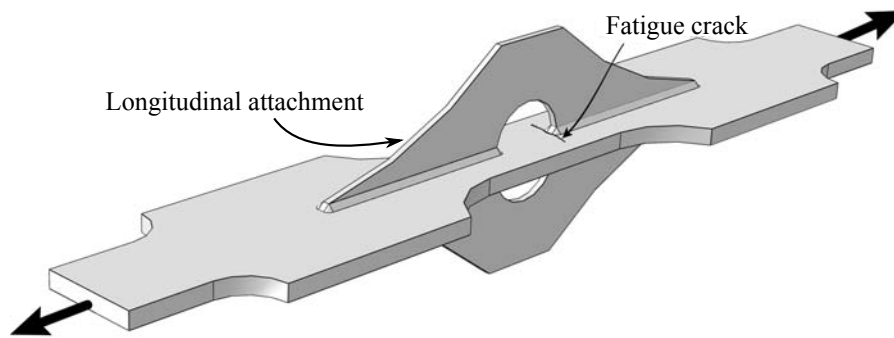
### 8.6.2 Post-weld treatment

A large number of weld toe improvement techniques are available but only a few of them are capable of being used in the bridge industry as a mature and efficient method. The weld toe grinding, TIG dressing and hammer peening are among those methods which appear to offer the most potential for the bridge structure applications.

Kirkhope et al. [83] experimentally investigated the aforementioned improvement techniques for a detail with cope-hole and concluded that a considerable level of improvement is expected such that for toe grinding and TIG dressing treatments an increase of 120% and for hammer peening an increase of 300% in terms of fa-

<sup>5</sup>Burr Grinding

<sup>6</sup>Ultrasonic Impact Treatment



**Figure 8.13:** *Cope-Hole test specimen tested at CTH*

tigue life. However, field-application feasibility and cost efficiency of these methods are other decisive parameters for bridge industry. According to [83, 84] the Burr Grinding (BG) method requires the least operator experience and is the least costly technique.

Post-weld treatment methods such as Burr Grinding and Ultrasonic Impact Treatment have been widely investigated and have in most cases been found to give substantial increases in fatigue strength [85]. However, usually a large difference exists between the obtained improvement levels. Haagensen and Maddox [85] suppose that the reason for such observation primarily initiates from a lack of standardization of the applied methods. In addition to that, the operator's skill also plays an important role in the effectiveness of the treatment.

The sharp transition from the plate surface to the weld on the one hand, and on the other, the presence of microscale pre-existing cracks make the weld toe a severe point of stress concentration. Hence, fatigue cracks initiate readily at these flaws.

Weld toe improvement methods principally aim to enhance the weld toe condition



(a) *Specimen treated with Burr Grinding*

(b) *AS Welded specimen*

**Figure 8.14:** *Cope-hole specimens tested at CTH*

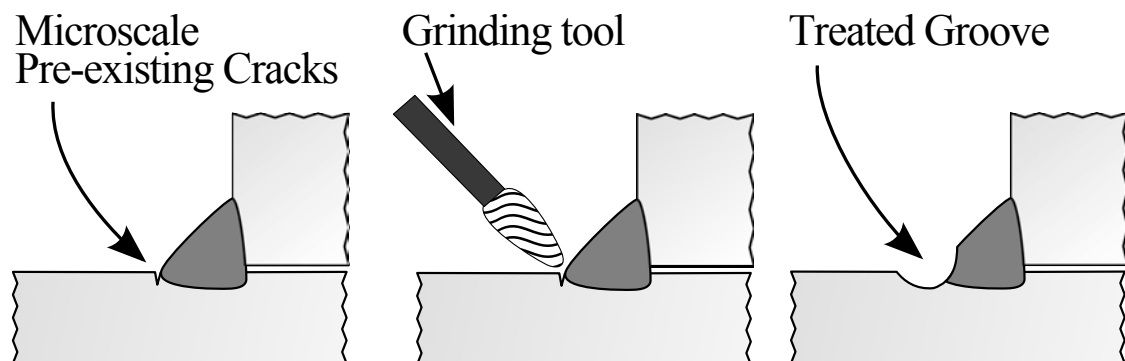
by means of:

- Reduction of the severity of the weld toe stress concentration
- Introduction of beneficial compressive residual stress

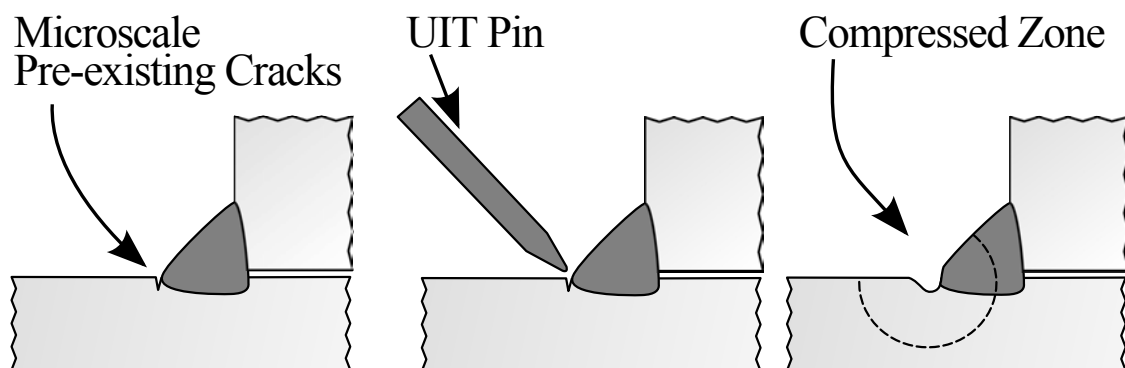
The severity of weld toe can primarily be achieved by removing the weld toe flaws. Subsequently, the crack initiation part of fatigue life will be extended. Furthermore, the local stress concentration due to sharp transition of weld profile can be reduced by introducing a smooth blend at the transition of plate and weld.

Some methods such as UIT, are capable of inducing high compressive residual stresses at the treated area. This way the applied tensile stress must first overcome the residual stress before it becomes damaging. As a result, the applied stress range becomes less destructive.

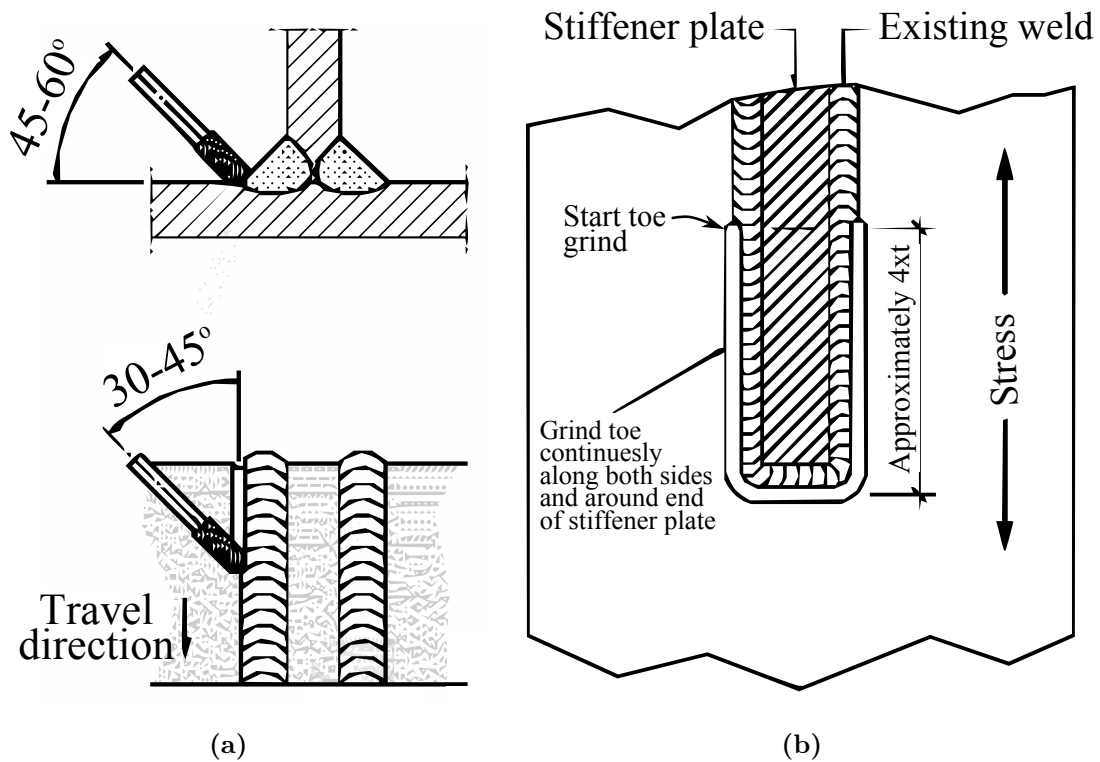
It has been shown in several research programs that Burr grinding method only improve the weld toe condition by reducing the severity of weld toe stress concentration, whereas UIT primarily enhance the fatigue performance by introducing compressive residual stresses. Figure 8.15 and Figure 8.16 demonstrate the principals of BG and UIT post-weld improvement methods respectively.



**Figure 8.15:** Burr Grinding technique as a method to enhance weld toe condition



**Figure 8.16:** Ultrasonic Impact treatment as a method to introduce compressive residual stresses and enhance weld toe condition



**Figure 8.17:** *Burr Grinding technique*

As it is shown in Figure 8.17b, According to the IIW recommendations on post weld improvement of steel and aluminium structures [85], the improvement should extend around the attachment end and should continue along both sides of the attachment. The length of treatment along the attachment sides should reach approximately four times of plate thickness. In this research, the treatment were extended approximately 50mm on both sides. Figure 8.17a shows other requirements of BG treatment application.

According to IIW, the depth of treatment should extend at least 0.5mm below any visible undercut. However, it shouldn't exceed the maximum allowable depth which is defined as 7% of the plate thickness. Thus, for a 20mm thick plate the maximum allowable treatment depth is 1.4mm. In this research it was anticipated that 1mm depth is the optimum value. Measurements after treatment application revealed a depth variation between 0.7–1.4mm with a groove of radius 4–5mm. Figure 8.18 depicts the BG treatment application while Figure 8.19 and Figure 8.20 show the final treatment after polishing the surface.



(a) Burr grinding tool



(b) BG of longitudinal attachment weld toe



(c) Cope-hole weld toe BG treatment



(d) Cope-hole weld toe BG treatment

**Figure 8.18:** Burr Grinding technique application



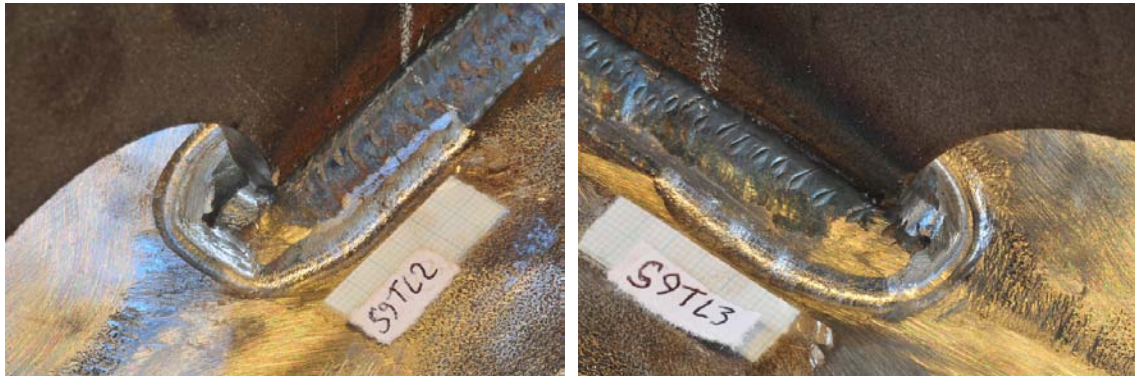
(a) Finished longitudinal attachment weld toe  
BG treated



(b) Finished longitudinal attachment weld toe  
BG treated

**Figure 8.19:** Finished BG treated specimens





(a) *Finished Cope-hole weld toe BG treated*      (b) *Finished Cope-hole weld toe BG treated*

**Figure 8.20:** *Finished BG treated specimens*

The UIT treatment technique was only applied on the cope-hole weld toes of 4 specimens as an alternative method. In this method, the weld toe was first compressed by means of a UIT pin with a radius of 1.5mm. This procedure formed a groove with depth of approximately 0.5–0.8mm. Additionally, in order to prevent the formation of small cracks as a result of hardening of the weld surface or improper treatment, the whole weld surface close to the treated zone was compressed with a 4-head pin. Figure 8.21 shows the procedure of UIT application along with a finished UIT treated weld toe.



(a) *UIT tool*



(b) *UIT application*



(c) *Half-way treated weld toe*



(d) *UIT application*



(e) *UIT application*



(f) *Finished UIT applied weld toe*

**Figure 8.21:** *Ultrasonic Impact Treatment application*



### 8.6.3 Test procedure

Fatigue testing was carried out to experimentally define the as-welded, BG-treated and UIT treated fatigue strength of welded cope-hole details. The constant amplitude fatigue tests were conducted at a frequency of 4–5hz and the ratio between minimum and maximum stress was  $R = \sigma_{min}/\sigma_{max} = 0.1$ . The tests were conducted using a 500kN hydraulic universal machine under axial tension loading in laboratory environment. Figure 8.22 shows the strain gages positioning for the specimens. The strain gage data are used to produce the structural stress value and to evaluate the probable secondary bending stresses.

Figure 8.23 demonstrates the test setup. The tests were carried on until the total rupture of specimen.

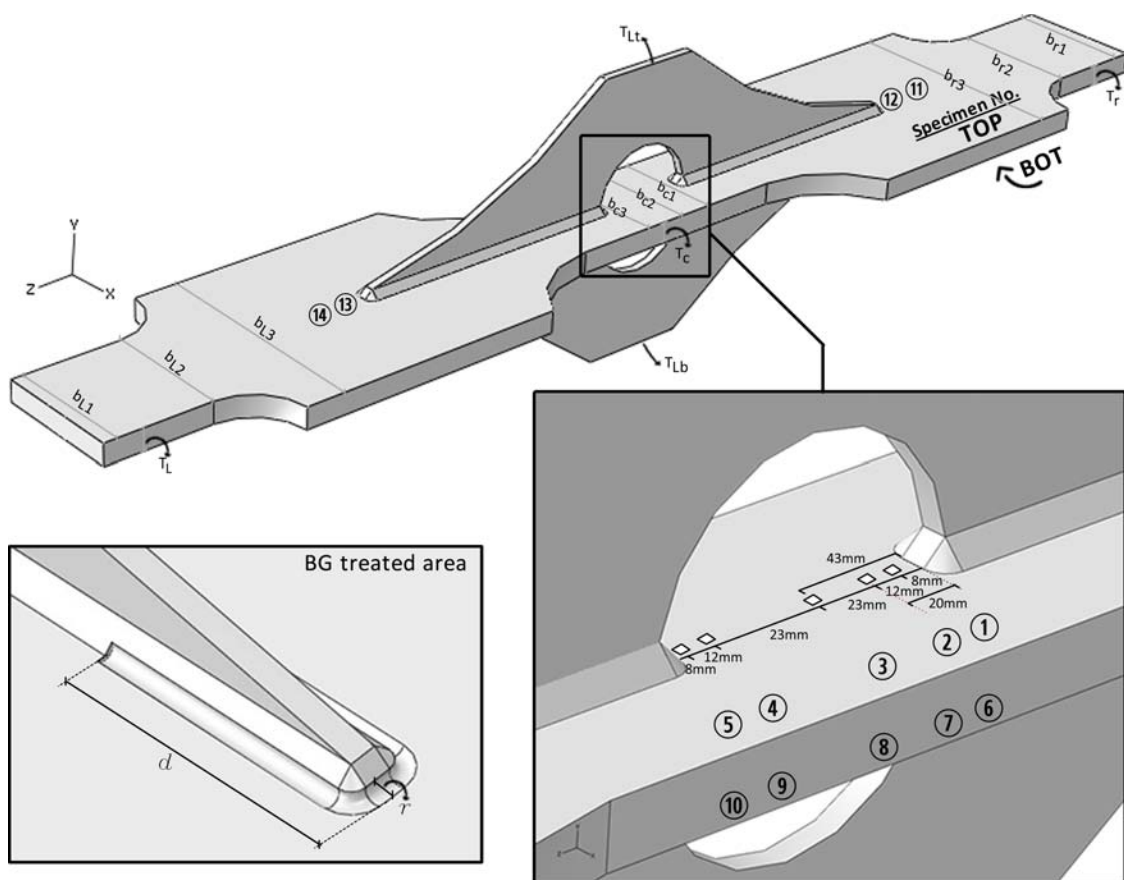


Figure 8.22: Strain gages positioning and designation



(a) *Test setup*                      (b) *Test setup*                      (c) *Strain gages placement*

**Figure 8.23:** *Axial tension fatigue test setup configuration*

#### 8.6.4 Test results

As discussed in Section 8.2, the obtained as-welded test results are consistent with the existing fatigue test data of cope-hole details. The fatigue crack in all the four as-welded specimens, initiated from the cope-hole weld toe which after propagation led to the final rupture of the specimen, see Figure 8.24.



(a)    (b)

**Figure 8.24:** *AS-welded specimen failed from weld toe*

Nevertheless, all the treated specimens except one failed from weld root of cope-hole. The only specimen which failed prematurely from the BG treated groove was suffering from improper treatment. Consequently, it can be concluded that,

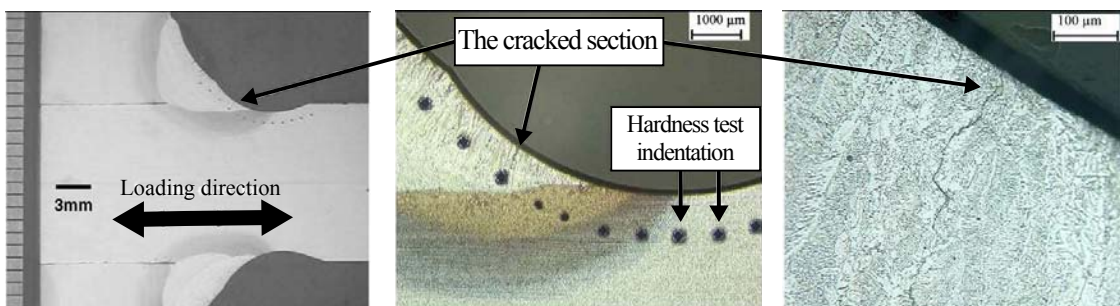


**Figure 8.25:** *UIT treated specimen failed from weld root*

providing the treatment is correctly applied, the weld toe becomes flaw-free and the crack initiation portion of fatigue life extends dramatically so that the weld fails due to root defects. Figure 8.25 shows a treated specimen failed from weld root.

However, as it was mentioned before, one treated specimen failed from the treated groove. The metallurgical investigations gained similar findings with those obtained by [86]. Zhang and Maddox [86] have mentioned the presence of small flaws in the weld metal at the groove, see Figure 8.26. This finding supports the low fatigue life behavior of the cope-hole test specimen failed at treated groove. It should be noted that the crack location in this specimen was not at the deepest point of the groove where the plate reduction is greater and thus undergoes the highest stress concentration factor. It is anticipated that by polishing the treated groove surface, the probability of having defects of this kind would become minimum.

The test results of all specimens are plotted in Figure 8.27 where the treated specimen failed at weld toe is marked with a cross. The results support the notion raised in other research that the treatment is more effective at high cycle fatigue. Statistical evaluation of the treated specimens test results, excluding the failure case due to improper treatment, indicates a slope of 3.55 and standard deviation of 0.098. When using a fixed slope of 3, a characteristic design value of 157.4 MPa



**Figure 8.26:** *Magnified photograph of toe ground welded specimen showing the initiation of the crack in weld metal at treated groove, after [86]*

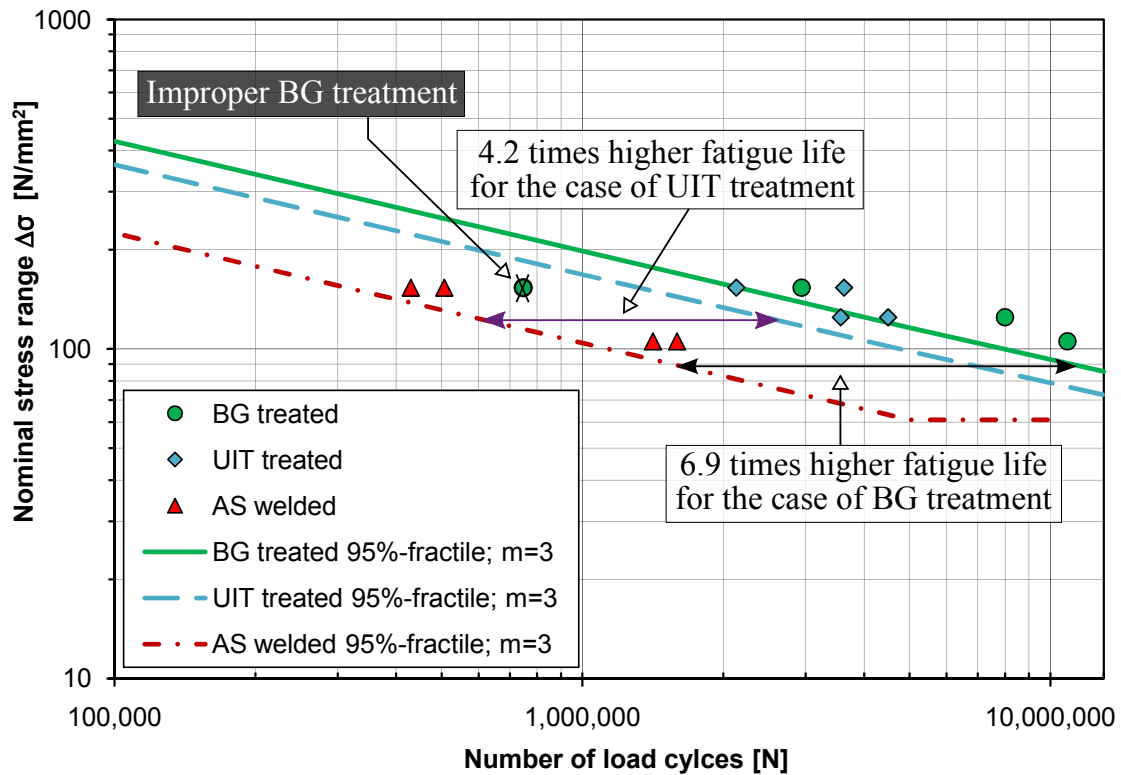


Figure 8.27: The fatigue test results of cope-hole specimens tested at CTH

is derived. This value indicates an increase of 190% in terms of fatigue strength compared to AS welded specimens.

The UIT treated specimens also show a good performance. The statistical evaluation of the UIT treated specimens, with a fixed slope of 3, reveals a characteristic fatigue strength of 133.6MPa accompanied by a standard deviation of 0.150. This indicates a fatigue life extension of approximately 4.2 times compared to the AS welded specimen. Finally, it should be noted that, the nominal stress for the specimens is defined as the total calculated force in main-plate at the midsection of cope-hole using a 3D solid FEM model divided by its area.

The constant amplitude fatigue test data are reported numerically in Appendix V.

## 9 Conclusions

### 9.1 Concluding remarks

Local fatigue assessment approaches, such as the structural hot spot stress method and the effective notch stress method, utilize the advantages of finite element method for fatigue assessment of welded steel details. As these methods include the stress raising effects caused by the geometrical variations, more types and variations of details compared to the conventional nominal stress method can be assessed by them. The structural hot spot stress method has been in use in other industries such as offshore and marine structures for more than 30 years. However, this method is rather new in the assessment of plate-type joints which mostly constitute bridges. Eurocode 3 has introduced these methods in its latest revision and thus, it is anticipated that the application of them will increase in the close future.

The application of the nominal stress, structural hot spot stress and the effective notch stress methods on the fatigue life evaluation of several frequently used bridge details was studied in this project. Table 9.1 represents a summary of the findings of this study. It is apparent that, although the findings of the nominal stress method is generally consistent with the current recommendations, the results obtained by the structural hot spot stress and the effective notch stress methods are not in good agreement with the available guidelines. With reference to the results, the current available recommendations based on the structural hot spot stress approach seem to be mostly on the unsafe side, whereas those based on the effective notch stress method appear very conservative.

In addition to that, special consideration is given to details with cope-holes. Besides the previous fatigue tested reported in the literature, a series of small scale fatigue tests has been performed. The results of the study show that if the cope holes are positioned in regions of high shear forces, the effect of shear stress should be considered in the fatigue design of the bridge girders. Altering the geometric shape of the cope hole gives very marginal change in the stress concentration at the weld toe. On the other hand, burr grinding gave very promising results in term of enhancing the fatigue category of the detail. The test results show an increase of 190% in terms of fatigue strength (Approximately 6.9 times higher fatigue life) for cope-holes treated with Burr Grinding. It was also observed that an increase of 4.2 times in terms of fatigue life is obtainable by applying the UIT treatment method.

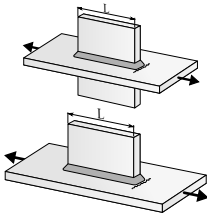
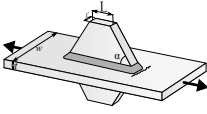
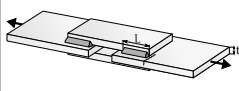
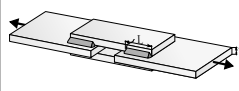
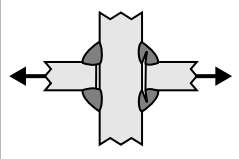
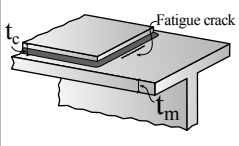
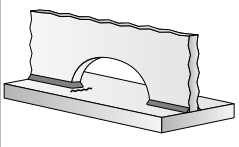
With reference to the finite element modeling analysis, the followings can be concluded:

- The modeled weld in the analysis based on the the structural hot spot stress method, has very little influence. Thus this method is specifically suitable for the analysis during the design phase. On the contrary, the effective notch stress method exhibited a great potential to reduce the scatter caused by the variations of the weld geometry. Therefore, it is expected to be more effective

for evaluation of the existing structures.

- The structural hot spot stress method is capable of reducing the scatter caused by the plate thickness variations for plates thinner than 25mm. However, conforming to the recommendations of Eurocode 3, a thickness correction factor should be used for thicker plates.
- The time and modeling effort required for the effective notch stress method is tremendously higher than the structural hot spot stress method. Considering the obtained results, it is apparent that within the field of bridge engineering, the application of the structural hot spot stress method is more reasonable. However, for root cracking, the structural hot spot stress approach is not applicable and the use of effective notch stress method is inevitable.
- As mentioned earlier, for the case of cope holes positioned in regions of high shear forces, the effect of shear stress should be considered in the fatigue design of the bridge girders. However, as the structural hot spot stress method is only applicable when the applied stress is predominantly perpendicular to the weld toe, it is recommended to use another method such as the effective notch stress method for the assessment of cope-holes subjected to severe shear stresses.

**Table 9.1:** Current and proposed fatigue design classes for the investigated welded joints according to the nominal stress, structural hot spot stress and effective notch stress methods

| Structural Detail   | Nominal stress                    |          | Hot spot stress  |          | Effective notch stress |  |      |      |
|---|-----------------------------------|----------|--|----------|------------------------|--|------|------|
|   | EC 3                              | Proposed | EC 3   | Proposed | EC 3                   | Proposed                                   |      |      |
|    | $L \leq 50$                       | C80      | $L \leq 150$   | C71      | C100                   | C90  | C225 | C300 |
|   | $50 < L \leq 80$                  | C71      |  |          |                        |  |      |      |
|   | $80 < L \leq 100$                 | C63      | $L > 150$  | C56      |                        |  |      |      |
|   | $L > 100$                         | C56      |  |          |                        |  |      |      |
|    | $L > 100$<br>$\alpha < 45^\circ$  | C71      | $L > 100$<br>$\alpha < 45^\circ$                             | C71      | C100                   | C90  | C225 | C300 |
|   | $100 < L \leq 120$<br>All t       | C56      | $100 < L \leq 120$<br>All t                                  | C56      | C90                    | C80<br>Quadratic<br>extrapolation          | C225 | C300 |
|   | $L > 120$<br>$t \leq 20$          | C56      | $L > 120$<br>$t \leq 20$                                     | C56      |                        |  |      |      |
|  | All configurations                | C45      | All configurations   | C45      | C90                    | C100                                       | C225 | C300 |
|  | All configurations                | C36      | All configurations   | C36      | [N/A]                  | [N/A]                                      | C225 | C225 |
|  | $t_c/t_m < 1$<br>$t_m \leq 20$    | C56      | $t_c/t_m < 1$<br>$t_m \leq 20$                               | C56      | C90                    | C100<br>Quadratic<br>extrapolation         | C225 | C300 |
|   | $t_c/t_m \geq 1$<br>$t_m \leq 20$ | C50      | $t_c/t_m \geq 1$<br>$t_m \leq 20$                            | C50      |                        |  |      |      |
|  | All configurations                | C71      | C71*<br>*Correction factor<br>for $\tau_a/\sigma_m \geq 0.2$ |          | C90                    | C90<br>Only for<br>$\tau_a/\sigma_m < 0.2$ | C225 | C225 |

## 9.2 Future work

Based on the results of this study, the followings are addressed for future work:

- The results of this study confirmed that, as long as the discussed local approaches are used, the accuracy of the evaluated fatigue tests is almost independent of the implemented method. Therefore, the evaluation of more welded details by these methods is of great interest.
- As it is listed in Table 9.1, when using the effective notch stress approach, except for two details, FAT300 is applicable to all other investigated details. As the effective notch stress method ideology is to use only one design class, more research is needed to investigate this observation.
- Dong stress method was applied to one of the investigated details. It was observed that the results obtained from this method are more consistent with the current recommendations for the studied detail. Therefore, applying the discussed SHSS determination methods other than the implemented surface stress extrapolation method to the investigated details, can shed light on their relative accuracy.
- A shear correction factor is derived for the cope-holes subjected to severe shear stresses. This equation needs to be further verified by experimental and analytical investigations to draw a firm conclusion.
- Improper burr grinding treatment was shown to be very destructive. As a result, methods to prevent the discussed treatment induced defects are needed to be investigated. In addition to that, numerical methods for the assessment of post-weld treated specimens can be studied.



## References

- [1] D. Radaj. *Design and analysis of fatigue resistant welded structures*. Woodhead Publishing, 1990.
- [2] T. R. Gurney. *Fatigue of Welded Structures*. Cambridge U.P., 1968.
- [3] Wolfgang Fricke. Fatigue analysis of welded joints: state of development. *Marine structures*, (16):185–200, 2003.
- [4] S J Maddox. *Fatigue strength of welded structures*. Abington Pub., 1991.
- [5] D. Radaj and C.M. Sonsino. *Fatigue assessment of welded joints by local approaches*. Woodhead publishing, 1998.
- [6] W. Fricke. Recommended hot-spot analysis procedure for structural details of ships and FPSOs based on round-robin FE analyses. *International Journal of Offshore and Polar Engineering*, 12(1):40–47, 2002.
- [7] I. Lotsberg. Fatigue design of plated structures using finite element analysis. *Ships Offshore Structures*, 1(1):45–54, 2006.
- [8] O. Doerk, W. Fricke, and C. Weissenborn. Comparison of different calculation methods for structural stresses at welded joints. *International journal of fatigue*, 25(5):359–369, 2003.
- [9] Eurocode3. *Design of steel structures - Part 1-9: Fatigue*. European Standard, May 2005.
- [10] A. Hobbacher. Recommendations for fatigue design of welded joints and components, iiw document no. Technical report, IIW-1823-07. International Institute of Welding, December 2008.
- [11] E. Niemi, W. Fricke, S.J. Maddox, and International Institute of Welding. *Fatigue Analysis of Welded Components: Designer's Guide to the Structural Hot-spot Stress Approach:(IIW-1430-00)*. Woodhead Publishing, 2006.
- [12] ASTM. *Standard Definitions of Fatigue*, volume ASTM E 1150-1987. ASTM, 1995.
- [13] Tore Dahlberg and Anders Ekberg. *Failure Fracture Fatigue, An Introduction*. Studentlitteratur AB, 2002. ISBN 9789144020969.
- [14] Jaap Schijve. *Fatigue of Structures and Materials*. Springer, 2nd edition, 2009. ISBN 1402068077.
- [15] Yan-Hui Zhang and Stephen J. Maddox. Fatigue life prediction for toe ground welded joints. *International Journal of Fatigue*, (31):1124–1136, 2009.
- [16] P Paris and F Erdogan. A critical analysis of crack propagation laws. *Journal of Basic Engineering*, pages 528–534, December 1963.

- [17] J. Schijve. Fatigue of structures and materials in the 20th century and the state of the art. *International Journal of Fatigue*, (25):679–702, 2003.
- [18] John M Barsom and Stanley T Rolfe. *Fracture and Fatigue Control in Structures, Applications of Fracture Mechanics*. American Society for Testing and Materials, 3rd edition, 1999. ISBN 9780803120822.
- [19] D Radaaj, C M Sonsino, and W Fricke. *Fatigue assessment of welded joints by local approaches*. Woodhead Publishing, second edition, 2006.
- [20] G Petterson. *Fatigue Assessment of Welded Structures with Non-Linear Boundary Conditions*. Dept. of Aeronautical and Vehicle Engineering, The Royal Institute of Technology, TRITA-AVE 2004-50, Stockholm, 2004.
- [21] M Byggnevi. Life predictions of a complex welded structure using different methods. In J Samuelsson, editor, *Design and Analysis of Welded high Strength Steel Structures*. EMAS, June 2002.
- [22] G. Marquis and J. Samuelsson. Modelling and fatigue life assessment of complex structures. *Materialwissenschaft und Werkstofftechnik*, 36(11):678–684, November 2005.
- [23] Åsa Eriksson, Anna-Maria Lignell, Claes Olsson, and Hans Spennare. *Weld evaluation using FEM: A guide to fatigue-loaded structures*. Industrilitteratur AB, Sweden, 2003. ISBN 9175486652.
- [24] A.F. Hobbacher. The new iiw recommendations for fatigue assessment of welded joints and components, a comprehensive code recently updated. *International Journal of Fatigue*, 31(1):50–58, January 2009.
- [25] T. R. Gurney. The influence of thickness on the fatigue strength of welded joints. *Proceedings of the Second International Conference on the Behaviour of Off-Shore Structures, held at Imperial College, London, England, Aug. 28th-31st 1979*.
- [26] Fidelis R. Mashiri and Xiao-Ling Zhao. Thickness effect in welded joints-a review. *Proceedings of the fifteenth international offshore and polar engineering conference, Seoul, Korea, June 2005*.
- [27] S. Berge and S. E. Webster. The size effect on the fatigue behaviour of welded joints. In *Proc. 3<sup>rd</sup> Int Conf on Steel in Marine Structures, SIMS'87*, pages 179–203, Delft, The Netherlands, June 1987.
- [28] E. Niemi. *Stress determination for fatigue analysis of welded components*. Woodhead Publishing, 1995.
- [29] I. Lotsberg and G. Sigurdsson. Hot spot stress S-N curve for fatigue analysis of plated structures. *Journal of offshore mechanics and Arctic engineering*, 128:330, 2006.

- [30] W. Fricke and A. Kahl. Comparison of different structural stress approaches for fatigue assessment of welded ship structures. *Marine structures*, 18(7-8): 473–488, 2005.
- [31] P. Dong. A structural stress definition and numerical implementation for fatigue analysis of welded joints. *International Journal of Fatigue*, 23(10): 865–876, 2001.
- [32] P. Dong, JK. Hong, and Z. Cao. Structural stress based master S-N curve for welded joints. *International Institute of Welding*, (IIW Doc XIII-1930-02/XV-1119-02), 2002.
- [33] Z.G. Xiao and K. Yamada. A method of determining geometric stress for fatigue strength evaluation of steel welded joints. *International journal of fatigue*, 26(12):1277–1293, 2004.
- [34] I. Poutiainen and G. Marquis. A fatigue assessment method based on weld stress. *International journal of fatigue*, 28(9):1037–1046, 2006.
- [35] H. Petershagen, W. Fricke, and T. Massel. Application of the local approach to the fatigue strength assessment of welded structures in ships. *International Institute of Welding*, (IIW Doc. XIII-1409-91), 1991.
- [36] W. Fricke and H. Petershagen. Detail design of welded ship structures based on hot-spot stresses. 1992.
- [37] Wolfgang Fricke and Hans Paetzoldt. Fatigue strength assessment of scallops; an example for the application of nominal and local stress approaches. *Marine Structures*, 8(4):423 – 447, 1995.
- [38] E. Niemi and G.B. Marquis. Structural hot spot stress method for fatigue analysis of welded components. *Metal structures-Design, Fabrication, and Economy*, (90-77017), 2003.
- [39] SJ. Maddox. Hot-spot stress design curves for fatigue assessment of welded structures. *International Journal of Offshore and Polar Engineering*, 12(2): 134–141, 2002.
- [40] C. Miki and K. Tateishi. Fatigue strength of cope hole details in steel bridges. *International Journal of Fatigue*, 19(6):445–455, 1997.
- [41] G. Savaidis and M. Vormwald. Hot-spot stress evaluation of fatigue in welded structural connections supported by finite element analysis. *International journal of fatigue*, 22(2):85–91, 2000.
- [42] British Standard BS 7608:1993. Code of practice for fatigue design and assessment of steel structures. *British Standards Institution, London, ISBN 0, 580:212815*, 1993.
- [43] E. Niemi and G.B. Marquis. Introduction to the structural stress approach to fatigue analysis of plate structures. In *Proceedings of the IIW fatigue seminar*, pages 73–90, Tokyo, 2002.

- [44] M. Wagner. Fatigue strength of structural members with in-plane notches. *IIW Doc XIII-1730-98*, 1998.
- [45] E. Niemi and P. Tanskanen. Hot spot stress determination for welded edge gussets. *Welding in the World*, 44(5):31–37, 2000.
- [46] I. Poutiainen, P. Tanskanen, and G. Marquis. Finite element methods for structural hot spot stress determination—a comparison of procedures. *International journal of fatigue*, 26(11):1147–1157, 2004.
- [47] P. Dong, JK Hong, and Z. Cao. A mesh-insensitive structural stress procedure for fatigue evaluation of welded structures. *IIW doc*, 13:1902–01, 2001.
- [48] B.W. Noh, J.I. Song, and S.I. Bae. Fatigue strength evaluation of the load-carrying cruciform fillet welded joints using hot-spot stress. *Key Engineering Materials*, 324:1281–1284, 2006.
- [49] G. Notaro, C. M. Rizzo, F. Casuscelli, and M. Codda. An application of the hot spot stress approach to a complex structural detail. In *Maritime industry, ocean engineering and coastal resource. Proceedings of the 12th International Congress of the International Maritime Association of the Mediterranean IMAM 2007*, Varna, Bulgaria, Septemeber 2–6 2007.
- [50] MH Kim and SW Kang. Testing and analysis of fatigue behaviour in edge details: a comparative study using hot spot and structural stresses. *Proceedings of the Institution of Mechanical Engineers, Part C: Journal of Mechanical Engineering Science*, 222(12):2351–2363, 2008.
- [51] Feltz O. Fricke, W. Fatigue tests and numerical analyses of partial-load and full-load carrying fillet welds at cover plates and lap joints. *Welding in the World*, 54(7-8):R225–R233, 2010.
- [52] D. Radaj, CM Sonsino, and W. Fricke. Recent developments in local concepts of fatigue assessment of welded joints. *International Journal of Fatigue*, 31(1): 2–11, 2009.
- [53] Notch stress concepts for the fatigue assessment of welded joints – background and applications. *International Journal of Fatigue*, 34(1):2 – 16, 2012. ISSN 0142-1123.
- [54] W. Fricke. Guideline for the fatigue assessment by notch stress analysis for welded structures. *International Institute of Welding*, 2008.
- [55] IJ Smith, IFC Smith, and SJ Hurworth. A 3-d analysis of the longitudinal non-load carrying fillet welded fatigue specimen. *The Welding Institute Research Report*, 184:1982, 1982.
- [56] IFC Smith and TR Gurney. Changes in the fatigue life of plates with attachments due to geometrical effects. *Welding Research Supplement*, pages 244s–250s, 1986.

- [57] A. Hobbacher. Stress intensity factors of welded joints. *Engineering fracture mechanics*, 46(2):173–182, 1993.
- [58] T. Dahle and B. Larsson. Fatigue life predictions of longitudinal non-load-carrying fillet welded specimens based on current flaw distribution. In *Fatigue under spectrum loading and in corrosive environments: proceedings of a conference held 26-27th August 1993 at the Technical University of Denmark, Lyngby*, page 149. Engineering Materials Advisory Services, 1993.
- [59] I. Huther, HP Lieurade, N. Sayhi, and R. Buisson. Fatigue strength of longitudinal non-load-carrying welded joints. *WELD WORLD SOUDAGE MONDE*, 41(4):298–313, 1998.
- [60] A. Version. 6.9 online documentation. *SIMULIA Inc.*
- [61] Farshid Zamiri Akhlaghi. Fatigue life assessment of welded bridge details using structural hot spot stress method, a numerical and experimental case study. Master’s thesis, Chalmers university of technology, 2009.
- [62] GS Booth. Constant amplitude fatigue tests on welded steel joints performed in air. In *European Offshore Steels Research Seminar; Cambridge*. The Welding Institute, Abington Hall, Abington, Cambridge, CB 1 6 AL, England, 1978.
- [63] TR Gurney. *The Influence of Artificially Induced Residual Stresses on the Fatigue Strength of Load-carrying Fillet Welded Joints in Mild Steel*. British Welding Research Assoc., 1961.
- [64] L.R. Hall, J.E. Stallmeyer, Welding Research Council (U.S.). Fatigue Committee, University of Illinois at Urbana-Champaign. Dept. of Civil Engineering, and United States. Bureau of Public Roads. *The fatigue strength of flexural members*. [Civil engineering studies: Structural research series. University of Illinois, Dept. of Civil Engineering, 1959.
- [65] J.W. Fisher, KH Frank, MA Hirt, and BM McNamee. *Effect of weldments on the fatigue strength of steel beams*. Highway Research Board, National Research Council, 1970.
- [66] R.E. Slockbower and J.W. Fisher. *Fatigue strength of full scale cover-plate beams*. Fritz Engineering Laboratory, Report No. 386-9(77), 1977.
- [67] W.H. Munse and J.E. Stallmeyer. Fatigue in welded beams and girders. *Highway Research Board Bulletin*, 1962.
- [68] S. Kainuma and I.T. Kim. Fatigue strength evaluation of load-carrying cruciform fillet-welded joints made with mild steel plates of different thickness. *International journal of fatigue*, 27(7):810–816, 2005.
- [69] S. Kainuma and T. Mori. A fatigue strength evaluation method for load-carrying fillet welded cruciform joints. *International journal of fatigue*, 28(8): 864–872, 2006.

- [70] N.N. United kingdom offshore steels research projec, final report to ecsc contract no.7210 kb/8/801, volume 1 and 2. Technical report, Department of Energy, London, 1980.
- [71] A. Neumann. *Theorie der Dauerfestigkeit von Schweißverbindungen*. Schweißtechnik, Heft 2, S. 423-431, 1958.
- [72] A. Neumann. Probleme der dauerfestigkeit von schweißverbindungen. Technical report, VEB Verlag Technik, Berlin, 1966.
- [73] D.S. Macfarlane and J.D. Harrison. Some fatigue tests of load-carrying transverse fillet welds. *British Welding Journal*, (12):613–623, 1965.
- [74] E. Haibach and M. Hempel. Ertragbare spannungen für zwei typische schweißverbindungen aus stahl st 37 und stahl st 52 bei hohen werten des spannungsverhältnisses und bei verschiedenen nahtausführungen. Technical report, Laboratorium für Betriebsfestigkeit, Darmstadt und Max-Planck-Institut für Eisenforschung, Düsseldorf, 1966.
- [75] E. Haibach and G. Bierett. Abhängigkeit der ertragbaren spannungen schwingbeanspruchter schweißverbindungen vom beanspruchungskollektiv bericht nr. fb-79. Technical report, Laboratorium für Betriebsfestigkeit, Darmstadt, 1968.
- [76] K. Latzin and Chr. Petersen. Auntersuchungsergebnisse für die stahlbaupraxis, dvs-bericht 31. Technical report, Deutscher Verlag für Schweißtechnik, Düsseldorf, 1974.
- [77] W. Fricke, A. von Lilienfeld-Toal, and H. Paetzold. Fatigue strength investigations of welded details of stiffened plate structures in steel ships. *International Journal of Fatigue*, 2011.
- [78] J.E. Stallmeyer and J.W. Fisher. *Behavior of welded built-up beams under repeated loads*. Civil engineering studies: Structural research series. Dept. of Civil Engineering, University of Illinois, 1958.
- [79] O. Izdinsky. Engine room section in the building of river ships and the welding of steel reinforcements to the bottom cover ship. *ZVARANIE*, 2(12):363–368, 1958.
- [80] Z. Xiao and K. Yamada. Fatigue strength of intersecting attachments. *Journal of Structural Engineering*, 131(6):924–932, 2005.
- [81] W. Fricke. Guideline for the fatigue assessment by notch stress analysis for welded structures. *International Institute of Welding*, 2008.
- [82] Rautaruukki. *Designer's guide, Steel products*. 1996.
- [83] K.J. Kirkhope, R. Bell, L. Caron, R.I. Basu, and K.-T. Ma. Weld detail fatigue life improvement techniques. part 1: review. *Marine Structures*, 12(6):447 – 474, 1999. ISSN 0951-8339.

- [84] K.J Kirkhope, R Bell, L Caron, R.I Basu, and K.-T Ma. Weld detail fatigue life improvement techniques. part 2: application to ship structures. *Marine Structures*, 12(7-8):477 – 496, 1999. ISSN 0951-8339.
- [85] PJ Haagensen and SJ Maddox. Iiw recommendations on post weld improvement of steel and aluminium structures. *International Institute of Welding. IIW Doc. XIII-2200r1-07*, 2008.
- [86] Yan-Hui Zhang and Stephen J. Maddox. Fatigue life prediction for toe ground welded joints. *International Journal of Fatigue*, 31(7):1124 – 1136, 2009. ISSN 0142-1123.

# Appendix I: An example of Dong stress calculation

This example demonstrates the calculation procedure of structural Dong stress for a 3D over-lapped joint. The finite element analysis results selected along certain pathes are the input data and the outcome is the structural Dong stress.

In this example, the Dong stress is calculated for detail OM1 and at distance  $\delta=0.9t=11.43mm$ .

Moreover, the attachment is welded on both sides of the main plate and thus, as discussed earlier, the stress distribution through thickness is non-monotonic. However, since the detail and loading type are symmetric, the through thickness stress linearization can be performed for half of the plate thickness.

## Input Data

Stress components up to half of the plate thickness at a section at distance  $\delta$  from the weld toe:

$$X := \begin{pmatrix} 0 \\ 1.5875 \\ 3.175 \\ 4.7625 \\ 6.35 \end{pmatrix} \text{ mm} \quad \sigma_{xx} := \begin{pmatrix} 1.14303 \\ 1.14031 \\ 1.1377 \\ 1.1323 \\ 1.12678 \end{pmatrix} \text{ MPa} \quad \tau_{xy} := \begin{pmatrix} -6.1591E-008 \\ 0.00174922 \\ 0.00369033 \\ 0.00235829 \\ 0.00111507 \end{pmatrix} \text{ MPa}$$

Stress components up to distance  $\delta$  from the weld toe at mid-plate section:

$$x_b := \begin{pmatrix} 0 \\ 0.84668 \\ 1.69336 \\ 2.54004 \\ 3.38666 \\ 4.23334 \\ 5.08002 \\ 6.66748 \\ 8.255 \\ 9.84253 \\ 11.43 \end{pmatrix} \text{ mm} \quad \sigma_{yy} := \begin{pmatrix} 0.277577 \\ 0.247718 \\ 0.254296 \\ 0.211195 \\ 0.141069 \\ 0.114083 \\ 0.0846233 \\ 0.0459059 \\ 0.0127364 \\ 0.00637722 \\ -0.000371797 \end{pmatrix} \text{ MPa} \quad \tau_{yx} := \begin{pmatrix} -4.82425E-005 \\ -3.194E-005 \\ -8.15187E-006 \\ -7.28923E-006 \\ -8.97655E-006 \\ -3.57046E-006 \\ -1.88593E-008 \\ 5.5274E-007 \\ 9.74171E-007 \\ 2.89852E-007 \\ -6.1591E-008 \end{pmatrix} \text{ MPa}$$

## Geometry

$$t_y := 6.35 \text{ mm} \quad w := 4.04 \text{ mm} \quad \text{delta} := 11.43 \text{ mm}$$



**Calculation procedure:**

Lower limit of the integral  $a$        $a := 0\text{mm}$

Upper limit of the integral  $b$        $b := 6.35\text{mm}$

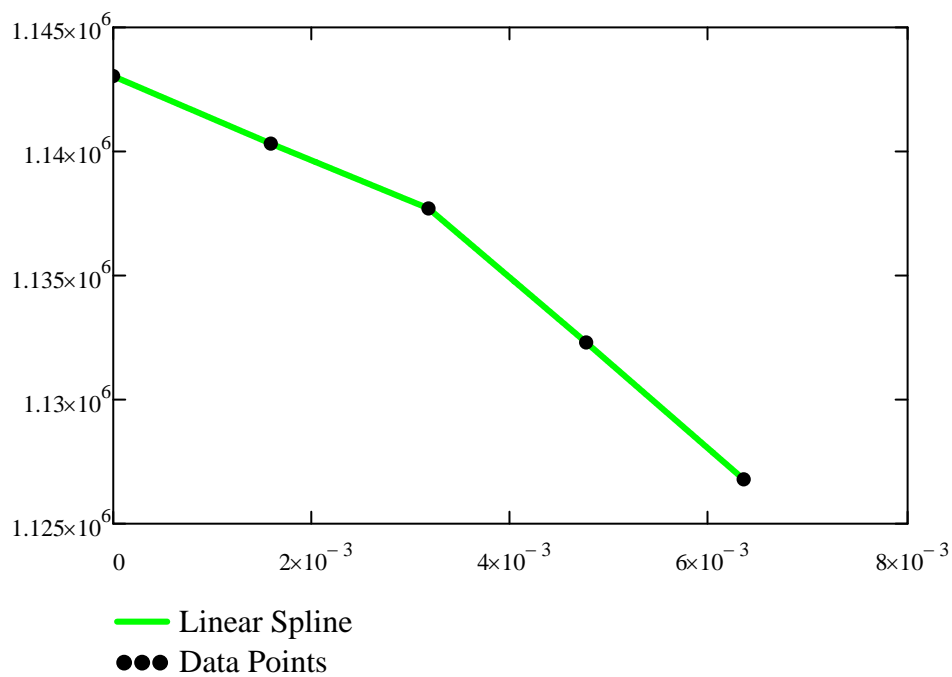
range :=  $X_0, X_0 + 0.01\text{mm}.. X_{\text{rows}(X)-1}$

**$\sigma_{xx}$ : Linear Spline Interpolation**

$$f_{\text{linear}}(x) := \text{linterp}(X, \sigma_{xx}, x)$$

$$F_{\text{axial.xx}} := \int_a^b f_{\text{linear}}(x) dx$$

$$F_{\text{axial.xx}} = 0.007 \cdot \frac{\text{kN}}{\text{mm}} \text{ Axial force per unit length}$$



**Figure AI.1:** Linear Spline Interpolation

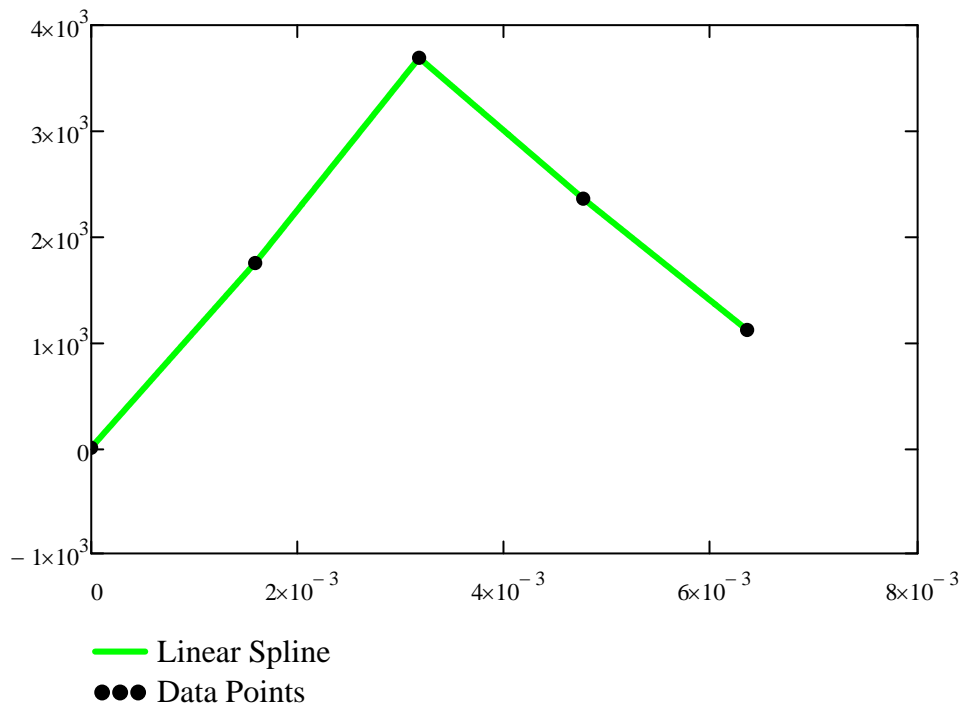
**$\tau_{xy}$ : Linear Spline Interpolation**

$$\text{range} := X_0, X_0 + 0.01\text{mm} .. X_{\text{rows}(X)-1}$$

$$g_{\text{linear}}(t) := \text{linterp}(X, \tau_{xy}, t)$$

$$F_{\text{shear.xy}} := \int_a^b g_{\text{linear}}(t) dt$$

$$F_{\text{shear.xy}} = 0 \cdot \frac{\text{kN}}{\text{mm}} \quad \textit{Shear force per unit length}$$



**Figure AI.2:** *Linear Spline Interpolation*

### *Dong stress determination*

$$F_{\text{bending.xx}} := \int_a^b f_{\text{linear}(x)} \cdot x \, dx$$

$$F_{\text{bending.xx}} = 0.023 \cdot \text{kN}$$

$$\sigma_m := \frac{1}{t_y} \cdot F_{\text{axial.xx}} = 1.136 \cdot \text{MPa} \quad \text{The resultant value of Equation 3.22}$$

Guess  $\sigma_{bx} := 20 \text{MPa}$

Given

$$\sigma_m \cdot \frac{t_y^2}{2} + \sigma_{bx} \cdot \frac{t_y^2}{6} = F_{\text{bending.xx}} - \text{delta} \cdot F_{\text{shear.xy}}$$

$$\sigma_b := \text{Find}(\sigma_{bx}) = -0.031 \cdot \text{MPa} \quad \text{The resultant value of the bending stress defined in Equation 3.23}$$

$$\sigma_s := \sigma_m + \sigma_b = 1.106 \cdot \text{MPa} \quad \text{The calculated Dong stress according to Equations 3.22 and 3.23}$$

The above calculated Dong stress disregards the vertical and shear stress distribution along a path at mid-plate section. However, as mentioned before, in this case the stress raised to the aforementioned stress components should be also considered.

***Dong stress determination for non-monotonic stress distribution***

$$q_{\text{linear}}(w) := \text{linterp}(x_b, \tau_{yx}, w)$$

$$F_{\text{shear.yx}} := \int_0^{\text{delta}} q_{\text{linear}}(w) dw$$

$$F_{\text{shear.yx}} = -0 \cdot \frac{\text{kN}}{\text{mm}}$$

$$\sigma_{m2} := \sigma_m - \frac{1}{t_y} \cdot F_{\text{shear.yx}} = 1.136 \cdot \text{MPa}$$

*The new membrane stress after considering the non-monotonic stress distribution according to Equation 3.24*

$$Y_{\text{linear}}(u) := \text{linterp}(x_b, \sigma_{yy}, u)$$

$$F_{\text{moment.yy}} := \int_0^{\text{delta}} Y_{\text{linear}}(u) \cdot u du$$

$$F_{\text{moment.yy}} = 3.141 \times 10^{-3} \cdot \text{kN}$$

Given  $\sigma_{bx2} := 30 \text{MPa}$

$$\sigma_{m2} \cdot \frac{t_y^2}{2} + \sigma_{bx2} \cdot \frac{t_y^2}{6} = F_{\text{bending.xx}} - \text{delta} \cdot F_{\text{shear.xy}} + F_{\text{moment.yy}}$$

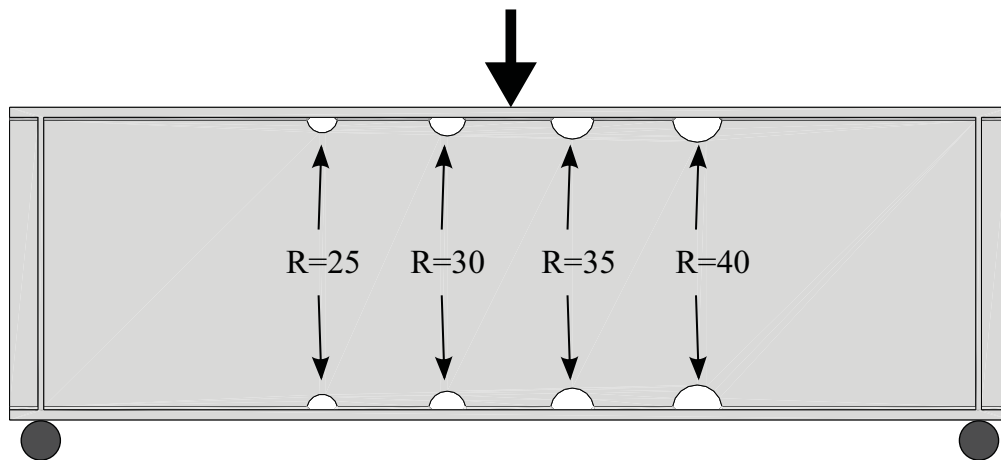
$$\sigma_{b2} := \text{Find}(\sigma_{bx2}) = 0.437 \cdot \text{MPa}$$

$$\sigma_{s2} := \sigma_{b2} + \sigma_{m2} = 1.573 \cdot \text{MPa}$$

*The calculated Dong stress according to Equations 3.24 and 3.25*

As can be seen, the new calculated Dong stress is significantly larger than the former calculated one.

## Appendix II: The modified nominal stress calculation for cope-hole details



**Figure AII-1:** *The investigated cope-hole detail*

In this Appendix, the modified nominal stress for a cope-hole detail subjected to a high shear to normal stress ratio is calculated. The cope-hole has a radius of 40mm and is depicted in the Figure AII-1.

The Input data are given below:

### Steel Girder at cope-hole location

|               |                           |                         |  |
|---------------|---------------------------|-------------------------|--|
| Top flange    | $b_{tf} := 250\text{mm}$  | $t_{tf} := 16\text{mm}$ |  |
| Web           | $h_w := 468\text{mm}$     | $t_w := 9\text{mm}$     |  |
| Bottom flange | $b_{bf} := 250\text{mm}$  | $t_{bf} := 16\text{mm}$ |  |
|               | $E_{st} := 210\text{GPa}$ | $\nu_{st} := 0.3$       | $G_{st} := \frac{E_{st}}{2(1 + \nu_{st})} = 80.769\cdot\text{GPa}$ |

### Cope Hole

|   |               |                            |                          |
|---|---------------|----------------------------|--------------------------|
| $R_{cp} := 40\text{mm}$                         | $n_{cp} := 2$ | $x_{cp} := 450\text{mm}$   | $L_b := 1500\text{mm}$   |
| $x_{load} := \frac{L_b}{2} = 750\cdot\text{mm}$ |               | $\sigma_N := 28\text{MPa}$ | $R_{ref} := 25\text{mm}$ |

### Calculation of neutral axis

From the top

$$y_n := \frac{b_{tf} \cdot t_{tf} \cdot \frac{t_{tf}}{2} + (h_w - 2 \cdot R_{cp}) \cdot t_w \cdot \left( t_{tf} + \frac{h_w}{2} \right) + b_{bf} \cdot t_{bf} \cdot \left( t_{tf} + h_w + \frac{t_{bf}}{2} \right)}{b_{tf} \cdot t_{tf} + (h_w - 2 \cdot R_{cp}) \cdot t_w + t_{bf} \cdot b_{bf}} = 250 \cdot \text{mm}$$

### Calculation of moment of inertia

$$\begin{aligned} I_{xx} &:= \frac{1}{12} \cdot b_{tf} \cdot t_{tf}^3 + b_{tf} \cdot t_{tf} \cdot \left( y_n - \frac{t_{tf}}{2} \right)^2 \dots \\ &+ \frac{1}{12} \cdot t_w \cdot (h_w - 2 \cdot R_{cp})^3 + t_w \cdot (h_w - 2 \cdot R_{cp}) \cdot \left[ y_n - \left( t_{tf} + \frac{h_w}{2} \right) \right]^2 \dots \\ &+ \frac{1}{12} \cdot t_{bf}^3 \cdot b_{bf} + t_{bf} \cdot b_{bf} \cdot \left[ y_n - \left( t_{tf} + h_w + \frac{t_{bf}}{2} \right) \right]^2 \\ I_{xx} &= 512.49097 \times 10^6 \cdot \text{mm}^4 \end{aligned}$$

### Calculation of Load

$$F_{\text{load}} := \frac{\sigma_N \cdot I_{xx} \cdot 2}{x_{cp} \cdot (h_w + t_{tf} - y_n)} = 272.55 \cdot \text{kN}$$

### Shear correction factor for an I section

$$y_{na.frtop} := \frac{t_{tf} \cdot b_{tf} \cdot \frac{t_{tf}}{2} + t_w \cdot h_w \cdot \left( t_{tf} + \frac{h_w}{2} \right) + t_{bf} \cdot b_{bf} \cdot \left( t_{tf} + h_w + \frac{t_{bf}}{2} \right)}{t_{tf} \cdot b_{tf} + t_w \cdot h_w + t_{bf} \cdot b_{bf}} = 250 \cdot \text{mm}$$

$$h_{\text{section}} := t_{bf} + h_w + t_{tf} = 500 \cdot \text{mm}$$

$$y_{na} := h_{\text{section}} - y_{na.frtop} = 250 \cdot \text{mm}$$

$$\begin{aligned} I_{\text{section}} &:= \frac{1}{12} \cdot b_{bf} \cdot t_{bf}^3 + b_{bf} \cdot t_{bf} \cdot \left( y_{na} - \frac{t_{bf}}{2} \right)^2 \dots = 5.456 \times 10^8 \cdot \text{mm}^4 \\ &+ \frac{1}{12} \cdot t_w \cdot h_w^3 + t_w \cdot h_w \cdot \left( y_{na} - t_{bf} - \frac{h_w}{2} \right)^2 \dots \\ &+ \frac{1}{12} \cdot b_{tf} \cdot t_{tf}^3 + b_{tf} \cdot t_{tf} \cdot \left( y_{na.frtop} - \frac{t_{tf}}{2} \right)^2 \end{aligned}$$

Shear area correction factor (1/A.s):

$$\begin{aligned}
 en_{Ih} := & \int_0^{t_{bf}} \left[ \frac{z \cdot \left( y_{na} - \frac{z}{2} \right)}{I_{section}} \right]^2 \cdot b_{bf} dz \dots \\
 & + \int_0^{y_{na} - t_{bf}} \left[ \frac{z \cdot t_w \cdot \left( y_{na} - t_{bf} - \frac{z}{2} \right) + (t_{bf} \cdot b_{bf}) \cdot \left( y_{na} - \frac{t_{bf}}{2} \right)}{I_{section} \cdot t_w} \right]^2 \cdot t_w dz \dots \\
 & + \int_0^{y_{na.frtop} - t_{tf}} \left[ \frac{z \cdot t_w \cdot \left( y_{na.frtop} - t_{tf} - \frac{z}{2} \right) + t_{tf} \cdot b_{tf} \cdot \left( y_{na.frtop} - \frac{t_{tf}}{2} \right)}{I_{section} \cdot t_w} \right]^2 \cdot t_w dz \dots \\
 & + \int_0^{t_{tf}} \left[ \frac{z \cdot \left( y_{na.frtop} - \frac{z}{2} \right)}{I_{section}} \right]^2 \cdot t_{tf} dz
 \end{aligned}$$

$$A_{section} := t_{bf} \cdot b_{bf} + t_{tf} \cdot b_{tf} + t_w \cdot h_w = 1.221 \times 10^4 \cdot \text{mm}^2$$

$$A_s := \frac{1}{en_{Ih}} = 4.444 \times 10^3 \cdot \text{mm}^2$$

$$A_{web} := t_w \cdot (t_{tf} + h_w + t_{bf}) = 4.5 \times 10^3 \cdot \text{mm}^2 \quad \kappa_{st} := \frac{A_s}{A_{section}} = 0.364$$

$$V_{support} := \frac{F_{load}}{2} = 136.275 \cdot \text{kN} \quad V_{cp.s} := \frac{F_{load}}{2} = 136.275 \cdot \text{kN}$$

$$Q := b_{bf} \cdot t_{bf} \cdot \left( y_{na} - \frac{t_{bf}}{2} \right) = 9.68 \times 10^5 \cdot \text{mm}^3$$

$$\tau_s := \frac{V_{cp.s} \cdot Q}{I_{section} \cdot t_w} = 26.866 \cdot \text{MPa}$$

### Shear to Normal stress ratio

$$\frac{\tau_s}{\sigma_N} = 0.9595$$

$$x_{\text{left}} := x_{\text{cp}} - R_{\text{cp}} = 410 \cdot \text{mm}$$

$$V_{\text{left}} := \frac{F_{\text{load}}}{2} = 136.275 \cdot \text{kN}$$

$$M_{\text{effective.left}} := \frac{(V_{\text{support}} + V_{\text{left}}) \cdot x_{\text{left}}}{2} = 55.873 \cdot \text{kN} \cdot \text{m}$$

$$\omega_{\text{st.left}} := \frac{M_{\text{effective.left}}}{G_{\text{st}} \cdot A_{\text{s}}} = 0.156 \cdot \text{mm}$$

$$x_{\text{right}} := x_{\text{cp}} + R_{\text{cp}} = 490 \cdot \text{mm}$$

$$V_{\text{right}} := \frac{F_{\text{load}}}{2} = 136.275 \cdot \text{kN}$$

$$M_{\text{effective.right}} := \frac{(V_{\text{support}} + V_{\text{right}}) \cdot x_{\text{right}}}{2} = 66.775 \cdot \text{kN} \cdot \text{m}$$

$$\omega_{\text{st.right}} := \frac{M_{\text{effective.right}}}{G_{\text{st}} \cdot A_{\text{s}}} = 0.186 \cdot \text{mm}$$

### Relative shear deformation of cope-hole weld toes

$$\delta_{\text{st.shear}} := \omega_{\text{st.right}} - \omega_{\text{st.left}} = 0.03 \cdot \text{mm}$$

$$I_{\text{bf}} := \frac{1}{12} \cdot (t_{\text{w}} + 15 \text{mm}) \cdot t_{\text{bf}}^3 = 8.192 \times 10^3 \cdot \text{mm}^4$$

$$M_{\text{reaction}} := \frac{6 \cdot E_{\text{st}} \cdot I_{\text{bf}} \cdot \delta_{\text{st.shear}}}{(2 \cdot R_{\text{cp}})^2} \cdot \frac{\tau_{\text{s}}}{\sigma_{\text{N}}} \cdot \frac{R_{\text{cp}}}{R_{\text{ref}}} = 0.075 \cdot \text{kN} \cdot \text{m}$$

$$\sigma_{\text{add.new}} := \frac{M_{\text{reaction}} \cdot \frac{t_{\text{bf}}}{2}}{I_{\text{bf}}} = 73.433 \cdot \text{MPa}$$

### New modified nominal stress:

---


$$\sigma_{\text{modified}} := \sigma_{\text{N}} + \sigma_{\text{add.new}} = 101.433 \cdot \text{MPa}$$


---



## Appendix III: The modified nominal stress calculation for an existing composite bridge

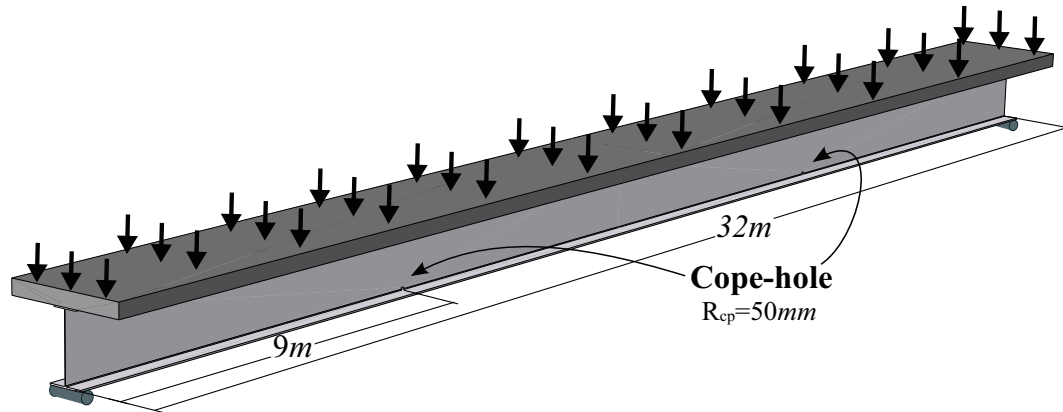


Figure AIII-1: *Composit steel-concrete bridge with cope-holes*

### Input data

#### Effective Concrete Deck at cope-hole location

$$b_{cn} := 2.45\text{m} \quad t_{cn} := 300\text{mm} \quad E_{cn} := 30\text{GPa}$$

$$\nu_{cn} := 0.2$$

$$G_{cn} := \frac{E_{cn}}{2(1 + \nu_{cn})} = 12.5 \cdot \text{GPa}$$

#### Steel Girder at cope-hole location

$$\text{Top flange} \quad b_{tf} := 500\text{mm} \quad t_{tf} := 25\text{mm}$$

$$\text{Web} \quad h_w := 1343\text{mm} \quad t_w := 13\text{mm}$$

$$\text{Bottom flange} \quad b_{bf} := 700\text{mm} \quad t_{bf} := 32\text{mm}$$

$$E_{st} := 210\text{GPa} \quad \nu_{st} := 0.3$$

#### Cope Hole

$$R_{cp} := 50\text{mm} \quad n_{cp} := 1 \quad G_{st} := \frac{E_{st}}{2(1 + \nu_{st})} = 80.769 \cdot \text{GPa}$$

$$V_{cp} := 100\text{kN} \quad M_{cp} := 120\text{kN}\cdot\text{m} \quad L_0 := 25\text{mm}$$

## Solution

$$E_{\text{ref}} := E_{\text{st}} = 210 \cdot \text{GPa} \quad n := \frac{E_{\text{cn}}}{E_{\text{st}}} = 0.143$$

$$b_{\text{tr.cn}} := n \cdot b_{\text{cn}} = 350 \cdot \text{mm}$$

### a) Bending stress

Section with cope-hole:

$$y_n := \begin{cases} \frac{b_{\text{tr.cn}} \cdot t_{\text{cn}} \cdot \frac{t_{\text{cn}}}{2} + b_{\text{tf}} \cdot t_{\text{tf}} \cdot \left( t_{\text{cn}} + \frac{t_{\text{tf}}}{2} \right) + (h_w - 1 \cdot R_{\text{cp}}) \cdot t_w \cdot \left( t_{\text{cn}} + t_{\text{tf}} + \frac{h_w - R_{\text{cp}}}{2} \right) \dots}{b_{\text{tr.cn}} \cdot t_{\text{cn}} + b_{\text{tf}} \cdot t_{\text{tf}} + (h_w - 1 \cdot R_{\text{cp}}) \cdot t_w + b_{\text{bf}} \cdot t_{\text{bf}}} & \text{if } n_{\text{cp}} = 1 \\ \frac{b_{\text{tr.cn}} \cdot t_{\text{cn}} \cdot \frac{t_{\text{cn}}}{2} + b_{\text{tf}} \cdot t_{\text{tf}} \cdot \left( t_{\text{cn}} + \frac{t_{\text{tf}}}{2} \right) + (h_w - 2 \cdot R_{\text{cp}}) \cdot t_w \cdot \left( t_{\text{cn}} + t_{\text{tf}} + \frac{h_w}{2} \right) \dots}{b_{\text{tr.cn}} \cdot t_{\text{cn}} + b_{\text{tf}} \cdot t_{\text{tf}} + (h_w - 2 \cdot R_{\text{cp}}) \cdot t_w + b_{\text{bf}} \cdot t_{\text{bf}}} & \text{otherwise} \end{cases}$$

$$y_n = 470.348 \cdot \text{mm} \quad \text{From top}$$

$$I_{\text{xx}} := \begin{cases} \frac{1}{12} b_{\text{tr.cn}} \cdot t_{\text{cn}}^3 + b_{\text{tr.cn}} \cdot t_{\text{cn}} \cdot \left( y_n - \frac{t_{\text{cn}}}{2} \right)^2 \dots & \text{if } n_{\text{cp}} = 1 \\ + \frac{1}{12} b_{\text{tf}} \cdot t_{\text{tf}}^3 + b_{\text{tf}} \cdot t_{\text{tf}} \left[ y_n - \left( t_{\text{cn}} + \frac{t_{\text{tf}}}{2} \right) \right]^2 \dots \\ + \frac{1}{12} t_w (h_w - 1 \cdot R_{\text{cp}})^3 + t_w (h_w - 1 \cdot R_{\text{cp}}) \left[ y_n - \left( t_{\text{cn}} + t_{\text{tf}} + \frac{h_w - R_{\text{cp}}}{2} \right) \right]^2 \dots \\ + \frac{1}{12} t_{\text{bf}}^3 \cdot b_{\text{bf}} + t_{\text{bf}} \cdot b_{\text{bf}} \left[ y_n - \left( t_{\text{cn}} + t_{\text{tf}} + h_w + \frac{t_{\text{bf}}}{2} \right) \right]^2 \\ \frac{1}{12} b_{\text{tr.cn}} \cdot t_{\text{cn}}^3 + b_{\text{tr.cn}} \cdot t_{\text{cn}} \cdot \left( y_n - \frac{t_{\text{cn}}}{2} \right)^2 \dots & \text{otherwise} \\ + \frac{1}{12} b_{\text{tf}} \cdot t_{\text{tf}}^3 + b_{\text{tf}} \cdot t_{\text{tf}} \left[ y_n - \left( t_{\text{cn}} + \frac{t_{\text{tf}}}{2} \right) \right]^2 \dots \\ + \frac{1}{12} t_w (h_w - 2 \cdot R_{\text{cp}})^3 + t_w (h_w - 2 \cdot R_{\text{cp}}) \left[ y_n - \left( t_{\text{cn}} + t_{\text{tf}} + \frac{h_w}{2} \right) \right]^2 \dots \\ + \frac{1}{12} t_{\text{bf}}^3 \cdot b_{\text{bf}} + t_{\text{bf}} \cdot b_{\text{bf}} \left[ y_n - \left( t_{\text{cn}} + t_{\text{tf}} + h_w + \frac{t_{\text{bf}}}{2} \right) \right]^2 \end{cases}$$

$$I_{xx} = 51.4345 \times 10^9 \cdot \text{mm}^4$$

$$q := 9 \frac{\text{kN}}{\text{m}^2}$$

$$x_{cp} := 9000\text{mm} = 9 \text{ m}$$

$$L_b := 32\text{m}$$

$$M_{cp,b} := \frac{q \cdot b_{cn} \cdot x_{cp}}{2} \cdot (L_b - x_{cp}) = 2.282 \cdot \text{MN} \cdot \text{m}$$

$$\sigma_b := \frac{M_{cp,b} \cdot (h_w + t_{tf} + t_{cn} - y_n)}{I_{xx}} = 53.14 \cdot \text{MPa}$$

### Section without cope-hole:

$$y_{nn} := \frac{b_{tr.cn} \cdot t_{cn} \cdot \frac{t_{cn}}{2} + b_{tf} \cdot t_{tf} \cdot \left( t_{cn} + \frac{t_{tf}}{2} \right) + (h_w) \cdot t_w \cdot \left( t_{cn} + t_{tf} + \frac{h_w}{2} \right) \dots + b_{bf} \cdot t_{bf} \cdot \left( t_{cn} + t_{tf} + h_w + \frac{t_{bf}}{2} \right)}{b_{tr.cn} \cdot t_{cn} + b_{tf} \cdot t_{tf} + (h_w) \cdot t_w + b_{bf} \cdot t_{bf}}$$

$$y_{nn} = 475.192 \cdot \text{mm}$$

$$I_{xx,n} := \frac{1}{12} b_{tr.cn} \cdot t_{cn}^3 + b_{tr.cn} \cdot t_{cn} \cdot \left( y_{nn} - \frac{t_{cn}}{2} \right)^2 \dots + \frac{1}{12} b_{tf} \cdot t_{tf}^3 + b_{tf} \cdot t_{tf} \cdot \left[ y_{nn} - \left( t_{cn} + \frac{t_{tf}}{2} \right) \right]^2 \dots + \frac{1}{12} t_w \cdot (h_w)^3 + t_w \cdot (h_w) \cdot \left[ y_{nn} - \left( t_{cn} + t_{tf} + \frac{h_w}{2} \right) \right]^2 \dots + \frac{1}{12} t_{bf}^3 \cdot b_{bf} + t_{bf} \cdot b_{bf} \cdot \left[ y_{nn} - \left( t_{cn} + t_{tf} + h_w + \frac{t_{bf}}{2} \right) \right]^2$$

$$I_{xx,n} = 52.32476 \times 10^9 \cdot \text{mm}^4$$

$$M_{cp,design} := 2.550 \text{MN} \cdot \text{m}$$

$$\sigma_{b,design} := \frac{M_{cp,design} \cdot (t_{bf} + h_w + t_{tf} + t_{cn} - y_n)}{I_{xx,n}} = 59.926 \cdot \text{MPa}$$

## b) Shear stress

$$V_{cp.s} := q \cdot b_{cn} \cdot \left( \frac{L_b}{2} - x_{cp} \right) = 154.35 \cdot \text{kN}$$

$$Q := b_{bf} \cdot t_{bf} \cdot \left( \frac{t_{bf}}{2} + h_w + t_{tf} + t_{cn} - y_{nn} \right) = 2.708 \times 10^7 \cdot \text{mm}^3$$

$$\tau_s := \frac{V_{cp.s} \cdot Q}{I_{xx.n} \cdot t_w} = 6.144 \cdot \text{MPa} \quad \tau_{s.bf} := \frac{V_{cp.s} \cdot Q}{I_{xx.n} \cdot b_{bf}} = 0.114 \cdot \text{MPa}$$

$$\frac{\tau_s}{\sigma_b} = 0.116$$

$$Q_{\max} := t_w \cdot \left[ y_{nn} - (t_{cn} + t_{tf}) \right] \cdot \left[ y_{nn} - \left[ \frac{y_{nn} - (t_{cn} + t_{tf})}{2} \right] \right] \dots = 3.696 \times 10^7 \cdot \text{mm}^3$$

$$+ t_{tf} \cdot b_{tf} \cdot \left[ y_{nn} - \left( t_{cn} + \frac{t_{tf}}{2} \right) \right] \dots$$

$$+ b_{tr.cn} \cdot t_{cn} \cdot \left( y_{nn} - \frac{t_{cn}}{2} \right)$$

$$\tau_{h_{\text{section}}} := t_{bf} + h_w + t_{tf} = 1.4 \times 10^3 \cdot \text{mm}$$

$$V_{\text{support}} := q \cdot b_{cn} \cdot \frac{L_b}{2} = 352.8 \cdot \text{kN}$$

$$x_{\text{left}} := x_{cp} - R_{cp} = 8.95 \text{ m}$$

$$V_{\text{left}} := q \cdot b_{cn} \cdot \left( \frac{L_b}{2} - x_{\text{left}} \right) = 155.453 \cdot \text{kN}$$

$$M_{\text{effective.left}} := V_{\text{support}} \cdot x_{\text{left}} = 3.158 \times 10^3 \cdot \text{kN} \cdot \text{m}$$

$$x_{\text{right}} := x_{cp} + R_{cp} = 9.05 \text{ m}$$

$$V_{\text{right}} := q \cdot b_{cn} \cdot \left( \frac{L_b}{2} - x_{\text{right}} \right) = 153.247 \cdot \text{kN}$$

$$M_{\text{effective.right}} := V_{\text{support}} \cdot x_{\text{right}} = 3.193 \times 10^3 \cdot \text{kN} \cdot \text{m}$$

$$I_{bf} := \frac{1}{12} \cdot (2 \cdot t_w) \cdot t_{bf}^3 = 7.1 \times 10^4 \cdot \text{mm}^4$$

$$A_{\text{section}} := t_{bf} \cdot b_{bf} + t_{tf} \cdot b_{tf} + t_w \cdot h_w = 5.236 \times 10^4 \cdot \text{mm}^2$$

## Bending deflections

$$\delta_{\text{bending.left}} := \frac{q \cdot b_{\text{cn}} \cdot (x_{\text{cp}} - R_{\text{cp}})}{24 \cdot E_{\text{st}} \cdot I_{\text{xx.n}}} \cdot \left[ L_{\text{b}}^3 - 2 \cdot L_{\text{b}} \cdot (x_{\text{cp}} - R_{\text{cp}})^2 + (x_{\text{cp}} - R_{\text{cp}})^3 \right] = 21.221 \cdot \text{mm}$$

$$\delta_{\text{bending.right}} := \frac{q \cdot b_{\text{cn}} \cdot (x_{\text{cp}} + R_{\text{cp}})}{24 \cdot E_{\text{st}} \cdot I_{\text{xx.n}}} \cdot \left[ L_{\text{b}}^3 - 2 \cdot L_{\text{b}} \cdot (x_{\text{cp}} + R_{\text{cp}})^2 + (x_{\text{cp}} + R_{\text{cp}})^3 \right] = 21.39 \cdot \text{mm}$$

$$\delta_{\text{bending.diff}} := \delta_{\text{bending.right}} - \delta_{\text{bending.left}} = 0.168 \cdot \text{mm}$$

## Shear deflections including concrete deck

$$y_{\text{na.cn.top}} := \frac{b_{\text{tr.cn}} \cdot t_{\text{cn}} \cdot \frac{t_{\text{cn}}}{2} + b_{\text{tf}} \cdot t_{\text{tf}} \cdot \left( t_{\text{cn}} + \frac{t_{\text{tf}}}{2} \right) + (h_{\text{w}}) \cdot t_{\text{w}} \cdot \left( t_{\text{cn}} + t_{\text{tf}} + \frac{h_{\text{w}}}{2} \right) \dots}{b_{\text{tr.cn}} \cdot t_{\text{cn}} + b_{\text{tf}} \cdot t_{\text{tf}} + (h_{\text{w}}) \cdot t_{\text{w}} + b_{\text{bf}} \cdot t_{\text{bf}}} \dots$$

$$y_{\text{na.cn.top}} = 475.192 \cdot \text{mm}$$

$$I_{\text{xx.cn}} := \frac{1}{12} b_{\text{tr.cn}} \cdot t_{\text{cn}}^3 + b_{\text{tr.cn}} \cdot t_{\text{cn}} \cdot \left( y_{\text{nn}} - \frac{t_{\text{cn}}}{2} \right)^2 \dots$$

$$+ \frac{1}{12} b_{\text{tf}} \cdot t_{\text{tf}}^3 + b_{\text{tf}} \cdot t_{\text{tf}} \cdot \left[ y_{\text{nn}} - \left( t_{\text{cn}} + \frac{t_{\text{tf}}}{2} \right) \right]^2 \dots$$

$$+ \frac{1}{12} t_{\text{w}} \cdot (h_{\text{w}})^3 + t_{\text{w}} \cdot (h_{\text{w}}) \cdot \left[ y_{\text{nn}} - \left( t_{\text{cn}} + t_{\text{tf}} + \frac{h_{\text{w}}}{2} \right) \right]^2 \dots$$

$$+ \frac{1}{12} t_{\text{bf}}^3 \cdot b_{\text{bf}} + t_{\text{bf}} \cdot b_{\text{bf}} \cdot \left[ y_{\text{n}} - \left( t_{\text{cn}} + t_{\text{tf}} + h_{\text{w}} + \frac{t_{\text{bf}}}{2} \right) \right]^2$$

$$I_{\text{xx.cn}} = 52.5876 \times 10^9 \cdot \text{mm}^4$$

$$y_{\text{na.cn}} := h_{\text{section}} - y_{\text{na.cn.top}} = 924.808 \cdot \text{mm}$$

### Shear correction factor:

$$\begin{aligned}
 en_{lh.cn} := & \int_0^{t_{bf}} \left[ \frac{z \cdot \left( y_{na.cn} - \frac{z}{2} \right)}{I_{xx.cn}} \right]^2 \cdot \frac{b_{bf}}{G_{st}} dz \dots \\
 & + \int_0^{y_{na.cn} - t_{bf}} \left[ \frac{z \cdot t_w \cdot \left( y_{na.cn} - t_{bf} - \frac{z}{2} \right) + (t_{bf} \cdot b_{bf}) \cdot \left( y_{na.cn} - \frac{t_{bf}}{2} \right)}{I_{xx.cn} \cdot t_w} \right]^2 \cdot \frac{t_w}{G_{st}} dz \dots \\
 & + \int_0^{y_{na.cn.top} - t_{tf} - t_{cn}} \left[ \frac{z \cdot t_w \cdot \left( y_{na.cn.top} - t_{tf} - t_{cn} - \frac{z}{2} \right) \dots \right. \\
 & \quad \left. + \left[ t_{tf} \cdot b_{tf} \cdot \left( y_{na.cn.top} - t_{cn} - \frac{t_{tf}}{2} \right) \dots \right. \right. \\
 & \quad \left. \left. + b_{tr.cn} \cdot t_{cn} \cdot \left( y_{na.cn.top} - \frac{t_{cn}}{2} \right) \right]}{I_{xx.cn} \cdot t_w} \right]^2 \cdot \frac{t_w}{G_{st}} dz \dots \\
 & + \int_0^{t_{tf}} \left[ \frac{z \cdot b_{tf} \cdot \left( y_{na.cn.top} - t_{cn} - \frac{z}{2} \right) + b_{tr.cn} \cdot t_{cn} \cdot \left( y_{na.cn.top} - \frac{t_{cn}}{2} \right)}{I_{xx.cn} \cdot b_{tf}} \right]^2 \cdot \frac{t_{tf}}{G_{st}} dz \dots \\
 & + \int_0^{t_{cn}} \left[ \frac{z \cdot b_{tr.cn} \cdot \left( y_{na.cn.top} - \frac{z}{2} \right)}{I_{xx.cn} \cdot b_{cn}} \right]^2 \cdot \frac{b_{tr.cn}}{G_{cn}} dz
 \end{aligned}$$

$$A_{s.cn} := \frac{1}{G_{st} \cdot en_{lh.cn}} = 5.086 \times 10^4 \cdot \text{mm}^2$$

$$A_{\text{section.cn}} := A_{\text{section}} + b_{tr.cn} \cdot t_{cn} = 1.574 \times 10^5 \cdot \text{mm}^2 \quad \kappa_{s.cn} := \frac{A_{s.cn}}{A_{\text{section.cn}}} = 0.323$$

$$\omega_{\text{section.left}} := \frac{M_{\text{effective.left}}}{G_{st} \cdot A_{s.cn}} = 0.769 \cdot \text{mm} \quad \omega_{\text{section.right}} := \frac{M_{\text{effective.right}}}{G_{st} \cdot A_{s.cn}} = 0.777 \cdot \text{mm}$$

### Relative shear deformation by Hand calculations:

$$\delta_{\text{section.shear}} := \omega_{\text{section.right}} - \omega_{\text{section.left}} = 0.009 \cdot \text{mm}$$

## Deflections and stresses from FEM model

$$\delta_{\text{fem.left}} := 23.0795 \text{ mm}$$

$$\delta_{\text{fem.right}} := 23.257 \text{ mm}$$

$$\delta_{\text{fem.diff}} := \delta_{\text{fem.right}} - \delta_{\text{fem.left}} = 0.178 \cdot \text{mm}$$

$$\delta_{\text{shear}} := \delta_{\text{fem.diff}} - \delta_{\text{bending.diff}} = 0.009 \cdot \text{mm}$$

$$F_{\text{reaction.fem}} := \frac{12 \cdot E_{\text{st}} \cdot I_{\text{bf}} \cdot \delta_{\text{shear}}}{(2 \cdot R_{\text{cp}})^3} = 1.641 \cdot \text{kN}$$

$$M_{\text{reaction.fem}} := \frac{6 \cdot E_{\text{st}} \cdot I_{\text{bf}} \cdot \delta_{\text{shear}}}{(2 \cdot R_{\text{cp}})^2} \cdot \frac{\tau_{\text{s}}}{\sigma_{\text{b}}} \cdot \frac{R_{\text{cp}}}{L_0} = 0.019 \cdot \text{kN} \cdot \text{m}$$

$$\sigma_{\text{add.fem}} := \frac{M_{\text{reaction.fem}} \cdot \frac{t_{\text{bf}}}{2}}{I_{\text{bf}}} = 4.276 \cdot \text{MPa}$$

$$\sigma_{\text{nominal}} := \frac{M_{\text{cp.b}} \cdot (h_{\text{w}} + t_{\text{tf}} + t_{\text{cn}} - y_{\text{n}})}{I_{\text{xx}}} = 53.14 \cdot \text{MPa}$$

## Additional stresses from the deflection calculated by FEM

$$\sigma_{\text{modified}} := \sigma_{\text{nominal}} + \sigma_{\text{add.fem}} = 57.416 \cdot \text{MPa}$$

## Additional stresses from theoretical model

$$M_{\text{reaction.theo}} := \frac{6 \cdot E_{\text{st}} \cdot I_{\text{bf}} \cdot \delta_{\text{section.shear}}}{(2 \cdot R_{\text{cp}})^2} \cdot \frac{\tau_{\text{s}}}{\sigma_{\text{b}}} \cdot \frac{R_{\text{cp}}}{L_0} = 0.018 \cdot \text{kN} \cdot \text{m}$$

$$\sigma_{\text{add.theo}} := \frac{M_{\text{reaction.theo}} \cdot \frac{t_{\text{bf}}}{2}}{I_{\text{bf}}} = 4.004 \cdot \text{MPa}$$

$$\sigma_{\text{nominal}} = 53.14 \cdot \text{MPa}$$

$$\sigma_{\text{modified.theo}} := \sigma_{\text{nominal}} + \sigma_{\text{add.theo}} = 57.144 \cdot \text{MPa}$$

## Appendix IV: The modified nominal stress calculation for an existing railway bridge

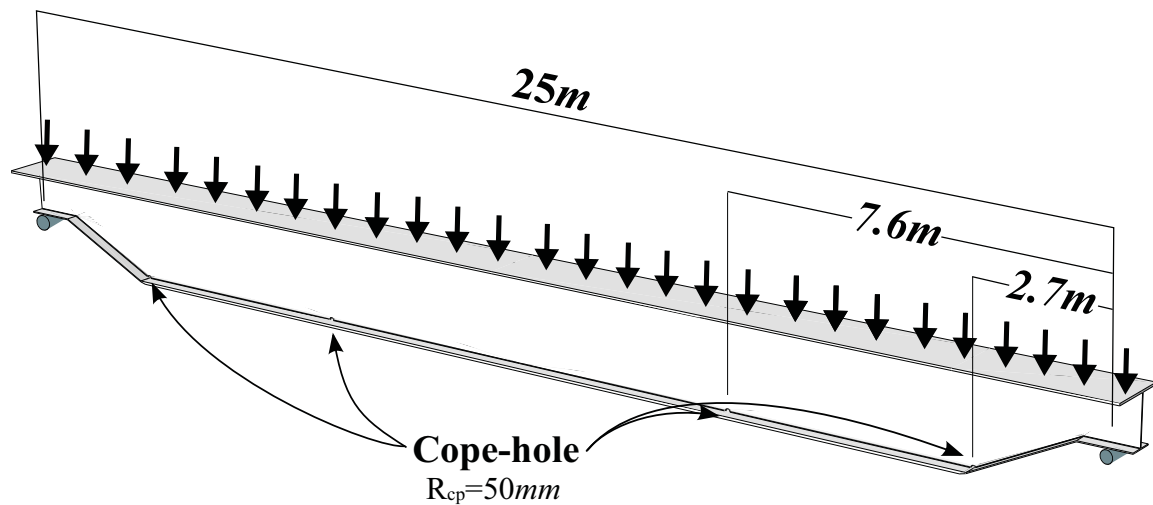


Figure AIV-1: existing railway bridge with cope-holes

### Input data

#### Effective Concrete Deck at cope-hole location

$$b_{cn} := 0m \quad t_{cn} := 0mm \quad E_{cn} := 30GPa \quad \nu_{cn} := 0.2 \quad G_{cn} := \frac{E_{cn}}{2(1 + \nu_{cn})} = 12.5 \cdot GPa$$

#### Steel Girder at cope-hole location

$$\text{Top flange} \quad b_{tf} := 1200mm \quad t_{tf} := 40mm \quad t_{bf.effective} := 50mm$$

$$\text{Web} \quad h_w := 1910mm \quad t_w := 20mm$$

$$\text{Bottom flange} \quad b_{bf} := 500mm \quad t_{bf} := 50mm$$

$$E_{st} := 210GPa \quad \nu_{st} := 0.3 \quad G_{st} := \frac{E_{st}}{2(1 + \nu_{st})} = 80.769 \cdot GPa$$

#### Cope Hole

$$R_{cp} := 50mm \quad n_{cp} := 2 \quad x_{cp} := 7600mm \quad L_b := 24400mm$$

$$q := 80 \frac{kN}{m} \quad R_{ref} := 25mm$$



### Calculation of neutral axis

From the top

$$y_n := \frac{b_{tf} \cdot t_{tf} \cdot \frac{t_{tf}}{2} + (h_w - 2 \cdot R_{cp}) \cdot t_w \cdot \left( t_{tf} + \frac{h_w}{2} \right) + b_{bf} \cdot t_{bf} \cdot \left( t_{tf} + h_w + \frac{t_{bf}}{2} \right)}{b_{tf} \cdot t_{tf} + (h_w - 2 \cdot R_{cp}) \cdot t_w + t_{bf} \cdot b_{bf}} = 790.788 \cdot \text{mm}$$

### Calculation of moment of inertia

$$I_{xx} := \frac{1}{12} \cdot b_{tf} \cdot t_{tf}^3 + b_{tf} \cdot t_{tf} \cdot \left( y_n - \frac{t_{tf}}{2} \right)^2 \dots$$
$$+ \frac{1}{12} \cdot t_w \cdot (h_w - 2 \cdot R_{cp})^3 + t_w \cdot (h_w - 2 \cdot R_{cp}) \cdot \left[ y_n - \left( t_{tf} + \frac{h_w}{2} \right) \right]^2 \dots$$
$$+ \frac{1}{12} \cdot t_{bf}^3 \cdot b_{bf} + t_{bf} \cdot b_{bf} \cdot \left[ y_n - \left( t_{tf} + h_w + \frac{t_{bf}}{2} \right) \right]^2$$

$$I_{xx} = 74.98057 \times 10^9 \cdot \text{mm}^4$$

### Calculation of Load

$$h_{\text{section}} := t_{bf} + h_w + t_{tf} = 2000 \cdot \text{mm}$$

$$y_{cp} := h_{\text{section}} - y_n - t_{bf} = 1159.212 \cdot \text{mm}$$

$$M := q \cdot \frac{L_b}{2} \cdot x_{cp} - q \cdot x_{cp} \cdot \frac{x_{cp}}{2} = 5.107 \times 10^3 \cdot \text{kN} \cdot \text{m}$$

$$\sigma_N := \frac{M \cdot y_{cp}}{I_{xx}} = 78.958 \cdot \text{MPa}$$

### Shear correction factor for an I section

$$y_{na.frtop} := \frac{t_{tf} \cdot b_{tf} \cdot \frac{t_{tf}}{2} + t_w \cdot h_w \cdot \left( t_{tf} + \frac{h_w}{2} \right) + t_{bf} \cdot b_{bf} \cdot \left( t_{tf} + h_w + \frac{t_{bf}}{2} \right)}{t_{tf} \cdot b_{tf} + t_w \cdot h_w + t_{bf} \cdot b_{bf}} = 794.46 \cdot \text{mm}$$

$$y_{na} := h_{\text{section}} - y_{na.frtop} = 1205.54 \cdot \text{mm}$$

$$I_{\text{section}} := \frac{1}{12} \cdot b_{\text{bf}} \cdot t_{\text{bf}}^3 + b_{\text{bf}} \cdot t_{\text{bf}} \cdot \left( y_{\text{na}} - \frac{t_{\text{bf}}}{2} \right)^2 \dots = 7.684 \times 10^{10} \cdot \text{mm}^4$$

$$+ \frac{1}{12} t_{\text{w}} \cdot h_{\text{w}}^3 + t_{\text{w}} \cdot h_{\text{w}} \cdot \left( y_{\text{na}} - t_{\text{bf}} - \frac{h_{\text{w}}}{2} \right)^2 \dots$$

$$+ \left[ \frac{1}{12} b_{\text{tf}} \cdot t_{\text{tf}}^3 + b_{\text{tf}} \cdot t_{\text{tf}} \cdot \left( y_{\text{na.frtop}} - \frac{t_{\text{tf}}}{2} \right)^2 \dots \right]$$

$$+ 7.5 \cdot 7.5 \cdot 900^2 \text{mm}^4$$

$$V_{\text{cp.s}} := q \cdot \left( \frac{L_{\text{b}}}{2} - x_{\text{cp}} \right) = 368 \cdot \text{kN}$$

$$Q := b_{\text{bf}} \cdot t_{\text{bf}} \cdot \left( y_{\text{na}} - \frac{t_{\text{bf}}}{2} \right) = 2.951 \times 10^7 \cdot \text{mm}^3$$

$$\tau_{\text{s}} := \frac{V_{\text{cp.s}} \cdot Q}{I_{\text{section}} \cdot t_{\text{w}}} = 7.067 \cdot \text{MPa} \quad \tau_{\text{s.bf}} := \frac{V_{\text{cp.s}} \cdot Q}{I_{\text{section}} \cdot b_{\text{bf}}} = 0.283 \cdot \text{MPa}$$

## Shear to normal stress ratio

$$\frac{\tau_{\text{s}}}{\sigma_{\text{N}}} = 0.0895$$

## Shear Correction factor

$$e_{\text{Ih}} := \int_0^{t_{\text{bf}}} \left[ \frac{z \cdot \left( y_{\text{na}} - \frac{z}{2} \right)}{I_{\text{section}}} \right]^2 \cdot b_{\text{bf}} \, dz \dots$$

$$+ \int_0^{y_{\text{na}} - t_{\text{bf}}} \left[ \frac{z \cdot t_{\text{w}} \cdot \left( y_{\text{na}} - t_{\text{bf}} - \frac{z}{2} \right) + (t_{\text{bf}} \cdot b_{\text{bf}}) \cdot \left( y_{\text{na}} - \frac{t_{\text{bf}}}{2} \right)}{I_{\text{section}} \cdot t_{\text{w}}} \right]^2 \cdot t_{\text{w}} \, dz \dots$$

$$+ \int_0^{y_{\text{na.frtop}} - t_{\text{tf}}} \left[ \frac{z \cdot t_{\text{w}} \cdot \left( y_{\text{na.frtop}} - t_{\text{tf}} - \frac{z}{2} \right) + t_{\text{tf}} \cdot b_{\text{tf}} \cdot \left( y_{\text{na.frtop}} - \frac{t_{\text{tf}}}{2} \right)}{I_{\text{section}} \cdot t_{\text{w}}} \right]^2 \cdot t_{\text{w}} \, dz \dots$$

$$+ \int_0^{t_{\text{tf}}} \left[ \frac{z \cdot \left( y_{\text{na.frtop}} - \frac{z}{2} \right)}{I_{\text{section}}} \right]^2 \cdot t_{\text{tf}} \, dz$$

$$A_{\text{section}} := t_{\text{bf}} \cdot b_{\text{bf}} + t_{\text{tf}} \cdot b_{\text{tf}} + t_{\text{w}} \cdot h_{\text{w}} = 1.112 \times 10^5 \cdot \text{mm}^2$$

$$A_{\text{s}} := \frac{1}{e_{\text{nlh}}} = 3.946 \times 10^4 \cdot \text{mm}^2$$

$$A_{\text{web}} := t_{\text{w}} \cdot (t_{\text{tf}} + h_{\text{w}} + t_{\text{bf}}) = 4 \times 10^4 \cdot \text{mm}^2 \quad \kappa_{\text{st}} := \frac{A_{\text{s}}}{A_{\text{section}}} = 0.355$$

$$V_{\text{support}} := \frac{q \cdot L_{\text{b}}}{2} = 976 \cdot \text{kN}$$

$$x_{\text{left}} := x_{\text{cp}} - R_{\text{cp}} = 7.55 \times 10^3 \cdot \text{mm}$$

$$V_{\text{left}} := V_{\text{support}} - q \cdot x_{\text{left}} = 372 \cdot \text{kN}$$

$$M_{\text{effective.left.new}} := V_{\text{support}} \cdot x_{\text{left}} = 7.369 \times 10^3 \cdot \text{kN} \cdot \text{m}$$

$$\omega_{\text{st.left.new}} := \frac{M_{\text{effective.left.new}}}{G_{\text{st}} \cdot A_{\text{s}}} = 2.312 \cdot \text{mm}$$

$$x_{\text{right}} := x_{\text{cp}} + R_{\text{cp}} = 7.65 \times 10^3 \cdot \text{mm}$$

$$V_{\text{right}} := V_{\text{support}} - q \cdot x_{\text{right}} = 364 \cdot \text{kN}$$

$$M_{\text{effective.right.new}} := V_{\text{support}} \cdot x_{\text{right}} = 7.466 \times 10^3 \cdot \text{kN} \cdot \text{m}$$

$$\omega_{\text{st.right.new}} := \frac{M_{\text{effective.right.new}}}{G_{\text{st}} \cdot A_{\text{s}}} = 2.343 \cdot \text{mm}$$

## Relative shear deflection by hand calculations

$$\delta_{\text{st.shear.new}} := \omega_{\text{st.right.new}} - \omega_{\text{st.left.new}} = 0.031 \cdot \text{mm}$$

## Additional stress calculation

$$I_{bf} := \frac{1}{12} \cdot (t_w + 15\text{mm}) \cdot t_{bf.effective}^3 = 3.646 \times 10^5 \cdot \text{mm}^4$$

$$F_{reaction} := \frac{12 \cdot E_{st} \cdot I_{bf} \cdot \delta_{st.shear.new}}{(2 \cdot R_{cp})^3} = 28.137 \cdot \text{kN}$$

$$M_{reaction.new} := \frac{6 \cdot E_{st} \cdot I_{bf} \cdot \delta_{st.shear.new}}{(2 \cdot R_{cp})^2} \cdot \frac{\tau_s}{\sigma_N} \cdot \frac{R_{cp}}{R_{ref}} = 0.252 \cdot \text{kN} \cdot \text{m}$$

$$\sigma_{add.new.new} := \frac{M_{reaction.new} \cdot \frac{t_{bf.effective}}{2}}{I_{bf}} = 17.27 \cdot \text{MPa}$$

## Modified nominal stress

$$\sigma_N = 78.958 \cdot \text{MPa}$$

$$\sigma_{modified.new} := \sigma_N + \sigma_{add.new.new} = 96.228 \cdot \text{MPa}$$

## FEM Evaluation

$$\delta_{\text{fem.right}} := -1 \cdot \begin{pmatrix} -22.2927 \\ -22.2911 \\ -22.2896 \\ -22.2883 \\ -22.2871 \\ -22.2859 \end{pmatrix} \text{mm} \quad \delta_{\text{fem.left}} := -1 \cdot \begin{pmatrix} -22.0954 \\ -22.0939 \\ -22.0927 \\ -22.0915 \\ -22.0904 \\ -22.0893 \end{pmatrix} \text{mm}$$

$$\delta_{\text{fem}} := \delta_{\text{fem.right}} - \delta_{\text{fem.left}} = \begin{pmatrix} 0.1973 \\ 0.1972 \\ 0.1969 \\ 0.1968 \\ 0.1967 \\ 0.1966 \end{pmatrix} \cdot \text{mm}$$

$$\delta_{\text{bending.left}} := \frac{q \cdot (x_{\text{left}})}{24 \cdot E_{\text{st}} \cdot I_{\text{section}}} \cdot \left[ L_{\text{b}}^3 - 2 \cdot L_{\text{b}} \cdot (x_{\text{left}})^2 + (x_{\text{left}})^3 \right] = 18.989 \cdot \text{mm}$$

$$\delta_{\text{bending.right}} := \frac{q \cdot (x_{\text{right}})}{24 \cdot E_{\text{st}} \cdot I_{\text{section}}} \cdot \left[ L_{\text{b}}^3 - 2 \cdot L_{\text{b}} \cdot (x_{\text{right}})^2 + (x_{\text{right}})^3 \right] = 19.151 \cdot \text{mm}$$

$$\delta_{\text{shear.fem}} := \delta_{\text{fem}_3} - (\delta_{\text{bending.right}} - \delta_{\text{bending.left}}) = 0.035 \cdot \text{mm}$$

## Relative shear deflection by FEM

$$\sigma_{\text{add.fem}} := \frac{\frac{6 \cdot E_{\text{st}} \cdot I_{\text{bf}} \cdot \delta_{\text{shear.fem}}}{(2 \cdot R_{\text{cp}})^2} \cdot \frac{\tau_{\text{s}}}{\sigma_{\text{N}}} \cdot \frac{R_{\text{cp}}}{R_{\text{ref}}} \cdot \frac{t_{\text{bf.effective}}}{2}}{I_{\text{bf}}} = 19.805 \text{ MPa}$$

## New modified stress by deflection from FEM

$$\sigma_{\text{N}} = 78.958 \cdot \text{MPa}$$

$$\sigma_{\text{modified.fem}} := \sigma_{\text{N}} + \sigma_{\text{add.fem}} = 98.763 \cdot \text{MPa}$$

## Appendix V: Constant amplitude fatigue test data

**Table 9.2:** *AS-welded cope-hole specimens test results*

| Specimen ID | $R$ | $\Delta\sigma_{Nom}$<br>[MPa] | $N_{tot}$ | Crack location     |
|-------------|-----|-------------------------------|-----------|--------------------|
| ASW-S1      | 0.1 | 105.5                         | 1,415,031 | Cope-Hole weld toe |
| ASW-S2      | 0.1 | 153.5                         | 429,753   | Cope-Hole weld toe |
| ASW-S3      | 0.1 | 105.5                         | 1,593,031 | Cope-Hole weld toe |
| ASW-S4      | 0.1 | 153.5                         | 506,688   | Cope-Hole weld toe |

**Table 9.3:** *UIT-treated cope-hole specimens test results*

| Specimen ID | $R$ | $\Delta\sigma_{Nom}$<br>[MPa] | $N_{tot}$ | Crack location      |
|-------------|-----|-------------------------------|-----------|---------------------|
| UIT-S5      | 0.1 | 153.5                         | 3,621,769 | Cope-Hole weld root |
| UIT-S6      | 0.1 | 153.5                         | 2,131,468 | Cope-Hole weld root |
| UIT-S7      | 0.1 | 124.8                         | 3,563,853 | Cope-Hole weld root |
| UIT-S8      | 0.1 | 124.8                         | 4,957,781 | Cope-Hole weld root |

**Table 9.4:** *BG-treated cope-hole specimens test results*

| Specimen ID | $R$ | $\Delta\sigma_{Nom}$<br>[MPa] | $N_{tot}$  | Crack location           |
|-------------|-----|-------------------------------|------------|--------------------------|
| BG-S9       | 0.1 | 105.5                         | 10,876,310 | Cope-Hole weld root      |
| BG-S10      | 0.1 | 153.5                         | 2,939,228  | Cope-Hole weld root      |
| BG-S11      | 0.1 | 153.5                         | 746,546    | Cope-Hole treated groove |
| BG-S12      | 0.1 | 124.8                         | 7,746,010  | Cope-Hole weld root      |

# Paper A

## **A comparative study on different fatigue failure assessments of welded bridge details**

M.Aygül, M.Bokesjö, M.Heshmati and M.Al-Emrani

*Submitted for publication to International Journal of Fatigue,  
February 2012*





# A comparative study on different fatigue failure assessments of welded bridge details

Mustafa Aygül, Mathias Bokesjö, Mohsen Heshmati and Mohammad Al-Emrani  
Chalmers University of Technology, Gothenburg, Sweden

## Abstract

Five different welded joints frequently used in steel bridges have been selected to investigate the accuracy and applicability of three fatigue assessment methods. The first and basic method, also categorized the global method, is the nominal stress method while the more advanced methods are the hot spot and the effective notch stress method. Solid element based finite element models for the welded bridge details were created by following the modelling requirements of each fatigue assessment method. A statistical evaluation based on the results from the finite element analyses and the fatigue test data collected from the literature was performed to determine the mean and characteristic fatigue strength. In addition, the standard deviation for each data series was also determined to conclude how well each method describes the fatigue strength of each welded detail. A method with a lower standard deviation is considered as a more accurate one. Also the evaluated results from each method were compared with the recommended fatigue strength values in Eurocode 3 and IIW codes. In the light of the test results in this study it appears that the standards are in reasonable agreement with the test data even though a few examples of the opposite occurred. The conclusion based on the revised results in this article indicates that the nominal stress method yields sufficient results despite its simplicity. When considering the effort of creating FE models for numerical analysis it seems clear that the choice of the nominal method is fairly acceptable.

**Keywords:** fatigue assessment methods, plate edge details, overlapped joints, longitudinal attachments, cope-hole details, cover plate details, nominal stress, hot spot stress, notch stress

## 1 Introduction

It ought to be obvious that steel bridges should be designed in such a way that they provide sufficient static capacity corresponding to, for example, an evenly distributed load over the entire bridge surface. However, as the loads consist of traffic loads from cars, lorries and trains, which cause fluctuating loading, the governing design state will in most cases be the fatigue limit state, FLS. When a train with a number of coaches passes over the bridge, the fluctuating stress in different details will arise due to the traffic loads. It will become evident that during the service life of the bridge, the total number of load cycles will exceed several millions. As a result the fatigue problems for critical details should be controlled by using a correct fatigue life estimation procedure. Over the years, a substantial number of tests have been performed in order to categorize fatigue loaded details and thus determine their fatigue strength. A wide range of different plate thicknesses, throat sizes, fillet welds, butt welds, angles, widths and lengths and combinations of these have been used in these fatigue tests. This large amount of information has been processed and is introduced in most design standards and recommendations.

The most renowned and widely used method for assessing fatigue of welded structures is the nominal stress method [1-3]. In fatigue design codes such as Eurocode 3 [4] or IIW [5] a large

number of structural details with corresponding to fatigue strength curves are given. However, the welded details in steel bridge structures are in many cases far more complicated than the basic and common details presented in design codes. It can be difficult sometimes to identify a suitable detail or using a simplified detail can lead to inaccurate fatigue life estimations. To overcome this problem a local stress determination method using the finite element method, which takes into account the stress-raising effects due to the geometrical changes and complex loading conditions, might provide an accurate estimation of the load effects in fatigue critical details.

The aim of this article is to investigate the accuracy and gainfulness for choosing a more advanced method when assessing the fatigue strength of commonly used welded details in steel and composite bridges. These methods are the nominal stress, the hot spot stress and the effect notch stress method. The fatigue experiment data of the five frequently used welded details in steel and composite bridge structures has been collected from the literature to confirm the performance of these three most frequently used fatigue assessment methods.

The five selected details for this study are presented in the next chapter together with a description of how the evaluation procedure regarding to the fatigue assessment methods has been performed. The results for each individual detail using these methods are then presented and discussed.

## **2 Methodology**

As stated earlier, the first method is the nominal stress method that has been used within the fatigue design of steel structures from early on. This method is included in several design codes and may be regarded as a sort of standard method by which the other two will be compared. The second method is the hot spot stress method at which considers a fictitious stress at a fatigue critical point, the so-called hot spot point, where the stress is considered representative of the component [6, 5, 2]. The hot spot stress is generally extrapolated based on two or three reference points on the surface of the detail depending on whether linear or quadratic extrapolation is used. The hot spot stress method takes into account all stress raising effects emanating from the macro-geometrical changes of the detail in the stresses calculation except the weld itself. The method is fairly easy to use and will keep the size of the models at a rather moderate level. FE models could either be created using 2D plane elements or 3D shell as well as solid elements. The weld is usually included in FE models with solid elements while in FE models with shell elements the welds are generally modelled in welded details with complex geometry [7]. The calculated hot spot stress at the weld toe is then used together with the recommended S-N-curve to estimate the fatigue life of welded details. However, the method is only applicable for fatigue failures starting from the weld toe [8].

The third fatigue life assessment method used in this study is the effective notch stress method which proposed by Radaj [9]. Apart from taking the geometrical changes into account, as with the hot spot method, the effective notch stress method also takes the effects of the weld itself into account. This method is based on stress averaging in the Neuber's micro-support theory with a reference radius of 1 mm in plate thickness of 5 mm and above [10]. For smaller plate thicknesses, Zhang [11] has proposed the use of a reference radius of 0.05 mm, which is based on the relationship between the stress intensity factor and the notch stress. The effective notch stress method can be used both in 2D plane elements or 3D solid elements. The effective notch stress at fatigue critical points can be computed using the sub-modelling technique since a very fine meshed region around the critical points are required to capture the maximum elastic stress [5]. The finite element sub-modelling technique is

generally performed to transfer the displacements when defining node-base sub-regions or to transfer the stresses at the integration points when defining surface-based sub-regions from the coarsely meshed global model to the refined meshed local models.

The following five welded details frequently used in steel and composite bridges have been selected to conduct the study.

- Plate edge details
- Overlapped joints
- Longitudinal attachments
- Cope-hole details
- Cover plate details

A large amount of test results were available in the literature. But only the test data where all the information about the specimen like the width, length, thickness, weld size, material data, etc. were available have been selected for re-analysis. This is to be able to create well-defined finite element models of the specimens which are then to be used to calculate the relevant stresses. Totally 1500 fatigue test results have been re-analysed.

The stress defined at fatigue critical points, i.e. crack initiation points, according to the three methods is computed for each test series. For the sake of consistency, only 3D solid elements were used in the finite element models following the IIW recommendations for the modelling works. In all finite element models, the welds were modelled and second order of solid elements were used. For the determination of hot spot stresses at the weld toe in the investigated details, the quadratic surface stress extrapolation technique recommended by IIW was used. As mentioned earlier, since the determination of the effective notch stress requires a very finely meshed model around the critical point to capture the maximum elastic stress, the sub-modelling technique was used for computing the effective notch stresses.

The fatigue tests collected from the literature contained only the tests performed under CAFL. Also to exclude the beneficial effects of compression stress caused by fatigue loading, the fatigue test specimens only subjected to stress ratios of  $R > 0$  were considered. The numbers of cycles to failure are then plotted against the computed stresses in a logarithmic scale. The test results are then evaluated by using linear regression analysis by which the characteristic fatigue strength, the slope of the curve, the standard deviation, etc. can be determined. Finally, the result from the evaluation procedures is compared with the recommended S-N curves given in Eurocode 3 and IIW codes.

## **2.1 Fatigue life evaluation of the welded details**

In this chapter the results of the evaluation for the three methods based on the chosen five details are being presented.

### **2.2 Plate edge details**

Plate edge details are rather common in fatigue loaded structures. A typical example is gusset plates in bridge beams. For this detail, a total number of 1016 test specimens have been evaluated [12-24]. The specimens cover a wide range of different geometries and dimensions; see Figure 2-1 and Table 2-1.

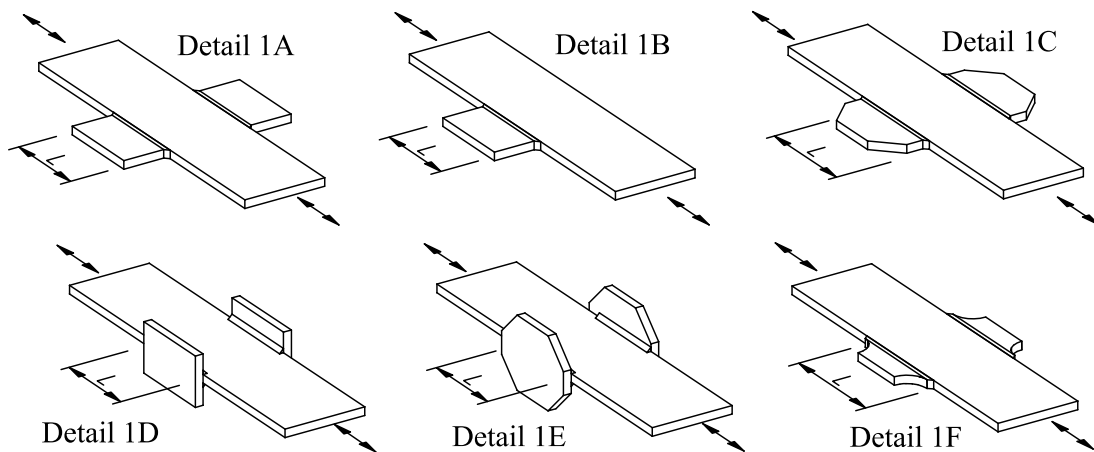


Figure 2-1 Different types of investigated plate edge details

Table 2-1 Dimensions and number of evaluated fatigue test specimens

| Types of joints | No. of specimens | Main Plate     |            | Gusset plate   |             |
|-----------------|------------------|----------------|------------|----------------|-------------|
|                 |                  | Thickness [mm] | Width [mm] | Thickness [mm] | Length [mm] |
| Detail 1A       | 710              | 8 – 20         | 40 – 170   | 8 – 20         | 50 – 400    |
| Detail 1A*      | 24               | 8              | 100 – 200  | 8              | 80 – 200    |
| Detail 1B       | 46               | 10 – 20        | 50 – 120   | 10 – 12.7      | 50 – 450    |
| Detail 1C       | 120              | 18 – 20        | 30 – 200   | 8 – 20         | 60 – 450    |
| Detail 1D       | 17               | 12.7 – 31.75   | 114        | 12.7           | 102 – 203   |
| Detail 1E       | 57               | 10             | 60         | 10             | 150         |
| Detail 1F       | 44               | 8 – 20         | 170 – 200  | 8 – 20         | 100 – 320   |

\*with no return welds

### 2.2.1 Fatigue life evaluation according to the nominal stress approach

The results from the fatigue test data based on the nominal stress amplitude are presented in Table 2. For this type of attachments, the length and the geometrical shape of the gusset plate has a significant influence on the magnitude of stress concentration at the plate termination; i.e. where fatigue cracks initiate. Therefore, the fatigue test data was evaluated by considering the variations in geometry of the specimens, see Figure 2-2. Apart from detail 1F, which is a special case, it is clear that the fatigue strength of plate edge attachments is dependent on the length of the cover plate, being reduced when the length of the attachment is increased. The 30 tests of Detail 1C show however a higher fatigue strength, even though the attachment length is the longest. These tests belong to one specific series in which the attachment was tapered with  $63^\circ$  and in which the gusset plate was thinner than the main plate. These two reasons might explain the relatively high fatigue strength of this particular test series. Details 1D and 1E – with the gusset plate being normal to the main plate – show the same trend as the other detail types.

It is worth mentioning here that Eurocode 1993-1-9 disregards the effect of the attached plate length on the fatigue strength of plate edge details. In addition a detail category 40 is assigned

to this detail (irrespective of the length of the gusset plate), which – considering the results from the current evaluation – seems to be rather conservative.

Table 2-2 Fatigue test results based on nominal stress approach

| Detail configurations                        | No. of specimens | St. dev. | $\Delta\sigma_{\text{mean}}$ [N/mm <sup>2</sup> ] | $\Delta\sigma_{\text{C}}$ [N/mm <sup>2</sup> ] |
|--|------------------|----------|---|--|
| $L \leq 100$ , (Detail 1A, 1A*, 1B and 1C)   | 386              | 0.180    | 81.3  | 64.7   |
| $100 < L \leq 200$ , (All details except 1F) | 80               | 0.226    | 70.8  | 52.9   |
| $200 < L \leq 300$ , (Detail 1A, 1B and 1D)  | 53               | 0.223    | 67.4  | 50.0   |
| $L > 300$ (Detail 1C)                        | 30               | 0.244    | 84.5  | 60.0   |
| $1/6 < r/L < 1/3$ (Detail 1F)                | 41               | 0.170    | 87.1  | 68.9   |
| Detail 1D – $L = 102$                        | 6                | 0,060    | 81,4  | 73,1   |
| Detail 1D – $L = 203$                        | 11               | 0.0,093  | 76,2  | 65,7   |
| Detail 1E – $L = 150$                        | 57               | 0.084    | 77.5  | 68.7   |

\*with no return welds

2.2.2 Fatigue life evaluation according to the hot spot stress approach

The results from the evaluation of the 616 test points (considered only  $R > 0$ ) according to the hot spot stress approach are plotted in Figure 2-2.

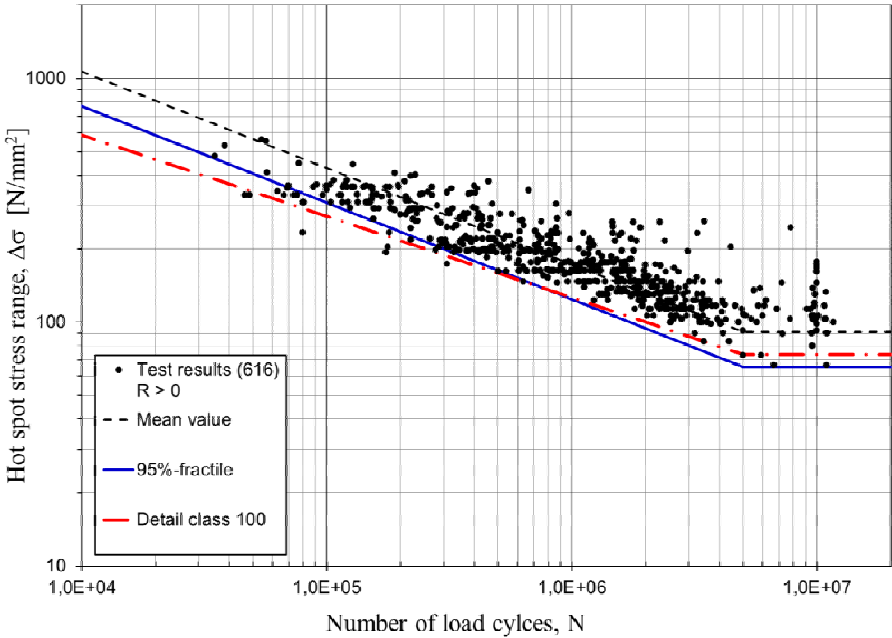


Figure 2-2 Fatigue test results for plate edge joints according to hot spot stress approach

Per definition, the effect of all geometrical parameters of the different specimens is implicitly considered in the hot-spot method. One S-N curve is needed to describe the fatigue strength of all tests. Of course, variation in welding technique, weld quality, possible size effects, etc. are

still expected to contribute to some scatter in test results. The standard deviation when all tests are considered is 0.219 when performing a linear regression analysis with a free slope with a mean value of 131.1MPa and a characteristic value of 94.3MPa. With a fixed slope of 3, the characteristic value is calculated to 103.6MPa with a standard deviation increasing to 0.232.

It was expected that the scatter when evaluating the experimental data using hot spot stress approach would be smaller than the scatter from the nominal stress approach since according to the definition of the hot spot stress method, the calculated stress includes the geometrical effects of the details. As shown in the Table 2-2, the hot spot stress method yields standard deviation in excess of that obtained with the nominal stress evaluation. One reasonable explanation to this observation is that the scatter inherent in the test results is primarily caused by welding techniques, weld quality, and the type and size of local defects rather than by the variation of the geometrical properties of the test specimens. Nevertheless, Fatigue category 100 seems to give a good representation of the fatigue strength of this particular detail.

**2.2.3 Fatigue life evaluation according to the effective notch stress approach**

The results for evaluating the fatigue test data according to the effective notch stress approach are presented in Figure 3. The standard deviation is 0.270 and the slope is 2.27 when performing a linear regression analysis with free slope. The mean and characteristic values when considering a slope of 3 are 331.9 and 235.7MPa respectively. Again, the standard deviation here is in excess of that obtained in the nominal stress and the hot spot stress evaluation, which confirms the conclusion made above. Detail category 225 which is proposed in the IIW recommendations for fatigue evaluation with the effective notch stress approach seems here to give a reasonable representation.

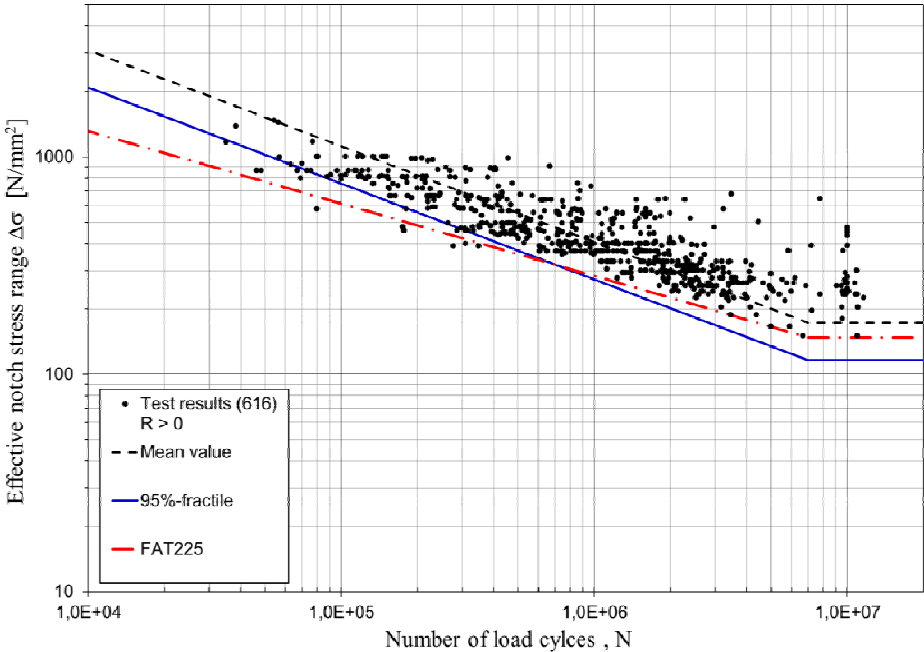


Figure 2-3 Fatigue test results for plate edge joints according to effective notch stress approach

### 2.3 Overlapped joints

The evaluation of fillet welded overlapped joints included 19 test specimens [25] with the configuration shown in Figure 2-4. The geometrical parameters that are considered for this detail are given in Table 2-3. Two different failure modes are recognized; cracking in the main plate, denoted 2MP1 and 2MP2 and cracking in the cover plates, denoted 2CP1 and 2CP2.

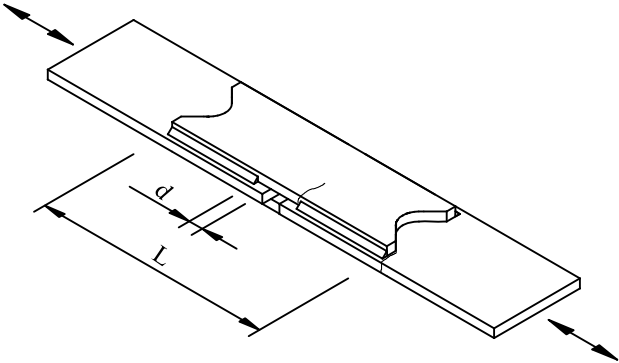


Figure 2-4 Overlapped specimens for fatigue testing.

Table 2-3 Dimensions and number of evaluated fatigue test specimens.

| Types of joints | No. of specimens | Main plate     |            | Cover plate    |             |        |
|-----------------|------------------|----------------|------------|----------------|-------------|--------|
|                 |                  | Thickness [mm] | Width [mm] | Thickness [mm] | Length [mm] | D [mm] |
| Detail 2MP1     | 5                | 12.7           | 114.3      | 12.7           | 228.6       | 0*     |
| Detail 2MP2     | 5                | 12.7           | 114.3      | 12.7           | 381         | 12.7   |
| Detail 2CP1     | 4                | 12.7           | 114.3      | 9.5            | 228.6       | 12.7   |
| Detail 2CP2     | 5                | 12.7           | 114.3      | 9.5            | 381         | 12.7   |

\*Welded to the edge of the cover plate.

#### 2.3.1 Fatigue life evaluation according to the nominal stress approach

The results from the statistical evaluation according to the nominal stress approach are presented in Table 4 for the two different cracking modes.

Table 2-4 Fatigue test results based on nominal stress approach.

| Crack location       | No. of specimens | St. dev. | $\Delta\sigma_{mean}$ [N/mm <sup>2</sup> ] | $\Delta\sigma_c$ [N/mm <sup>2</sup> ] |
|----------------------|------------------|----------|--|---------------------------------------|
| Main plate cracking  | 10               | 0.135    | 78.0                                       | 61.8                                  |
| Cover plate cracking | 9                | 0.169    | 54.2                                       | 41.1                                  |

It is apparent from the results that the fatigue strength of welded overlapped joints is higher when fatigue cracking takes place in the main plate. This has been recognized by some design codes, such as Eurocode. Another observation is that specimens with longer welds show slightly higher fatigue strength in both cracking modes (compare specimens 2MP2 and 2CP2

to specimens 2MP1 and 2CP1. However the number of available test results is not enough to draw a firm conclusion regarding the effect of the weld length in this detail.

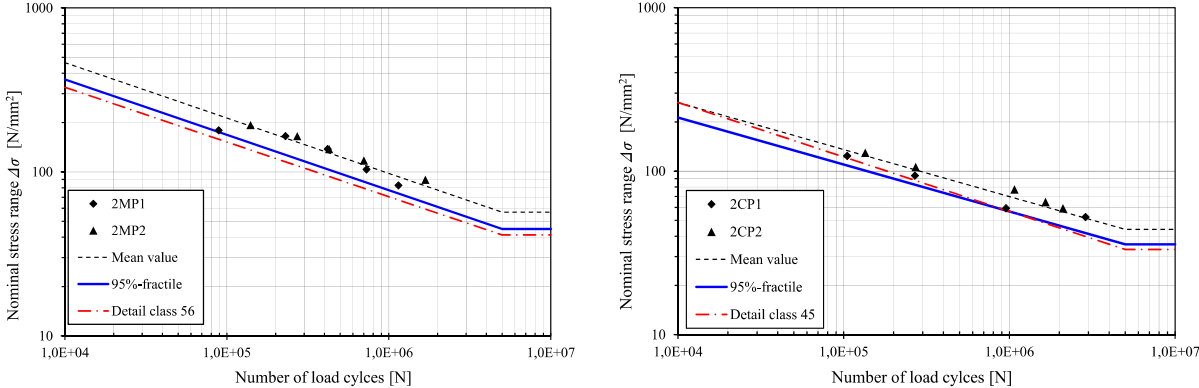


Figure 2-5 Test results based on nominal stress approach; left cracking in the main plate; right cracking in the cover plate.

**2.3.2 Fatigue life evaluation according to the hot spot stress approach**

The results from the evaluation according to the hot spot stress approach are presented in Table 2-5. Again the test data have been divided into two groups depending on the location of cracking. Although the number of available test data is rather limited, the results clearly indicate distinct fatigue strength values for the two cracking modes. The Eurocode suggests C90 for both cracking modes. Considering the test data in hand this value seems to be inappropriate concerning cracking in the main plate. The recommended C-class seems to be in better agreement regarding the second cracking mode; i.e. cracking in the cover plate. Apparently, more test data on details with similar configuration is needed before a firm conclusion can be made.

Table 2-5 Fatigue test results based on hot spot stress approach.

|                      | No. of specimens | St. dev. | $\Delta\sigma_{\text{mean}}$ [N/mm <sup>2</sup> ] | $\Delta\sigma_c$ [N/mm <sup>2</sup> ] |
|----------------------|------------------|----------|---|---------------------------------------|
| All test data        | 19               | 0.202    | 110.3   | 82.3                                  |
| Main plate cracking  | 10               | 0.120    | 98.7  | 80.3                                  |
| Cover plate cracking | 9                | 0.141    | 124.7   | 98.9                                  |

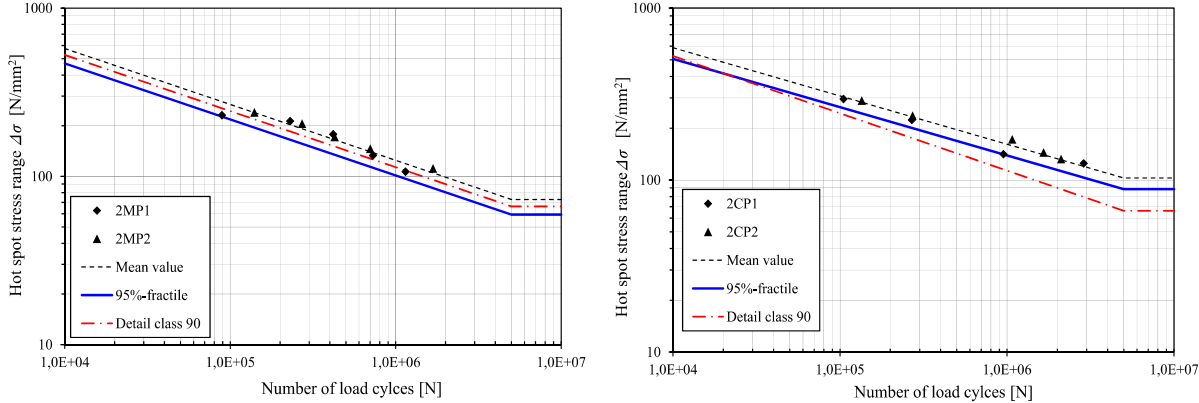


Figure 2-6 Fatigue test results for overlapped joints according to hot spot stress approach.



**2.3.3 Fatigue life evaluation according to the effective notch stress approach**

The results for the effective notch stress method are very dependent on how the weld end is modelled. The complicated weld geometry for this specific joint made it rather difficult to use the effective notch stress method. In this investigation, a simplified model for the weld end has been adopted; see Figure 2-7 (a). The test data is presented in Figure 2-7 (b) in terms of the effective notch stress. With all test data evaluated together with a fixed slope of 3, the standard deviation is 0.195 with a characteristic strength of 303.2 MPa. All test data lie well above FAT 225, which is proposed in the IIW recommendations for evaluation with the effective notch stress method. Also here the fatigue test data is clearly separated for the two different cracking modes. As in the case of the hot spot stress, the specimens with cracking starting in the main plate show slightly lower fatigue strength. This indicates that the lower fatigue strength for this cracking mode is an inherent feature in these tests specimens rather than a result of a higher stress concentration at the weld end.

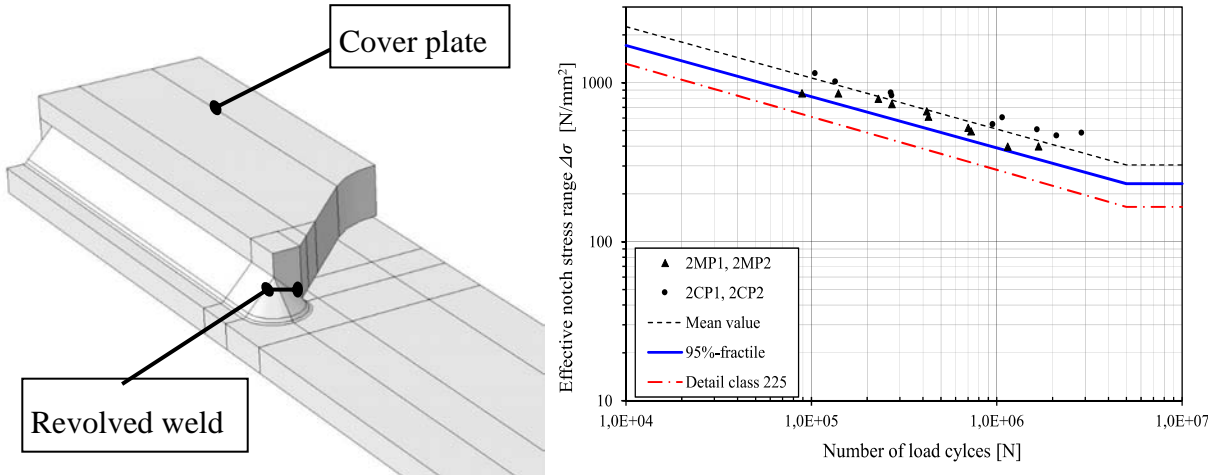


Figure 2-7 (a) Revolved weld end used for notch stress analysis. (b) Fatigue test results for overlapped joints according to effective notch stress approach.

**2.4 Longitudinal attachments**

This detail covers in total 286 test results [26-41] with a wide variation in dimensions and geometrical properties. As the fatigue strength of plates with longitudinal non-load-carrying attachments is known to be a function of the length of the attachment plate, the test results were primarily categorized according to the attachment length, in five different classes as shown in Table 3.

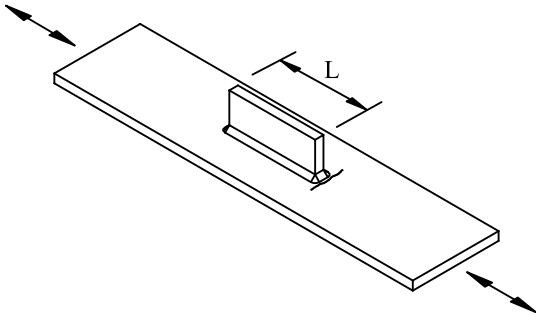


Figure 2-8 Investigated longitudinal attachment

Table 2-6 Number of specimens and geometry of investigated welded details.

| [mm]    | No. of specimens | $t_{\text{attachment}}$ [mm] | $t_{\text{main}}$ [mm] | $l_{\text{attachment}}$ [mm] | Width [mm] |
|---------|------------------|------------------------------|------------------------|------------------------------|------------|
| L = 200 | 10               | 4                            | 4                      | 200                          | 100        |
| L = 150 | 193              | 4.8 – 25.4                   | 4.8 – 25.4             | 150                          | 75 – 100   |
| L = 100 | 55               | 10-25                        | 10 – 25                | 100                          | 80 – 152.4 |
| L = 60  | 11               | 16                           | 16                     | 60                           | 90         |
| L = 50  | 17               | 8                            | 8                      | 50                           | 80         |

### 2.4.1 Fatigue life evaluation according to the nominal stress approach

The results from evaluating the test results based on the nominal stress approach are presented in Table 2-7. The C-classes for this detail are divided into groups according to their length. The test results are in agreement with Eurocode except for the joints with the 50 mm long attachment which shows slightly lower fatigue life (77.3 MPa) than specified in the standard (C80). Test data can be seen in Figure 2-9.

Table 2-7 Fatigue test results based on nominal stress approach.

| [mm]    | No. of specimens | St. dev. | $\Delta\sigma_{\text{mean}}$ [N/mm <sup>2</sup> ] | $\Delta\sigma_c$ [N/mm <sup>2</sup> ] |
|---------|------------------|----------|---|---------------------------------------|
| L = 200 | 10               | 0.157    | 75.4  | 56.9                                  |
| L = 150 | 193              | 0.123    | 88.8  | 75.9                                  |
| L = 100 | 55               | 0.164    | 91.3  | 73.6                                  |
| L = 60  | 11               | 0.056    | 85.8  | 77.9                                  |
| L = 50  | 17               | 0.088    | 88.6  | 77.3                                  |

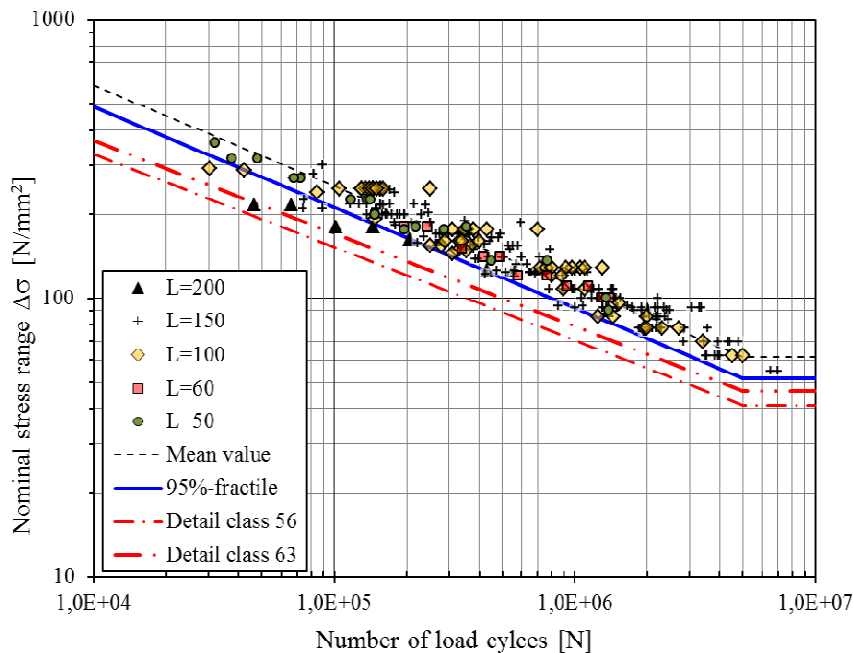
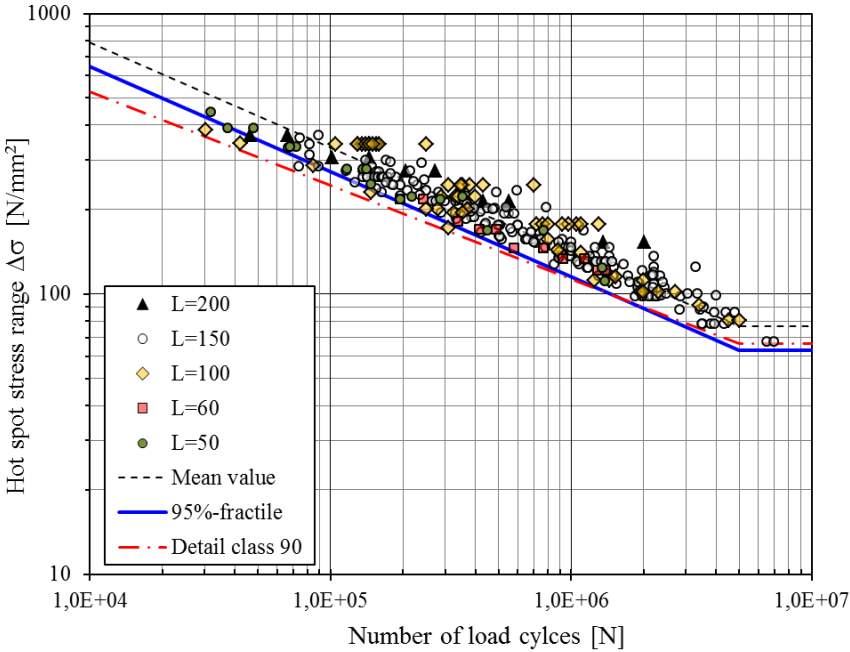


Figure 2-9 Fatigue test results for longitudinal attachments according to nominal stress approach.

**2.4.2 Fatigue life evaluation according to the hot spot stress approach**

Test results for the hot spot stress approach are plotted in Figure 2-10. In this figure quadratic extrapolation of the hot spot stress has been used. The standard deviation is 0.138 and the slope 2.67 evaluated with free linear regression. The characteristic strength is 88.8 MPa. With a fixed slope of 3 the standard deviation becomes 0.150 and the characteristic fatigue strength 94.2 MPa. Linear extrapolation was also examined for this detail, giving a standard deviation of 0.150 and characteristic fatigue strength of 93.1 MPa. Considering the results in Figure 2-10 it seems that C90 should be used for this detail instead of the C100 which is recommended by the Eurocode.



*Figure 2-10 Fatigue test results for longitudinal attachments according to hot spot stress approach.*

**2.4.3 Fatigue life evaluation according to the effective notch stress approach**

Among the 286 test specimens considered for this detail, only a limited number of tests were fully described in the source literature. Therefore only these tests [27, 32-34] are included in the effective notch stress evaluation. The results are presented in Figure 2-11. The standard deviation is 0.136 and the slope is 2.70 using the free linear regression. When the slope is set to 3 the standard deviation is 0.145 and the characteristic strength 301.1 MPa. As can be seen from Figure 2-11 the test data are in good agreement with the recommendations concerning detail category of 225 for the effective notch stress method.

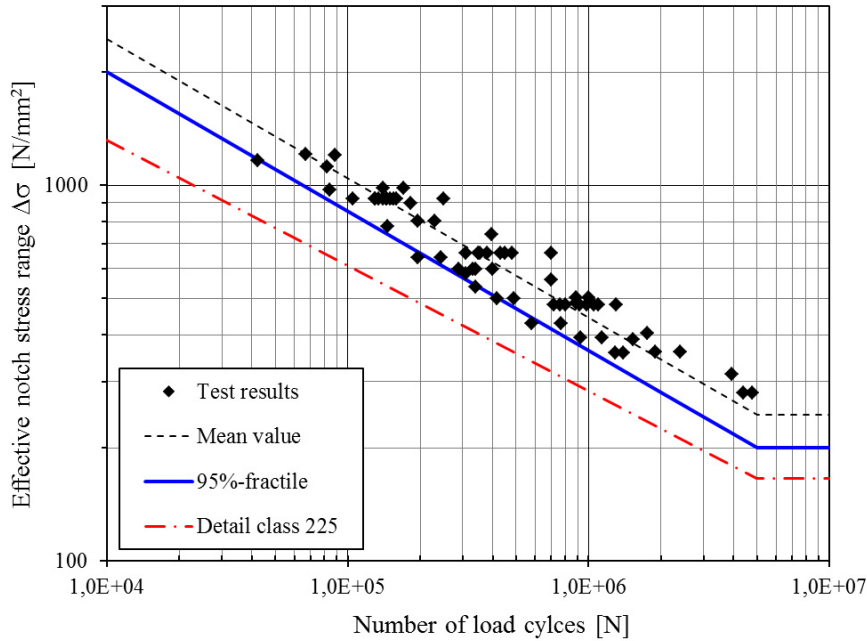


Figure 2-11 Fatigue test results for longitudinal attachments according to effective notch stress approach.

## 2.5 Cope-hole details

Cope-holes are usually used as field-welded joints in bridge girders to facilitate for the transversal butt welds in the flanges and avoid weld crossing. The size of the cope-hole is also chosen to give access for the NDT of the butt welds. The fatigue test results of 29 different specimens from 4 different sources [42-45] have been collected as to evaluate this detail. Table 2-8 represents a detailed overview of various test configurations as illustrated in Figure 2-12.

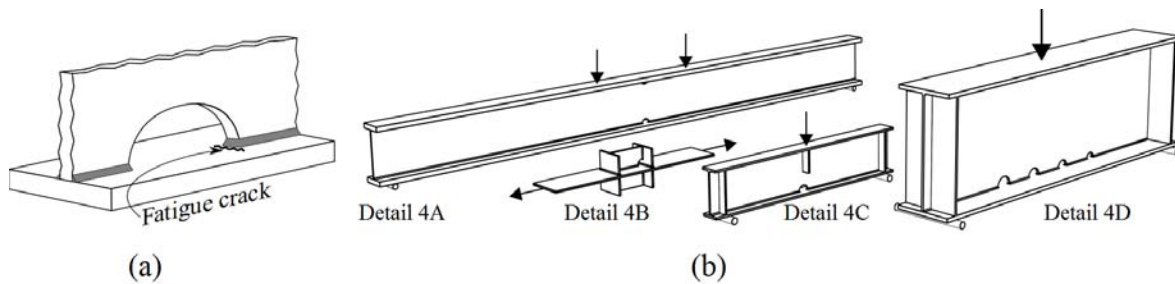


Figure 2-12 (a) Fatigue crack location in specimens with cope-hole; (b) Different cope-hole test configurations

Table 2-8 Dimensions and number of evaluated fatigue test specimens for cope-holes

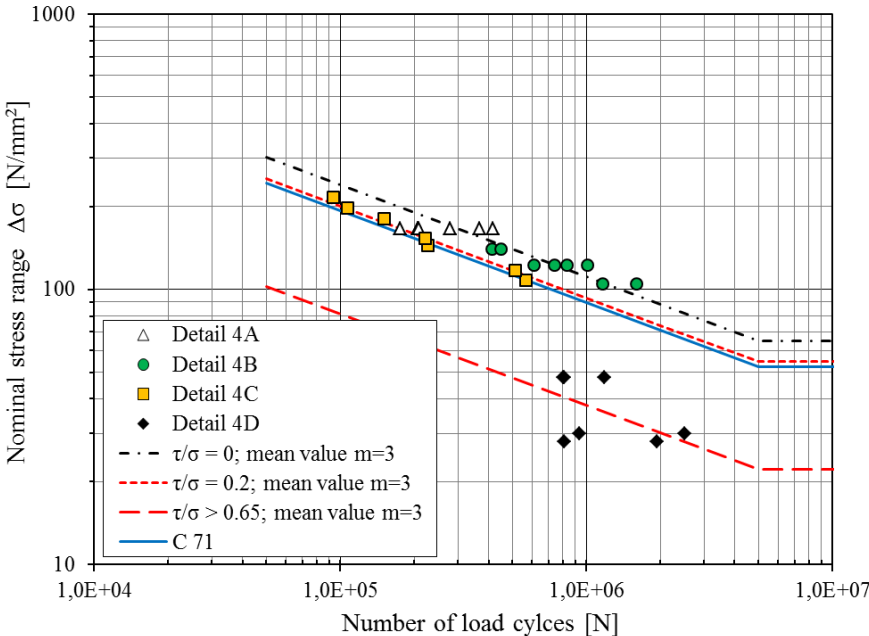
| Types of joints | No. of specimens | Main Plate     |            | Attachment     |                       | $\tau_a/\sigma_m$ |
|-----------------|------------------|----------------|------------|----------------|-----------------------|-------------------|
|                 |                  | Thickness [mm] | Width [mm] | Thickness [mm] | Cope-Hole Radius [mm] |                   |
| Detail 4A       | 7                | 25.4           | 127        | 4.8            | 25.4                  | 0                 |
| Detail 4B       | 8                | 9              | 200        | 9              | 35                    | 0                 |
| Detail 4C       | 7                | 8              | 80         | 6              | 26                    | 0.2               |
| Detail 4D       | 7                | 16             | 250        | 9              | 25-40                 | 0.67-0.98         |

**2.5.1 Fatigue life evaluation according to the nominal stress approach**

As it is listed in Table 2-9, the fatigue strength of the evaluated cope-hole details is very inconsistent. A closer look at the results in Figure 2-13 reveals that despite the conspicuous geometrical variation of details 4A and 4B, they exhibit almost identical fatigue strength. However, detail 4D which is more similar to 4A shows a dramatic fall in terms of fatigue strength. A more thorough assessment of the tests, reveals a pronounced dependency of fatigue life of cope-hole details on the ratio of shear stress to normal stress in the specimens ( $\tau_a/\sigma_m$ ), see Figure 2-13. It is clear that the relatively low fatigue strength of details in the test series 4D is due to presence of considerable shear stresses at the anticipated crack location i.e. weld toe at cope-hole section. The destructive effect of shear stresses on the fatigue life of cope-hole details has been previously confirmed by Miki et. al. [43]. Therefore, evaluation of the test results, based on the nominal stress in these details, should consider to the ratio  $\tau_a/\sigma_m$  as an important parameter that affects the fatigue strength of cope-hole details. While this has been recognized in IIW, the Eurocode 1993-1-9 assigns detail category 71 to cope-hole details irrespective of the ratio  $\tau_a/\sigma_m$ .

*Table 2-9 Statistical evaluation of cope-hole test results using linear regression analysis with a fixed slope of 3*

| Type of joint | St. dev. | $\Delta\sigma_{mean}$<br>[N/mm <sup>2</sup> ] | $\Delta\sigma_C$<br>[N/mm <sup>2</sup> ] |
|---------------|----------|---|--|
| Detail 4A     | 0.157    | 83.8  | 72.5                                     |
| Detail 4B     | 0.093    | 88.9  | 71.9                                     |
| Detail 4C     | 0.055    | 74  | 64.7                                     |
| Detail 4D     | 0.345    | 30  | 16.7                                     |



*Figure 2-13 Fatigue test results for cope-hole details distinguished by shear to normal stress ratio.*

**2.5.2 Fatigue life evaluation according to the hot spot stress approach**

The test results of all cope-hole details evaluated based on the hot spot stresses are plotted in Figure 2-14. It is apparent that although the test data do not lie in one group, the scatter of the results, compared to the nominal stress method, is decreased. Linear regression analysis with a fixed slope of 3 gives a standard deviation of 0,281 compared with the value of 0.614 obtained from the nominal stress method. However, the calculated characteristic fatigue strength of 70.6 MPa is considerably lower than what is specified in IIW and Eurocode (FAT 100). If the results from detail 4D which undergoes the highest  $\tau_a/\sigma_m$  ratio are excluded, FAT 100 appears to be a reasonable representation.

The low hot spot stress value obtained for Detail 4D is assumed to be due to the presence of high amount of shear stresses in the web which causes the weld to become load carrying. In such a case, the weld at the cope-hole transfers the existing shear stresses in addition to the normal stresses caused by the bending of the beam. Thus, in order to account for such severe loading conditions, it is recommended to apply a further reduction of design class to FAT90 for cope-holes in beams when using the hot spot stress approach.

It is noteworthy that for Detail 4C, for which the surface stress extrapolation according to IIW recommendation was not feasible due to the small radius of the cope-hole in relation to the flange thickness, hot spot stress is calculated as  $1.12 \cdot \sigma \cdot 0.5t$  according to [46]. Moreover, in order to calculate the hot spot stress concentration factor, the nominal stress for beam specimens is calculated as the stress in the mid-section of the cope hole using the net cross section and the simple beam theory formula.

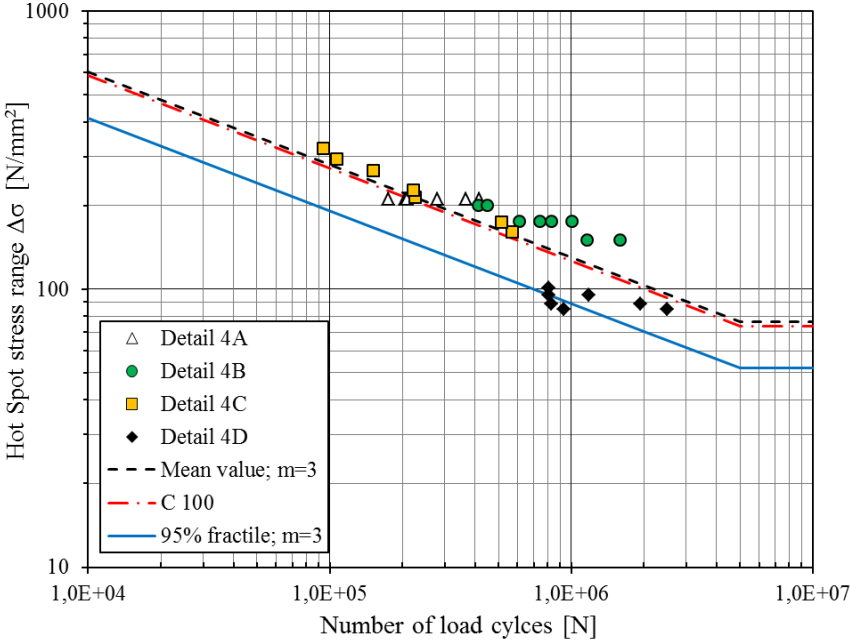


Figure 2-14 Fatigue test results for cope-hole details according to hot spot stress approach.

**2.5.3 Fatigue life evaluation according to the effective notch stress approach**

Considering Figure 2-15, in which the fatigue test data are evaluated with the effective notch stress method, the scatter of the test data is noticeably reduced. All test data lie within the same narrow scatter band. Moreover, linear regression analysis reveals a slope of 2.74

accompanying by the characteristic value of 216.1 MPa and standard deviation of 0.162, which is the lowest obtained standard deviation for this detail based on different evaluation methods. When the slope is set to 3 the standard deviation is 0.155 and the characteristic strength 230.3 MPa. As can be seen from Figure 2-15, the test data are in good agreement with the recommendations concerning detail category of 225 for the effective notch stress method. Eventually, the IIW recommended fatigue class of 225 appears to be in good agreement with the evaluated cope-hole details in this study.

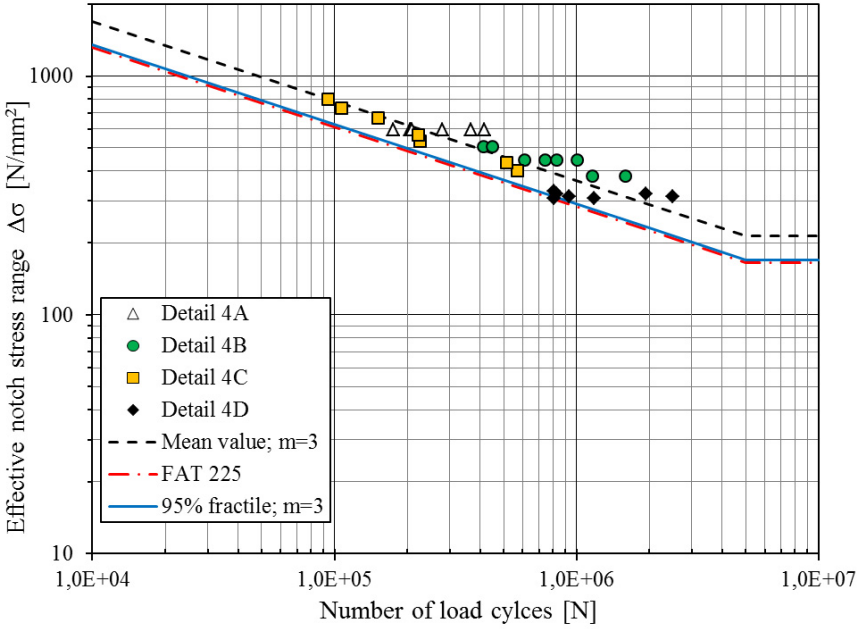


Figure 2-15 Fatigue test results for cope-hole details according to effective notch stress approach.

**2.6 Cover-Plate details**

Partial-length Cover-Plates are usually welded to the flanges of steel bridge girders in order to increase the moment capacity and consequently the allowable traffic load and span of the bridge. Herein, the constant amplitude fatigue test results of 183 cover-plate specimens have been evaluated [47, 48]. The specimens accommodate a wide range of geometric variations such as the cover-plate to main plate thickness ratio ( $t_c/t_m$ ) and the cover-plate end shape; see Figure 2-16 and Table 2-10.

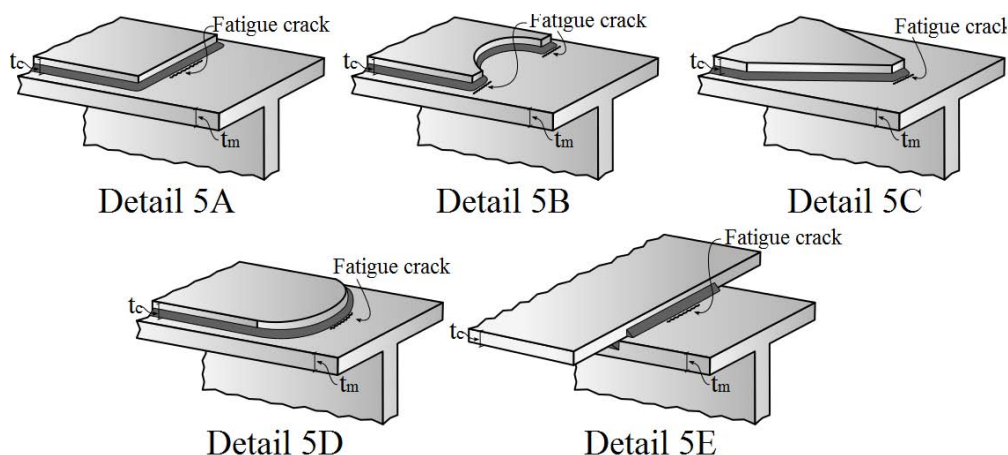


Figure 2-16 Different cover-plate test configurations.

Table 2-10 Dimensions and number of evaluated fatigue test specimens for cover-plate details.

| Types of joints | No. of specimens | Main Plate     |            | Cover Plate    |            | $t_c/t_m$ |
|-----------------|------------------|----------------|------------|----------------|------------|-----------|
|                 |                  | Thickness [mm] | Width [mm] | Thickness [mm] | Width [mm] |           |
| Detail 5A1      | 30               | 9.525          | 171        | 19.05          | 114        | 2         |
| Detail 5A2      | 102              | 9.525          | 171        | 14.3           | 114        | 1.5       |
| Detail 5A3      | 5                | 19.05          | 127        | 12.7           | 101.6      | 0.67      |
| Detail 5B       | 5                | 19.05          | 127        | 12.7           | 101.6      | 0.67      |
| Detail 5C       | 6                | 19.05          | 127        | 12.7           | 101.6      | 0.67      |
| Detail 5D       | 5                | 19.05          | 127        | 12.7           | 101.6      | 0.67      |
| Detail 5E       | 30               | 9.525          | 171        | 14.3           | 229        | 1.5       |

### 2.6.1 Fatigue life evaluation according to the nominal stress approach

Conforming to the data shown in Figure 2-17 and Table 2-11, the fatigue strength of cover plates seems to be particularly affected by the ratio  $t_c/t_m$ . It is apparent that cover plates with the lowest  $t_c/t_m$  ratio exhibit the highest fatigue strength. However, this effect disappears for details with  $t_c/t_m > 1$ . These details demonstrate the same fatigue strength. Moreover, as the fatigue test results of cover plates with various end shapes lie latently within the same scatter band, it can be concluded that changing the cover plate end shape does not affect the fatigue strength of cover plate details.

While Eurocode 3 has limited the effect of  $t_c/t_m$  to ratios only less than and higher than one, IIW code considers several intervals. Consequently, considering the evaluated data in this study, Eurocode recommendations appear to be more consistent.



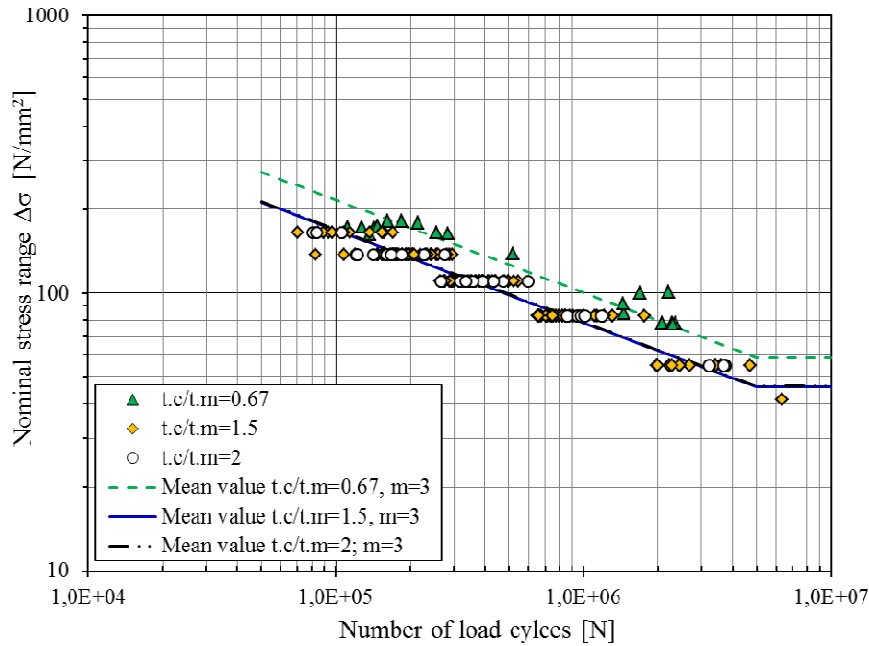


Figure 2-17 Fatigue test results for cover-plate details categorized by cover plate to main plate thickness ratio.

Table 2-11 Statistical evaluation of cover-plate test results using linear regression analysis with a fixed slope of 3.

| Category         | No. of specimens | St. dev. | $\Delta\sigma_{\text{mean}}$ [N/mm <sup>2</sup> ] | $\Delta\sigma_c$ [N/mm <sup>2</sup> ] |
|------------------|------------------|----------|---|---------------------------------------|
| $t_c/t_m = 0.67$ | 21               | 0.147    | 79.7  | 64.8                                  |
| $t_c/t_m = 1.5$  | 132              | 0.104    | 62.2  | 54.4                                  |
| $t_c/t_m = 2$    | 30               | 0.103    | 62.7  | 54.3                                  |

## 2.6.2 Fatigue life evaluation according to the hot spot stress approach

The test results of all cover-plate details are shown in Figure 2-18. As it was expected, the geometrical effects of different shapes and configurations are implicitly accounted for by the hot spot stress approach and all the data lie within one scatter band. This observation is supported by the statistical analysis as well. The standard deviation of all test data decreases significantly from 0.149 in the nominal stress approach to 0.116 for the hot spot stress approach. The recommended C100 seems also to be a reasonable representation for the fatigue strength of this detail.

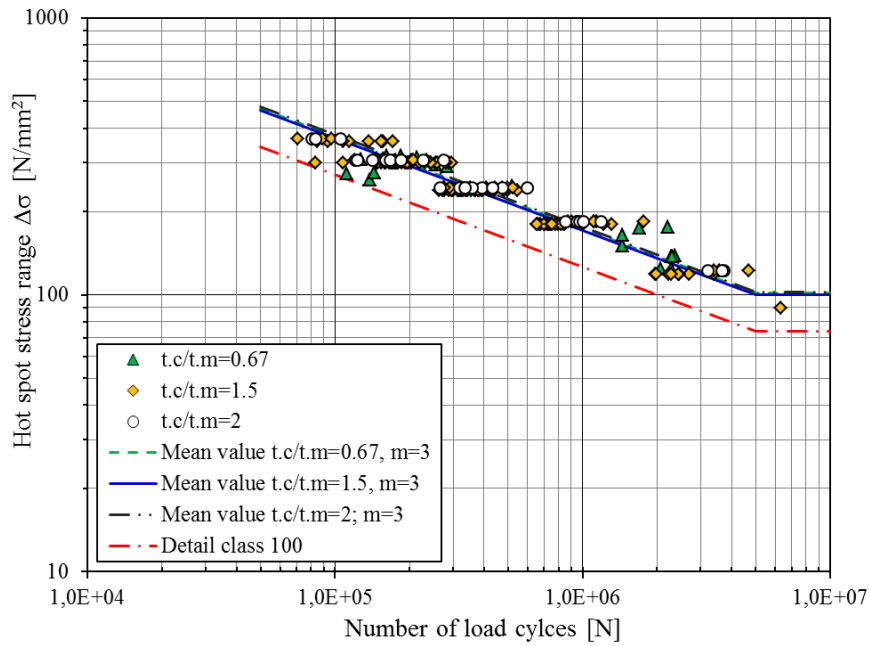


Figure 2-18 Fatigue test results for cover-plate details according to hot spot stress approach.

### 2.6.3 Fatigue life evaluation according to the effective notch stress approach

The test results according to the effective notch stress approach are shown in Figure 2-19. It is apparent that although the scatter of the test data is reduced compared to the nominal stress method, they don't lie within one scatter band. The reason for this anomalous observation is assumed to stem from the fact that, when using effective notch stress method, the exact weld geometry should be modelled in order to obtain accurate results. However, the precise weld geometry is often unknown when assessing the test data.

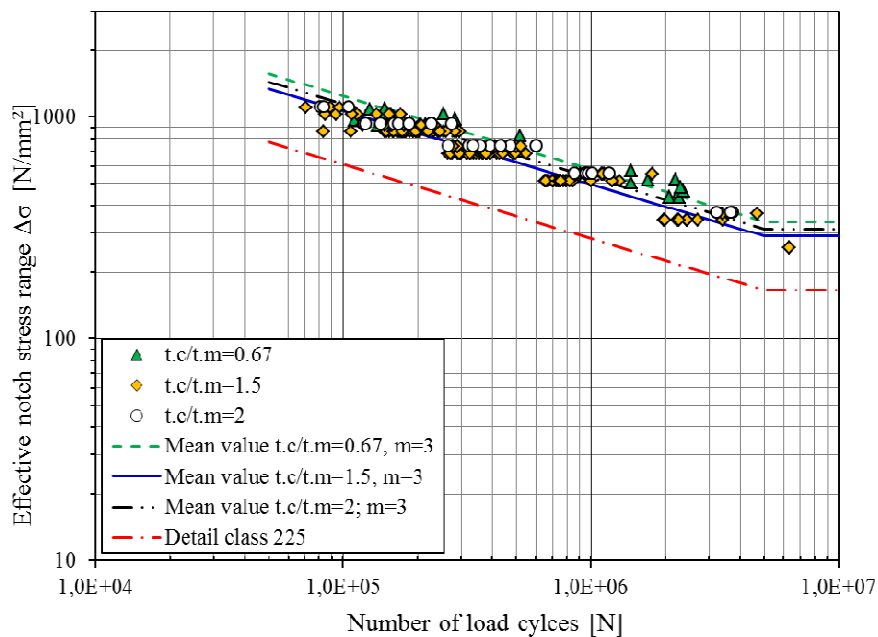


Figure 2-19 Fatigue test results for cover-plate details according to effective notch stress approach

### **3 Discussion of results**

#### **General conclusions**

The standard deviations obtained from the three different methods are all of the same magnitudes (more and less) which were unexpected. Since the refined and advanced methods take into account the stress raising effects, it was expected to that these methods would produce smaller scatter. However, variations in welding technique, weld quality and possible size effects may be contributed to some scatter in test results which is confirmed by the scatter obtained from the hot spot stress method. The scatter from this method for example was the smallest one due to the fact that the method ignores the weld effects in the stress calculations. Despite the scatter from the three life assessment methods is more and less same, the results for estimating of the fatigue life of the welded details when using the advanced methods are in better agreement with the fatigue test results in comparison with estimating the fatigue life of the fatigue test specimens when using the nominal stress method.

Another common conclusion for the studied welded details is that the fatigue category FAT225 recommended by the IIW for the effective notch stress method appears to give reasonable agreement with the fatigue test results.

#### **Plate edge details**

The length of the attached plates has a significant effect on the fatigue strength capacity of welded plate edge joints. The fatigue strength of the joints will decrease as the length of the plate increases. This is however not recognized in Eurocode 3 where the fatigue strength of 40 MPa is assigned to this detail irrespective of the length of the attached plate. This recommendation appears to be rather conservative considering the results from the current evaluation.

The IIW recommends using fatigue strength of 90 and 100 MPa depending on the length of the attached plates for the hot spot stress method while there is no recommendation given in Eurocode 3. According to the definition of the method, only one S-N curve should be sufficient for this detail. The reason for the two S-N curves is that the attached plate might become more load-carrying with increased length.

#### **Overlapped joints**

A distinct difference in fatigue strengths could be seen for this detail depending on the failure location. The fatigue strength was higher when the fatigue failure occurs in the main plate. This difference is also recognized in both the Eurocode and in the IIW.

The Eurocode and IIW recommend using fatigue strength of 90 MPa when using the hot spot stress method. Based on the current results this seems to be inappropriate for cracking in the main plate. It provides however a better estimate for cracking in the cover plate.

#### **Longitudinal attachment**

The fatigue strength for this type of detail is a function of the length of the attached plates. This has been recognized in both Eurocode 3 and IIW recommendations. The results from in this investigation showed that Eurocode 3 provides a good representation of the fatigue strength of this detail. However, the result for the 50 mm length of the attached plates appears to be non-conservative. The IIW recommendation for the failure in the main plate with the present test results is consistent with the test results, except the attached plate length of 200 mm.

Based on the present results, fatigue class of C90 should be more consistent with the test results instead of the recommended fatigue strength curve of C100 when using the hot spot stress method.

#### **Cope-hole details**

For cope-hole details shear stress has quite an adverse effect on the fatigue strength. This effect has been recognized by the IIW where the fatigue strength of this detail is a function of the ratio of shear ( $\tau$ ) to normal ( $\sigma$ ) stress. In Eurocode 3 however, one C-class is assigned irrespective of the  $\tau_a/\sigma_m$ -ratio.

From the present evaluation it can be seen that FAT100 recommended by IIW for non-load carrying welds for the hot spot stress method is not consistent with the test results. However, if the results from detail 4D which undergoes the highest  $\tau_a/\sigma_m$  ratio are excluded, FAT100 appears to be a reasonable representation.

#### **Cover plate details**

The fatigue strength is dependent on the  $t_c/t_m$ -ratio; it increases as the ratio decreases. This effect has been recognized by both Eurocode 3 and IIW recommendations. The present evaluation study showed that the recommendations given by Eurocode 3 is more consistent with suggesting either of two values, for the ratio above or below 1. In the IIW there are several intervals given. The results from the evaluation of the fatigue test also indicate that the fatigue strength is independent of the shape of the weld end.

The recommended fatigue strength of 100 MPa in EC3 and IIW for the hot spot stress method appears to give reasonable agreement with the results from the current evaluation.

## **4 Conclusions**

The standard deviations for the five different details in this investigation are approximately same magnitude for most of them regardless the choice of method. An exception is, however, cope-hole details where the standard deviation not only decreases as sophisticated methods are used, the difference between the basic and most advanced method is also quite large. However, it is difficult to decide for which details the more advanced methods will provide a significant improvement in the estimation of the fatigue strengths. Moreover, there are no recommendations for how to model weld ends for complex details such as cover plates when applying the effective notch stress method. The advanced methods also require a significant effort for both for modelling and computation. This is especially true for the effective notch stress method because of the requirements regarding the mesh density which results in very large models to be solved by sub-modelling technique.

## **4 Acknowledgment**

This investigation within the framework of the research project (Brifag – Bridge Fatigue Guidance) is being carried out with a financial grant from the Research Fund for Coal and Steel (RFCS) of the European Community and the Swedish Transport Administration, Granted under Contract No. RFSR-CT-2008-00033.

## 5 References

- [1] Fricke, W., Fatigue analysis of welded joints: State of development, Marine structures, Vol. 16 (2003) pp. 185-200.
- [2] Niemi, E., Stress determination for Fatigue Analysis of Welded Components, IIW doc. IIS/IIW-1221-93, The International Institute of Welding, (1995).
- [3] Radaj, D., Sonsino, C. M., Fricke, W., Fatigue Assessment of Welded Joints by Local Approaches. 2. Ed, Woodhead Publishing, Cambridge, 2006.
- [4] Eurocode3, En-1993-1-9. Eurocode 3: Design of Steel Structures - Part 1-9: Fatigue, (2005).
- [5] Hobbacher, A., Recommendation for fatigue Design of Welded Joints and Components, The international Institute of Welding, IIW-1823-07 ex. XIII-2151r4-07/XV-1254r4-07, (2008).
- [6] Fricke, W., Recommended Hot Spot Analysis Procedure for Structural Details of FPSO's and Ships Based on Round-Robin FE Analyses, International Journal of Offshore and Polar Engineering, 12 (2001) 1-8.
- [7] Aygül, M., Al-Emrani, M., Urushadze, S., Modelling and fatigue life assessment of orthotropic bridge deck details using FEM, International Journal of Fatigue, (Article in Press) (2011).
- [8] Niemi, E., Tanskanen, P., Hot Spot Stress Determination for Welded Edge Gussets, The International Institute of Welding - IIW Doc. XIII-1781-99 (1999).
- [9] Radaj D, Sonsino C M, Fricke W, Fatigue Assessment of Welded Joints by Local Approaches., 2. Ed, Woodhead Publishing, Cambridge, (2006).
- [10] Hobbacher A, The IIW recommendations for fatigue design of welded joints and components, The International Institute of Welding, IIW-1823-07 ex XIII-2151r4-07/XV-1254r4-07 (2008).
- [11] Sonsino C M, A consideration of allowable equivalent stresses for fatigue design of welded joints according to the notch stress concept with the reference radii  $r_{ref} = 1.00$  and  $0.05$  mm, Welding in the World, 53, (2009).
- [12] Berger, P., Der neue Ermüdungsfestigkeitsnachweis in TG 2 13 500, Informationen des Veb MLK, Leipzig 18 2, (1979) 2-8.
- [13] Berger, P., Investigation on the fatigue strength of welded joints by full scale tests, VEB Metalleichtbaukombinat, Forschungsinstitut Leipzig und IIW-Document No. XIII-983-80.V. Metalleichtbaukombinat (1980)
- [14] Gurney, T. R., Further fatigue tests on mild steel specimens with artificially induced residual stresses, British Welding Journal 9, No. 11 (1962).
- [15] Gurney, T. R., Nekanda Trepka, L., Influence of local heating on fatigue behaviour of welded specimens, British Welding Journal 6, No. 10 (1959) 491-497
- [16] Haibach, E., Oliver, R., Fatigue investigation of higher strength structural steels in notched and in welded condition, Synthesis of results and tentative conclusions, Report No. TB-114 Laboratorium für Betriebsfestigkeit (1974)
- [17] Hirt, M. A., Crisinel, M., La resistance a la fatigue des pontres en ame pleine composees-soudees effect des plaquettes et goussets soudees a l' aile, Ecole Polytechnique Federale De Lausanne Departement de Gemi Civil Institut De La Construction Metallique, ICOM 017 (1975)
- [18] Kim, M.-H., Kang, S.-W., Testing and analysis of fatigue behaviour in edge details: a comparative study using hot spot and structural stresses, Journal of Mechanical Engineering Science, Vol. 222 (2008) pp.2351-2363.
- [19] Kim, W. S., Lotsberg, I., Fatigue test data for welded connections in ship-shape structures, OMAE Specialty Symposium on FPSO Integrity, OMAE-FPSO'04-0018 (2004) 1-8.

- [20] Krämer, W., Betriebsfestigkeitsversuche an Schweißverbindungen mit Lastkollektiven für Straßenbrücken, *Schweißtechnik* 17, Heft 11 (1967).
- [21] Müller, G., Ein Beitrag zur Betriebsfestigkeit geschweißter Konstruktionen, in: *ZIS-Mitteilungen*, 10/68, 1968, pp. 1640-1651.
- [22] Neumann, A., *ZIS*, I/1958 veröffentlicht in: Neumann A. Probleme der Dauerfestigkeit von Schweißverbindungen, in: *VEB Verlag Technik*, Berlin, 1960.
- [23] Puchner, O., Augmentation de la résistance à la fatigue par chauffage localisé de plats et de poutres comportant des goussets soudés in: *IIW-Doc. XIII-179*, 1959.
- [24] Wagner, M., Fatigue Strength of Structural Members with In-Plane Notches, *International Institute of Welding, Doc. XIII-1730-98* International Institute of Welding, Doc. XIII-1730-98 (1998)
- [25] Gurney T R, Influence of Artificially Induced Residual Stresses on Fatigue Strength of Load-Carrying Fillet Welded Joints in Mild Steel, Report D8/4/60 of the British Welding Research Association, (1961).
- [26] Berge S, Residual stress and stress interaction in fatigue testing of welded joints, Report SK/R 55, Division of Marine Structures, The University of Trondheim, The Norwegian Institute of Technology, (1981).
- [27] Booth, G. S., Constant amplitude fatigue tests on welded steel joints performed in air, *American Society of Mechanical Engineers (Paper)*, (1980) III/P4-1-15.
- [28] Gurney T R, Influence of elapsed time on fatigue strength of welded joints, *IIW-Document No. XIII-590-70*.
- [29] Gurney T R, Influence of residual stresses on fatigue strength of plates with fillet welded attachments, *British Welding Journal* 7, No. 6., (1960) 415-430.
- [30] Gurney T R, Fatigue tests on butt and fillet welded joints in mild and high tensile structural steels, *British Welding Journal* 9, No. 11., (1962) 614-620.
- [31] Gurney T R, Some fatigue tests on fillet welded mild and high tensile steel specimens in the as-welded and normalized conditions, *British Welding Journal* 13, No. 11., (1966) 648-651.
- [32] Han S H, Han J W, Kim J S, Rodopoulos C A, Estimating the fatigue life of welded joints considering statistical characteristics of weld toe shapes and multiple collinear surface cracks, (2006).
- [33] Jamada K, Makino T, Baba C, Kikuchi Y, Fatigue analysis based on crack growth from toe of gusset end weld, *Proceedings of ISCE 303*, Japan Society of Chemical Engineers, (1980).
- [34] Kawono H, Inoue K, A Local Approach for the Fatigue Strength Evaluation of Ship Structures, *Fatigue Design ESIS 16* (Edited by J. Solin, G. Marquis, A. Siljander, and S. Sipilä) Mechanical Engineering Publications, London, (1993) 95-108.
- [35] Knight J W, Some basic fatigue data for various types of fillet welded joints in structural steel, *Welding Research International* 9, No. 3., (1979) 22-41.
- [36] Maddox S J, A fracture mechanics analysis of the fatigue behaviour of a fillet welded joint, *IIW-Document No. XIII-722-74*.
- [37] Mang E, Bucak Ö, Untersuchungen an Verbindungen von geschlossenen und offenen Profilen aus hochfesten Stählen, Veröffentlichung Nr. P 11 und P 71 der Studiengesellschaft für Anwendungstechnik von Eisen und Stahl e.V., Düsseldorf, (1982).
- [38] N.N., Effect of peening and grinding on the fatigue strength of fillet welded joints, *British Welding Journal* 15, No. 12., (1968) 601-609.
- [39] N.N., United Kingdom Offshore Steels Research Project, Final Report to ECSC Contract No. 7210 KB/8/801, Volume 1 and 2, Department of Energy, London, (1980).

- [40] Ostermann H, Einfluß einer Entspannungsbehandlung auf die Zeitfestigkeit von geschweißtem Panzerstahl XH 113, Laboratorium für Betriebsfestigkeit, Darmstadt, Bericht Nr. 2670 (unveröffentlicht), (1972).
- [41] Weck R, Results of fatigue tests on mild steel specimens with welded attachments, IIW-Document No. XIII-154, (1958).
- [42] Izdinsky O, et. al., Engine room section in the building of river ships and the welding of steel reinforcements to the bottom cover ship. , ZVARANIE VII/12:, (1958) 363-368.
- [43] Miki C, Tateishi K, Fatigue strength of cope-hole details in steel bridges., International journal of fatigue, Vol. 19 No.6: (1997) 445-455.
- [44] Stallmeyer J E, al, e., Behaviour of welded built-up beams under repeated loads., Structural research series No.135, (1957).
- [45] Xiao Z, Yamada K, Fatigue strength of intersecting attachments., Journal of structural engineering ACSE:, (2005) 924-932.
- [46] Lotsberg I, Sigurdsson G, Hot Spot Stress S-N Curve for Fatigue Analysis of Plated Structures., Journal of Offshore Mechanics and Arctic Engineering, 128(4) (2006) 330-336.
- [47] Fisher J W, al., e., Effect of weldments on the fatigue strength of steel beams., Fritz engineering laboratory report No. 334.2, (1969).
- [48] Hall L R, Stallmeyer J E, The fatigue strength of flexural members., Fatigue committee – welding research council., (1959).





# Paper B

## Fatigue strength of cope-hole details in steel bridges

M.Heshmati & M.Al-Emrani

*Submitted to Journal of bridge engineering*



# Fatigue strength of cope-hole details in steel bridges

Mohsen Heshmati\*, Mohammad Al-Emrani

*Chalmers University of Technology, Department of Structural Engineering,  
Sven Hultins gata 8, 412 96, Gothenburg, Sweden*

---

## Abstract

Cope-holes are usually used in field-welded joints in bridge girders to facilitate for the transversal butt welds in the flanges and avoid weld crossing. The size of the cope hole is also chosen to give access for the NDT of the butt welds. Details with cope holes are today determining for the design of steel and composite bridges due to their relatively low fatigue resistance. Therefore an upgrading of the fatigue strength of these details is of great interest to the bridge industry.

The low fatigue strength of details with cope-holes is mainly a result of high stress concentration close to the weld toe which are caused by the cope-hole. In this study, the fatigue strength of welded details with cope holes is studied. Besides the previous fatigue tested reported in the literature, a series of small scale fatigue tests has been performed. The study also includes an examination of the load effects in these details in two existing bridges. Additionally, different methods of improving the fatigue strength of cope-hole details are studied. The effects of altering the geometric shape of cope-holes and the corresponding stress concentration at the probable crack initiation areas are investigated with Finite Element Analysis (FEA). Furthermore, the fatigue strength enhancement of cope-hole details by means of post-weld treatment is evaluated experimentally by conducting constant amplitude fatigue tests. The results of the study show that if the cope holes are positioned in regions of high shear forces, the effect of shear stress should be considered in the fatigue design of the bridge girders. Altering the geometric shape of the cope hole gives very marginal change in the stress concentration at the weld toe. On the other hand, burr grinding gave very

---

\*Corresponding author

*Email address:* heshmati@student.chalmers.se (Mohsen Heshmati)

promising results in term of enhancing the fatigue category of the detail.

*Keywords:*

Fatigue strength, Finite elements, Structural fatigue tests, Post-weld treatment

---

## 1. Introduction

The steel girders in steel and composite bridges for medium and large spans are usually fabricated in several segments due to transportation limitations. Consequently, the steel girder segments have to be assembled on site through welded or riveted connections. When welded connections are used, and in order to facilitate for the transversal butt welds in the flanges and avoid weld crossing, cope-holes are introduced in the girder web, see Figure 1. Additionally, cope-holes give access for the required quality control of the transverse weld in the beam splice through the application of none-destructive testing. Even though, the recent advancements of welding technologies have eliminate the necessity of cope holes in such connections by improving the welding process and material, road and railway administrations in some countries such as Sweden still prefer to use cope-holes in welded girder splices for practical and safety considerations.

From a structural point of view, the existence of cope-holes results in an abrupt reduction of the stiffness of the section which causes high stress concentration close to the weld toe at the intersection of the web and flange. This will lead to a relatively low fatigue strength compared to the other constructional details in a steel bridge girder. Eurocode 3 [1] recommends fatigue design class FAT71 for welded joints with cope-holes in which the design stress is considered based on the nominal stress in the flange at the cope hole. This detail category is lower than that for welded stiffeners and other common welded joints in steel bridge girders. Subsequently the design stress for cope-holes will govern the design of the section at a low stress level which is not economical. Therefore, an increase of the fatigue strength (detail category) of cope-hole details and/or a decrease of the stress concentration in this detail is of great interest.

Fatigue test data on steel details with cope holes is rather limited [2–5]. Further fatigue tests are carried out in this study in order to evaluate the recommended fatigue design class of cope-holes. Besides the conventional nominal stress method, the structural hot spot stress approach and the effec-

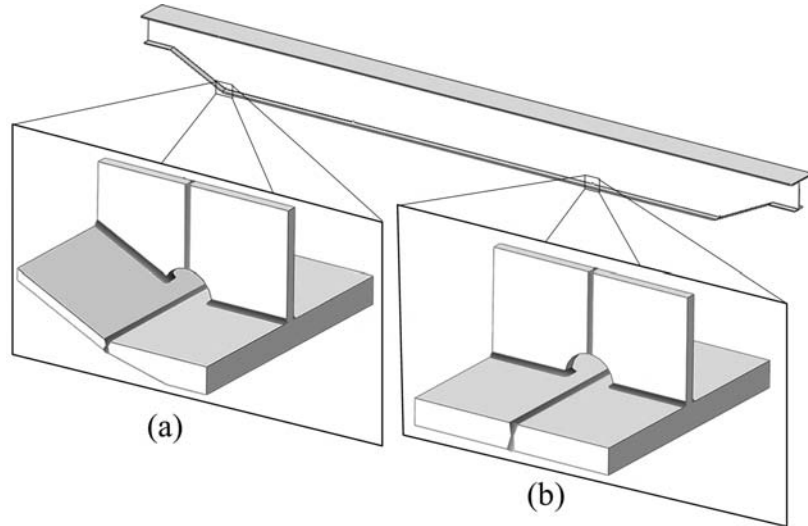


Figure 1: Application of cope-holes in a bridge girder: (a)Cope-hole at a splice due to section change, (b)Cope-hole at a splice due to transportation limitations

tive notch stress method have employed to investigate the validity of recommended design classes based on these approaches. As the last two mentioned methods require finite element analysis, the well-known IIW recommendations [6] are adopted in order for the results to be comparable with previous studies and recommendations [6, 7]. The evaluation of the fatigue test data reveals a noticeable dependency of fatigue life of the detail on the magnitude of shear stresses at the cope-hole section. This phenomenon was previously addressed by Miki and Tateishi [4] where fatigue tests on steel girders with cope holes were reported. Even though the results of the fatigue tests in Miki and Tateishi [4] clearly showed the effect of shear on the fatigue life of cope hole details, the applicability of these results to bridge girders might be doubtful. The test beams had a relatively high depth to span ratio and some of the cope holes were positioned very close to the supports, in high shear force regions, which is quite unlikely to be the case for field splices in real bridge girders.

In order to remove these doubts, the findings of the current study are presented in view of analysis conducted on several existing bridge girders containing cope-holes at various locations.

## 2. Review of existing fatigue tests

The number of available fatigue tests for cope-hole details is limited. In total 29 constant amplitude fatigue test results were found in the literature. All tests, coming from 4 different sources [2–5], were performed on as-welded specimens. In addition to the existing fatigue tests, a new test series was conducted on axially loaded specimens with cope-holes. The test program was aimed at supporting a newly produced guidelines at Chalmers University of Technology (CTH) [8] regarding the fatigue strength of bridge details with cope-holes. Table 1 represents a detailed overview of various test configurations as illustrated in Figure 2.

As listed in Table 2, the fatigue strength of the evaluated cope-hole details is very inconsistent. A closer look at the results in Figure 3 reveals that despite the conspicuous geometrical variation of specimens CH1, CH2 and CTH, these specimens exhibit almost identical fatigue strength. How-

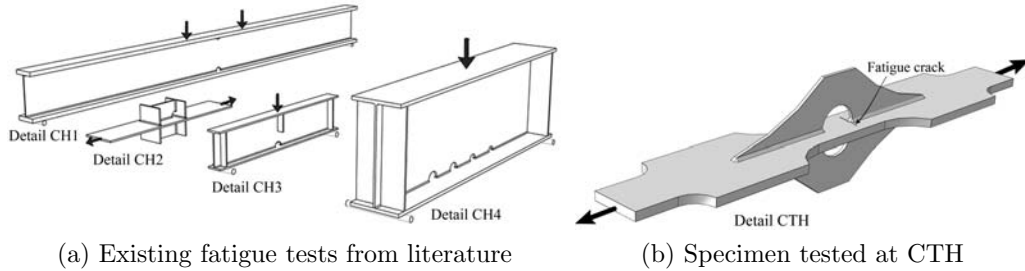


Figure 2: Schematics of various cope-hole test configurations

Table 1: Dimensions and quantity of the evaluated fatigue test specimens for cope-holes; all dimensions are in *mm*.

| Detail | Test data | Main plate |       | Attachment |        | $\tau_a/\sigma_m$ | Ref. |
|--------|-----------|------------|-------|------------|--------|-------------------|------|
|        |           | Thickness  | Width | Thickness  | Radius |                   |      |
| CH1    | 7         | 25.4       | 127   | 4.8        | 25.4   | 0                 | [2]  |
| CH2    | 8         | 9          | 200   | 9          | 35     | 0                 | [5]  |
| CH3    | 7         | 8          | 80    | 6          | 26     | 0.2               | [3]  |
| CH4    | 7         | 16         | 50    | 9          | 25-40  | 0.7-1             | [4]  |
| CTH    | 4         | 20         | 100   | 8          | 50     | 0                 | [8]  |

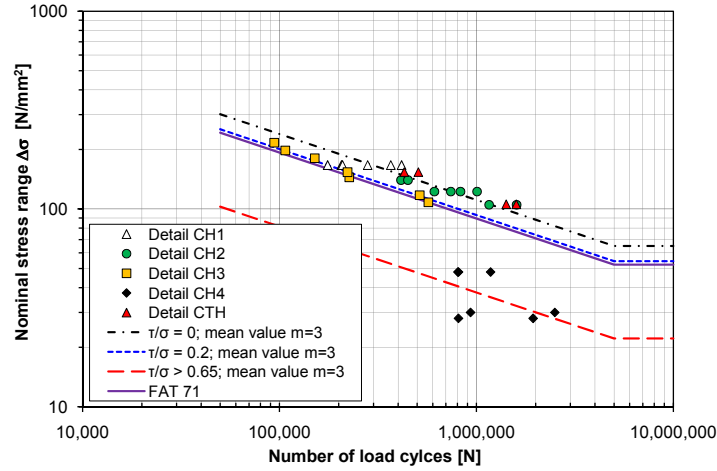


Figure 3: Fatigue test results for cope-hole details distinguished by shear to normal stress ratio

ever, specimen CH4 which is more similar to CH1 shows a dramatic fall in terms of fatigue strength. A more thorough assessment of the tests, reveals a pronounced dependency of fatigue life of cope-hole details on the ratio of shear stress to normal stress in the specimens ( $\tau_a/\sigma_m$ ), see Figure 3. It is clear that the relatively low fatigue strength of the specimens in the test series CH4 is due to the presence of considerable shear stresses in the web at the intersection of flange and web at the weld toe of cope-hole. The destructive effect of shear stresses on the fatigue life of cope-hole details has been previously confirmed in [4]. Therefore, evaluation of the test results, based on the nominal stress in these details, should consider the ratio  $\tau_a/\sigma_m$  as an important parameter that affects the fatigue strength of cope-hole details. While this has been recognized in IIW, the Eurocode 1993-1-9 assigns detail category 71 to cope-hole details irrespective of the ratio  $\tau_a/\sigma_m$ .

When using local approaches it is anticipated that the aforementioned effect should be covered. The test results of all specimens evaluated based on the hot spot stresses are plotted in Figure 4a. It is apparent that although the test data do not lie in one group, the scatter of the results is decreased, compared to the nominal stress method. Linear regression analysis with a fixed slope of 3 yields a standard deviation of 0.281 compared with the value of 0.598 obtained from the nominal stress method. Considering Figure 4b,

Table 2: Statistical evaluation of the cope-hole test results using linear regression analysis with a fixed slope of 3.

| Detail | $\Delta\sigma_{mean}$<br>$N/mm^2$ | $\Delta\sigma_C$<br>$N/mm^2$ | St.d. |
|--------|-----------------------------------|------------------------------|-------|
| CH1*   | 83.8                              | –                            | –     |
| CH2    | 88.9                              | 71.9                         | 0.093 |
| CH3    | 74                                | 64.7                         | 0.055 |
| CH4    | 30                                | 16.7                         | 0.345 |
| CTH    | 95.2                              | 82.7                         | 0.044 |

\* Since all the specimens were tested in one stress range, a statistical evaluation is not possible.

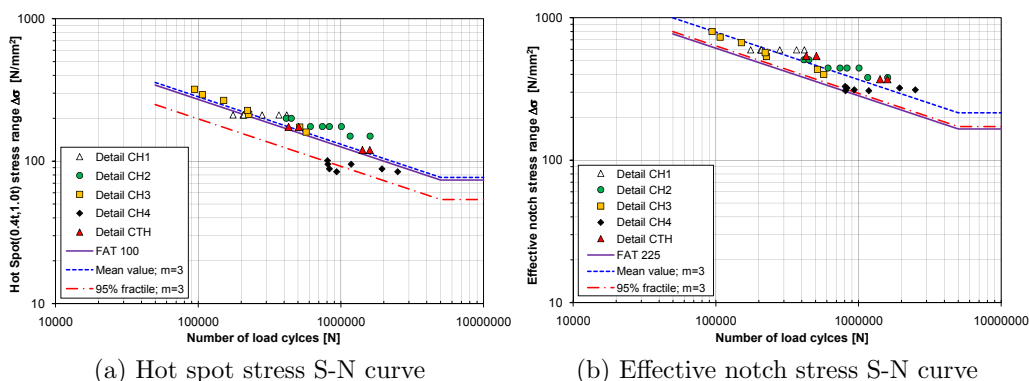


Figure 4: Fatigue test results for cope-hole details according to local approaches

in which the fatigue test data are evaluated with the effective notch stress method, the scatter of the test data is noticeably reduced. All test data lie within the same narrow scatter band. Moreover, linear regression analysis reveals a slope of 2.78 accompanied by a characteristic fatigue strength of 221.1 MPa and standard deviation of 0.158, which is the lowest obtained standard deviation for this detail based on different evaluation methods.

On this basis it may be inferred that the presence of high shear stresses at cope-hole location has a distinct destructive effect on the fatigue strength of this detail. The shear effect is investigated more elaborately in the next section.



### 3. Examination of load effects on bridges

The discussion in this section aims to illuminate the damaging effects of the shear stresses on the fatigue strength of cope-hole details. According to the principles of structural mechanics, the total deflection of any point along a beam which is subjected to an arbitrary loading is composed of two components: bending and shear deformation, see Figure 5a. Although, it has been argued that the deflection due to shear can be generally neglected in long span beams, the local effects of such deformations may be prominent. To illustrate the point clearly, the deformations of a beam section with cope-holes are further studied, see Figure 5b. It is apparent that as a result of the presence of shear, a relative displacement ( $\delta$ ) is induced between the sections before and after the cope-hole. Furthermore, considering that the lateral support of flange provided by web is no longer available in this section, the flange undergoes an additional deformation. In this instance, the flange plate is analogous to a beam with both ends fixed enduring an additional moment ( $M_{add}$ ) due to the relative displacement of the two ends ( $\delta$ ). As demonstrated in Figure 5c, the additional moment introduces secondary

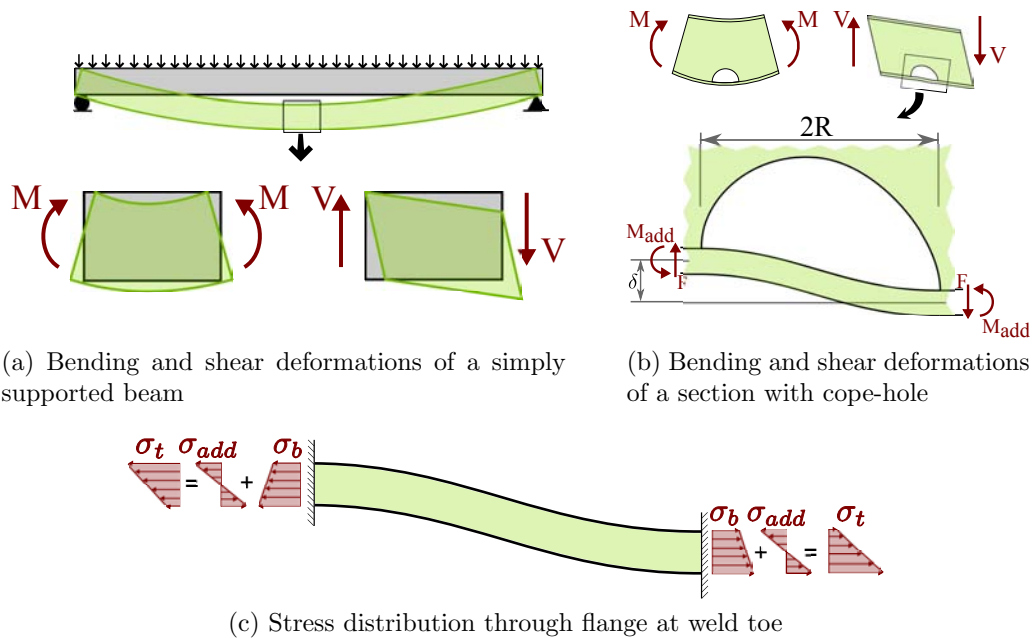


Figure 5: Schematic model for beam deformations

bending stresses ( $\sigma_{add}$ ) through the depth so that the total stress ( $\sigma_t$ ) at the inner surface of the flange at weld toe undergoes abrupt variations. The total stresses at the cope-hole weld toe on the inner surface of a flange at the tension side increases at one end and decreases at the other end. This peculiarity of stress state at a cope-hole section instigates the weld to experience higher stresses than the anticipated design ones.

To enlighten the importance of stress variations at cope-hole sections due to shear deformation, the discussed model is investigated numerically. The relative deformation of ‘beam’ ends can be obtained by subtracting the shear deflection of the sections before and after the cope-hole. For a cope-hole with radius  $R_{cp}$  located at  $x = L_1$  it yields

$$\delta = \omega_S(L_1 + R_{cp}) - \omega_S(L_1 - R_{cp}) \quad (1)$$

where

$$\omega_S(x) = \frac{V(x)}{GA_s} \quad (2)$$

and the shear area ( $A_s$ ) for an arbitrary section can be calculated based upon the conservation of energy law as follows

$$\frac{1}{2} \frac{V^2}{GA_s} = \frac{1}{2} \int \frac{\tau^2}{G} dA \quad (3)$$

Having obtained  $\delta$ , the additional moment can be obtained using Euler-Bernoulli beam theory as

$$M_{add} = \frac{6EI_f \delta}{(2R_{cp})^2} \quad (4)$$

However, further investigations have confirmed that the  $2R_{cp}/t_f$  and the  $\tau_a/\sigma_m$  ratios have also a considerable effect on stress redistributions through the flange depth. In order to consider the secondary stress redistribution, further finite element analysis of a satisfactory number of cope-hole details were performed. According to the results, the additional stress at the edges of the beam with a normalized cope-hole detail with  $R_{Ref} = 25mm$ , can be obtained from:

$$\sigma_{add} = \frac{M_{add} t_f}{2I_f} \frac{\tau_a}{\sigma_m} \frac{2R_{cp}}{t_f R_{ref}} \quad (5)$$

As can be seen, by introducing a normalized cope-hole radius, the results can be linearly extrapolated for any other cope-hole detail geometry. However, as also mentioned by Eurocode 3, the cope-hole radius has to be limited to

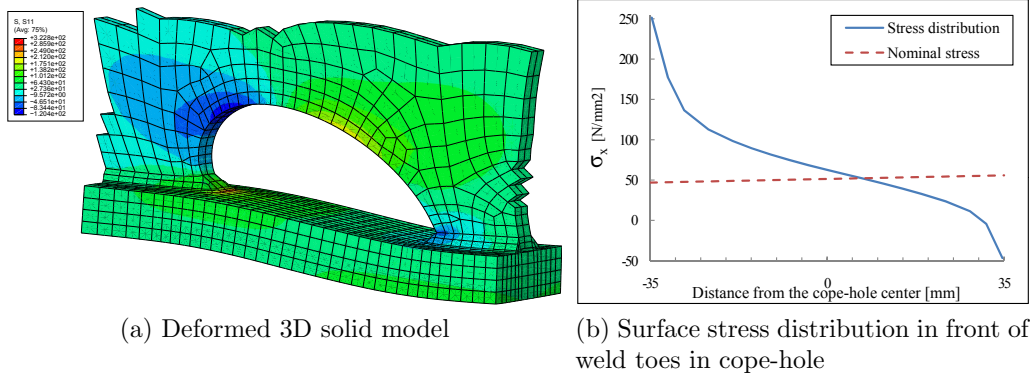


Figure 6: FEA results of a cope-hole subjected to high shear stresses

less than 60mm. From Equations 4 and 5, the additional stress at the inner edge of the flange at the weld toes is given by

$$\sigma_{add} = \frac{3}{4} \frac{Et_f \delta}{R_{cp}^2} \frac{\tau_a}{\sigma_m} \frac{2R_{cp}}{t_f R_{ref}} \quad (6)$$

Eventually, the total utilized stress at the weld toes of cope-hole is obtained through superposition

$$\sigma_t = \sigma_b \pm \sigma_{add} \quad (7)$$

In order to further evaluate the proposed model, finite element analysis of several beams with cope-holes are performed. Figure 6 shows the FEA results of a cope-hole located in a region of high shear stress in a bridge girder. It is apparent that the proposed shear deformation model is valid and that stresses at weld toes are affected by the high shear stresses in the girder at the location of the cope hole.

Evaluating the results from the FE-models, it is found that by modifying the nominal stress according to Equation 7 for bridge girders with cope holes located in regions with high shear stresses, the shear effect should be implicitly covered. In addition and in order to investigate the capability of the model to capture the effect of shear stress on the fatigue life of the studied detail, the previously discussed tests reported in [4] are re-analyzed. The mentioned test specimens were tested under severe shear stresses and consequently exhibited relatively poor fatigue strength. However, as plotted in Figure 7, when correcting the nominal stress at the cope hole according to the proposed model, the data are found to lie within the scatter band of all

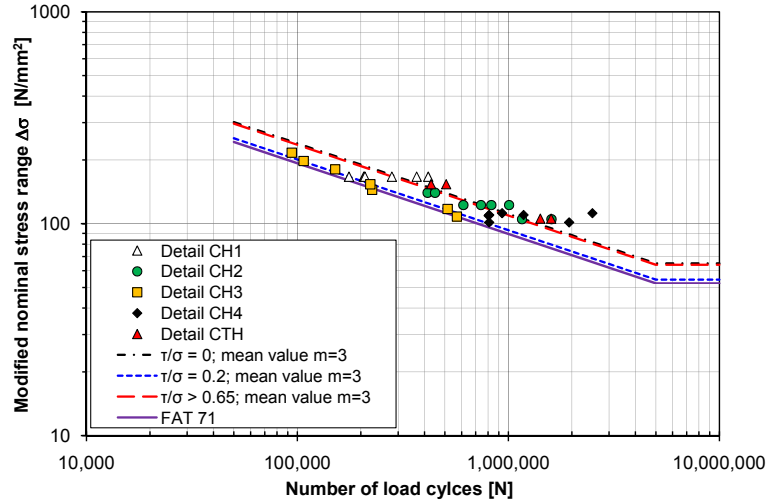


Figure 7: Fatigue test results for cope-hole details according to modified nominal stress

other tests, cf. Figure 3. This observation confirms the fact that when using a modified nominal stress for cope-holes a single design FAT class can be used irrespective of loading conditions. More important, it was clear that the calculated modified nominal stresses for this test series are up to three times larger than the conventional nominal stresses, i.e. when the shear effects are not considered. This is an evidence of the significance of stresses induced by shear deformations.

A survey, including a railway and a traffic bridge, is conducted to illuminate the ambiguities of load effects in existing bridges. The results of this study appears to reaffirm the proposed model for additional stress calculation. Moreover, as there is no conclusive criterion regarding the splices location, cope-holes are prone to endure high  $\tau_a/\sigma_m$  ratios e.g. splices close to mid support in multi-span bridges. In conclusion, the shear effect must be recognized and considered in fatigue design of bridges with cope-hole details.

#### 4. Cope-hole shape effect

The performed finite element analysis of the studied specimens with cope-holes revealed that the weld toes at introduced gap experience severe stress concentrations. Therefore, it is anticipated that by altering the cope-hole shape and consequently the local stress distribution around it, an enhancement in fatigue strength would be achieved. In order to investigate the local stress distribution in cope-holes with different shapes, FE analysis has been carried out on beams with four disparate cope-hole shapes as shown in Figure 8.

As a result of the applied loading configuration, the cope-hole in the middle experiences merely bending stresses, whereas the side holes are subjected to a combination of shear and bending stresses. The  $\tau_a/\sigma_m$  ratio is highest for

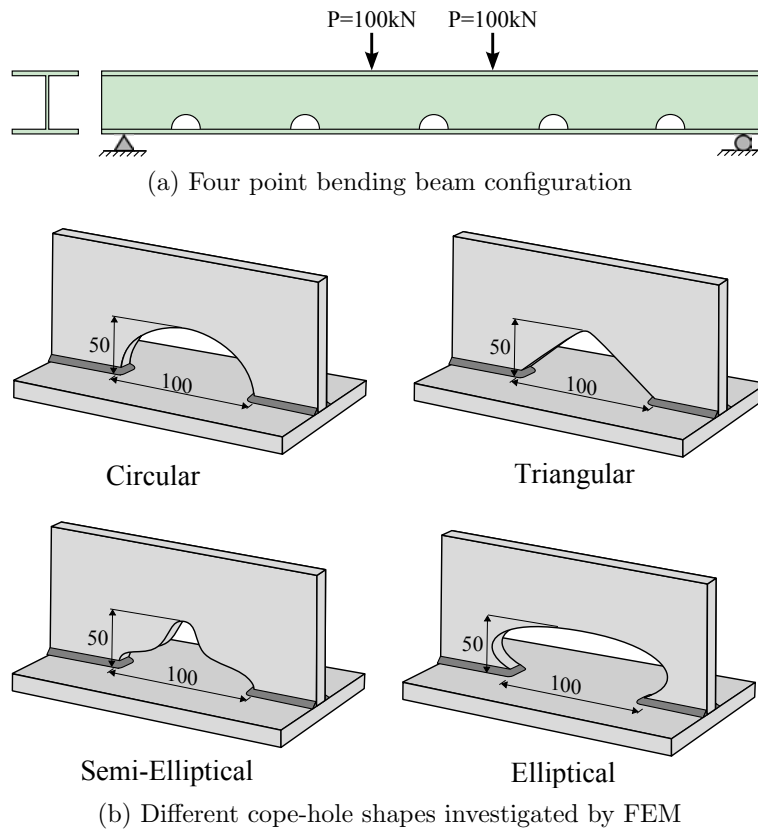
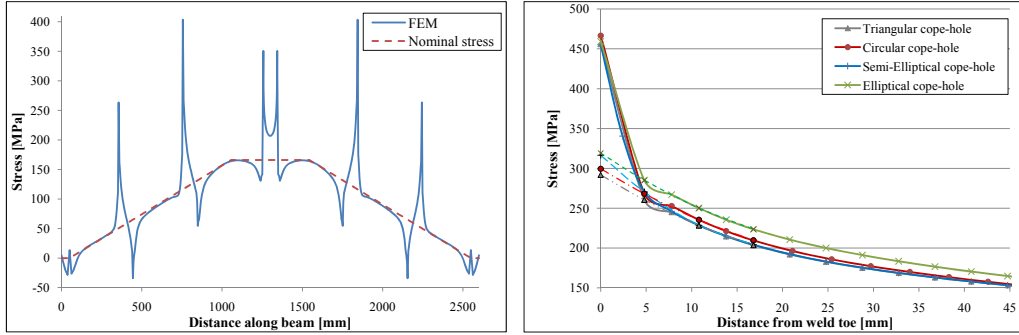


Figure 8: Cope-hole shape effect investigated models; All dimensions in *mm*.



(a) Stress distribution along the beam with circular cope-holes (b) Stress distribution and extrapolated hot spot stress in front of second cope-hole for different cope-hole shapes

Figure 9: Influence of loading and shape type on stress distribution

the cope-holes closest to the support.

As it is apparent from Figure 9a, for the cope-holes located in shear-present regions, the normal stress derived from FEM notably rises on the side of the cope-hole closer to the support and drops on the other side. On the other hand, the center cope-hole experience a symmetric stress distribution with stress peaks at the weld toes.

Figure 9b illustrates the stress distribution in front of the second cope-hole for different cope-hole shapes. A quadratic extrapolation of the stresses according to IIW recommendations [6] has been done to obtain structural hot spot stress at the weld toe as an acceptable criterion to compare different shapes. It is apparent that the triangular cope-hole exhibits the lowest hot spot stress while the highest stress belongs to the elliptical cope-hole. The higher hot spot stress for elliptical shape is a result of the more reduction in the cross section stiffness at cope-hole ends which consequently causes a higher additional stress.

Table 3 represents a comparison of hot spot stress concentration factors (SCF) for different cope hole shapes. The presented data confirms the unfavorable effect of using elliptical cope-holes, whereas the lowest SCF is obtained for triangular cope-holes. Further analysis reveals that an increase of 31.2% in fatigue life can be obtained by using triangular cope-holes instead of conventional circular ones. However, due to the fact that fatigue tests are usually accompanied by a large scatter, it is anticipated that the achieved improvement would be negligible.

Table 3: Comparison of fatigue strength for cope-holes with disparate shapes

| Cope-hole shape | Hot spot SCF |             |             | Fatigue life variation |             |             |
|-----------------|--------------|-------------|-------------|------------------------|-------------|-------------|
|                 | First hole   | Second hole | Center hole | First hole             | Second hole | Center hole |
| Circular        | 3.24         | 2.42        | 1.79        | –                      | –           | –           |
| Triangular      | 3.15         | 2.36        | 1.63        | +9%                    | +8.1%       | +31.2%      |
| Semi-Elliptical | 3.43         | 2.56        | 1.73        | -15.4%                 | -15.2%      | +11.2%      |
| Elliptical      | 3.42         | 2.58        | 1.89        | -14.5%                 | -17.3%      | -14.6%      |

## 5. Post weld treatment of cope-hole details

There are many weld toe improvement techniques which are applicable to fatigue life enhancement of welded connections. Some of these techniques are also used in the bridge industry. The weld toe grinding, TIG dressing and hammer peening are among those methods which appear to offer the most potential for the bridge structure applications.

Kirkhope et al. experimentally investigated the aforementioned improvement techniques for a detail with cope-hole and concluded that a considerable level of improvement can be expected such that for toe grinding and TIG dressing treatments an increase of 120% and for hammer peening an increase of 300% in terms of fatigue life was obtained. However, field-application feasibility and cost efficiency of these methods are other decisive parameters for bridge industry. According to [9, 10] the Burr Grinding (BG) method requires the least operator experience and is the least costly technique.

To date, the codes and guidelines recommendations regarding the fatigue design of post-weld treated details are controversial. A universally accepted S-N curve is missing and treatment application instructions are incomplete. In order to determine the fatigue strength of BG treated cope-hole details, four test specimens identical to Figure 2b were BG treated and tested. Figure 10 shows the weld toes of a BG treated and an AS welded cope-hole. It was observed that for all AS welded specimens the crack initiated at the weld toe of cope-hole and propagated until full rupture of the specimen. On the other hand, 3 out of 4 treated specimens failed due to root cracking of welds at the cope-hole section while only for one the crack initiated prematurely at the weld toe. Furthermore metallurgical investigations of the latter

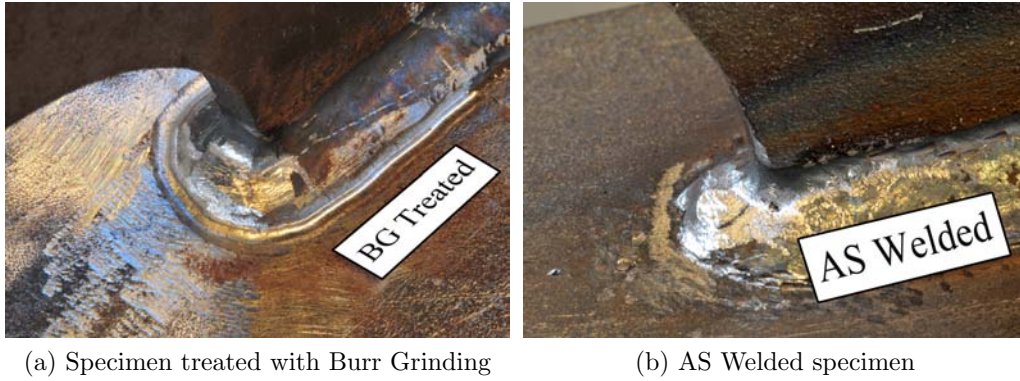


Figure 10: Cope-hole specimens tested at CTH

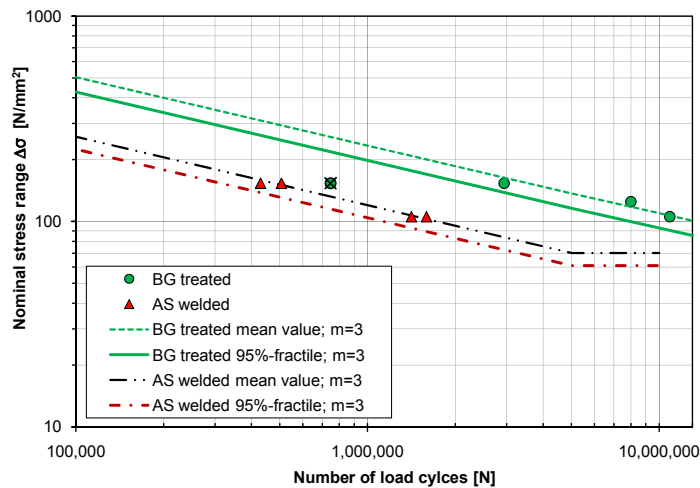


Figure 11: Fatigue test results of cope-hole details tested at CTH

specimen revealed that the weld toe failure was mainly as a result of pre-existing cracks formed due to improper treatment. The test results of all specimens are plotted in Figure 11 where the treated specimen failed at weld toe is marked with a cross. The results support the notion raised in other research that the treatment is more effective at high cycle fatigue. Statistical evaluation of the treated specimens test results, excluding the failure case due to improper treatment, indicates a slope of 3.55 and standard deviation of 0.098. When using a fixed slope of 3, a characteristic design value of



157.4 MPa is derived. This value indicates an increase of 190% in terms of fatigue strength compared to AS welded specimens.

## 6. Concluding remarks

The following conclusions can be drawn:

- A cope-hole specimen is a structural detail used to prevent weld crossing and facilitate weld quality control in splices.
- Cope-hole details are design governing details in bridge girders due to their low fatigue strength.
- The evaluation of existing test data seemed to reaffirm the IIW design FAT class for cope-hole details.
- The evaluation of existing fatigue test data reveals a dependency of the results to the  $\tau_a/\sigma_m$  ratio.
- The findings regarding the shear attributed effect appear to support the mentioned dependency. This effect is further investigated for existing bridge sections and the findings confirm the significance of shear deformation induced stresses even for such stiff sections.
- Cope-hole shape effect is also investigated in order to evaluate the achievable extent of enhancement in fatigue strength by altering the cope-hole shape. It is apparent that although the cope-hole shape has an effect on local stress distribution in front of cope-hole, it is not high enough to be recognizable in fatigue test data.
- Post-weld treatment effects on cope-hole details are evaluated experimentally. The test results show an increase of 190% in terms of fatigue strength (Approximately 6.9 times higher fatigue life) for cope-holes treated with Burr Grinding.

## 7. Acknowledgments

The research has been carried out at the Division of Structural Engineering of the Department of Civil and Environmental Engineering at Chalmers University of Technology. The work presented in this research is a part of the

research project BriFag - Bridge Fatigue Guidance with a financial grant from the Research Fund for Coal and Steel (contract No. RFSRCT-2008-00033) as well as the Swedish Transport Administration.

## References

- [1] Eurocode3, Design of steel structures - Part 1-9: Fatigue, European Standard, 2005.
- [2] J. Stallmeyer, J. Fisher, Behavior of welded built-up beams under repeated loads, Civil engineering studies: Structural research series, Dept. of Civil Engineering, University of Illinois, 1958.
- [3] O. Izdinsky, ZVARANIE 2 (1958) 363–368.
- [4] C. Miki, K. Tateishi, International Journal of Fatigue 19 (1997) 445–455.
- [5] Z. Xiao, K. Yamada, Journal of Structural Engineering 131 (2005) 924–932.
- [6] A. Hobbacher, Recommendations for fatigue design of welded joints and components, IIW document No, Technical Report, IIW-1823-07. International Institute of Welding, December 2008.
- [7] W. Fricke, International Institute of Welding (2008).
- [8] M. Heshmati, Fatigue life assessment of bridge details using finite element method, Master's thesis, Chalmers University of Technology, 2012.
- [9] K. Kirkhope, R. Bell, L. Caron, R. Basu, K.-T. Ma, Marine Structures 12 (1999) 447 – 474.
- [10] K. Kirkhope, R. Bell, L. Caron, R. Basu, K.-T. Ma, Marine Structures 12 (1999) 477 – 496.

# Paper C

## Fatigue design of plated structures using structural hot spot stress approach

M.Heshmati & M.Al-Emrani

*Accepted publication and oral presentation 6th Int. Conference on Bridge  
Maintenance, Safety and Management*

*IABMAS 2012*



# Fatigue design of plated structures using structural hot spot stress approach

M.Heshmati & M.Al-Emrani

*Chalmers University of Technology, Gothenburg, Sweden*

In most fatigue design codes, the nominal stress method is the predominant approach for fatigue design of structures. However, the known limitations of this method along with new advanced computational possibilities, have paved the way to search for more accurate stress based fatigue design approaches. The structural hot spot stress approach (SHSS) is one of these methods which has drawn a wide-spread attention since its advent. The SHSS designates the basic stress by taking into account the geometrical variations of the detail at the location of expected fatigue crack initiation (hot spot). In this paper, the fatigue strength of several frequently used structural details is investigated using both nominal stress and SHSS approaches. The aim of this investigation is to establish an equivalency between these two approaches with reference to the fatigue strengths of the studied details. A large database including available fatigue test results (from 1950s till present) is built up and used to produce hot spot stress S-N curves for the studied details.

## 1 INTRODUCTION

The nominal stress method has been the most widely used fatigue assessment method in the field of structural engineering for decades. This method is generally referred to as the classic fatigue assessment method. The ease of use for versatile structural details and the acceptable accuracy, compared to the work effort, are some advantages of this approach. However, the implementation of more complicated details in steel structures on the one hand, and the increasing demand for more efficient and accurate design methods on the other hand, has caused new limitations for designers to use the nominal stress method. Some of these limitations are remarked in the following paragraphs.

When using nominal stress method, the constructional detail and load type should fall under one of the design classes that are provided by the code. Nevertheless, not all structural details are listed in current fatigue regulations. Thus, in order to obtain a design class for such details, new laboratory tests should be carried out. After performing statistical analysis of the test results, the data can be consolidated into an S-N curve for that detail. This procedure is indeed expensive, time consuming and cumbersome.

Another limitation of nominal stress method is that in more complex structural details, the nominal stress is often affected by various macro geometrical

factors which make the task of defining a correct nominal stress very difficult, if not impossible. On the other hand, the growing use of finite element analysis in the new modern design workflow makes it even vaguer to distinguish the nominal stress in the vicinity of the welded joint. This is due to the fact that, finite element analysis, by definition, determines notch stress and not nominal stress. According to Hobbacher (2009), up to now, none of the available codes or guidelines has given explicit instructions of how to determine the nominal stress from FE results. The methods to determine nominal stress from FE results basically left to the engineering judgment of the designer.

Last but not least, the fatigue life of some details depends on the geometrical properties of the joint such as the length of attachment, transition radius, etc. For such details, IIW or Eurocode 3, usually define several FAT classes for different geometric combinations. The fatigue life, consequently, exhibits a stepwise trend whereas it is, in reality, continuous.

All these short comes and limitations make the application of the nominal stress method in some cases complicated, less accurate and less efficient.

The hot spot stress concept was first introduced for the fatigue design of tubular structures decades ago. Over the years, the advantages of this approach compared to the traditional nominal stress method provoked design associations to introduce guidelines and instructions regarding fatigue design of plated

structures using hot spot stress as well. By definition, the structural hot spot stress approach (SHSS) designates the basic stress, including stress concentration effects caused by geometrical variations of the detail at the expected fatigue crack initiation area (hot spot). SHSS disregards the notch effect caused by the weld profile and comprises all other geometric parameters. Hence, one hot spot stress S-N curve can be associated to several details.

The hot spot stress  $\sigma_{\text{Hot spot}}$  can be directly calculated from finite element analysis (FEA) as follows:

$$\sigma_{\text{Hot spot}} = K \cdot \sigma_{\text{Nominal}} \quad (1)$$

where K is the structural stress concentration factor derived from the FEA.

The results of several three-dimensional FEA have shown that certain instructions regarding the element types and meshing techniques should be followed in order to obtain comparable results.

In this paper, a large number of fatigue test data of frequently used details in plated steel structures are collected and used to produce nominal stress S-N curves. The results are discussed and compared with the IIW and Eurocode 1993-1-9 recommendations. The FEA instructions given by international welding institute (IIW) are adapted in order to create three-dimensional solid models with fine meshes. Both linear and quadratic extrapolation methods are exploited in order to obtain hot spot stress S-N curves. Eventually, an equivalency between these two approaches with reference to the fatigue strengths of the studied details is established.

## 2 FATIGUE EVALUATION OF PLATED DETAILS

### 2.1 Longitudinal non-load-carrying attachments

Longitudinal non-load-carrying attachments are commonly used in many fatigue loaded structures such as ships, cranes, offshore structures and bridges. The universal use of this type of attachment has made it one of the most frequent fatigue tested details. However, although the extensive number of available fatigue tests may facilitate the evaluation of their fatigue strength, these tests might include irrelevant and/or unsuitable test data. Therefore, in order to derive any valid conclusions, the test data should be first categorized and filtered. In the current study, after an initial evaluation of the whole available test data, a total number of 286 specimens are selected for further evaluations. In the initial evaluation phase, inappropriate test data such as tests with post-weld treatment, unusual ambient temperatures, negative stress ratios etc. were excluded. Table 1 lists a summary of the approved fatigue test series as depicted in Figure 1.

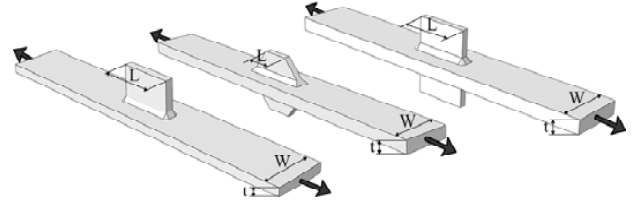


Figure 1. Different Longitudinal attachment test configurations

As the fatigue strength of plates with longitudinal non-load-carrying attachments is known to be a function of the length of the attachment plate, the test results were primarily categorized according to the attachment length, in five different classes.

Table 1. Dimensions and quantity of evaluated fatigue test specimens for longitudinal attachments; all dimensions are in mm.

| Attachment length | Test data | Main Plate |          | Attachment |        |
|-------------------|-----------|------------|----------|------------|--------|
|                   |           | Thickness  | Width    | Thickness  | Length |
| L = 200           | 10        | 4          | 100      | 4          | 200    |
| L = 150           | 193       | 4.8-25.4   | 75-100   | 4.8-25.4   | 150    |
| L = 100           | 55        | 10-25      | 80-152.4 | 10-25      | 100    |
| L = 60            | 11        | 16         | 90       | 16         | 60     |
| L = 50            | 17        | 8          | 80       | 8          | 50     |

#### 2.1.1 Evaluation according to the nominal stress method

The results from evaluating the test results based on the nominal stress method are presented in Table 2. It is clear that for specimens with attachment plates having a length up to 150 mm, FAT71 seems to provide a good representation for the fatigue strength of the detail. This complies very well with the recommendations in IIW. For test data with L=200, the evaluated fatigue strength at 2 million cycles is below the recommended FAT-category 63. Nevertheless, this category is only composed of one test series in which the main plate is very thin. Therefore, it is anticipated that by including more test data the characteristic value may improve. However, according to the tests evaluated in this study, the recommended FAT class of 63 seems to be unreliable. The test data are plotted in Figure 2.

Table 2. Statistical evaluation of longitudinal attachments test results using linear regression analysis with a fixed slope of 3.

| Configuration | $\Delta\sigma_{\text{mean}}$<br>N/mm <sup>2</sup> | $\Delta\sigma_c$<br>N/mm <sup>2</sup> | Standard deviation |
|---------------|---|---------------------------------------|--------------------|
| L = 200       | 75.4  | 56.9                                  | 0.157              |
| L = 150       | 88.7  | 75.9                                  | 0.123              |
| L = 100       | 91.3  | 73.6                                  | 0.164              |
| L = 60        | 85.8  | 77.9                                  | 0.056              |
| L = 50        | 88.6  | 77.3                                  | 0.088              |

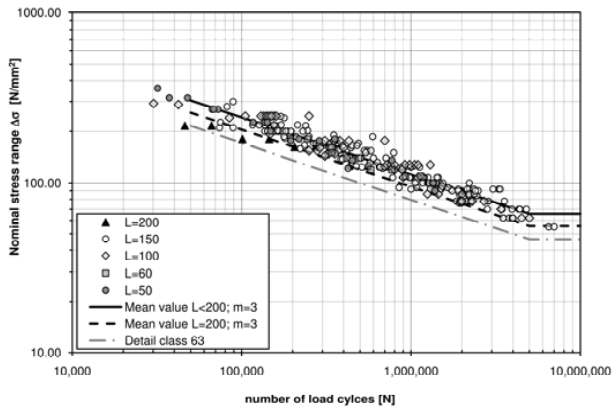


Figure 2. Fatigue test results for longitudinal attachments distinguished by length of attachment

### 2.1.2 Evaluation according to the hot spot stress approach

The collected fatigue test data for this detail dates back to 1950. As a result, a good documentation of the tests is missing in some cases. The weld leg length was one of the parameters that were missing in most of the tests. Therefore, since the whole geometry including the welds had to be modeled, the effect of weld leg length size variation on the stress concentration in the detail was investigated.

The results show that varying the weld leg length from 5 to 15 mm alters the calculated structural stress concentration factor with less than 5%. Nevertheless, as recommended by IIW, a minimum weld throat thickness equal to one third of the main plate thickness was assumed where the weld size was unknown.

Moreover, the effect of the main plate width on the fatigue strength of longitudinal attachments is also investigated. As shown in Figure 3, as the main plate becomes wider, the K factor increases. This effect is more pronounced for plates with the width of 50 to 150 mm. Since most of the tests have a plate width in the mentioned range, it is recommended to consider this parameter as well for evaluation based on the nominal stress method.

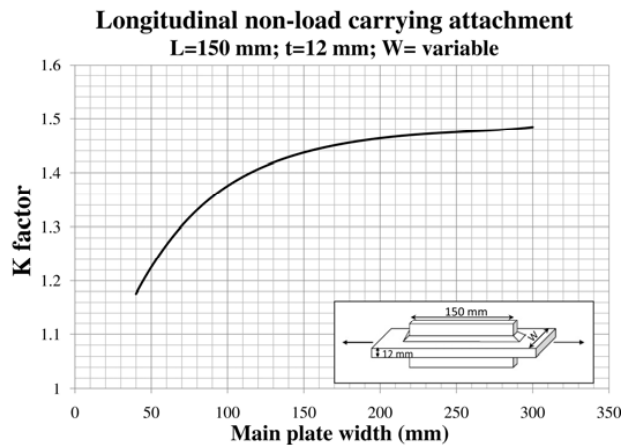


Figure 3. K factor as a function of main plate width

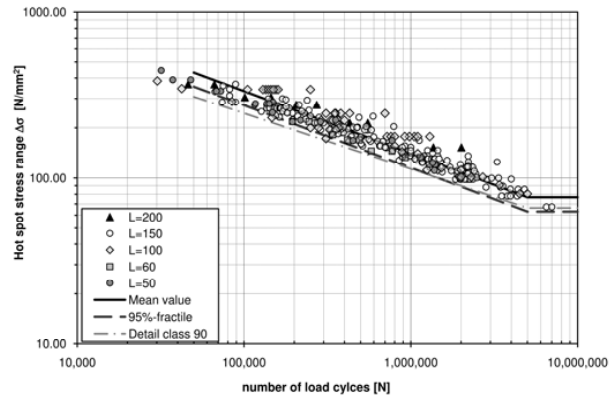


Figure 4. Fatigue test results for longitudinal attachments according to the hot spot stress approach

The test results for the hot spot stress approach are plotted in Figure 8. In this figure quadratic extrapolation of the hot spot stress has been used. The standard deviation is 0.138 and the slope 2.67 evaluated with free linear regression. The characteristic strength is 88.8 MPa. With a fixed slope of 3 the standard deviation becomes 0.150 and the characteristic fatigue strength is 94.2 MPa. Linear extrapolation was also examined for this detail, giving a standard deviation of 0.150 and characteristic fatigue strength of 93.1 MPa. Considering the results in Figure 3 it seems that FAT-category 90 should be used for this detail instead of the FAT100 which is recommended by the IIW.

### 2.2 Over-lapped joints with crack at main plate

Longitudinally loaded over-lapped joints with side welds are usually used in fatigue loaded structures to join different sections to the gusset plate.

The evaluation of fillet welded overlapped joints included 19 test specimens of which 10 failed in the main-plate and 9 in one of the cover-plates. Since the failure types and consequently the hot spot stress evaluation methods are substantially different, the evaluation of this detail is presented separately. Figure 5 demonstrates two different examined test specimens that had failed from the weld toe at the main plate. The geometrical parameters that are considered for this detail are given in Table 3.

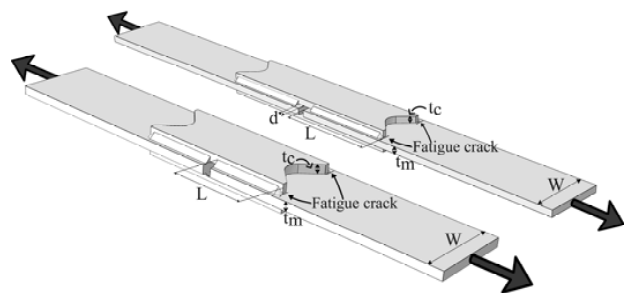


Figure 5. Different configurations of over-lapped joints

Table 3. Dimensions and quantity of evaluated fatigue test specimens for over-lapped joint with crack at main plate; all dimensions are in mm.

| Detail | Test data | Main plate |       | Cover plate |       | d    |
|--------|-----------|------------|-------|-------------|-------|------|
|        |           | $t_m$      | W     | $t_c$       | L     |      |
| 2A     | 5         | 12.7       | 114.3 | 12.7        | 108   | 0    |
| 2B     | 5         | 12.7       | 114.3 | 12.7        | 171.5 | 12.7 |

### 2.2.1 Evaluation according to the nominal stress method

As it is shown in Figure 6, the fatigue strength of over-lapped specimens with longer cover plates (2B) is slightly higher than the specimens in series 2A. The dependency of fatigue life on the weld length has been recognized by Eurocode as well.

Statistical analysis of the test results reveals mean values for the fatigue strength of 73.4 MPa for detail 2A and 82.9 MPa for detail 2B. The characteristic value of all the test data according to the nominal stress method is 61.8 MPa with a standard deviation of 0.135. The obtained value is consistent with FAT 56 recommended by Eurocode.

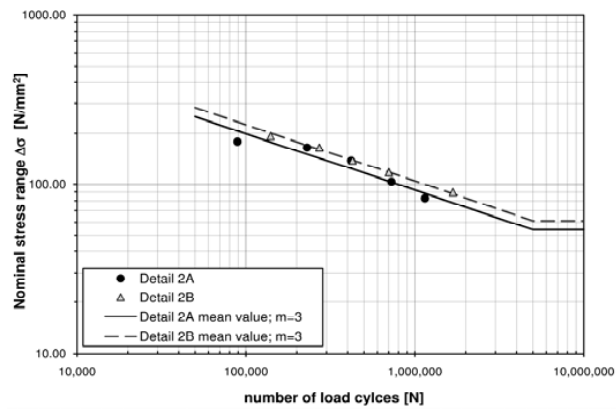


Figure 6. Fatigue test results for over-lapped joints with crack at main plate distinguished by detail type

### 2.2.2 Evaluation according to the hot spot stress approach

The hot spot stress S-N curve for over-lapped joints with crack at main plate are plotted in Figure 7.

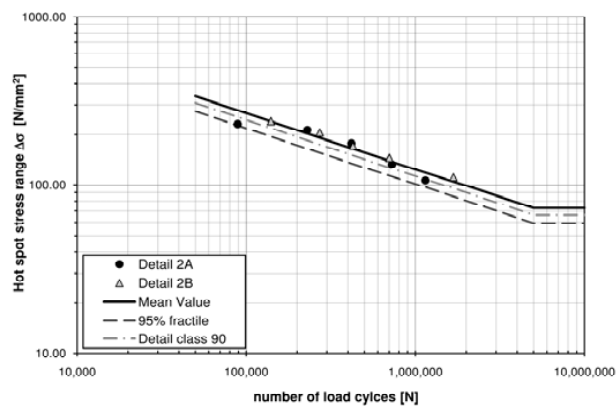


Figure 7. Fatigue test results for over-lapped joints with crack at main plate according to the hot spot stress approach

A linear regression analysis affirms a reduced standard deviation to 0.120 for all the data in this case.

The characteristic value for fatigue strength is 80.3 MPa which is lower than the recommended FAT100 strength in the IIW. The number of available tests is of course rather limited. Quadratic extrapolation is recommended for this detail as the stress increases very rapidly at the crack initiation point.

### 2.3 Over-lapped joints with crack at cover plate

A total number of 9 over-lapped specimens with cracking in the cover plate are evaluated in this section. The test data includes specimens with two different weld lengths (L). Table 4 lists the quantity and dimensions of the evaluated test data as shown in Figure 8.

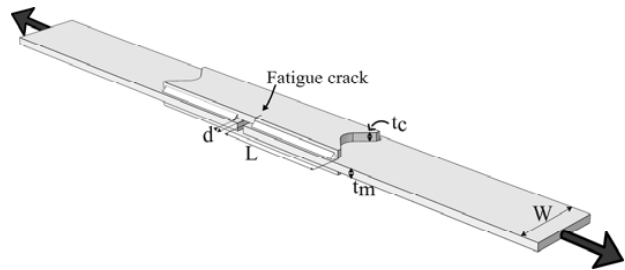


Figure 8. Schematic drawing of over-lapped joints with crack at cover-plate

Table 4. Dimensions and quantity of the evaluated fatigue test specimens for over-lapped joint with crack at cover plate; all dimensions are in mm.

| Detail | Test data | Main plate |       | Cover plate |       | d    |
|--------|-----------|------------|-------|-------------|-------|------|
|        |           | $t_m$      | W     | $t_c$       | L     |      |
| 3A     | 4         | 12.7       | 114.3 | 9.5         | 95.25 | 0    |
| 3B     | 5         | 12.7       | 114.3 | 9.5         | 171.5 | 12.7 |

#### 2.3.1 Evaluation according to the nominal stress method

The nominal stress evaluation results for the over-lapped joints with crack at cover plate are demonstrated in Figure 9. Similar to the case with crack at main plate, the longer plates exhibit an insignificant higher fatigue life.

The standard deviation when all tests are considered is 0.151 when performing a linear regression analysis with a free slope, giving a mean value of 57.3MPa and a characteristic value of 46.4MPa. With a fixed slope of 3, the characteristic value is calculated to 41.1MPa with a standard deviation increasing to 0.169. It is worth mentioning that both Eurocode and IIW neglect the plate length effect and recommend design classes 45 and 50 respectively. While the Eurocode recommendation appears to be a good representation, the IIW suggested FAT class



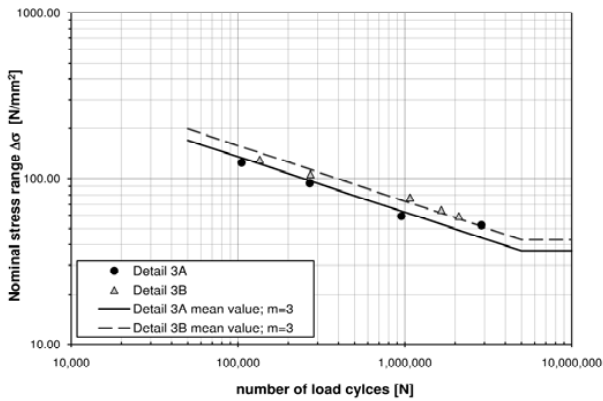


Figure 9. Fatigue test results for over-lapped joints with crack at cover plate distinguished by detail type

seems to be optimistic, when the tests at hand are evaluated.

### 2.3.2 Evaluation according to the hot spot stress approach

As it is shown in Figure 10, the scatter of the test data seems to be reduced when the hot spot stress is used, and the two test groups lie within a narrow scatter band. Linear regression analysis reveals a meaningful reduction of standard deviation to 0.109 when using a free slope. With a fixed slope of 3 the characteristic value becomes 98.9MPa.

According to IIW, the hot spot stress type of this specimen is specified as type b. However, neither IIW nor Eurocode suggest a FAT class base on the hot spot stress for this detail (i.e. for cracking at weld ends). Considering the evaluated tests in this study, FAT100 appears to give good representation. However, more test data on similar details with various configurations of different lengths and thicknesses are needed before a firm conclusion can be made.

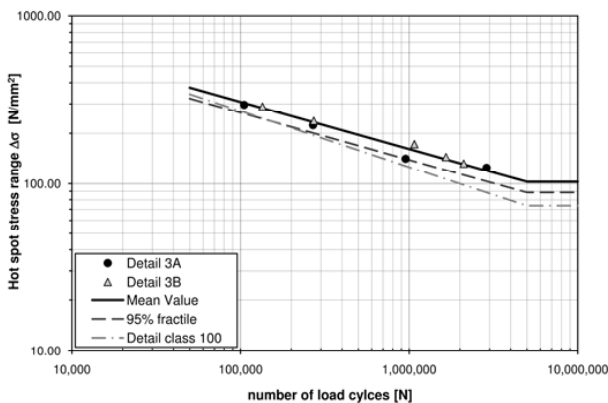


Figure 10. Fatigue test results for over-lapped joints with crack at main plate according to the hot spot stress approach

## 2.4 Cope-hole details

Cope-holes are usually used in field-welded joints in bridge girders to facilitate for the transversal butt welds in the flanges and to avoid weld crossing. The size of the cope-hole is also chosen to give access for the NDT of the butt welds. Constant amplitude fatigue test results of 29 different specimens from 4 different sources have been collected to evaluate this detail. Table 5 represents a detailed overview of various test configurations as illustrated in Figure 11.

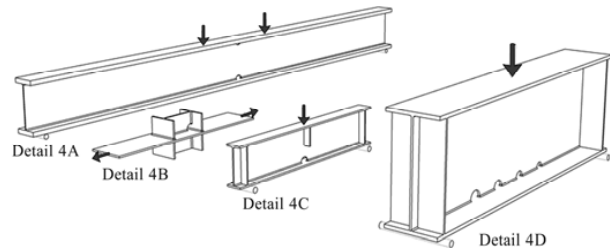


Figure 11. Different cope-hole test configurations

Table 5. Dimensions and quantity of the evaluated fatigue test specimens for cope-holes; all dimensions are in mm.

| Detail | Test data | Main plate |       | Attachment |        | $\tau_a/\sigma_m$ |
|--------|-----------|------------|-------|------------|--------|-------------------|
|        |           | Thickness  | Width | Thickness  | Radius |                   |
| 4A     | 7         | 25.4       | 127   | 4.8        | 25.4   | 0                 |
| 4B     | 8         | 9          | 200   | 9          | 35     | 0                 |
| 4C     | 7         | 8          | 80    | 6          | 26     | 0.2               |
| 4D     | 7         | 16         | 250   | 9          | 25- 40 | 0.7-1             |

### 2.4.1 Evaluation according to the nominal stress method

As listed in Table 6, the fatigue strength of the evaluated cope-hole details is very inconsistent. A closer look at the results in Figure 12 reveals that despite the conspicuous geometrical variation of details 4A and 4B, they exhibit almost identical fatigue strength. However, detail 4D which is more similar to 4A shows a dramatic fall in terms of fatigue strength. A more thorough assessment of the tests, reveals a pronounced dependency of fatigue life of cope-hole details on the ratio of shear stress to normal stress in the specimens ( $\tau_a/\sigma_m$ ), see Figure 12. It is clear that the relatively low fatigue strength of details in the test series 4D is due to the presence of considerable shear stresses at the anticipated crack location i.e. weld toe at cope-hole section. The destructive effect of shear stresses on the fatigue life of cope-hole details has been previously confirmed by Miki & Tateishi (1997). Therefore, evaluation of the test results, based on the nominal stress in these details, should consider the ratio  $\tau_a/\sigma_m$  as an important parameter that affects the fatigue strength of cope-hole details. While this has been recognized in IIW, the Eurocode 1993-1-9 assigns detail category 71 to cope-hole details irrespective of the ratio  $\tau_a/\sigma_m$ .

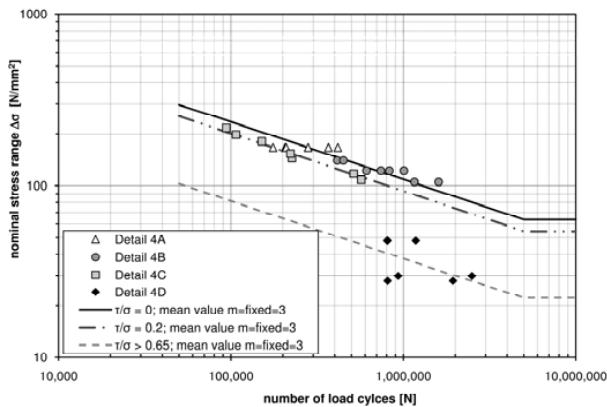


Figure 12. Fatigue test results for cope-hole details distinguished by shear to normal stress ratio

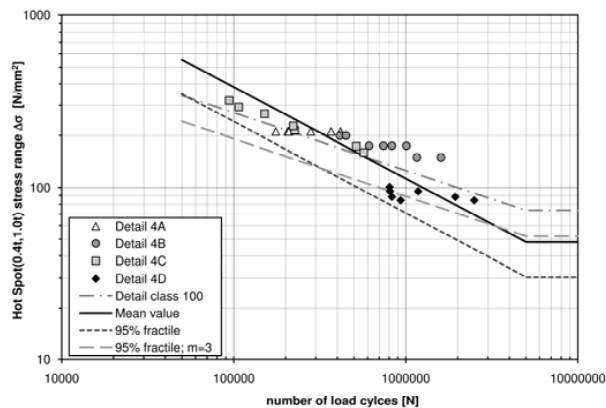


Figure 13. Fatigue test results for cope-hole details according to the hot spot stress approach

Table 6. Statistical evaluation of the cope-hole test results using linear regression analysis with a fixed slope of 3.

| Type of joint | $\Delta\sigma_{\text{mean}}$<br>N/mm <sup>2</sup> | $\Delta\sigma_C$<br>N/mm <sup>2</sup> | Standard deviation |
|---------------|---|---------------------------------------|--------------------|
| Detail 4A*    | 83.8  | --                                    | --                 |
| Detail 4B     | 88.9  | 71.9                                  | 0.093              |
| Detail 4C     | 74  | 64.7                                  | 0.055              |
| Detail 4D     | 30  | 16.7                                  | 0.345              |

\* Since all the specimens were tested in one stress range, a statistical evaluation is not possible.

#### 2.4.2 Evaluation according to the hot spot stress approach

The test results of all cope-hole details evaluated based on the hot spot stresses are plotted in Figure 13. It is apparent that although the test data do not lie in one group, the scatter of the results, compared to the nominal stress method, is decreased. Linear regression analysis with a fixed slope of 3 gives a standard deviation of 0,281 compared with the value of 0.614 obtained from the nominal stress method. However, the calculated characteristic fatigue strength of 70.6 MPa is considerably lower than what is specified in IIW and Eurocode (FAT100). If the results from detail 4D which undergoes the highest  $\tau_a/\sigma_m$  ratio are excluded, FAT100 appears to be a reasonable representation. The low hot spot stress value obtained for detail 4D is assumed to be because of the presence of high amount of shear stresses in the web which causes the weld to become load carrying. In such a case, the weld at the cope-hole transfers the existing shear stresses in addition to the normal stresses caused by the bending of the beam.

Thus, in order to account for such severe loading conditions, it is recommended to apply a further reduction of design class to FAT90 for cope-holes in beams when using the hot spot stress approach.

It is noteworthy that for Detail 4C, surface stress extrapolation according to IIW recommendation was not feasible due to the small radius of the cope-hole in relation to the flange thickness. Therefore, the hot spot stress was calculated as  $1.12 \cdot 0.5t$  according to Lotsberg & Sigurdsson (2006). Moreover, In order to calculate the hotspot stress concentration factor, the nominal stress for beam specimens is calculated as the stress in the mid section of the cope hole using the net cross section and the simple beam theory formula.

#### 2.5 Cover-plates on beams

Partial-length Cover-Plates are usually welded to the flanges of steel bridge girders in order to increase the moment capacity and consequently the allowable traffic load and span of the bridge. For this detail, constant amplitude fatigue test results of 183 cover-plate specimens have been evaluated. The specimens accommodate a wide range of geometric variations such as the cover-plate to main plate thickness ratio ( $t_c/t_m$ ) and the cover-plate end shape; see Figure 14 and Table 7.

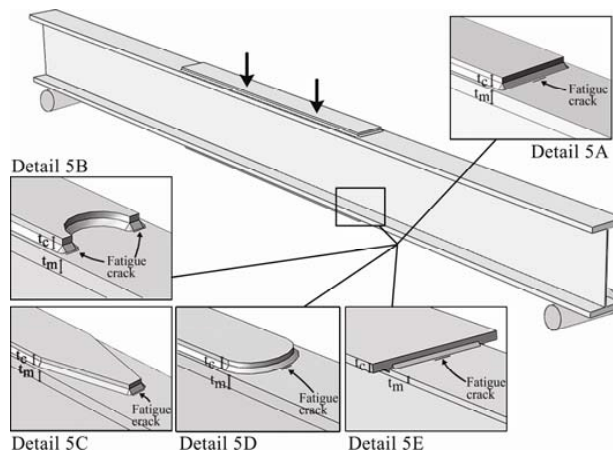


Figure 14. Different cover-plate test configurations

Table 7. Dimensions and quantity of the evaluated fatigue test specimens for cover-plates; all dimensions are in mm.

| Detail | Test data | Main plate |       | Cover plate |       | $t_c/t_m$ |
|--------|-----------|------------|-------|-------------|-------|-----------|
|        |           | Thickness  | Width | Thickness   | Width |           |
| 5A1    | 30        | 9.525      | 171   | 19.05       | 114   | 2         |
| 5A2    | 102       | 9.525      | 171   | 14.3        | 114   | 1.5       |
| 5A3    | 5         | 19.05      | 127   | 12.7        | 101.6 | 0.67      |
| 5B     | 5         | 19.05      | 127   | 12.7        | 101.6 | 0.67      |
| 5C     | 6         | 19.05      | 127   | 12.7        | 101.6 | 0.67      |
| 5D     | 5         | 19.05      | 127   | 12.7        | 101.6 | 0.67      |
| 5E     | 30        | 9.525      | 171   | 14.3        | 229   | 1.5       |

### 2.5.1 Evaluation according to the nominal stress method

Conforming to the data shown in figure 15 and Table 8, the fatigue strength of cover plates seems to be particularly affected by the ratio  $t_c/t_m$ . It is apparent that cover plates with the lowest  $t_c/t_m$  ratio exhibit the highest fatigue strength. However, this effect disappears for details with  $t_c/t_m > 1$ . These details demonstrate the same fatigue strength. Moreover, as the fatigue test results of cover plates with various end shapes lie latently within the same scatter band, it can be concluded that changing the cover plate end shape does not affect the fatigue strength of cover plate details.

While Eurocode has limited the effect of  $t_c/t_m$  to ratios only less than and higher than one, IIW considers several intervals. Consequently, considering the evaluated data in this study, Eurocode recommendations appear to be more consistent.

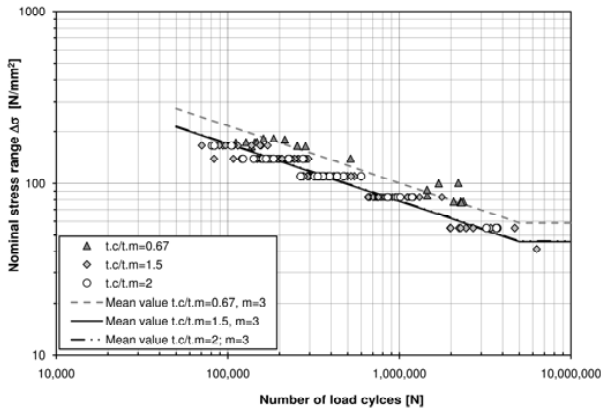


Figure 15. Fatigue test results for cover-plate details categorized by cover plate to main plate thickness ratio

Table 8: Statistical evaluation of the cover-plate test results using linear regression analysis with a fixed slope of 3.

| Configuration    | Test Data | $\Delta\sigma_{\text{mean}}$<br>N/mm <sup>2</sup> | $\Delta\sigma_c$<br>N/mm <sup>2</sup> | Standard deviation |
|------------------|-----------|---|---------------------------------------|--------------------|
| $t_c/t_m = 0.67$ | 21        | 79.7  | 64.8                                  | 0.147              |
| $t_c/t_m = 1.5$  | 132       | 62.2  | 54.4                                  | 0.104              |
| $t_c/t_m = 2$    | 30        | 62.7  | 54.3                                  | 0.103              |

### 2.5.2 Evaluation according to the hot spot stress approach

The test results of all cover-plate details are shown in Figure 13. As it was expected, the geometrical effects of different shapes and configurations are implicitly accounted for by the hot spot stress approach and all the data lie within one scatter band. This observation is supported by the statistical analysis as well. The standard deviation of all test data decreases significantly from 0.149 in the nominal stress approach to 0.116 for the hot spot stress approach. The recommended FAT100 seems also to be a reasonable representation for the fatigue strength of this detail.

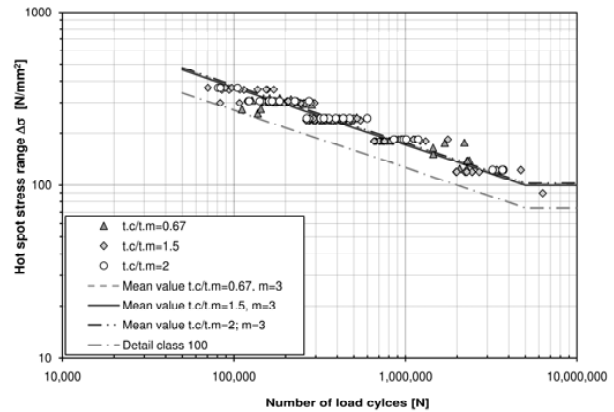


Figure 13. Fatigue test results for cover-plate details according to the hot spot stress approach

## 3 CONCLUSIONS

The following conclusions can be drawn:

- The hot spot stress method is capable of reducing the scatter caused by the geometrical variations. As a result, one hot spot stress S-N curve can be associated to several details.
- For longitudinal non-load-carrying attachments, the design recommendations according to IIW based on the nominal stress method appears to be consistent with the available test data. However, the recommended FAT100 for evaluation based on the hot spot stress approach seems to be inconsistent and should be replaced by FAT90.
- For evaluation of details with load carrying welds based on the hot spot stress approach, a further reduction of the suggested design class FAT90 to FAT80 is recommended based on the evaluated tests. This reduction is relevant for overlapped joints with crack at main plate.
- Quadratic extrapolation is recommended for longitudinally loaded overlapped joints with crack at main plate.
- According to the evaluated test data for overlapped joints with crack at cover plate, FAT100 is

recommended for type b cracks at cover plates when using hot spots stress approach.

- The ratio of the shear stress to the normal bending stress ( $\tau_a/\sigma_m$ ) in cope-hole details seems to effect the fatigue strength of these details considerably. This ratio should be considered by the designer when the fatigue design is made based on the nominal stress method.
- FAT90 is recommended for cope-hole details undergoing  $\tau_a/\sigma_m \leq 0.2$  according to the hot spot stress approach.
- Altering the shape of cover-plates end does not affect the fatigue strength.
- The suggested FAT100 seems to be a reasonable representation for the design of cover-plates based on the hot spot stress method.

Stallmeyer, J.E. et al. 1957. Behaviour of welded built-up beams under repeated loads. *Structural research series* No.135

Xiao, Z. & Yamada, K. 2005. Fatigue strength of intersecting attachments. *Journal of structural engineering* ACSE: 924-932

#### 4 ACKNOWLEDGEMENT

The work presented in this paper is a part of the research project Brifag – Bridge Fatigue Guidance with a financial grant from the Research Fund for Coal and Steel (contract No. RFSRCT-2008-00033) as well as the Swedish Transport Administration.

#### 5 REFERENCES

European standard, 2005. Eurocode 3: Design of steel structures - Part 1-9: Fatigue, Brussels: European Committee for Standardization

Fisher, J.W. et al. 1969. Effect of weldments on the fatigue strength of steel beams. *Fritz engineering laboratory report* No.334.2

Fricke, W. 2001. Recommended hot spot analysis procedure for structural details of FPSO's and ships based on round-robin FE analysis. *Int. 7 Offshore Polar Eng.*, 12(1)

Gurney, T.R. et al. 1961. Influence of artificially induced residual stresses on Fatigue strength of load carrying fillet welded joints in mild steel. *British welding journal*, 541-553

Hall, L.R & Stallmeyer, J.E. 1959. The fatigue strength of flexural members. *Fatigue committee – welding research council*.

Hobbacher, A. 2008. IIW document IIW-1823-07 ex XIII-2151r4-07/XV-1254r4-07

Hobbacher, A.F. 2009. The new IIW recommendations for fatigue assessment of welded joints and components: A comprehensive code recently updated. *International journal of fatigue* 31:50-58

Izdinsky, O. et al. 1958. Engine room section in the building of river ships and the welding of steel reinforcements to the bottom cover ship. *ZVARANIE* VII/12: 363-368

Lotsberg, I. & Sigurdsson, G., 2006. Hot Spot Stress S-N Curve for Fatigue Analysis of Plated Structures. *Journal of Offshore Mechanics and Arctic Engineering*, 128(4):330-336.

Miki, C. & Tateishi, K. 1997. Fatigue strength of cope-hole details in steel bridges. *International journal of fatigue* Vol. 19 No.6: 445-455